

# **Bio-Mediated Self-Assembly of Nanoscale Structures Using the M13 Bacteriophage**

By

Simon White

A thesis submitted in accordance with the requirements for the degree of Ph.D.

The University of Leeds

Faculty of Biological Sciences

August 2010

The candidate confirms that the work submitted is his own and that appropriate credit has been given where reference has been made to the work of others

This copy has been supplied on the understanding that it is copyright material and that no quotation from the thesis may be published without proper acknowledgement

© 2010 The University of Leeds and Simon White

---

# Acknowledgements

My PhD and thesis would not have been possible without the support and help of so many people. I would like to thank:

Prof. Peter Stockley for all his help and encouragement throughout this PhD.

Prof. Christoph Walti and Prof Giles Davies for their help and advice over in Electrical Engineering.

Atul Mohan for his never ending optimism.

Zulfi Hasan for his endless patience at the beginning of my PhD and Jamie Caryl and Pietro Taylor for showing me that things could always be worse.

Steve Johnson, Dave Evans and Rajan Sharma for their support, help and advice for a biologist learning about electronics. Especially Steve for his help with performing the DPI and Dave and Raj for their help with the AFM machine.

David Brockwell with his help with CD, Adrian and Martin for their help with TEM and Iain for his help with all things relating to HPLC.

The various people, past and present, that make up the Stockley lab: Dave, Nic, Rob, Francis, Olga, Gosia, Gabby, Ottar, Andrew and Asik. My apologies to anyone I have left out due to my awful memory.

My final thanks are to my family and my fiancé Kat Aviss: I am very lucky to have you!

---

## Abstract

The M13 bacteriophage is  $\sim 1 \mu\text{m}$  long, with a capsid comprised of five coat proteins. Small peptides can be displayed upon the coat proteins. The aim of this work was to use the phage display of small peptides for the purpose of fabricating a self-assembling molecular transistor with the M13 bacteriophage acting as the scaffold. Each aspect of this fabrication was considered.

Firstly, a 50 nm long microphage particle was re-created and used to produce a 215 nm long phage particle. These smaller phage particles could be used to make the transistor 100 nm in size. To create the scaffold, selenocysteine was displayed on the coat protein pIII and used to self-assemble two to four phage particles around 10 nm gold nanoparticles or quantum dots. These higher order structures were then purified using a linear sucrose gradient. So that the transistor could be directed to a specific area of an existing electronic circuit, the coiled-coil pair ACID:BASE was used. ACID was displayed on the coat protein pIX whilst a BASE peptide containing a C-terminal cysteine was immobilised onto a gold surface. It was shown that ACID and BASE form a coiled-coil when the BASE is immobilised on a surface and that the M13 bacteriophage, displaying ACID, can be anchored to the surface via coiled-coil formation. Finally, tyrosine was displayed on the major coat protein pVIII so that gold could be specifically reduced onto the M13 phage particle scaffold to create the gold electrodes of the transistor. Although within solution, and on a carbon surface, gold was reduced onto the phage particles, when the particles were adsorbed onto an  $\text{SiO}_2$  surface there was no gold deposition.

Therefore, although much progress was made towards the goal of a self assembling transistor, the aspects devised within this study need to be combined.

---

# Contents

<b>Chapter 1: Introduction</b> .....	1
1.0 Introduction.....	2
1.1 Bionanotechnology .....	2
1.2 Viruses and Nanotechnology .....	7
1.3 The M13 bacteriophage .....	11
1.3.1 The life-cycle of the M13 bacteriophage.....	14
1.3.2 Infection.....	15
1.3.3 Replication.....	16
1.3.4 The M13 bacteriophage viral pore.....	17
1.4 Phage Display .....	18
1.4.1 Phagemid phage display .....	21
1.4.2 Bio-panning .....	22
1.4.3 Bio-panning and peptides specific to inorganic materials.....	25
1.5 The M13 phage coat proteins and their uses in bionanotechnology.....	26
1.5.1 The minor coat proteins pIII, pIX. pVI and pVII .....	26
1.5.2 The major coat protein pVIII.....	30
1.5.2.1 Virion structure.....	31
1.5.2.2 pVIII phage display and bionanotechnology .....	32
1.5.2.3 Liquid crystal properties of the M13 bacteriophage.....	35
1.6 Summary of the M13 bacteriophage and bionanotechnology .....	38
1.7 Aims of the thesis and the molecular transistor .....	38
1.8 Scope of the work .....	41

---

<b>Chapter 2: Materials and Methods</b> .....	43
2.0 Materials .....	44
2.0.1 General Reagents .....	44
2.0.2 Bacterial Strains .....	44
2.0.3 Antibiotic stock and working concentrations .....	45
2.0.4 Media recipes .....	46
2.0.4.1 2xYT medium .....	46
2.0.4.2 Super broth (SB) medium .....	46
2.0.4.3 Agarose top .....	47
2.0.4.4 Agar.....	47
2.0.5 Buffers and other reagents .....	48
2.0.5.1 Phosphate buffered saline (PBS) pH 7.4.....	48
2.0.5.2 20% Polyethylene glycol (PEG) and 2.5 M NaCl solution (PEG/NaCl) .....	48
2.0.5.3 2x Protein loading buffer (Laemmli buffer) .....	49
2.0.5.4 10x $\lambda$ buffer for linear sucrose gradients .....	49
2.0.5.5 10x Glycine running buffer.....	50
2.0.5.6 Coomassie blue staining solution.....	50
2.0.5.7 De-stain solution .....	51
2.0.5.8 Tris-HCl buffer .....	51
2.1 General methods .....	52
2.1.1 Growth of overnight <i>E.coli</i> culture .....	52
2.1.2 Preparation of chemically competent <i>E.coli</i> cells.....	52
2.1.3 Transformation using chemically competent <i>E.coli</i> cells .....	52
2.1.4 Preparation of bacterial stocks for freezing .....	54
2.1.5 Preparation of phage stock.....	54

---

2.1.5.1 Growth of phage and PEG precipitation .....	54
2.1.5.2 Caesium chloride purification.....	55
2.1.5.3 Linear sucrose gradients .....	56
2.1.5.4 Fractionation .....	58
2.1.6 Measurement of phage concentration .....	60
2.1.6.1 Phage titering (measured in pfu/mL) .....	60
2.1.6.2 Spectrophotometry of phage particles .....	61
2.1.6.3 Definition of virions/mL and plaque forming units (pfu)/mL.....	61
2.1.7 Colony PCR .....	62
2.1.8 Transmission Electron Microscopy (TEM) .....	64
2.1.9 DNA Gel Electrophoresis .....	64
2.1.9.1 10% Polyacrylamide Gel .....	64
2.1.9.2 1% and 3% Agarose Gel .....	65
2.1.10 Protein Gel Electrophoresis Under Denaturing Conditions.....	65
2.1.10.1 Tris-glycine SDS Gel.....	65
2.1.11 Molecular biology techniques.....	67
2.1.11.1 Polymerase Chain Reaction (PCR) .....	67
2.1.11.2 Phenol Chloroform extraction of DNA and ethanol precipitation .....	69
2.1.11.3 Insertional PCR.....	70
2.1.11.4 Ligation of DNA fragments .....	72
2.2 Specific Methods for Chapter 3 .....	73
2.2.1 Creation of the microphage plasmid (pMicro) .....	73
2.2.2 Creation of longer microphage cassette (pMicroKan) .....	75
2.2.3 Creation of the helper plasmid pM13CP .....	75
2.2.4 Production of shorter length phage particles using M13KO7 .....	77
2.2.5 Production of shorter length phage particles using M13CP .....	78

---

2.2.6 Purification of shorter phage particles .....	78
2.2.7 Caesium chloride purification of shorter length phage particles ...	79
2.2.8 Linear sucrose density ultracentrifugation of shorter length phage particles .....	79
2.2.9 Size exclusion chromatography of shorter length phage particles.	79
2.2.10 Titering of shorter length phage particles .....	80
2.2.11 Measurement of shorter length phage particle length by TEM ...	80
2.3 Specific Methods for Chapter 4 .....	82
2.3.1 Insertion of selenocysteine into <i>gIII</i> .....	82
2.3.2 Production of selenocysteine containing phage .....	84
2.3.3 Production of microphage containing selenocysteine.....	84
2.3.4 Creation and production of pIII cysteine mutant .....	85
2.3.5 Binding of M13pIIISel and wild-type M13 to gold nanoparticles	85
2.3.6 Binding of M13pIIISel and wild-type M13 to quantum dots .....	86
2.3.7 Purification of phage:nanoparticle complexes on a linear sucrose gradient .....	89
2.3.8 Purification of higher order structures using size exclusion chromatography .....	89
2.3.9 Fabrication of microphage higher order structures .....	90
2.4 Specific Methods for Chapter 5 .....	91
2.4.1 Creation of pCGMTpIXHisACIDap and pCGMTpIXHisFOS .....	91
2.4.2 Production of M13pIXHisACIDap and M13pIXHisFOS phage...	92
2.4.3 Purification of M13pIXHisACIDap and M13pIXHisFOS phage .	92
2.4.4 Creation and production of M13pIIIACIDap phage.....	93
2.4.5 HPLC of ACIDap and BASEap peptides .....	94
2.4.6 Circular dichroism (CD) spectroscopy of ACIDap and BASEap peptides .....	95
2.4.7 Surface Plasmon Resonance (SPR) analysis.....	95
2.4.8 Dual Polarisation Interferometry (DPI) analysis.....	96

---

2.5 Specific Methods for Chapter 6 .....	98
2.5.1 Display of tyrosine on pVIII.....	98
2.5.2 Fabrication of gold coated phage in solution.....	99
2.5.3 Deposition of M13Y onto carbon and incubation with gold salt...	99
2.5.4 Attempts to deposit gold on M13 adsorbed to SiO <sub>2</sub> surface .....	100
2.5.4.1 Piranha cleaning of SiO <sub>2</sub> surface.....	100
2.5.4.2 Adsorption of M13 particles to SiO <sub>2</sub> surface and incubation with gold salt.....	101
2.5.5 AFM (Atomic Force Microscopy) .....	101
2.5.6 Scanning Electron Microscopy of gold nanowires .....	102
2.5.7 Conductivity measurements.....	102
<b>Chapter 3: The Microphage.....</b>	<b>103</b>
3.1 Introduction.....	104
3.1.1 The Microphage.....	104
3.1.2 The Helper phage M13KO7.....	110
3.1.3 The Helper Plasmid .....	113
3.1.4 Aims of the work described within this Chapter .....	114
3.2 Results and Discussion .....	115
3.2.1 Creation of microphage .....	115
3.2.2 Creation of pMicroKan.....	119
3.2.3 Creation of the pM13CP helper plasmid .....	120
3.2.4 Production of shorter phage using the helper plasmid pM13CP .	121
3.2.5 Production of shorter phage using the helper phage M13KO7....	125
3.2.6 Production of different length phage and purification.....	126
3.2.7 Examination of shorter phage particles.....	130

---

3.3 Conclusions and Future Work .....	135
<b>Chapter 4: Fabrication of Higher Order Structures .....</b>	<b>139</b>
4.1 Introduction.....	140
4.1.1 The importance of new fabrication techniques.....	140
4.1.2 Self-assembly of molecular transistors .....	142
4.1.3 Viral self-assembly into higher order structures.....	143
4.1.4 Selenocysteine.....	147
4.1.5 Aims of the work described within this Chapter .....	150
4.2 Results and Discussion .....	151
4.2.1 Display of selenocysteine on pIII .....	151
4.2.2 Incorporation of selenocysteine into M13pIIISel .....	153
4.2.3 Titer of M13pIIISel.....	153
4.2.4 Fabrication of higher order structures with gold nanoparticles ...	155
4.2.5 Investigation into the concentration relationship between M13pIIISel and gold nanoparticles.....	161
4.2.6 Fabrication of higher order structures with M13pIIISel and quantum dots.....	165
4.2.6.1 Fabrication using 14 nm quantum dots.....	165
4.2.6.2 Fabrication using 22 nm quantum dots.....	168
4.2.7 Purification of higher order structures using size exclusion chromatography .....	170
4.2.8 Fabrication of higher order structures using microphage .....	173
4.3 Conclusions and Future Work .....	175

---

**Chapter 5: Phage Particle Attachment to a Gold Surface** ..... 179

5.1 Introduction.....	180
5.1.1 Coiled-coils.....	180
5.1.2 Attachment of M13 phage particles to a surface .....	185
5.1.3 Aims of the work described within this Chapter .....	187
5.2 Results and Discussion .....	188
5.2.1 Production and purification of ACIDap and BASEap peptides...	188
5.2.2 Analysis of ACIDap/BASEap coiled-coil formation.....	190
5.2.3 Display of leucine zippers on the M13 bacteriophage.....	191
5.2.3.1 Display of ACIDap on pIX.....	191
5.2.3.2 Production and purification of M13pIXHisACID .....	192
5.2.3.3 Display of the leucine zipper FOS on pIX.....	196
5.2.3.4 Display of ACIDap on pIII .....	197
5.2.4 Surface Plasmon Resonance (SPR) and Dual Polarisation Interferometry (DPI) analysis of ACIDap:BASEap interaction .....	198
5.2.4.1 SPR analysis of BASEap:ACIDap coiled-coil formation.....	199
5.2.4.2 DPI analysis of BASEap:ACIDap coiled-coil formation.....	202
5.2.5 SPR analysis of M13pIXHisACIDap phage interaction with surface immobilised BASEap .....	205
5.3 Conclusions and Future Work .....	208

**Chapter 6: Fabrication of Gold-Coated M13 Bacteriophage** ..... 211

6.1 Introduction.....	212
6.1.1 Bio-mineralisation of nanoparticles.....	212

---

6.1.2 Amino acid reduction of metal salts .....	215
6.1.3 Aims of the work described within this Chapter .....	218
6.2 Results and Discussion .....	219
6.2.1 Display of tyrosine on pVIII.....	219
6.2.2 Fabrication of gold coated phage in solution.....	220
6.2.3 Deposition of M13Y onto carbon and patterning with gold.....	226
6.2.4 Attempts to deposit gold on M13 adsorbed to SiO <sub>2</sub> surface .....	228
6.3 Conclusions and Future Work .....	238
<b>Chapter 7: General Conclusions .....</b>	<b>241</b>
7.1 Conclusions from Chapter 3 .....	242
7.2 Conclusions from Chapter 4 .....	243
7.3 Conclusions from Chapter 5 .....	244
7.4 Conclusions from Chapter 6 .....	245
7.5 Closing remarks .....	246
<b>References.....</b>	<b>247</b>
<b>Appendix A.....</b>	<b>281</b>
1.0 DNA sequence of pM1 .....	282
2.0 DNA sequence of pMicro plasmid .....	282
3.0 DNA sequence of pMicrokan .....	283
4.0 DNA sequence of pM13CP .....	284
4.1 DNA and protein sequence of M13CP .....	289

---

<b>Appendix B</b> .....	293
1.0 DNA sequence of M13pIIISel phage.....	294
1.1 DNA and protein sequence of M13pIIISel phage .....	294
2.0 DNA sequence of M13pIIIC phage .....	295
2.1 DNA and protein sequence of M13pIIIC phage.....	295
3.0 DNA and protein sequence of wild-type pIII .....	295
 <b>Appendix C</b> .....	 297
1.0 Mass spectrometry data of ACIDap and BASEap peptides .....	298
1.1 Fraction 1 of HPLC purified BASEap peptide .....	298
1.2 Fraction 2 of HPLC purified BASEap peptide .....	298
1.3 HPLC purified ACIDap peptide .....	299
2.0 DNA sequence of pCGMTpIXHisACIDap.....	299
2.1 DNA and protein sequence of pCGMTpIXHisACIDap.....	300
3.0 DNA sequence of pCGMTpIXHisFOS .....	300
3.1 DNA and protein sequence of pCGMTpIXHisFOS.....	301
4.0 DNA sequence of M13pIIIACIDap.....	301
4.1 DNA and protein sequence of M13pIIIACIDap.....	302
5.0 SPR kinetic fits for ACIDap and M13pIXHisACID interacting with immobilised BASEap peptide.....	303
5.1 SPR kinetic fit for ACIDap interacting with immobilised BASEap (Chapter 5, Figure 5.10 B) .....	303
5.2 SPR kinetic fit for M13pIXHisACIDap interacting with immobilised BASEap (Chapter 5, Figure 5.13 B).....	304

---

<b>Appendix D</b> .....	305
1.0 DNA sequence of M13Y .....	306
1.1 DNA and protein sequence of M13Y .....	306
2.0 DNA and protein sequence of wild-type M13 pVIII.....	306

## List of Figures

<b>Chapter 1: Introduction</b> .....	1
Figure 1.1. Examples of nano-scale materials fabricated by Nature .....	3
Figure 1.2. The Tobacco Mosaic Virus .....	8
Figure 1.3. The structure of M13 bacteriophage.....	13
Figure 1.4. The life-cycle of the M13 bacteriophage.....	14
Figure 1.5. pIII interaction with F-pilus.....	16
Figure 1.6. Methods of phage display.....	20
Figure 1.7. Bio-panning .....	24
Figure 1.8. The minor coat protein pIII .....	28
Figure 1.9. A nano-ring created by the M13 bacteriophage .....	29
Figure 1.10. Amino acid sequence of the pVIII coat protein. ....	31
Figure 1.11. Model of M13 filamentous bacteriophage capsid determined by NMR spectroscopy. ....	32
Figure 1.12. M13 binding to gold nanoparticles.....	34
Figure 1.13. The liquid crystal structures .....	35
Figure 1.14. Self-assembling liquid crystal M13 bacteriophage layer .....	37
Figure 1.15. The Molecular transistor.....	39

---

Figure 1.16. Schematic of a possible fabrication protocol of a self-assembling molecular transistor.....	40
--	----

## **Chapter 2: Materials and Methods** ..... 43

Figure 2.1. Materials supplied with Biocomp gradient station.....	58
---	----

Figure 2.2. The Biocomp gradient station and fractionator .....	59
---	----

Figure 2.3. The gradient fractionator trumpet.....	60
--	----

Figure 2.4. Typical absorption spectrum of a purified (PEG/NaCl) M13 particle .....	62
---	----

Figure 2.5. Position of pIII and pVIII sequencing primers.....	63
--	----

Figure 2.6. Gel ladders for DNA and proteins.....	66
---	----

Figure 2.7. Vector Map of pJET1.2.....	75
--	----

Figure 2.8. The Qdot quantum dot from Invitrogen .....	87
--	----

Figure 2.9. The structure of sulfo-SMCC .....	87
---	----

## **Chapter 3: The Microphage**..... 103

Figure 3.1. An electron micrograph of microphage particles .....	107
--	-----

Figure 3.2. The structure of the microphage cassette .....	109
--	-----

Figure 3.3. The intergenic region of the M13 bacteriophage .....	112
--	-----

Figure 3.4. Schematic of method used to create pM13CP.....	114
--	-----

Figure 3.5. Maps of the pJet1.2 and pMicro vectors .....	115
--	-----

Figure 3.6. Insertion of packaging signal (PS) into the pET26-b vector .....	117
--	-----

Figure 3.7. Insertion of defective origin, (+) Ori $\Delta$ 29, into the pM1 vector.....	118
--	-----

Figure 3.8. Controlling the length of phage particles .....	120
---	-----

Figure 3.9. Creation of pM13CP helper plasmid.....	122
Figure 3.10. Phage produced using pM13CP and pMicro and pLitmus 28i.....	123
Figure 3.11. Titer of pLitmus28i and pM13CP .....	124
Figure 3.12. Production of microphage .....	125
Figure 3.13. Linear sucrose gradient fractionation of different length phage particles	126
Figure 3.14. Transmission electron micrographs of gradient fractionated phage particles; pMicro, pMicroKan, pLitmus, and M13KO7 helper phage .....	127
Figure 3.15. Size exclusion purification of microphage particles .....	128
Figure 3.16. Denaturing PAGE analysis of GroEL .....	130
Figure 3.17. Homogeneity of shorter phage particle populations.....	131
Figure 3.18. The length of different phage particles.....	132
Figure 3.19. CsCl gradient of different length phage particles.....	133
Figure 3.20. Titer of different length phage.....	134

## **Chapter 4: Fabrication of Higher Order Structures** ..... 139

Figure 4.1. Photolithography .....	141
Figure 4.2. AFM images of M13 bacteriophage higher order structures.....	144
Figure 4.3. Gold coated M13 bacteriophage higher order structures .....	146
Figure 4.4. Incorporation of selenocysteine into the opal stop codon in prokaryotes ..	149
Figure 4.5. Amplification of DNA fragment encoding for selenocysteine containing peptide.....	152
Figure 4.6. Linear sucrose gradient purification of M13pIIISel phage particles bound to gold nanoparticles .....	157

---

Figure 4.7. Linear sucrose gradient purification of M13pIIISel and wild-type M13 phage particles bound to gold nanoparticles.....	159
Figure 4.8. Linear sucrose gradient purification of M13pIIISel and phosphine stabilised gold nanoparticles .....	160
Figure 4.9. Concentration dependence of M13pIIISel and GNP10nm/cit in fabricating higher order structures .....	162
Figure 4.10. Quantitation of sucrose purified higher order structures.....	163
Figure 4.11. Fabrication of higher order structures using M13pIIISel phage and 525 nm emission QDs.....	167
Figure 4.12. Fabrication of higher order structures using M13pIIISel phage and 800 nm emission QDs.....	169
Figure 4.13. Purification of higher order structures using size exclusion chromatography .....	172
Figure 4.14. Higher order structures using microphagepIIISel .....	174
<b>Chapter 5: Phage Particle Attachment to a Gold Surface.....</b>	<b>179</b>
Figure 5.1. Structure of a coiled-coil .....	180
Figure 5.2. Schematic showing coiled-coil interactions .....	182
Figure 5.3. The ACID:BASE leucine zipper pair .....	184
Figure 5.4. Schematic of M13 phage particle attachment to a gold surface.....	186
Figure 5.5. HPLC purification of ACIDap and BASEap peptides .....	189
Figure 5.6. Circular dichroism of the ACIDap/BASEap leucine zipper pair .....	191
Figure 5.7. Display of the ACIDap peptide on pIX.....	193
Figure 5.8. HisTrap™ column purification of M13pIXHisACIDap and	

---

M13pIXHisFOS .....	195
Figure 5.9. Schematic of DPI and SPR sensor chips .....	199
Figure 5.10. SPR analysis of ACIDap:BASEap interactions .....	201
Figure 5.11. Dual Polarisation Interferometry (DPI) .....	203
Figure 5.12. DPI analysis of ACIDap:BASEap interactions .....	204
Figure 5.13. SPR analysis of M13 phage and immobilised BASEap .....	206
<b>Chapter 6: Fabrication of Gold-Coated M13 Bacteriophage .....</b>	<b>211</b>
Figure 6.1. The magnetotactic bacteria .....	214
Figure 6.2. Cartoon showing a proposed mechanism of metal reduction by tyrosine ..	216
Figure 6.3. A TEM image of M13 phage mixed with gold salt overnight in solution .	221
Figure 6.4. Time course of M13Y and wild-type phage mixed with gold salt .....	223
Figure 6.5. Phage particles on a carbon surface exposed to gold salt .....	227
Figure 6.6. M13 bacteriophage particles adsorbed to SiO <sub>2</sub> surface .....	228
Figure 6.7. M13 phage particles adsorbed to SiO <sub>2</sub> and incubated with gold salt for different times .....	229
Figure 6.8. M13 bacteriophage particles adsorbed to SiO <sub>2</sub> surface and incubated with varying amounts of gold salt .....	231
Figure 6.9. Height and width measurement of M13Y particles .....	232
Figure 6.10. M13Y phage on SiO <sub>2</sub> surface exposed to dilute hydrochloric acid .....	234
Figure 6.11. Scanning electron microscopy of M13Y phage exposed to 6 mM gold salt on a SiO <sub>2</sub> surface .....	235
Figure 6.12. Electronic characterisation of M13Y phage particles .....	236

---

## List of Tables

<b>Chapter 1: Introduction</b> .....	1
Table 1.1. The M13 proteins.....	11
Table 1.2. Peptides that show high affinity to inorganic materials.....	25
<b>Chapter 2: Materials and Methods</b> .....	43
Table 2.1 A list of the primers used in creating the microphage plasmid pMicro.....	73
Table 2.2 A list of the primers used in creating the helper plasmid M13CP.....	76
Table 2.3. Dimensions and composition of Qdot® nanocrystals .....	86
<b>Chapter 5: Phage Particle Attachment to a Gold Surface</b> .....	179
Table 5.1. Rate and equilibrium constants obtained from sensograms shown in Figures 5.10 B and 5.13. ....	207

---

# Abbreviations

AFM: Atomic Force Microscopy

CCD: Charge-coupled device

CD: Circular dichroism

CT: C-terminal

DMF: Dimethylformamide

DPI: Dual Plasmon Interferometry

dUMP: Deoxyuridine monophosphate

GNP: Gold Nanoparticles

HEPES: 4-(2-hydroxyethyl)-1-piperazineethanesulfonic acid

HPLC: High-performance liquid chromatography

IPA: Isopropyl alcohol

IPTG: Isopropyl  $\beta$ -D-1-thiogalactopyranoside

LPEI: Linear-polyethylenimine

NEB: New England Biolabs

Ni-NTA: Nickel(II)-nitrilotriacetic acid

O-mRNA: Orthogonal messenger ribonucleic acid

O-ribosome: Orthogonal ribosome

PAA: Polyacrylic acid

PCR: Polymerase Chain Reaction

PEG: Polyethylene glycol

PMMA: Poly(methyl methacrylate)

PS: Packaging signal

QD: Quantum dot

RBS: Ribosome binding sequence

---

RF DNA: Replicative Form Deoxyribonucleic acid

PS: Packaging Signal

SB: Super broth

SPR: Surface Plasmon Resonance

TFA: Trifluoroacetic acid

TMV: Tobacco Mosaic Virus

TNT: Trinitrotoluene

UPRT: Uracyl phosphoribosyltransferase

# Chapter 1

---

Introduction

## 1.0 Introduction

In the winter of 1959, the physicist Richard Feynman gave a presentation to the West Coast division of the American Physical Society entitled '*There's plenty of room at the bottom*' (Feynman, 1960). Within the talk he laid out the concepts for a new area of science which, in time, became known as nanotechnology. What he discussed, as the title suggests, was "the manipulation and control of atoms and molecules on the small scale". Why, he pondered, was it not possible to "write the entire 24 volumes of the Encyclopaedia Britannica on the head of a pin?" or to manoeuvre "things atom by atom" when it was well within the realms of physics to carry out such tasks.

Although not widely cited at the time, just seven times until 1980 (Toumey, 2009), it is now widely accepted as a prescient presentation that foresaw the coming together of a diverse range of disciplines to focus on answering the questions that Feynman pondered upon in his presentation; and therefore producing the nanoscale materials and devices we see today.

### 1.1 Bionanotechnology

One aspect the talk focused on was biology, where cells act as entire factories producing a plethora of complex nanoscale machines and materials (Figure 1.1 highlights some well known nanoscale materials). Feynman had the imagination to 'Consider the possibility that we too can make a thing very small [the cell] which does what we want--that we can manufacture an object that manoeuvres at that level!' (Feynman, 1960).

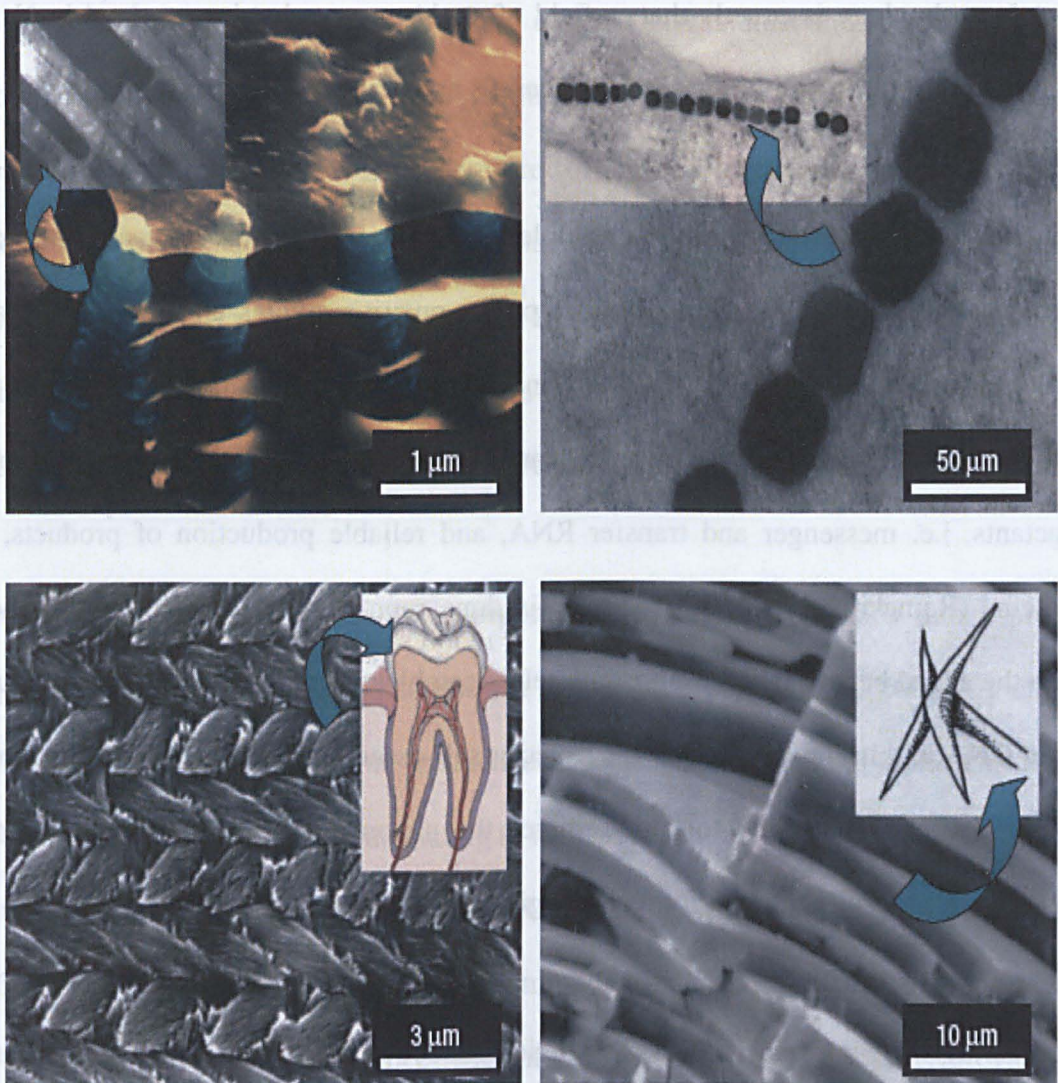


**Figure 1.1. Examples of nano-scale materials fabricated by Nature.** All images are from a scanning electron micrograph (taken from Sarikaya, 2003).

**A** shows the growth edge of an abalone, a sea mollusc known for its brightly coloured mother of pearl (nacre) shell. It shows platelets (blue) separated by an organic film (orange) that form the mother of pearl. The layers provide a very strong and tough bi-composite. The inset picture shows a transmission electron micrograph of the same structure.

**B** shows an ordered array of magnetite nanoparticles created by a magnetotactic bacterium which allow the bacterium to migrate using the Earth's magnetic field; the inset shows a transmission electron micrograph of these ordered nanoparticles.

**C** shows hydroxyapatite crystallites woven together to form an ordered, tough structure which makes up mouse teeth enamel (inset).

**D** shows a sponge (Rosella) spicule (inset) which is created from layered silica and has properties similar to fibre optic cables.

# Chapter 1

---

Bionanotechnology is exactly that: a field of study to use what has evolved in Nature and manipulate it to produce desirable materials and devices at the nanoscale.

The ribosome is perhaps the best example of a biological nanoscale machine and as George Whitesides (a Harvard chemist) points out; it provides an “existence proof” (editorial in *Nature Materials*, 2009) that nanotechnology can work. The ribosome is a protein and RNA complex, 20 nm in diameter, which shows specific recognition of reactants, i.e. messenger and transfer RNA, and reliable production of products, i.e. proteins (Ramakrishnan, 2002). All this is done reproducibly in ambient conditions, with the added benefit that the ribosome self-assembles from discrete particles produced from DNA within the cell. It is these aspects; self-assembly, reproducibility at ambient conditions, and the ability to “programme” the nanomachine using DNA, that make nature such an exciting target for technological applications.

Comparing the ribosome with the synthetic production of a small peptide provides an example to show the potential benefits of harnessing Nature’s nanoscale machines. Synthetic production is normally a slow process with a current upper limit of 100 amino acid long chains. The fabrication of these chains requires the step-wise deprotection of the N-terminus of the chain and the formation of a peptide bond with the next amino acid. The reaction is carried out in a non-aqueous solvent; typically TFA (trifluoroacetic acid) and DMF (dimethylformamide), both of which are toxic. Assuming a high yield of 99% with each step, after only 26 amino acids the yield would already be down to ~75%. Contrast this with the ribosome which can produce proteins hundreds of amino acids long, in an aqueous solution, with a high yield and with no toxic chemicals involved.

# Chapter 1

---

However, the ribosome has evolved to use the 64 DNA codons and the 20 genetically encoded amino acids, 22 if you include pyrrolysine (Srinivasan, 2002) and selenocysteine (Bock, 1991). It is therefore difficult to incorporate un-natural amino acids into a protein sequence using the ribosome, e.g. fluorescent amino acids which can be used to study peptide folding. Aside from allowing the investigation of proteins, it is thought that the incorporation of un-natural amino acids could allow for the evolution of proteins with novel functions (Xie, 2006).

Currently, the favoured system to incorporate un-natural amino acids into a protein sequence using the ribosome is to use the amber stop codon (Xie, 2006). A unique tRNA molecule was derived from the archaeal species *Methanococcus jannaschii* which recognises the amber stop codon, leading to incorporation of an un-natural amino acid at that site (Wang, 2000). The amber codon (UAG) is the least used stop codon (Benzer, 1962) and so incorporation of un-natural amino acids in response to this codon means that there is minimal interference with normal cellular translation. However, the efficiency of un-natural amino acid incorporation in this way can be as low as 20% (Barrett, 2010). Likewise, incorporating multiple different un-natural amino acids using this approach is not possible as there is no way to specify which un-natural amino acid is translated at each amber stop codon. In contrast, the step-wise construction of proteins using synthetic methods allows far easier incorporation of multiple un-natural amino acids.

Therefore many scientists have been attempting to combine the advantages of both synthetic production and the ribosome. The aim is to have a self-assembling synthetic ribosome, with all the associated benefits, which is able to incorporate multiple un-

# Chapter 1

---

natural amino acids efficiently. Recently, the group of Dr Jason Chin has focused on creating an orthogonal ribosome (O-ribosome), i.e. a ribosome that recognises mRNA molecules which cannot be recognised by wild-type ribosomes (Rackham, 2005; Barrett, 2010; Neumann, 2010). They have evolved the ribosome and mRNA, within *E.coli*, and focused on the ribosome binding sequence (RBS) within the mRNA and its complementary partner in the 16S RNA sequence of the ribosome (Rackham, 2005). The RBS has been shown to be main determinant in translational efficiency, i.e. it is the main recognition site of the mRNA by the ribosome. The RBS within the mRNA and 16S RNA were randomly mutated to create libraries of ribosomes and mRNA, each with a different RBS sequences. The mRNA used within the library encoded for the enzyme uracyl phosphoribosyltransferase (UPRT) and for chloramphenicol resistance. To select for orthogonal mRNA (O-mRNA), i.e. mRNA that could not be recognised by wild-type ribosomes, the mRNA library was transformed into *E.coli* and grown in the presence of 5-fluorouracil; this is converted by UPRT to 5-fluoro-dUMP, which in turn strongly inhibits thymidylate synthase and so causes cell death. Therefore *E.coli* cells which survived growth in the presence of 5-fluorouracil contained mRNA mutants which were not recognised by wild-type ribosomes.

These cells were then transformed with the ribosome library and grown in the presence of chloramphenicol. Only ribosomes that recognised the O-mRNA, encoding chloramphenicol resistance, could translate it and so provide the cell with chloramphenicol resistance. By selecting for specific RBSs within the ribosome and mRNA, it was possible to create orthogonal ribosomes and mRNA which when present within an *E.coli* cell acted independently of the endogenous ribosomes and mRNA (Rackham, 2005). Therefore these O-ribosome and O-mRNA can create proteins with

minimal interference of endogenous cellular functions. The O-ribosome was then used to select O-ribosomes that could efficiently decode quadruplet codons, e.g. AGGA (Neumann, 2010). The selection was again carried out by using mRNA that encoded for chloramphenicol resistance. However, the mRNA contained the quadruplet sequence AGGA. A quadruplet anti-codon tRNA<sup>Ser</sup> was produced by a plasmid within the cell which recognised the AGGA sequence. Only O-ribosomes which could accommodate the quadruplet tRNA<sup>Ser</sup> would provide the *E.coli* cell with chloramphenicol resistance. The use of quadruplet codons means that there are blank codons, i.e. there are no natural tRNAs that will recognise them, into which un-natural amino acids can be incorporated via the quadruplet t-RNA (Neumann, 2010). What they have therefore created is a ribosome that can read the genetic sequence in a novel way and incorporate multiple un-natural amino acids into a protein sequence. This example highlights how the understanding of cellular nanoscale mechanisms can be used to manipulate them and change their function whilst retaining the benefits of working in aqueous solutions and ambient conditions.

## 1.2 Viruses and Nanotechnology

The field of bionanotechnology is rapidly growing with scientists exploiting DNA (Dietz, 2009), proteins (Naik, 2002), and even whole cells (such as the magnetotactic bacteria in Figure 1.1). There is, however, one area of research which exploits all three; that involving viruses and bacteriophages (the subtle distinction between the two is that phage infect only bacteria). These are miniscule replicating units, on the scale of nanometres: between 10-100 nm, containing a simple genome, either DNA or RNA, coated in a protective protein shell, that utilise a host cell's machinery to replicate.

Typically the protein coat is made up of a small repertoire of proteins encoded by the viral genome, which self-assemble into ordered, symmetrical structures.

It is the properties of self assembly; simple manipulation of the coat proteins using genetic modification of the genome and the ease of large-scale production (Shenton, 1999; Lee, 2006) which make viruses such inviting targets for nanotechnology applications. Some of the earliest work in this field focused on the plant virus TMV (Tobacco Mosaic Virus); which is a rod-shaped virus in which the coat is made up of 2130 copies of an identical coat protein (Dujardin, 2003; Figure 1.2 A) encoded for within the viral genome.

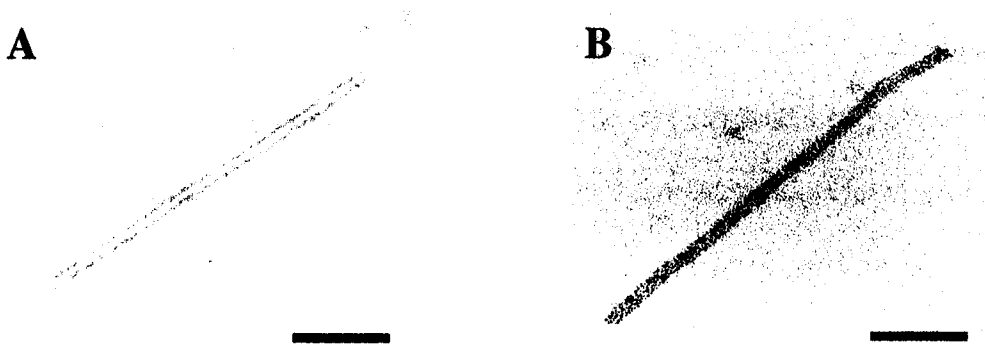


**Figure 1.2. The Tobacco Mosaic Virus.** TEM image showing a wild-type TMV capsid stained with 2% uranyl acetate (A). TMV mutant coat proteins displaying a solution exposed hexahistidine tag at position 1 were re-assembled into a capsid-like particle, but lacking any genomic RNA, at pH 8. The hexahistidine tag was used to spontaneously order citrate-stabilised 2 nm gold nanoparticles via electrostatic binding along the capsid-like particle (B). Images kindly provided by Dr Gosia Wnek. Scale bar equals 100 nm.

# Chapter 1

---

A large proportion of bionanotech research with TMV focuses on using the viral capsid as a scaffold for the deposition of materials, e.g. gold (Figure 1.2 B) to create “nanowires”. By altering the genome of TMV, Lee, *et al.* (2005), inserted two cysteine residues at positions 2 and 3 of the TMV coat protein which were solvent exposed on the surface of the TMV capsid (Lee, 2005). Transfection of tobacco plants with the genome led to the production of TMV virus particles, 300 nm in length, displaying 2 cysteines on every coat protein for the entire length of the virus. Cysteine contains a single sulphur atom which forms a strong covalent bond with gold atoms (Grandbois, 1999; Jadzinsky, 2007). The displayed cysteines were used to bind to the gold nanoclusters, irregularly shaped nanoparticles ~10 nm in size, which had been created from the chemical reduction of a gold salt solution. Using this method the TMV particle was entirely coated in gold nanoclusters. The majority of work involving TMV, and other viruses, has followed this approach, i.e. the alteration of key amino acid residues of the coat protein by DNA manipulation so that specific chemical groups are exposed in the viral capsid and then using these groups to bind metal ions to the outside of the virus.

One of the challenges of bionanotechnology is that of interfacing self-assembled macromolecular structures within an electronic circuit. Thus many groups have focused on manipulating TMV into creating a device that self-assembles into a specific location that is connected to the surrounding circuit. Yi, *et al.* (2005), achieved this by incubating TMV virus particles at pH 8, which dissociated some of the coat proteins from the 5' end of the RNA genome and exposed this portion of the nucleic acid to solution. By hybridising the protein-free 5' end of RNA genome to a complementary strand of DNA covalently bound to a gold electrode, it was possible to attach the TMV

via nucleic acid hybridisation (Yi, 2005). Numerous small peptides have been discovered by phage display (section 1.4) that recognise specific targets, e.g. cocaine (Carrera, 2004), cancer markers (Brissette, 2006) and the explosive TNT (Goldman, 2002). These could be displayed on the surface of the TMV virus; thus creating a self-assembling biosensor.

Another group utilised the TMV virus displaying two cysteine residues created by Lee, *et al.* (2005), to bind the viral particles to a specified area of a gold surface and then used the same particles as sites for metal deposition. The displayed cysteines were used to create a layer of TMV particles on a gold surface via thiol-gold bonds (Gerasopoulos, 2010). The immobilised TMV particles were then coated with nickel via electroless plating, i.e. chemical reduction of a nickel salt to randomly coat the TMV particles. A pre-fabricated zinc layer was then placed above the nickel coated TMV layer. The two layers acted as the anode and cathode, respectively, of a battery (Gerasopoulos, 2008). A 1 M KOH solution was then used as the battery electrolyte so that electrons could migrate between the anode and the cathode. The increased surface area that the nickel coated TMV provided increased the initial capacity of the battery by a factor of six compared to batteries without the virus. Working with TMV therefore shows us that viruses can be used as scaffolds that can bind spontaneously to a pre-determined area and at the same time act as nucleation sites for inorganic materials, creating a self-assembling nanodevice.

## 1.3 The M13 bacteriophage

A parallel branch of bionanotechnology research has involved the M13 bacteriophage. This is a filamentous phage of the *Inovirus* family (Clackson, 2004), so named because of its discovery in Munich waste water (hence the M) in 1963 (Hofschneider, 1963). Specifically, it is part of the Ff (F-pilus specific) class of phage, of which f1 and fd are also members (Marvin, 1963). The Ff nomenclature relates to the observation that the phage infect *Escherichia coli* (*E.coli*) via the F-pilus, a membrane appendage used by bacteria for transferring DNA plasmids between one another (Marvin, 1998). The three phage of the Ff group share 98% DNA sequence homology and their gene products are interchangeable (Clackson, 2004). This fact is important since it means that protein II, involved in the recognition and initiation of Ff reproduction, will recognise any Ff viral origin of replication, e.g. protein II of M13 will recognise the commonly used f1 origin of replication.

**Table 1.1. The M13 proteins.** This lists the M13 gene names, the size of proteins encoded, and functions of those proteins. Gene I encodes both protein I and XI. (Makowski, 1984; Russel, 1991)

Gene	Protein	Size (aa)	Function
I	I	348	Assembly/export
	XI	108	Assembly/export
II	II	410	Replication
III	III	427	Capsid
IV	IV	426	Assembly/export
V	V	87	Replication
VI	VI	112	Capsid
VII	VII	33	Capsid
VIII	VIII	73	Capsid
IX	IX	32	Capsid
X	X	110	Replication

# Chapter 1

---

The wild-type M13 virion is a flexible rod (Figure 1.3 A and B), persistence length  $\sim 1$  micron (Khalili, 2007), with a 7,222 nucleotide single-stranded DNA genome (Figure 1.3 C) contained within a  $\sim 1 \mu\text{m}$  long capsid (Clackson, 2004; Marvin, 1966). Although the genome encodes 11 proteins (denoted by Roman numerals I – XI, Table 1.1), only five are incorporated into the viral capsid. The others are involved in the replication and assembly of the virion (Clackson, 2004). The five coat proteins (pIII, pVI, pVII, pVIII and pIX) function to encapsulate the ssDNA genome of the M13 bacteriophage. They are split into two families; the major, and minor coat proteins. pVIII comprises the only major coat protein and  $\sim 2800$  copies of pVIII form the phage coat. It is thought that this is the smallest number of pVIII coat proteins that can be used to encapsulate the 7,222 base DNA genome (Greenwood, 1991). However the number of pVIII molecules changes with the length of the ssDNA (Clackson, 2004).

The minor coat proteins, pIII, pVI, pVII and pIX, are located at either end of the virion, and in theory these may be distinguished by electron microscopy, one end appearing blunt, whilst the opposite end looks pointed (Dogic, 2006). However it is often difficult to differentiate between each end (Figure 1.3 B). By using shorter phage particles it is possible to detect the larger pIII proteins (Figure 1.3 B inset). This “pointed” end contains 3-5 copies of both pIII and pVI, whilst the “blunt” end is once again composed of 3-5 copies each of pVII and pIX (Figure 1.3 A – Dogic, 2006). However, it is common practice in schematics of the M13 bacteriophage to show 5 copies of each coat protein.

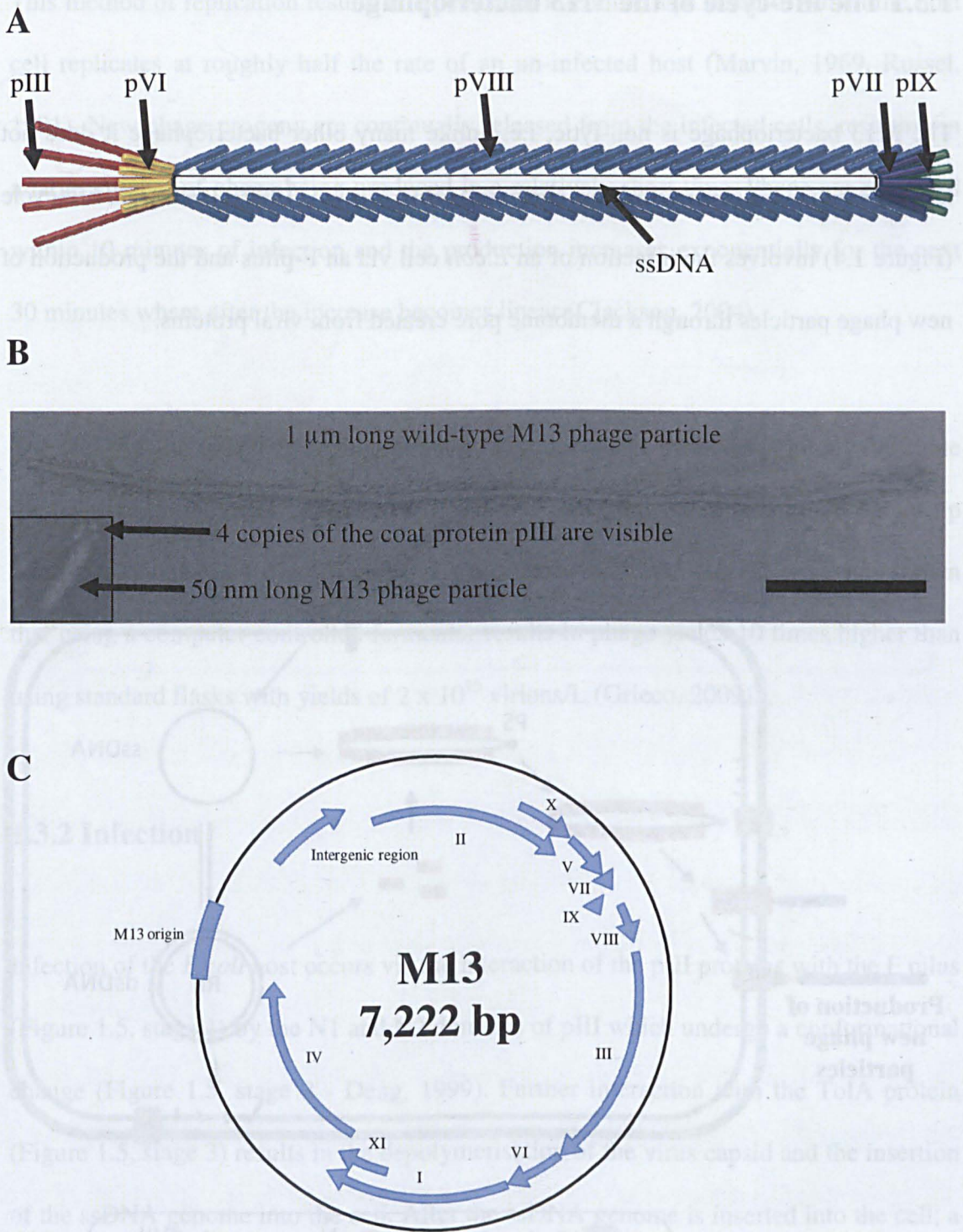


**Figure 1.3. The structure of M13 bacteriophage.** A shows a schematic of the M13 bacteriophage. B shows a transmission electron micrograph of a single M13 phage negatively stained with uranyl acetate. Inset shows a 50 nm long microphage particle. C shows the genetic map of wild-type M13 bacteriophage. Scale bar equals 200 nm.

1.3.1 The life-cycle of the M13 bacteriophage

The M13 bacteriophage is non-lytic, i.e. unlike many other bacteriophage it does not kill the host cell in order to release phage progeny (Marvin, 1969). Instead its life-cycle (Figure 1.4) involves the infection of an *E.coli* cell via an F-pilus and the production of new phage particles through a membrane pore created from viral proteins.

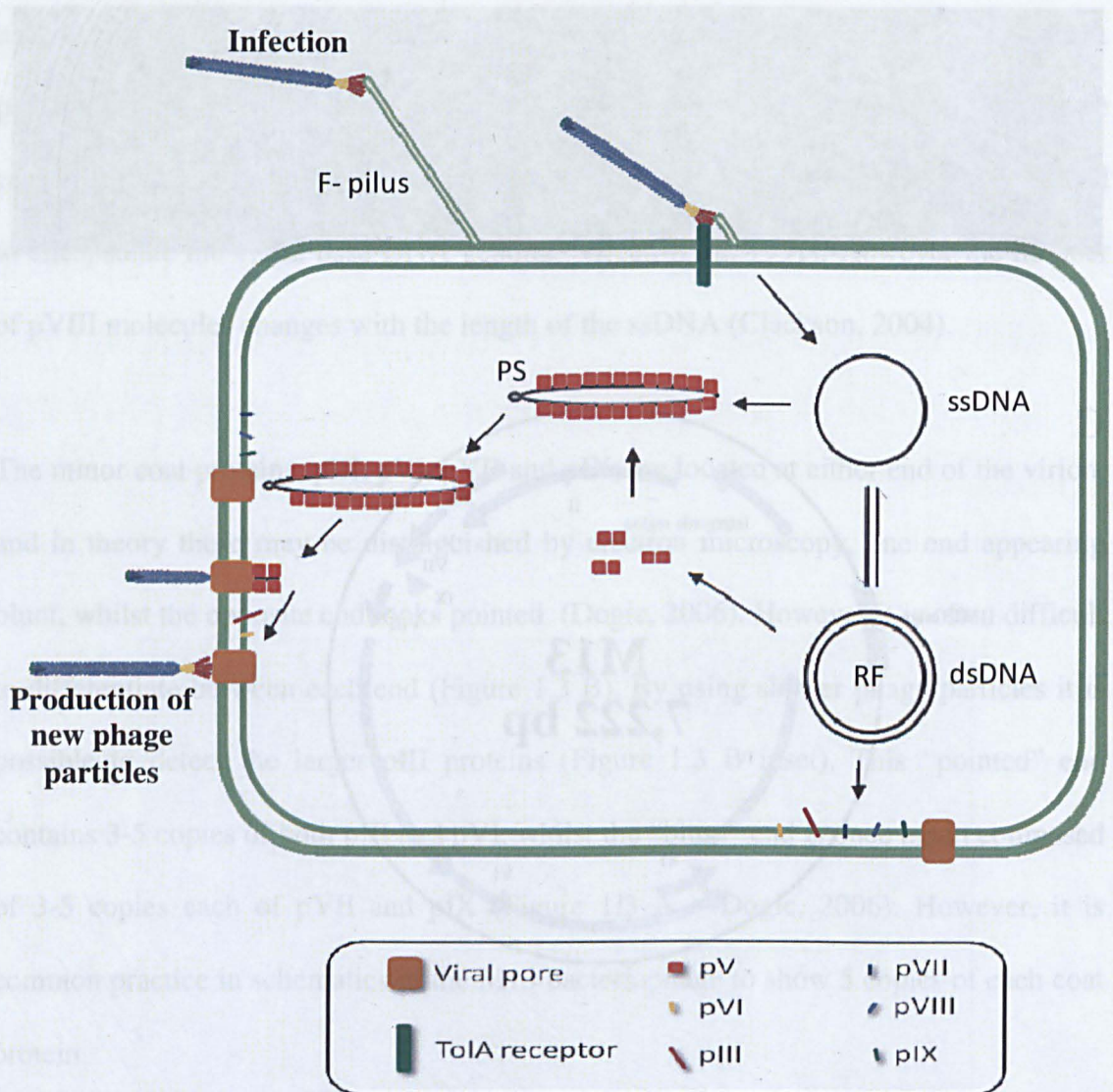


Figure 1.4. The life-cycle of the M13 bacteriophage. Adapted from Clackson, 2004.

This method of replication results in a persistent infection, as a result of which the host cell replicates at roughly half the rate of an un-infected host (Marvin, 1969, Russel, 1991). New phage progeny are continually released from the infected cells, resulting in a large number of phage being produced in a relatively short time. Phage are produced within 10 minutes of infection and the production increases exponentially for the next 30 minutes where after the increase becomes linear (Clackson, 2004).

The fact that the infected *E.coli* continually produce phage particles is highly desirable for possible commercial applications given that industrial fermenters could be set up relatively cheaply and used to grow vast quantities of phage. Recent work has shown that using a computer controlled fermenter results in phage yields 10 times higher than using standard flasks with yields of  $2 \times 10^{15}$  virions/L (Grieco, 2009).

### 1.3.2 Infection

Infection of the *E.coli* host occurs via the interaction of the pIII proteins with the F pilus (Figure 1.5, stage 1) by the N1 and N2 domains of pIII which undergo a conformational change (Figure 1.5, stage 2 - Deng, 1999). Further interaction with the TolA protein (Figure 1.5, stage 3) results in the depolymerisation of the virus capsid and the insertion of the ssDNA genome into the cell. After the ssDNA genome is inserted into the cell, a complementary strand is then synthesised from the ssDNA to create a double stranded circular piece of DNA (Geider, 1974) termed the replicative form (RF). It is from the RF DNA that all the viral proteins are transcribed and progeny ssDNA copied.

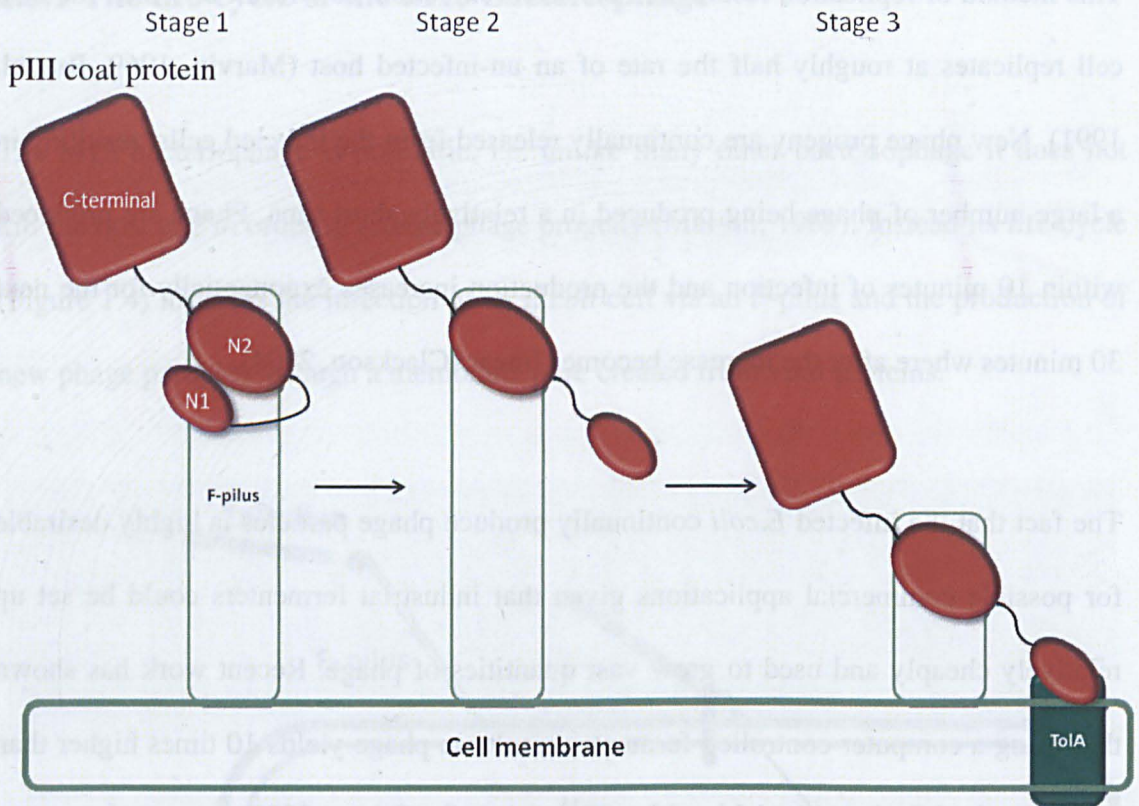


**Figure 1.5. pIII interaction with F-pilus.** A diagram showing the binding sites and conformational changes of pIII.

### 1.3.3 Replication

It has been shown that pV forms a dimer which then binds to the ssDNA (Salstrom, 1971). In the early stages of infection when pV levels are low, unbound ssDNA is rapidly converted to RF DNA (Figure 1.4). Only when pV is at a high enough concentration are phage particles produced (Salstrom, 1971). The pV dimers bind along the viral + strand ssDNA strand, collapsing it into a rod like shape (Gray, 1989) with the packaging signal (PS), a DNA hairpin structure, exposed at one end: pV binds preferentially to ssDNA (Bauer, 1988; Mou, 1999; Alberts, 1972).

### 1.3.4 The M13 bacteriophage viral pore

The viral pore is a complex of pI, pIV and pXI. pIV is known to assemble into approximately 12 to 14 600 kDa subunits that form a 24 nm long cylindrical structure within the outer membrane (Russel, 1991) with a gated channel (Marciano, 2001) running through the centre with a diameter of 8 nm (Linderoth, 1997). It is through this channel that the M13 particle is thought to pass (Marciano, 2001).

pI and pXI are essentially the same protein but pXI lacks a 240 amino acid long sequence starting from the N-terminal domain of pI. It is the result of an internal translation re-initiation event (Rapoza, 1995). pXI is known to be essential to phage production but its specific function(s) is still unknown (Rapoza, 1995). The C-terminal domain of pI and pXI contains a conserved nucleotide binding motif which extrudes into the cytoplasm whilst the N-terminal domain of pI contains a pIV binding domain (Rapoza, 1995). pI and pXI form a complex containing 5-6 copies of each protein that spans the inner membrane. It is thought they may form a pore as well although it is still not known (Clackson, 2004).

Little is known about how the phage passes through the viral pore. It is thought that the coat proteins pIX and pVII, which cap one end of the bacteriophage, interact with the PS along with the C-termini of the pI/pXI complex (Feng, 1999). The ssDNA then passes through the pore with pVIII coat proteins replacing the pV dimers along the ssDNA backbone; this process is known to be powered by ATP hydrolysis and the membrane potential (Feng, 1997).

Once the ssDNA has passed through the pore the end is “capped” by binding of pIII and pVI to complete the phage (Rakjonac, 1999). It has been shown that when pIII or pVI is absent the phage stays tethered to the pore and that more ssDNA can be packaged behind it, resulting in phage particles 10 times longer than wild-type (Rakjonac, 1998). Within typical phage populations it has been found that 5% of the phage particles are double in length (Salivar, 1967), suggesting that “capping” errors do occur frequently, perhaps because the levels of pIII and pVI are not high enough within the *E.coli* cell at the time.

## 1.4 Phage Display

Phage display is the term used to describe the display of short, non-phage, peptide sequences on the phage coat proteins (which is reviewed in Clackson, 2004) and is one of the primary reasons for the use of the M13 bacteriophage in bionanotechnology. It was developed in 1985 when George Smith discovered that the pIII protein could tolerate insertions of small peptides, creating fusion proteins that were incorporated into the viral capsid without stopping infection of the *E.coli* host (Smith, 1985). A 171 bp DNA fragment of the gene that encodes for the endonuclease EcoRI was inserted into the BamHI site at position 2220 of the f1 bacteriophage. Therefore a 57 amino acid fragment of EcoRI was displayed at position 198 of the mature pIII coat protein, i.e. in the middle of the pIII coat protein. When the phage was purified and incubated with an anti-EcoRI antibody the phage became non-infective: the anti-body was binding to the EcoRI fragment and inhibiting pIII interaction with the *E.coli*. Wild-type phage were unaffected by the antibody and the effect could be reversed in a low pH buffer, after which the peptide-displaying phage become infective again, although at levels 100

# Chapter 1

---

times lower than wild-type. After this proof of principle experiment, other groups showed that small peptides could be displayed at position 1 of pIII (Parmley, 1988), position 2 of pVIII (Ilyichev, 1989) and on the three remaining coat proteins, pVI, pVII and pIX (Jespers, 1995; Kwasnikowski, 2005, Gao, 1997; Gao, 1999).

The following section will describe how phage display is carried out. It focuses primarily on pIII display at position 1; however, the principle is the same for the display of peptides on any of the other coat proteins.

To display a peptide on a specific coat protein, a DNA sequence that encodes for the desired peptide is inserted between the start of *gene III* (which corresponds to position 1 of the mature protein) and the signal sequence (Figure 1.6 B). The signal sequence ensures that the protein is transported to the *E.coli* membrane for incorporation into the virion before being cleaved off by the endogenous leader peptidase (Clackson, 2004). The insertion of the displayed peptide's DNA into *gIII* is carried out using the RF form of the phage genome. Once the modified phage genome is inserted into a suitable *E.coli* host, the RF DNA produces phage particles containing the pIII coat protein displaying the peptide. This is the simplest method of phage display and results in every copy of pIII displaying a peptide: termed, polyvalent display.

However, it is not always possible to have polyvalent display due to physical constraints. For example, pVIII cannot express peptides longer than 8 amino acids on every copy of pVIII (Petrenko, 1996; Malik, 1996), or a peptide expressed on pIII may interfere with infection (Smith, 1988). However, it is possible to overcome this

limitation by using a phagemid system (section 1.4.1), which allows peptides longer than 8 amino acids to be displayed (Clackson, 2004).

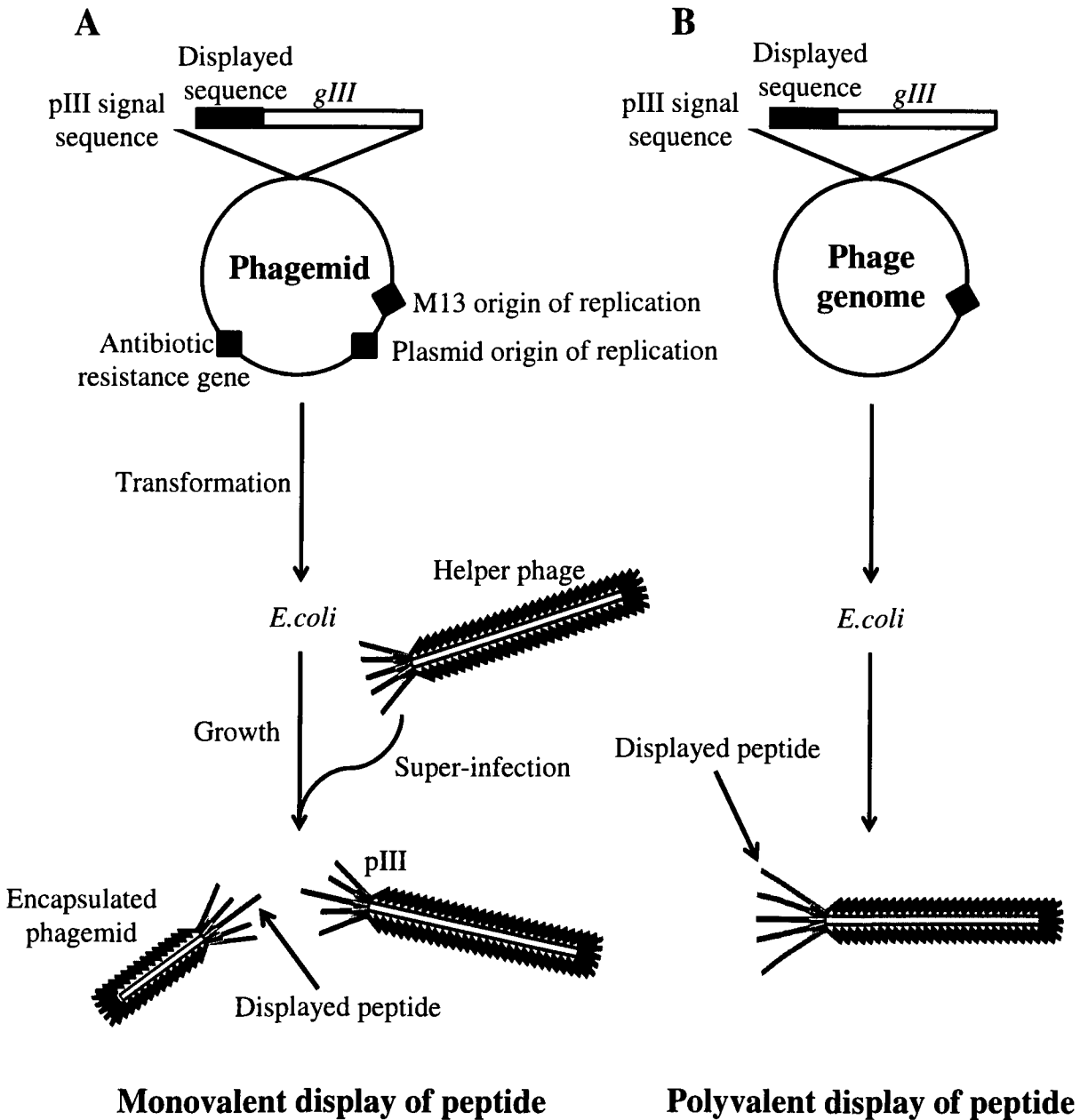


**Figure 1.6. Methods of phage display.** Two commonly used methods of phage display; insertion into the phagemid vector (A) or insertion into the phage itself (B).

Adapted from Clackson *et al.* (2004).

## 1.4.1 Phagemid phage display

A phagemid vector (Figure 1.6 A) is a bacterial plasmid that contains an altered phage coat protein gene, e.g. *gene III* with inserted DNA corresponding to a displayed peptide, a bacterial origin of replication and an M13 origin of replication. When inserted into *E.coli*, the phagemid behaves as a bacterial plasmid and is replicated and transferred to all daughter cells of the original *E.coli*. This means that the entire culture contains a copy of the phagemid. However, no phage particles are produced since only the altered *gIII* is present. A helper phage is needed in order to produce phage particles displaying the desired peptide. The helper phage is an M13 phage with a defective viral origin of replication so that the ssDNA of the phagemid is preferentially encapsulated (discussed further in Chapter 3).

The viral coat protein within the phagemid is typically under the control of the *lacZ* operon and therefore along with the helper phage, isopropyl  $\beta$ -D-1-thiogalactopyranoside (IPTG) is added to induce the production of the altered coat protein. Within the *E.coli*, thereafter, there is production of all the phage proteins (I-XI) from the helper phage along with the altered pIII coat protein from the phagemid, i.e. there are two populations of pIII coat protein: the wild-type pIII and the pIII displaying the peptide produced from the phagemid. The two populations “compete” to be encapsulated into phage capsids. Typically 10% or less of the phage particles in a phagemid preparation will contain a pIII protein displaying the peptide: termed monovalent display (Clackson, 2004).

## 1.4.2 Bio-panning

Peptides that have an affinity for a specific material are identified using the method of “bio-panning” and this is the same whether the genome or phagemid system is used (Clackson, 2004). By inserting sequences of degenerate codons, typically encoding 7 – 15 amino acids, into *gene III* it is possible to create random sequences of peptides that are displayed at position 1 of pIII. A single culture of *E.coli* is able to produce upwards of  $10^{11}$  phage particles (Noren, 2001) and therefore it is possible to create billions of phage particles, each with a different peptide sequence displayed on the surface (Figure 1.7); this is termed a “phage library” (Petrenko, 1996).

In order to identify a peptide that has a high affinity for an inorganic material, or in fact any material, the phage library is exposed *in vitro* to the immobilised target (Figure 1.7, 1). Any phage that display a peptide with an affinity for the target will then become attached. Washing with a pH neutral buffer containing a small amount of the non-ionic detergent Tween to stop phage-phage interactions removes all the other phage, leaving only the phage with an affinity for the target (Figure 1.7, 2). These phage are then eluted (Figure 1.7, 3), typically with an acidic wash, e.g. glycine-HCl pH 2.2, to break the phage interaction with the immobilised target. The eluted phage are then amplified by infecting host bacteria before being extracted and purified (Figure 1.7, 4 and 5). Subsequent rounds of bio-panning, normally 3 – 5 rounds, lead to the enrichment of a few bacteriophage displaying peptides with a high affinity for the target substrate. The DNA of these bacteriophage is then extracted and sequenced to identify the binding peptide (Figure 1.7, 6), which can then be used in other applications.

## Chapter 1

---

Although phage display and bio-panning are excellent techniques there are issues that make them non-ideal. As has been pointed out by Bassindale *et al.* (2007), there is the possibility of inherent bias in the selection of certain sequences. These biases manifest themselves as sequences that may be the “best” binders to the target, yet they inhibit the infection or production of that phage particle and so are selected against in the amplification step (Figure 1.7). Likewise during the elution step (Figure 1.7), the acidic buffer glycine-HCl, used to disrupt the peptide-target interactions, may have a greater effect on highly basic peptides meaning these are released more readily compared to acidic peptides. Naik *et al.* (2004) have devised a modification of the phage display method to remove the glycine-HCl step bias. Their method follows the standard bio-panning protocol (Steps 1 – 3 of Figure 1.7). However, they made the assumption that glycine-HCl would not remove all the bound phage from the target and that the tightest binders would still be associated. Therefore they treated the target with glycine-HCl and then washed away any unbound phage. They then heated the target, and any remaining bound phage, to 95°C for 10 minutes to break down the phage particles and release their ssDNA genome. They then used the released ssDNA as the template for PCR using primers specific to *gene III* to amplify the displayed peptide DNA sequence. They used this method to obtain unique peptide sequences specific to 10 nm cobalt nanoparticles that were not found using the traditional bio-panning procedure. However, they did not report whether these sequences had a higher affinity than those found with traditional bio-panning (Naik, 2004).

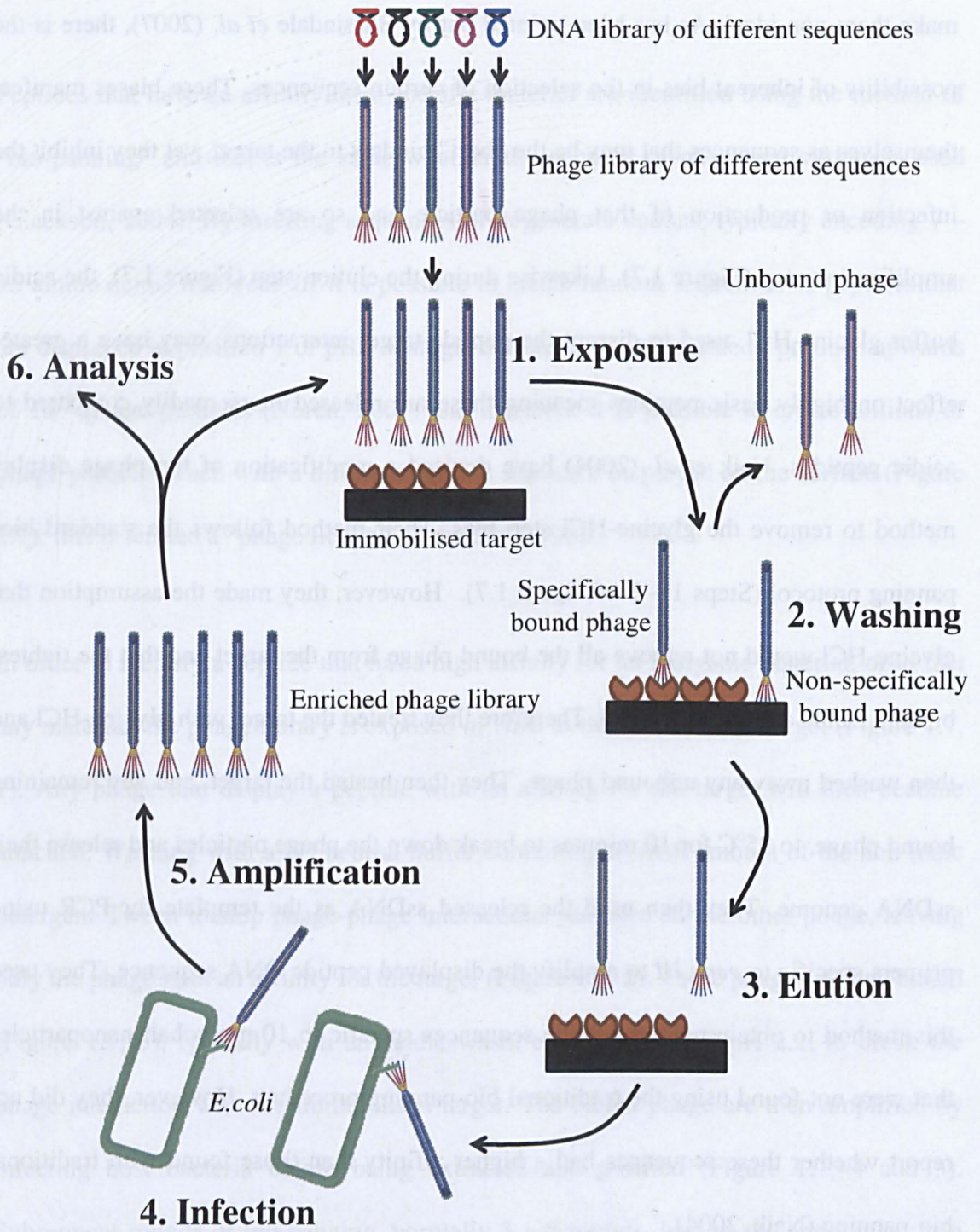


**Figure 1.7. Bio-panning.** Cartoon showing the principal aspects of M13 bacteriophage bio-panning using a pIII expressed library. Adapted from Willats, 2002.

## 1.4.3 Bio-panning and peptides specific to inorganic materials

The use of bio-panning has identified numerous inorganic binding peptides that may have a practical use in bionanotechnology (Table 1.2).

**Table 1.2. Peptides that show high affinity to inorganic materials.** A list highlighting some examples of materials where phage display has been used to find peptide sequences specific to that material.

	Peptide Sequence	Material it binds to	Size	Library	Reference
Noble Metals	VSGSSPDS	Gold (Au)	8	pIII	Huang, 2005
	CDRTSTWRC	Platinum (Pt)	9	pIII	Sarikaya, 2003
	CAYSSGAPMPFPC	Silver (Ag)	14	pIII	Naik, 2002
	CSVTQNKYC	Palladium (Pd)	9	pIII	Sarikaya, 2003
Semiconductors	AQNPSDNNTHTH	Gallium arsenide (GaAs)	12	pIII	Whaley, 2000
	CTYSRLHLC	Cadmium sulphide (CdS)	9	pIII	Flynn, 2003
	CNNPMHQNC	Zinc sulphide (ZnS)	9	pIII	Flynn, 2003
	HGHPYQHLLRVL	Carbon Nanotubes	12	pIII	Lee, 2009
Oxides	ATWVSPY	Titanium oxide (TiO <sub>2</sub> )	7	pIII	Liu, 2009
	EAHVMHKVAPRPGGGSC	Zinc oxide (ZnO)	17	pIII	Umetsu, 2005
	TVVQTYSMVTRA	Silicon oxide (SiO <sub>2</sub> )	12	pIII	Eteshola, 2005
Minerals	CHAALTMQC	Mica	9	pIII	Donatan, 2009
	CMLPHHGAC	Hydroxyapatite	9	pIII	Gungormus, 2008
	DVFSSFNKHMARG	Calcite (Calcium carbonate)	12	pIII	Gaskin, 2000
	HTQNMRYEPWFG	Argonite (Calcium carbonate)	12	pIII	Gaskin, 2000
Biocompatible substrates	MSPHPHRHHHT	Silica (SiO <sub>2</sub> )	12	pIII	Naik, 2002
	YPSAPPQWLNT	Titania (TiO <sub>2</sub> )	12	pIII	Fang, 2008
	THRTSTLDYFVI	Chlorine-doped polypyrrole (PPyCl)	12	pIII	Sanghvi, 2005

However, peptides have been identified that show not just specificity to a particular material but also specificity to the structure of that material. Whaley *et al.* (2000) panned for sequences that were specific to the different crystal faces of GaAs (gallium arsenide). A pIII library, displaying random 12-mer peptides, was used to select for sequences that were specific for GaAs(100). When the GaAs(100) specific phage were then incubated with GaAs(111), i.e. gallium arsenide with a different crystal lattice structure, the phage failed to interact with the surface.

A similar experiment was carried out using a pIII 7-mer library to find peptide sequences specific to surface defects within a sheet of germanium (Sinensky, 2006), e.g. the boundary between two germanium crystals, or large changes in surface morphology. Two rounds of bio-panning were carried out using a germanium film on a silicon surface (Ge-on-Si) as the target. Ge-on-Si is created from a vapour of germanium, in a vacuum, which forms a single crystal of germanium on the silicon substrate. However, this process leads to numerous defects in the germanium layer (Colace, 2000). The phage selected were therefore specific to defects and germanium alike. In order to select specificity for the defects, a round of negative selection was carried out, i.e. by bio-panning the selected phage against a germanium wafer. The wafer was created by cleaving a single germanium crystal, which produces far fewer defects. They identified two sequences (CSYHRMATC and CTSPHTRAC) which showed a 10:1 preference for Ge-on-Si over germanium wafers compared to wild-type M13 phage, i.e. the sequences were more specific to the defects of the germanium than to the germanium crystal itself. The two experiments described above highlight the versatility of phage display and bio-panning, and that specific peptide sequences can be identified that are specific to almost any material and the different forms that the material may have.

## **1.5 The M13 phage coat proteins and their uses in bionanotechnology**

### **1.5.1 The minor coat proteins pIII, pIX, pVI and pVII**

The viral gene *gIII* encodes a 406 amino acid long peptide (Hill, 1982), pIII. It is by far the largest viral coat protein. In contrast, pIX and pVII are 32 and 33 amino acids long, respectively, and are two of the smallest ribosomally translated proteins known

# Chapter 1

---

(Clackson, 2004). The remaining minor coat protein pVI is 112 amino acids long (Rakonjac, 1999). pIII differs from the other coat proteins since it has a large hydrophilic domain, whilst the other proteins are mostly hydrophobic (Beck, 1978). It is perhaps the most important coat protein since it is responsible for the recognition of the bacterial F-pilus and TolA receptor, both of which must be bound to by pIII for successful infection (Deng, 1999).

Work by the Strengle and Kremser laboratories using mutagenesis and protein analysis of pIII (Kremser, 1994; Strengle, 1990) have indicated that it is divided into three domains: N1, N2 and C-terminal (Figure 1.8 A), which are separated by glycine rich linker sequences. The N1 and N2 domains consist primarily of  $\beta$  strands with a single alpha helix in each domain (Lubowski, 1998). It is thought, from crystallographic studies of the first 217 residues (Figure 1.8 A), that N1 and N2 interact extensively (Lubowski, 1998), thus creating a 'horseshoe shape' (Figure 1.8 B). This conformation exposes the polar residues, Lys22, Asp24, Lys25 and Asp28, in the N1 domain, and threonine residues in the N2 domain. These exposed residues on the N1 and N2 domains interact, forming a central channel between the two domains (Figure 1.8 B) with the hydrophobic residues stabilising the structure (Lubowski, 1998). It has been suggested that this channel acts as the binding site for the F-pilus (Lubowski, 1998; Chatellier, 1999).

Whilst the N1 and N2 domains are required for infection, pIII deletion mutants containing only the C-terminal (CT) domain show that it plays an important structural role and is required for both pVI interaction and phage release from the cell (Rakonjac,

1999). Whereas the two N-terminal domains are exposed to solution, it is thought that the C-terminal is buried within the phage capsid (Rakonjac, 1999).

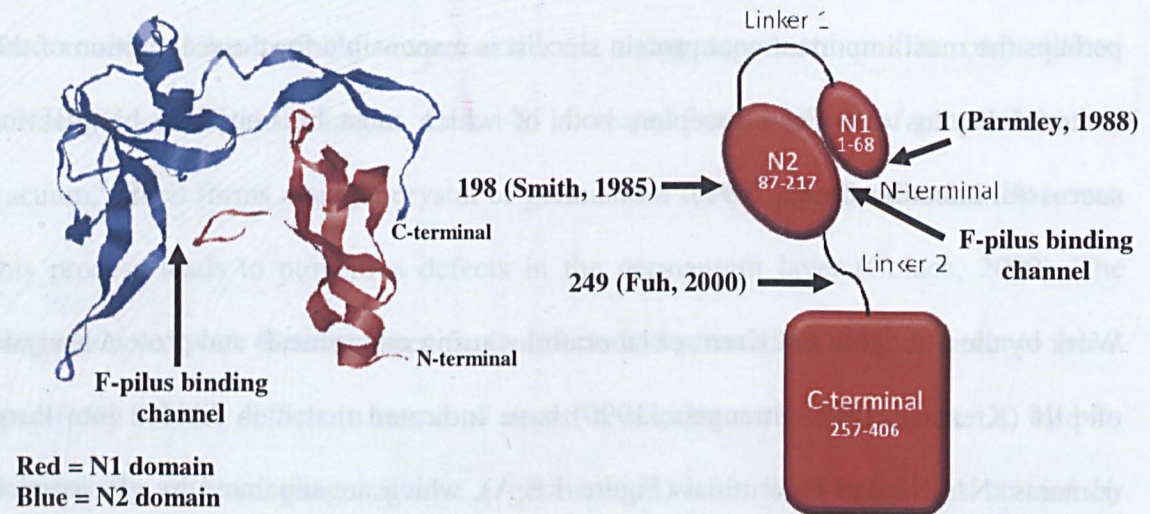


**Figure 1.8. The minor coat protein pIII.** A shows the crystal structure, at 1.46 Å, of the first 217 amino acids of the M13 coat protein pIII. PDB code: 1g3p (Lubowski, 1998). B shows a schematic of the three main domains of pIII (N1, N2 and C-terminal), linked by glyceric rich sequences, and their position within the protein sequence, e.g. N1: 1-68. The commonly used areas for peptide display, and sites of peptide insertion within the protein sequence, are highlighted by arrows, together with the reference of the first report to successfully phage display at these sites.

Little is known about the remaining minor coat proteins. The lack of structural and functional data about these coat proteins reflects their lack of biotechnology applications with 99% of phage display studies utilising pIII and pVIII. However, pIX is increasingly used to express small peptides (Gao, 1997) and has been used in M13 bionanotechnology (Nam, 2004; Khalil, 2007).

Two examples highlight how using minor coat protein phage display can result in potentially useful structures. Both used pIII and pIX peptide display within the same phage particle. Nam, *et al.* in 2004 used M13 to create a nano-ring, i.e. they engineered the M13 phage particle so that it joined end to end, creating a loop or ring-like structure (Figure 1.9).

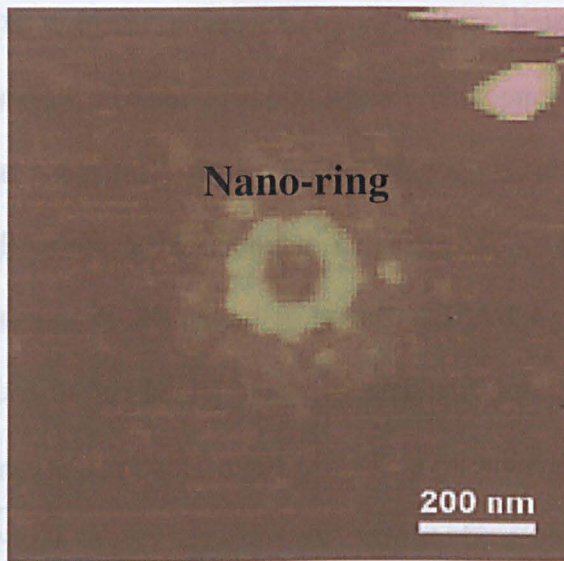


**Figure 1.9. A nano-ring created by the M13 bacteriophage.** An Atomic Force Microscopy (AFM) image of M13 bacteriophage joined end to end to create a loop structure called a nano-ring. Taken from Nam, 2004.

They created an M13 phage mutant that displayed an anti-streptavidin peptide on pIII and a hexahis tag (HHHHHH) on pIX: both at position 1 within the two coat proteins. By mixing this phage with a linker molecule consisting of streptavidin conjugated to a Ni(II)-nitrilotriacetic acid complex (Ni-NTA) it formed a nano-ring. The pIII peptide bound to the streptavidin whilst the hexahis tag on pIX bound tightly to the Ni-NTA complex (Figure 1.9). As expected, the formation of nano-rings was very inefficient unless the amounts of phage and linker molecule were at equal concentrations. At higher or lower concentrations of phage: linker molecule, then very few nano-rings

were observed. By adding imidazole (which competed with the hexahis tag binding to the Ni-NTA complex) it was possible to reverse this reaction and break up the rings. Therefore they essentially created a biological nano-switch where the nano-ring could be open or closed by adding or removing imidazole.

Sweeney, *et al.* created another hetero bi-functional phage that displayed pairs of leucine zippers. These are short, helical polypeptides which associate with their specific partner, e.g. the leucine zipper ACID has a high affinity to its leucine zipper partner BASE (O'Shea, 1993). They created a mutant M13 phage that displayed ACID at position 1 on pIII and BASE at position 1 on pIX. When these phage were mixed together they formed long filaments of phage joined end-to-end via the leucine zipper pairs, with some filaments up to 15  $\mu\text{m}$  long. However, there was no mechanism to control the length of these filaments.

Although the structures described above are relatively simple, they provide a proof of principle that the M13 bacteriophage minor coat proteins can be programmed using simple genetic manipulation to self-assemble into higher order structures.

## **1.5.2 The major coat protein pVIII**

The pVIII coat protein is 50 amino acids long (Clackson, 2004). Currently it is thought that pVIII exists as a continuous alpha helix between residues 10-46 (Vos, 2009) and can be split into four domains (Figure 1.10): an acidic domain located at the N-terminal end followed by regions that are largely amphipathic and hydrophobic and finally a basic region located at the C-terminal end (Papavoine, 1998). Some groups have argued

that the amphipathic domain and hydrophobic domains are connected by a flexible hinge-region (Papavoine, 1998); more recently this has been refined into a theory that pVIII has the ability to undergo helical deformations between residues 38-50, which allow the protein to a) have a simple tilt mechanism in order to fit into the membrane, and b) undergo efficient incorporation into the phage particle (Vos, 2009). The basic domain located at the C-terminus is known to interact with the ssDNA genome (Hunter, 1987; Rowitch, 1988). Substitutions of the positively charged lysines within the basic C-terminal region with negatively charged glutamate residues have shown that the positive charge of the lysines are needed to negate the negative charges of the DNA phosphate backbone (Hunter, 1987; Rowitch, 1988).

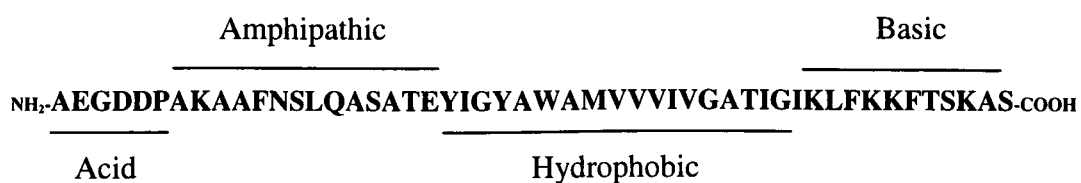


**Figure 1.10. Amino acid sequence of the pVIII coat protein.**

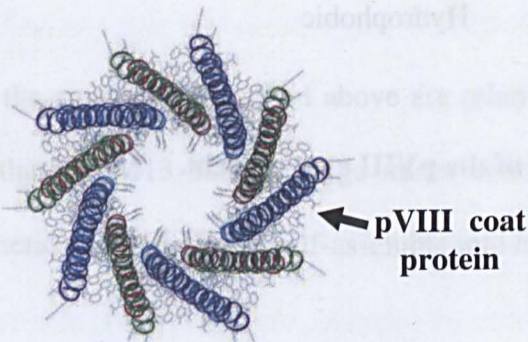
## 1.5.2.1 Virion structure

Within the assembled virion, the pVIII protein has a linear 'I' shape (Vos, 2009). The ~2800 copies of pVIII assemble into a helix around the circular ssDNA genome with 2.4 nucleotides per pVIII subunit (Clackson, 2004). The pVIII proteins have been found by Raman microspectroscopy to tilt away from the DNA by approximately 16° (Overman, 1996) and overlap one another, giving a so-called fish scale or roof tile appearance to the viral capsid. The overlapping structure of the pVIII coat proteins

results in the negatively charged N-terminal acid domain being exposed to the solvent and giving the phage particle an overall negative charge (Clackson, 2004). The coat proteins show a 5-fold (pentamer) rotation axis around the ssDNA with a 2-fold screw axis of 32 Å pitch; i.e. each pentamer is rotated 180° and translated by 16 Å (Figure 1.11) from the previous pentamer (Marvin, 1966). This creates a helical structure where each turn of the helix contains five pVIII proteins (Wen, 1997). It has, however, been suggested that M13, and related filamentous phage, show structural polymorphism (Wang, 2006) and that this is averaged out by the various techniques that have been utilised to study its structure.

**A**

View of an M13 phage particle along the helical axis



**B**

View of a section of the M13 phage particle from the side

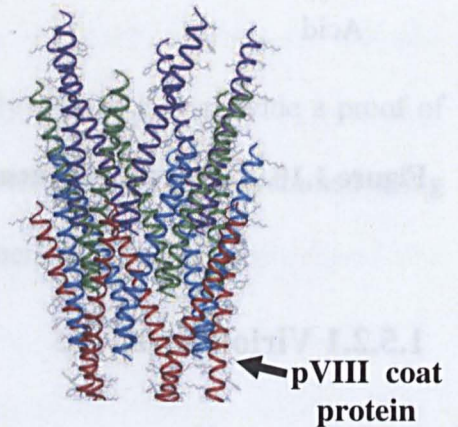


**Figure 1.11. Model of M13 filamentous bacteriophage capsid determined by NMR spectroscopy.** A and B show the arrangement of the pVIII coat proteins in the capsid along the helical axis of the M13 phage particle (A) and from the side (B). The various colours show different pVIII pentamer sets. Taken from Zeri, 2003.

## 1.5.2.2 pVIII phage display and bionanotechnology

Peptides are typically displayed on pVIII by replacing the EGD amino acids at positions, 2 to 4, with the desired sequence. However, it has been found that only relatively short peptides can be displayed on pVIII, typically 6 – 8 amino acids (Clackson, 2004). The exact reason for this is unknown but it is thought it may be that the displayed peptides may interfere with the passage of the phage particle through the viral pore as it passes out of the *E.coli* membrane (Clackson, 2004). Another reason may be that the displayed peptide may obstruct pVIII interactions with the minor coat proteins at the ends of the phage particle (V. Petrenko, personal communication). Whatever the mechanism, it limits the flexibility of display on pVIII. However this does not stop the display of peptides on pVIII from being used to produce nanoscale devices.

Using pVIII phage display has led to the fabrication of some of the simplest nanoscale devices: a conducting nanowire. The M13 bacteriophage is an excellent shape to act as a scaffold for deposition of materials to create nanowires, i.e. the phage particle is long and thin. By displaying small peptides on pVIII that nucleate a specific material Angela Belcher and her group have created gold (Huang 2005), cobalt: platinum (Lee 2009), cobalt oxide (Nam 2006), cadmium sulphide, and zinc sulphide nanowires (Flynn 2003). Huang, *et al.* in 2005 used a pVIII 8-mer phage display library to isolate a peptide sequence that had an affinity for a gold surface. It was found that the gold binding peptide (VSGSSPDS), which was displayed on all the copies of pVIII, also had an affinity for 5 nm gold nanoparticles. Mixing the mutant M13 phage with 5 nm gold nanoparticles resulted in the nanoparticles spontaneously ordering themselves along the length of the phage (Figure 1.12 A). Chloroauric acid ( $\text{HAuCl}_4$ ), as a source of gold

## Chapter 1

ions ( $\text{Au}^{3+}$ ), was then reduced with sodium borohydride in the presence of the decorated phage particles. The 5 nm gold nanoparticles acted as a nucleating site for the reduced gold and the nanoparticles increased in size until they merged to create a continuous nanowire (Figure 1.12 B). Importantly, the nucleation of these materials was done under ambient conditions. This is in contrast to more traditional techniques for the fabrication of nanowires which require harsh conditions, such as high temperature and organic solvents (Huang, 2005). The continuous gold coating on the mutant M13 phage particles was found to be conducting and showed a linear relationship between current and voltage, i.e. the gold coated mutant phage behaved like a gold nanowire. However, the gold coated mutant phage had an average resistance of  $\sim 600 \Omega$ , which is  $\sim 100$  times greater than that of bulk gold.

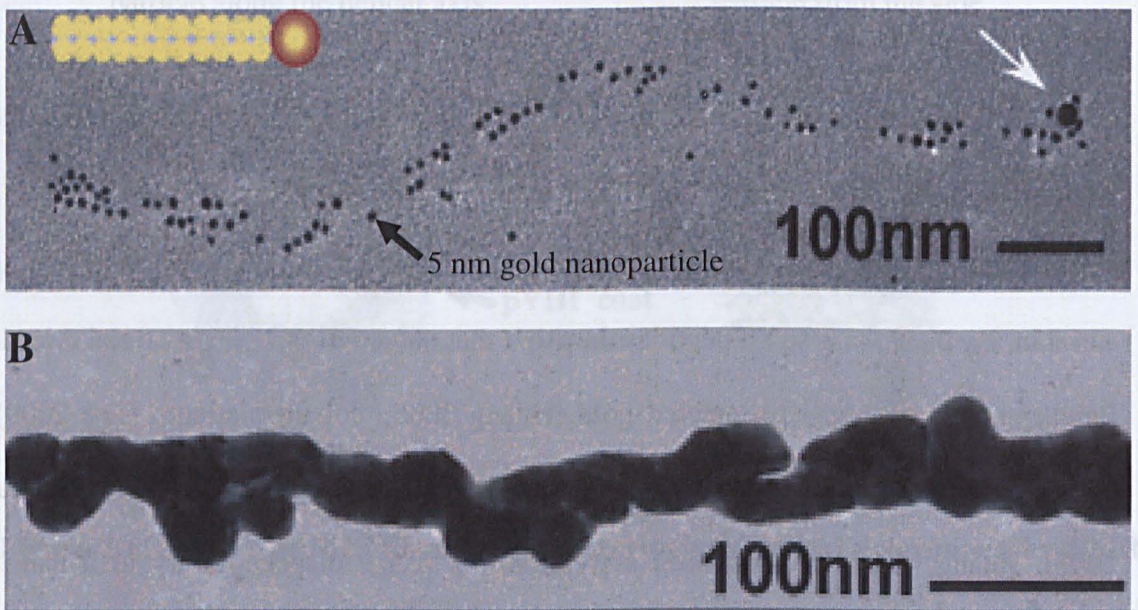


**Figure 1.12. M13 binding to gold nanoparticles.** M13 phage particles displaying a gold binding peptide bound to 5 nm gold nanoparticles (A) and after gold deposition (B). Taken from Huang, 2005.

### 1.5.2.3 Liquid crystal properties of the M13 bacteriophage

Perhaps the most interesting property of the M13 bacteriophage is that at high concentrations it shows liquid crystal properties (Welsh, 1996; Clackson, 2004). The liquid crystal phase is a stable phase between the solid crystal and isotropic liquid phases (Kumar, 2001); i.e. the M13 particles spontaneously self-assemble into ordered lattices. Liquid crystals can be broadly divided into two distinct groups; the first is thermotropic where the liquid crystalline properties vary with temperature; and lyotropic where the liquid crystalline properties vary with concentration. The M13 bacteriophage behaves as a lyotropic liquid crystal because of its rod-like structure (Welsh, 1996).

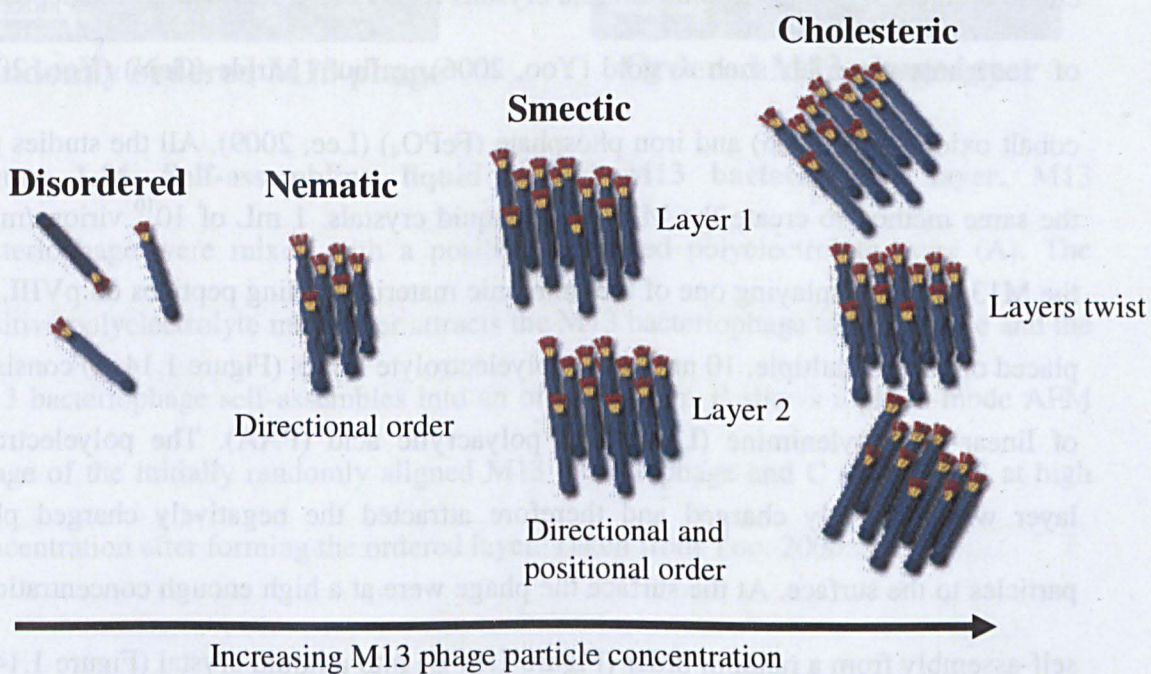


**Figure 1.13. The liquid crystal structures.** A schematic showing the different types of liquid crystal categories using the M13 bacteriophage.

The structure of the liquid crystal phase can be subdivided into three categories: nematic, smectic and cholesteric (Figure 1.13; Kumar, 2001). These refer to the level of

## Chapter 1

---

order found within the phase. Therefore with regard to M13, the more concentrated a solution gets, the phase order will shift first from nematic to smectic, and then at higher concentrations the order will shift to cholesteric. M13 particles found in the nematic phase will all point in the same direction; whereas those found in the smectic phase will point the same direction but will also be organised into layers, i.e. they have directional and positional ordering. Thus by controlling the concentration of M13 it is possible to control the level of order that the particles will self-assemble into and so create a higher ordered structure.

Various studies have used the liquid crystal properties of the M13 bacteriophage to create ordered M13 bacteriophage liquid crystals that act as a scaffold for the deposition of inorganic materials such as gold (Yoo, 2006), gallium nitride (GaN) (Yoo, 2006), cobalt oxide (Yoo, 2006) and iron phosphate ( $\text{FePO}_4$ ) (Lee, 2009). All the studies used the same method to create the M13 phage liquid crystals. 1 mL of  $10^{10}$  virions/mL of the M13 phage, displaying one of the inorganic material binding peptides on pVIII, was placed on top of multiple, 10 nm thick, polyelectrolyte layers (Figure 1.14 A) consisting of linear-polyethylenimine (LPEI) and polyacrylic acid (PAA). The polyelectrolyte layer was positively charged and therefore attracted the negatively charged phage particles to the surface. At the surface the phage were at a high enough concentration to self-assembly from a random order (Figure 1.14 B) into a liquid crystal (Figure 1.14 C). The packing density of the phage, i.e. the number of phage particles per  $\text{mm}^2$ , could be controlled by the pH of the phage solution, with very dense packing of the phage at pH 4.8 and very sparse packing when the pH was increased to pH 5.5. The displayed peptides on pVIII were still solvent accessible and were used to bind the specific inorganic materials and so coating the phage.

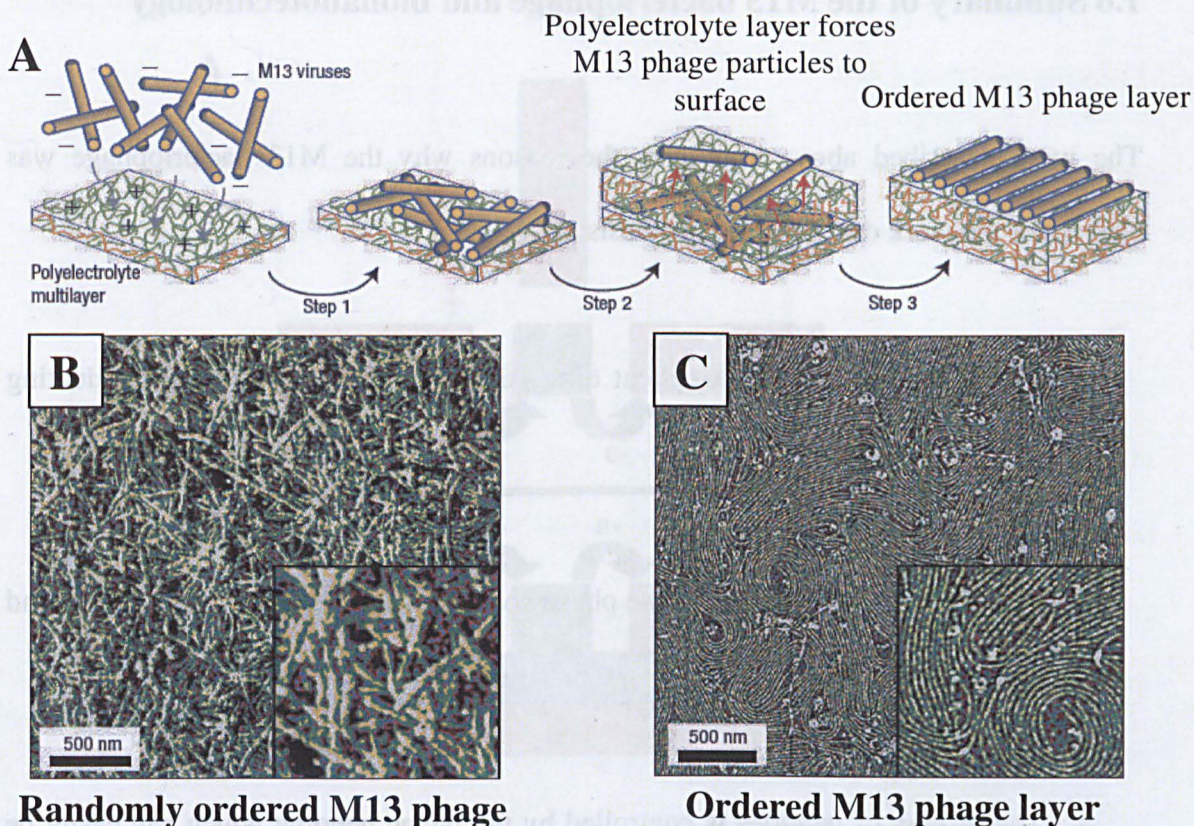


**Figure 1.14. Self-assembling liquid crystal M13 bacteriophage layer.** M13 bacteriophage were mixed with a positively charged polyelectrolyte layer (A). The positive polyelectrolyte multilayer attracts the M13 bacteriophage to the surface and the M13 bacteriophage self-assembles into an ordered layer. B shows a phase-mode AFM image of the initially randomly aligned M13 bacteriophage and C shows M13 at high concentration after forming the ordered layer. Taken from Yoo, 2006.

The M13 phage liquid crystals have been used to create a simple lithium ion battery (Lee, 2009). Two different M13 phage layers were created; one coated with cobalt oxide and the other coated with iron phosphate. These two layers were used as the anode and cathode of the battery, respectively. When used as part of a lithium ion battery they were shown to perform almost as well as existing macroscopic lithium ion batteries (Cahoon, 2009).

## 1.6 Summary of the M13 bacteriophage and bionanotechnology

The work described above highlights the reasons why the M13 bacteriophage was chosen for the work described in this thesis:

1. The phage particle has excellent dimensions for the fabrication of conducting nanowires.
2. Peptides can be displayed on the phage coat proteins in order to specifically bind inorganic materials.
3. The display of peptides is controlled by the phage genome which can easily be altered using simple molecular biology techniques.
4. The M13 bacteriophage can be programmed, via phage display, to self-assemble into high order structures which can be used as simple nano-scale devices.

## 1.7 Aims of the thesis and the molecular transistor

The aim of the work described within this thesis has been to use the properties of the M13 bacteriophage described above to create a self-assembling molecular transistor. The transistor is a ubiquitous device within all electronics. At its most basic the transistor is a switch with two states: On and off. The on and off states equate to the 1 and 0 of the binary language which is used for the various calculations that computer chips carry out (Kastner, 2000).

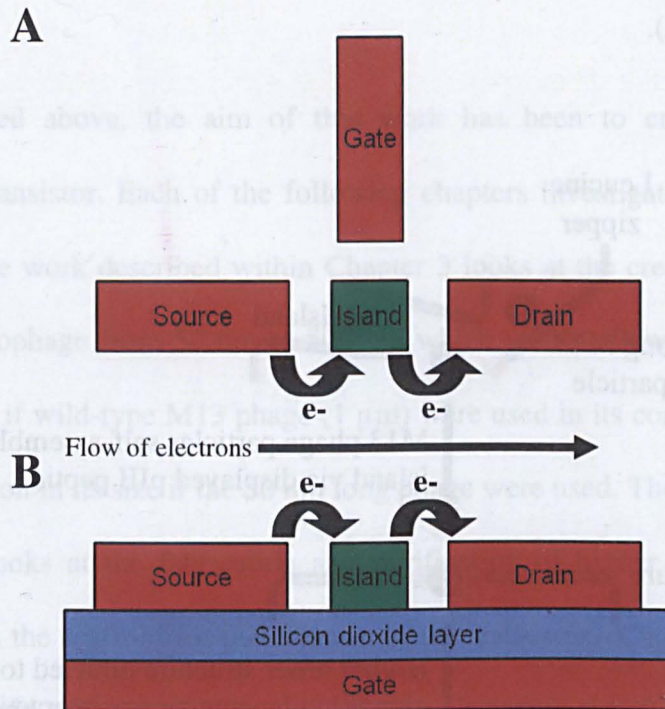


**Figure 1.15. The Molecular transistor.** A schematic showing the two basic layouts of a transistor. A shows the gate associated with the source and drain electrodes on the same plane. B shows the gate underneath the source and drain electrodes separated by a silicon dioxide layer.

A transistor consists of four main components (Figure 1.15); three metallic electrodes (source, drain and gate) surrounding a metallic or semi-conducting island. Electrons flow from the source electrode to the drain electrode via the island. A voltage applied across the gate electrode is used to control this flow of electrons. Altering the voltage applied across the gate changes the energy state of the island. Applying enough voltage changes the energy state to allow electrons to “hop” from the source to the island and then “hop” again from the island to the drain. The work described within this thesis focuses on genetically programming the M13 bacteriophage to self-assemble around a

# Chapter 1

nanoparticle island and then to act as a scaffold for the deposition of gold to create the electrodes (Figure 1.16).

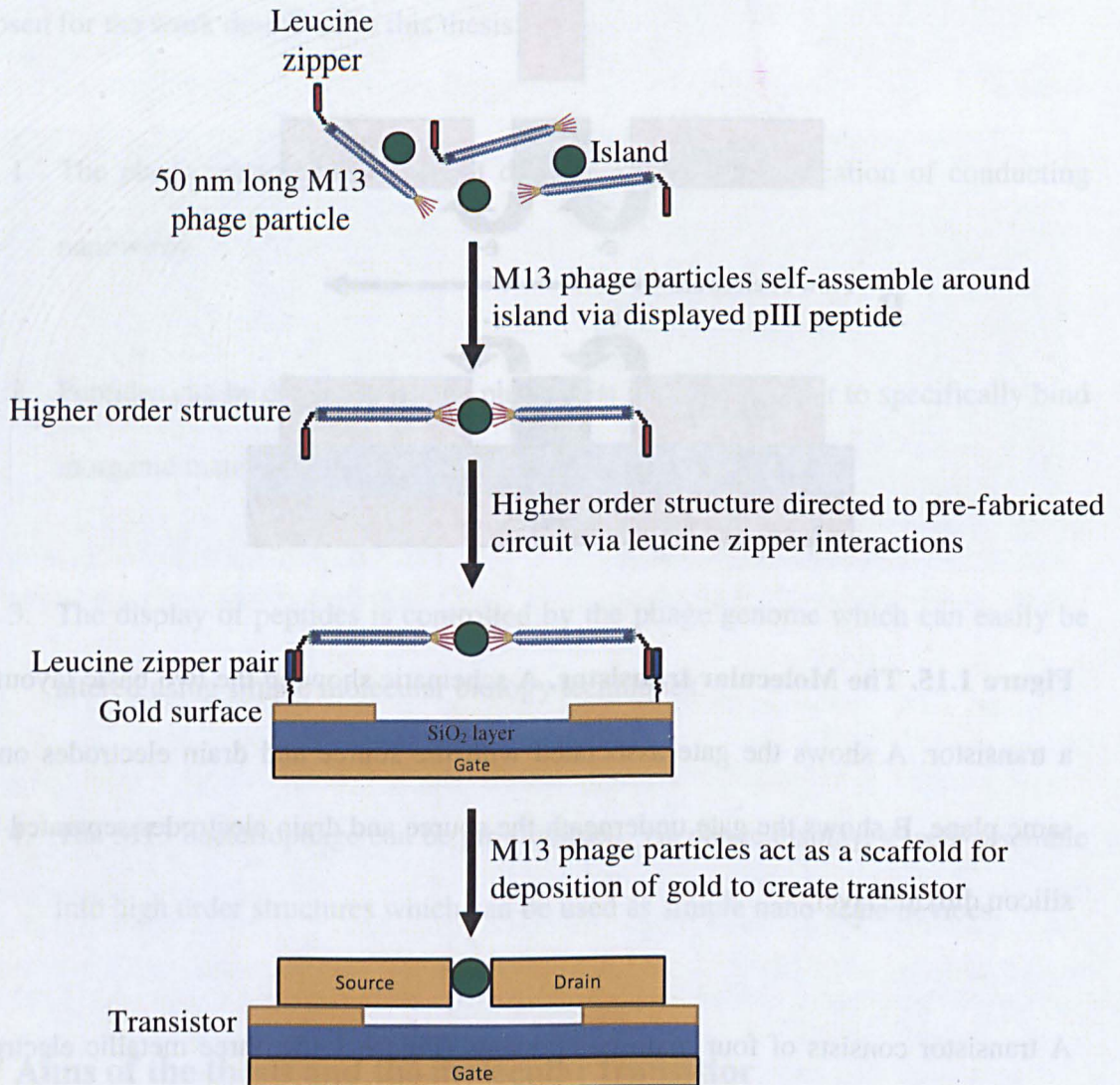


**Figure 1.16. Schematic of a possible fabrication protocol of a self-assembling molecular transistor.** A schematic showing the proposed steps involved in the creation of a self-assembling molecular transistor using M13 phage.

## 1.8 Scope of the work

As mentioned above, the aim of this work has been to create a self-assembling molecular transistor. Each of the following chapters investigates a different aspect of this aim: The work described within Chapter 3 looks at the creation of bespoke length M13 bacteriophage from 50 nm to 500 nm which would allow the transistor to be far smaller than if wild-type M13 phage (1  $\mu\text{m}$ ) were used in its construction; i.e. a 20 fold miniaturisation in its size if the 50 nm long phage were used. The work described within Chapter 4 looks at the fabrication and purification of higher order structures which would act as the scaffold for the creation of the transistor. Chapter 5 looks at how the transistor could self-assemble into an existing electronic circuit by using leucine zipper pairs to direct the higher order structures to specific locations on a surface. Finally work described within Chapter 6 looks at using the M13 bacteriophage as a scaffold to deposit gold onto the phage particles to create the electrodes of the transistor.

**This page is intentionally blank**

# Chapter 2

---

Materials and Methods

## 2.0 Materials

### 2.0.1 General Reagents

All chemicals were purchased from Sigma-Aldrich (St. Louis, MO, U.S.A.) unless otherwise stated. All primers were purchased from MWG-Biotech (Ebersberg, Germany) with High Purity Salt Free (HPSF) purification. DNA sequencing was carried out by The Sequencing Service at Dundee University, U. K. or GATC Biotech Ltd (Cambridge, U.K.). Restriction enzymes were purchased from New England Biolabs (Hitchin, U.K.).

### 2.0.2 Bacterial Strains

*E.coli* K12 ER2738 ([F' *proA*<sup>+</sup>*B*<sup>+</sup> *lacI*<sup>f</sup>  $\Delta$ (*lacZ*)M15 *zzf*::*Tn10*(Tet<sup>R</sup>)] *fhuA2 glnV*  $\Delta$ (*lac-proAB*) *thi-1*  $\Delta$ (*hsdS-mcrB*)5) was obtained from New England Biolabs, Cat. No. E4104S.

NEB 5-alpha F'I<sup>f</sup> Competent *E. coli* (High Efficiency) ([F' *proA*<sup>+</sup>*B*<sup>+</sup> *lacI*<sup>f</sup>  $\Delta$ (*lacZ*)M15 *zzf*::*Tn10* (Tet<sup>R</sup>)] *fhuA2* $\Delta$ (*argF-lacZ*)*UI169 phoA glnV44*  $\Phi$ 80 $\Delta$ (*lacZ*)M15 *gyrA96 recA1 endA1 thi-1 hsdR17*) was obtained from New England Biolabs, Cat. No. C2992H.

XL1-Blue supercompetent cells (*recA1 endA1 gyrA96 thi-1 hsdR17 supE44 relA1 lac* [F' *proAB lacIqZ* $\Delta$ M15 *Tn10* (Tetr)]) was obtained from Stratagene (La Jolla, California, U.S.A.) as part of the QuikChange® II mutagenesis kit (Cat. No. 200523).

XL1-Blue Competent cells (*recA1 endA1 gyrA96 thi-1 hsdR17 supE44 relA1 lac* [F' *proAB lacIqZΔM15 Tn10* (Tetr)]) were obtained from Stratagene (La Jolla, California, U.S.A.), Cat. No. 200249.

All of the above bacterial strains contain the common characteristic of F-pilus expression linked to tetracycline resistance. This results in a high expression of F-pili (needed for M13 infection) in the presence of tetracycline. In theory, any bacterial strain with this characteristic can be used to grow M13.

### **2.0.3 Antibiotic stock and working concentrations**

Carbenicillin disodium salt (Cat. No. C1389): 100 mg/mL in 70% (v/v) ethanol (1000x stock). Working concentration: 100 μg/mL. Mode of action: inhibits bacterial cell-wall synthesis (peptidoglycan cross-linking) by inactivating transpeptidases on the inner surface of the bacterial cell membrane. Carbenicillin was used instead of ampicillin due to its increased resistance to degradation from beta-lactamase enzymes.

Chloramphenicol (Cat. No. C0378): 34 mg/mL in 100% (v/v) ethanol (1000x stock). Working concentration: 34 μg/mL. Mode of Action: Inhibits translation on the 50S ribosomal subunit at the peptidyltransferase step (elongation inhibition).

Kanamycin B sulphate salt (Cat. No. B5264): 50 mg/mL in ddH<sub>2</sub>O (1000x stock). Working concentration: 50 μg/mL. Mode of Action: Binds to 70S ribosomal subunit; inhibits translocation and elicits miscoding.

Tetracycline hydrochloride (Cat. No. T7660): 10 mg/mL in 70% (v/v) ethanol (1000x stock). Working concentration: 10 µg/mL. Mode of Action: Inhibits protein synthesis (elongation) by preventing binding of aminoacyl-tRNA to the 30S subunit.

All antibiotics were 0.22 µm filtered and stored at -20°C. All stocks were made at 1000x concentration; therefore 1 µL of antibiotic was added per 1 mL of medium.

### **2.0.4 Media recipes**

#### **2.0.4.1 2xYT medium**

Per litre.

To 900 mL of ddH<sub>2</sub>O added:

- 16 g tryptone
- 10 g yeast extract
- 5 g NaCl

Mixed until powder had dissolved, adjusted to pH 7 with 5 N NaOH and adjusted the volume to 1 L with ddH<sub>2</sub>O. The medium was then autoclaved.

#### **2.0.4.2 Super broth (SB) medium**

Per litre.

To 900 mL of ddH<sub>2</sub>O added:

- 32 g typtone
- 20 g yeast extract

- 5 g NaCl

Mixed until powder had dissolved, adjusted to pH 7.4 with 5 N NaOH and adjusted the volume to 1 L with ddH<sub>2</sub>O. The medium was then autoclaved.

### 2.0.4.3 Agarose top

Per litre.

To 900 mL of ddH<sub>2</sub>O added:

- 10 g tryptone
- 5 g yeast extract
- 5 g NaCl
- 1 g MgCl<sub>2</sub>•H<sub>2</sub>O (magnesium chloride hexahydrate)
- 7 g Agarose

Mixed until powder had dissolved, adjusted to pH 7.4 with 5 N NaOH and adjusted the volume to 1 L with ddH<sub>2</sub>O. The agarose top was then dispensed into 50 mL aliquots in 80 mL bottles and autoclaved.

### 2.0.4.4 Agar

Per litre.

To 900 mL of ddH<sub>2</sub>O added:

- 16 g tryptone
- 10 g yeast extract
- 5 g NaCl
- 15 g agar

Mixed until powder had dissolved, adjusted to pH 7.4 with 5 N NaOH and adjusted the volume to 1 L with ddH<sub>2</sub>O before autoclaving. Agar was allowed to cool to ~ 50°C before antibiotics were added.

### **2.0.5 Buffers and other reagents**

#### **2.0.5.1 Phosphate buffered saline (PBS) pH 7.4**

PBS was made using phosphate buffered saline (Dulbecco A) tablets (Oxoid, part of Thermo Fisher Scientific, Cat. No. BR0014G). One tablet was used per 100 mL of dd H<sub>2</sub>O; so for 1 L 10 tablets were used. Typical formula in 1 L ddH<sub>2</sub>O:

- 8 g NaCl
- 0.2 g Potassium chloride
- 1.15 g Di-sodium hydrogen phosphate
- 0.2 g Potassium dihydrogen phosphate

Tablets produced a PBS solution of pH 7.4. After dissolving the tablets into the ddH<sub>2</sub>O, the solution was autoclaved (or when needed, sterilised with a 0.22 µm filter)

#### **2.0.5.2 20% Polyethylene glycol (PEG) and 2.5 M NaCl solution (PEG/NaCl)**

Per litre:

- 200 g PEG (Sigma-Aldrich, Cat. No. P5413)

- 146.1 g NaCl

The solution was autoclaved and then allowed to cool. As PEG cools it splits into two layers. Therefore it is important to keep mixing the PEG every 10 minutes or so which will create a white cloudy solution. Eventually it cools to a point where the solution suddenly becomes clear upon mixing. Occasionally after PEG has been left overnight it develops a very slight cloudiness; this does not affect its performance.

### **2.0.5.3 2x Protein loading buffer (LaemmLi buffer; LaemmLi, 1970)**

To make 5 mL:

- 0.625  $\mu$ L 1 M Tris-HCl, pH 6.8 (0.125 M)
- 2 mL 10% SDS (4%)
- 1 mL Glycerol (20%)
- 0.5 mL 2-mercaptoethanol (10%)
- 1 mg (approx.) Bromophenol blue (approx. 0.004%)
- 0.875 mL ddH<sub>2</sub>O (to 5 mL)

Stored at 4 °C.

### **2.0.5.4 10x $\lambda$ buffer for linear sucrose gradients**

Per litre:

- 24.5 g HEPES (4-(2-hydroxyethyl)-1-piperazineethanesulfonic acid)
- 58.44 g NaCl

Mixed until powder had dissolved and adjusted the volume to 1 L with ddH<sub>2</sub>O before filtering with a 0.22  $\mu$ m filter.

## Chapter 2

---

To use for linear sucrose gradients: 25 mL of 10x  $\lambda$  buffer was added to 1 mL of 0.25 M EDTA (ethylenediaminetetraacetic acid) and made up to 250 mL with ddH<sub>2</sub>O. Within 1x  $\lambda$  buffer the final concentrations were as follows: 100 mM HEPES, 1 M NaCl, 1.25 mM EDTA.

### 2.0.5.5 10x Glycine running buffer

Per litre:

- 10 g Sodium lauryl sulfate (SDS)
- 30.3 g Tris-base
- 144.1 g glycine

Adjust volume to 1 L with ddH<sub>2</sub>O and store at room temperature. Add 100 mL 10x glycine buffer to 900 mL ddH<sub>2</sub>O to create 1x glycine running buffer.

### 2.0.5.6 Coomassie blue staining solution

Per litre:

- 2.5 g Coomassie brilliant blue R-250 (Cat. No. B8647)
- 450 mL methanol
- 100 mL acetic acid

Adjust volume to 1 L with ddH<sub>2</sub>O and store at room temperature.

### 2.0.5.7 De-stain solution

Per litre:

- 450 mL methanol
- 100 mL acetic acid

Adjust volume to 1 L with ddH<sub>2</sub>O and store at room temperature.

### 2.0.5.8 Tris-HCl buffer

Per litre:

- 20 mL Trizma-HCl (Cat. No. T3253)
- 29.22 g NaCl

Adjust volume to 1 L with ddH<sub>2</sub>O and 0.22 µm filter sterilised. Store at room temperature.

### 2.1 General methods

#### 2.1.1 Growth of overnight *E.coli* culture

A single colony of *E.coli* was picked and placed into 50 mL red-topped Falcon tube containing 10 mL of 2xYT medium and tetracycline. Culture was grown at 37°C with shaking at 220 rpm overnight.

#### 2.1.2 Preparation of chemically competent *E.coli* cells

1 mL of an overnight culture of *E.coli* was added to 10 mL of 2xYT media containing tetracycline and grown for ~1 hour at 37°C with shaking at 220 rpm to an optical density at 600 nm (OD<sub>600</sub>) of ~0.5. The cells were spun down in a Sorvall RC-5B refrigerated super-speed centrifuge at 1500 rpm (200 x g) for 10 minutes at 4°C. The supernatant was removed and the cells placed on ice. The cell pellet were re-suspended with 1/5<sup>th</sup> volume (2 mL) of ice cold 50 mM CaCl<sub>2</sub> and left on ice for 20 minutes and were spun down again at 1500 rpm for 10 minutes at 4°C. The supernatant was removed and the cells re-suspended with 1/10<sup>th</sup> volume (1 mL) of ice cold 50 mM CaCl<sub>2</sub> and left on ice for 1 hour. The cells were used directly for transformation.

#### 2.1.3 Transformation using chemically competent *E.coli* cells

Competent *E.coli* cells (prepared in section 2.1.2) were dispensed into aliquots of 200 µL in 1.5 mL Eppendorf tubes that had been pre-cooled on ice for 10 minutes. Up to

100 ng of DNA (either phage RF DNA or plasmid DNA) was added to the cells, mixed gently by flicking the tube, and then incubated on ice for 40 minutes. Cells were heat shocked in a water bath at 42°C for 90 seconds and returned to ice and incubated for a further 2 minutes. 0.8 mL of 2xYT broth was added to each aliquot of cells and incubated at 37°C with shaking at 220 rpm for 1 hour in order for the cells to regain normal membrane permeability. 10 µL, 100 µL and 890 µL were plated out onto three 2xYT agar plates containing tetracycline and, if required, other antibiotics (depending on plasmid DNA). When using plasmid DNA the solution was pipetted onto the surface of the agar plate and spread evenly across the surface with a glass spreader.

When transforming phage RF DNA, the transformed cells were added to 3 mL of molten agarose top (stored in 5 mL tubes in a water bath at a temperature of 47°C) and 200 µl of an overnight *E.coli* culture (section 2.1.1). The solution was mixed by inversion and then quickly poured onto a 2xYT agar plate containing tetracycline and swirled to ensure complete and even coverage of the agar by the molten agarose top. The agarose top was allowed to set for 10 minutes at room temperature before being incubated overnight at 37°C. When transforming phage RF DNA a negative control was used that contained no DNA in order to check for phage cross-contamination. If plaques were present on negative control then other plates were discarded and the transformation repeated.

### 2.1.4 Preparation of bacterial stocks for freezing

900  $\mu\text{L}$  of overnight *E.coli* culture (section 2.1.1) was mixed with 100  $\mu\text{L}$  of 80% 0.22  $\mu\text{m}$  filtered glycerol (8% final concentration) in a 1.5 mL Eppendorf tube and stored in a  $-80^{\circ}\text{C}$  freezer.

### 2.1.5 Preparation of phage stock

#### 2.1.5.1 Growth of phage and PEG precipitation

A single plaque was picked from an agar plate and used to inoculate 1 mL of 2xYT medium (in a 50 mL Falcon tube) containing tetracycline and 10  $\mu\text{l}$  of an overnight *E.coli* ER2738 culture (section 2.1.1); giving a 1 in 100 dilution of the *E.coli*. This culture was incubated at  $37^{\circ}\text{C}$ , with shaking at 220 rpm, for  $\sim 4.5$  hours. The culture was transferred to a 1.5 mL Eppendorf tube and spun at 10000 rpm (9167 x g) at  $4^{\circ}\text{C}$  using a table top microcentrifuge (1-15K, Sigma, Osterode am Harz, Germany) for 10 minutes to pellet the cells. The supernatant (containing the phage particles) was removed to a clean 1.5 mL Eppendorf tube and the pellet discarded. 400  $\mu\text{L}$  of the supernatant was added to 100 mL of 2xYT (in a 500 mL conical flask) containing tetracycline and 1 mL of overnight *E.coli* ER2738 culture. The culture was incubated at  $37^{\circ}\text{C}$  with shaking at 220 rpm for  $\sim 4.5$  hours. The culture was transferred to a 250 mL centrifugation tube (Nalgene, Rochester NY USA, Cat. No. 3120-0250) and spun at 10000 rpm (8000 x g) using a JA-14 rotor (Beckman Coulter, Part No. 339247) in a Sorvall RC-5B refrigerated super-speed centrifuge (Thermo Fisher Scientific Inc, Waltham MA USA)

for 10 minutes to pellet the cells. The supernatant was transferred to a fresh 250 mL tube and the pellet discarded.

1/6<sup>th</sup> volume of PEG/NaCl (20% PEG/2.5 M NaCl) was added to the supernatant in order to precipitate the phage particles and left overnight at 4°C. The supernatant was spun down at 10,000 rpm (6500 x g) for 10 minutes at 4°C to pellet the phage. The supernatant was removed and discarded and the pellet re-suspended in 1 mL of PBS buffer (pH 7.4) and transferred to a 1.5 mL Eppendorf tube. 1/6<sup>th</sup> volume of PEG/NaCl was added and the solution left overnight at 4°C. The solution was spun down at 10,000 rpm for 10 minutes as before and the supernatant removed. The pellet was re-suspended in 1 mL of PBS buffer (pH 7.4) and the solution spun down at 10,000 rpm (9200 x g) for 10 minutes at 4°C in a table top microcentrifuge (GenFuge 24D, Progen Scientific London UK, Cat. No. C-2400) to remove any in-soluble matter. The supernatant (containing the purified phage) was transferred to a clean 1.5 mL Eppendorf tube and stored at 4°C. Concentration of the phage stock was found via titring or spectrophotometry.

### **2.1.5.2 Caesium chloride purification**

This method was developed by Prof. George Smith at the University of Missouri. 4.83 g of 98% pure CsCl (Cat. No. C4036-250G) was weighed out into a 50 mL glass beaker (zero the balance using the glass beaker). The balance was then zeroed again with the glass beaker containing the CsCl. The PEG purified phage was added to the beaker and ddH<sub>2</sub>O added to make the final weight 10.75 g. The mixture was swirled gently until the caesium chloride had dissolved and poured into a 12 mL (14 x 95 mm) open-top

## Chapter 2

---

polyclear tubes (Seton scientific, Los Gatos CA USA, Cat. No. 7031). Seton tubes must be used since they are the only ones that work with the gradient fractionator (Biocomp instruments, Fredericton NB Canada, Cat. No. 152-002). The tube (along with another balanced tube) was then loaded onto a SW 32 Ti open bucket rotor (Beckman Coulter, Brea CA USA, Part No. 369650) and spun at 30,000 rpm for 48 hours using an Optima L-80 XP (Beckman Coulter, Part No. 392051). The phage were fractionated using a gradient fractionator as in section 2.1.5.4; the phage appear as a milky band roughly a quarter way down the tube.

### 2.1.5.3 Linear sucrose gradients

A stock of 2 M (68.4%) ultrapure sucrose (USB corporation Cleveland OH USA, Cat. No. 21938) was prepared in 1x  $\lambda$  buffer by weighing out 171 g of sucrose and making the solution up to 250 mL with 1x  $\lambda$  buffer. The buffer was chosen as it was part of an established protocol. The sucrose solution was mixed with a magnetic stirrer overnight at 4°C to dissolve the sucrose. 2 M sucrose can be stored for long periods at 4°C; however, when diluted, i.e. down to 60%, solutions should be used on the same day.

Linear sucrose gradients were created using a gradient station (Biocomp, Cat. No. 153-002), the same machine as used for fractionation in section 2.1.4.4 (Figure 2.2), and open-top polyclear tubes (Seton scientific). To create a gradient, two solutions were made using the 2 M sucrose stock and  $\lambda$  buffer; i.e. for a 30 – 60% gradient then 30% and 60% solutions were made (for six 12 mL seton tubes then 50 mL of each solution is enough). The gradient station comes with a marker block (Figure 2.1 A) which was

used to mark the 12 mL seton tubes (the higher mark, which is for rate zonal gradients, was used) using a permanent pen.

The lower concentration of sucrose (i.e. 30%) was then poured into the tubes until the meniscus was just above the pen line. A 20 mL disposable syringe was then filled with the higher concentration of sucrose (i.e. 60%); this must be refilled for each tube. A long metal needle was then attached to the syringe and pushed to the bottom of the tube. The higher concentration of sucrose was slowly pushed into the tube so that it displaced the lower concentration of sucrose up to the marked line. Therefore within the 12 mL tube the higher concentration (i.e. 60%) was below the lower concentration (i.e. 30%) sucrose. The tubes were then capped with the rate zonal caps supplied by Biocomp (Figure 2.1 B) and left at 4°C for 30 minutes to allow the sucrose to settle.

The Biocomp gradient station comes pre-programmed with a selection of sequences for different tubes and sucrose concentrations to create a linear sucrose gradient. The correct sequence was selected and the tubes placed into the supplied Magnabase (Figure 2.1 C). This was then placed onto the magnetic base on the gradient station (Figure 2.2 A), which had been levelled. The sequence was then started to create the linear sucrose gradient. The tubes were then stored for 1 hour at 4°C to allow the sucrose to settle.

The caps were carefully removed from the tubes and an equivalent volume of sucrose to the PEG purified phage sample taken from the top of gradient. The PEG purified phage were loaded onto the top of the gradient with care taken to avoid disturbing the gradient. The tubes were balanced with ddH<sub>2</sub>O and loaded onto a SW 32 Ti open bucket rotor (Beckman Coulter, Brea CA USA, Part No. 369650). The phage were spun at 18,500

## Chapter 2

rpm overnight (typically 17 hours) using an Optima L-80 XP (Beckman Coulter, Part No. 392051). The phage were fractionated using a gradient fractionator (Biocomp instruments, Fredericton NB Canada, Cat. No. 152-002) as in section 2.1.5.4.

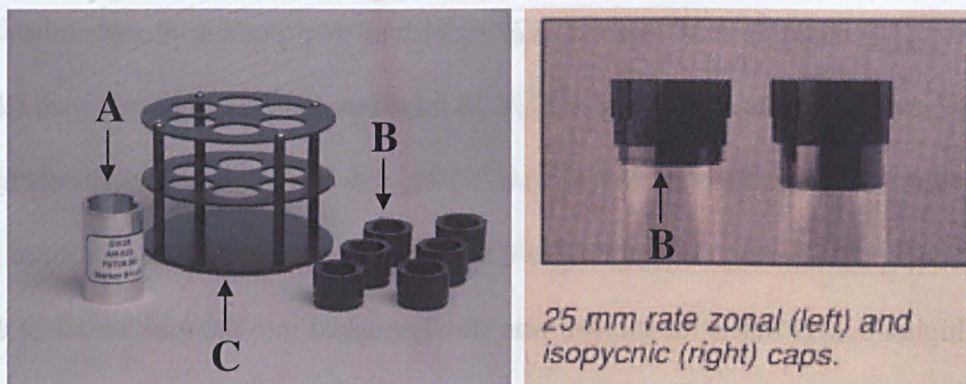


**Figure 2.1. Materials supplied with Biocomp gradient station.** These were used to create linear sucrose gradients. A) Marker block, B) Rate zonal cap, C) Magnabase. Taken from Biocomp gradient station manual.

### 2.1.5.4 Fractionation

All phage, after ultracentrifugation using open-top polyclear tubes (Seton scientific), were fractionated using a gradient fractionator (Biocomp instruments – Figure 2.2). Samples were fractionated continuously at a speed of 0.3 mm/second whilst measuring the absorbance at 260 nm. The gradient fractionator utilises a specialized trumpet (Figure 2.2 D) that is attached to a piston (Figure 2.2 E). The centrifuge tube is aligned under the trumpet using the supplied tube holder (Figure 2.2 C). The piston then pushes the trumpet down into the tube. The trumpet forms an air-tight seal within the tube so that the liquid in the tube is forced up though the trumpet and into the connected tubing (Figure 2.3). Biocomp state that the trumpet provides better sample resolution compared to needle fractionation. The liquid then passes through a UV detector (Pharmacia UV-M

II, GE Healthcare, Cat. No. 18-1001-10) which measures the absorbance at 260 nm. The UV detector was connected to a DI-158U USB data acquisition device (DataQ instruments, Akron OH USA) which was in turn connected to a PC which records the absorbance using the WinDaq®/Lite waveform browser (DataQ instruments) Finally the liquid passes out of the tubing where it can be collected.

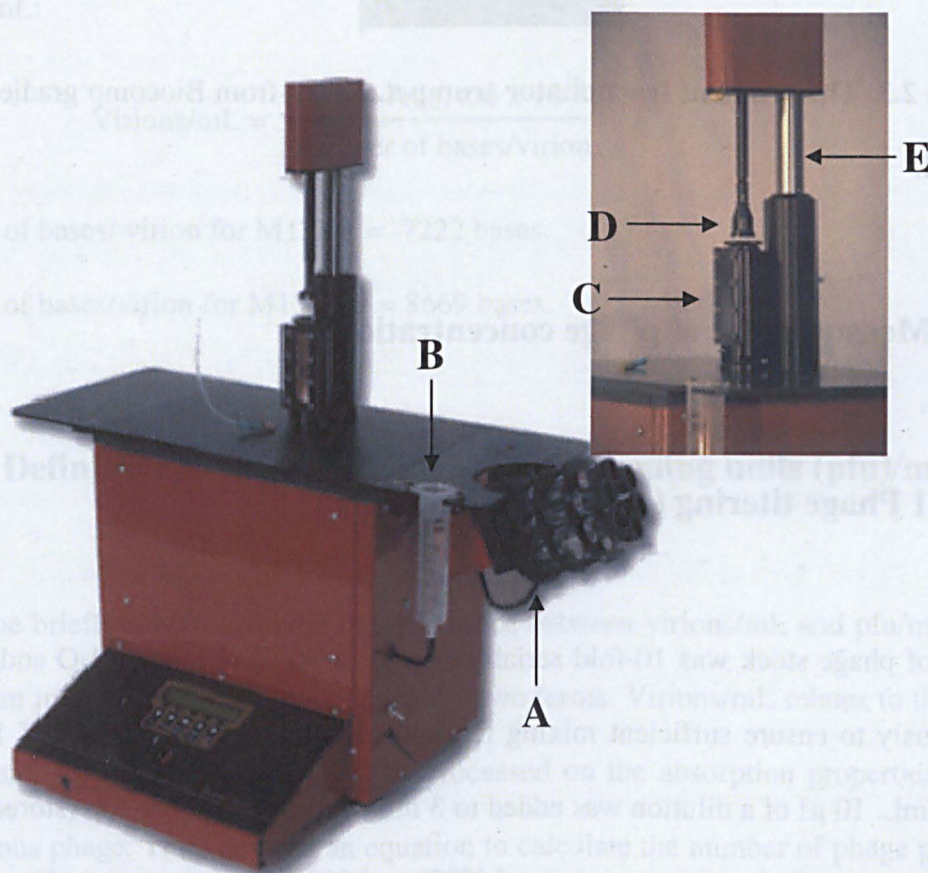


**Figure 2.2. The Biocomp gradient station and fractionator.** A) shows the magnetic base which is used to form the gradients. B) is the syringe used for washing the system. C) is the tube holder. D) shows the trumpet and E) shows the piston. Taken from Biocomp gradient station manual.

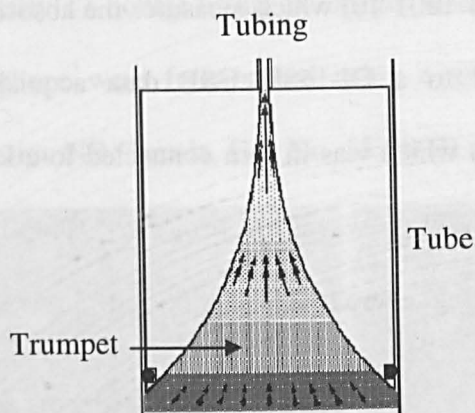


**Figure 2.3. The gradient fractionator trumpet.** Taken from Biocomp gradient station manual.

### 2.1.6 Measurement of phage concentration

#### 2.1.6.1 Phage titering (measured in pfu/mL)

10  $\mu$ l of phage stock was 10-fold serially diluted in 90  $\mu$ l of sterile H<sub>2</sub>O and vortexed vigorously to ensure sufficient mixing to yield estimated concentrations of  $10^6$  -  $10^{10}$  phage/mL. 10  $\mu$ l of a dilution was added to 3 mL of molten agarose top (stored in 5 mL tubes in a water bath at a temperature of 47°C) and 200  $\mu$ l of an overnight *E.coli* culture. The solution was mixed by inversion and quickly poured onto 2xYT agar plates containing tetracycline and swirled to ensure complete and even coverage of the agar by the molten agarose top. The agarose top was allowed to set for 10 minutes at room temperature before being incubated overnight at 37°C. Plates that had plaque numbers greater than 100 were used and the number of plaques counted. This number was then multiplied by the dilution factor to find the plaque forming units (pfu) in 10  $\mu$ l of the stock solution. The pfu was then multiplied by 100 to provide pfu/mL.

### 2.1.6.2 Spectrophotometry of phage particles (measured in virions/mL)

Absorbance of phage stock (2  $\mu$ L) at 269 nm and 320 nm was measured using a Nanodrop 3300 spectrophotometer (Nanodrop products, Wilmington, Delaware, U.S.A.). Absorbance values were used in the equation below to calculate the number of virions/mL:

$$\text{Virions/mL} = \frac{(A_{269} - A_{320}) \times 6 \times 10^{16}}{\text{Number of bases/virion}}$$

Number of bases/ virion for M13KE = 7222 bases.

Number of bases/virion for M13KO7 = 8669 bases.

### 2.1.6.3 Definition of virions/mL and plaque forming units (pfu)/mL

It must be briefly mentioned here the difference between virions/mL and pfu/mL since there is an important distinction between the two terms. Virions/mL relates to the work of Day and Wiseman, 1978. Their work focussed on the absorption properties of the filamentous phage. They devised an equation to calculate the number of phage particles in a solution from the absorbance at 269 nm and 320 nm:

$$\text{Virions/mL} = \frac{(A_{269} - A_{320}) \times 6 \times 10^{16}}{\text{Number of bases/virion}}$$

The 269 nm value comes from the maxima of the broad peak seen in the absorption spectrum between 260 and 280 nm (highlighted by the arrow in Figure 2.4). The broad peak arises from the fact that the filamentous phage has 6 times more protein than DNA (Day, 1978). The 320 nm value is used to correct for phage particle light scattering and other contaminants.

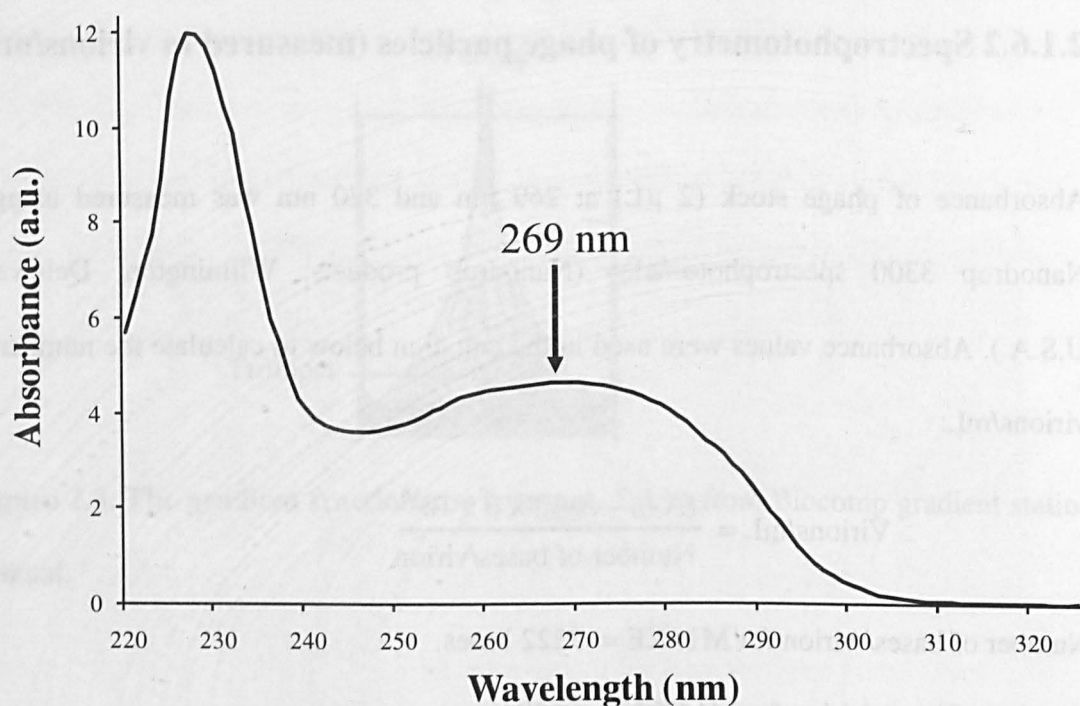


**Figure 2.4. Typical absorption spectrum of a purified (PEG/NaCl) M13 particle.**

The other standard measurement of phage is plaque forming units (pfu). This is a direct measurement of how many infective particles are contained within a solution. Therefore although virions/mL is a measure of all virus particles in a solution it does not differentiate between infective and un-infective particles; importantly, with respect to M13, this is likely to reflect whether the pIII protein is intact or not. Typically, it is found (and was also observed in this work) that the pfu/mL value is 10 times lower than virions/mL.

### 2.1.7 Colony PCR

Viral plaques were picked from agar plates using a sterile pipette tip and used to inoculate 200  $\mu$ l of 2xYT broth in a 1.5 mL Eppendorf tube (it is important to tap the tube three times on the bench after inoculation) and incubated for 1 hour at 37°C with

## Chapter 2

shaking at 220 rpm. Primers were designed to amplify either *gene III* (Seq-g3-for: 5'-CACCTCGAAGCAAGCTGATAAAC -3', Seq-g3-rev: 5'-GACAACCCTCATAGTTAGCGTAACG -3') or *gene VIII* (Seq-g8-for: 5'-GCTATGCCT TCGTAG TGGCATTACG -3', Seq-g8-rev: 5'-AACGCAGCTTGCTTTTCGAGGTG -3'). Figure 2.5 shows the primer positions.

```
1201 CAAAGATGAG TGTTTTAGTG TATTCTTTG CCTCTTTCGT TTAGGTTGG
      Seq-g8-for →
1251 TGCCCTCGTA GTGGCATTAC GTATTTTACC CGTTTAATGG AAACCTCCTC
1301 ATGAAAAAGT CTTTAGTCCT CAAAGCCTCT GTAGCCGTTG CTACCCTCGT
      Pst I           Bam HI
1351 TCCGATGCTG TCTTTCGCTG CAGAGGGTGA GGATCCCGCA AAAGCGGCCT
1401 TTAACTCCCT GCAAGCCTCA GCGACCGAAT ATATCGGTTA TGCGTGGGCG
1451 ATGGTTGTTG TCATTGTCGG CGCAACTATC GGTATCAAGC TGTTTAAGAA
      ← Seq-g8-rev
1501 ATTCCACCTCG AAAGCAAGCT GATAACCGA TACAATTAAGGCTCCTTTT
      Seq-g3-for →
1551 GGAGCCTTTT TTTTGGAGAT TTTCAACGTG AAAAAATTAT TATTCGCAAT
      Acc 65 I           Eag I
1601 TCCTTTAGTG GTACCCTTCT ATTCTCACTC GGCCGAAACT GTTGAAAGTT
1651 GTTTAGCAAA ATCCCATACA GAAAATTCAT TACTAACGT CTGGAAAGAC
      ← Seq-g3-rev
1701 GACAAAACCTT TAGATCGTTA CGCTAACTAT GAGGGCCTGTC TGTGGAATGC
```

**Figure 2.5. Position of pIII and pVIII sequencing primers.** *gVIII*: 1301-1522 (start 1301), *gIII*: 1578-2852 (start 1578). The Pst I and Bam HI restriction sites show the approximate position of *gVIII* inserts, whilst the Acc65 I and Eag I sites show the position of *gIII* inserts. *gIII* PCR product: 237 bp. *gVIII* PCR product: 279 bp. Sequence is M13KE, which is available from New England Biolabs.

PCR was carried out using 2 µl of the 1 hour culture as a template in the reaction. 1 U of Taq DNA polymerase (Invitrogen, Cat. No. 18038-026), 1 x concentration of provided buffer, 1.5 mM MgCl<sub>2</sub> (Invitrogen), 0.5 mM dNTPs (Invitrogen) and 1 pmol/µl of the

relevant primers were used in a final volume of 20  $\mu$ l. PCR conditions used were 95°C for 30 seconds, followed by 24 cycles of: 95°C for 30 seconds, 55°C for 1 minute, and 72°C for 1 minute. Final step was 68°C for 10 minutes. An M13KE (grown from a plaque as above) and negative ddH<sub>2</sub>O control were also used in the PCR. Products were run directly on a 10% polyacrylamide gel (section 2.1.9.1)

### **2.1.8 Transmission Electron Microscopy (TEM)**

5  $\mu$ l of sample was applied directly to charged ultra-thin carbon-coated copper grids (Agar Scientific, Essex, U.K.). After 1 minute the liquid was removed carefully with filter paper. Staining (if necessary) was done using 2% (w/v) uranyl acetate (in pH 4 ddH<sub>2</sub>O). A Philips CM10 (Philips Electronics UK Ltd, Guildford, U.K.) or Jeol 1200EX (Jeol Inc, Tokyo, Japan) transmission electron microscope was used to visualise the samples at 80 keV.

### **2.1.9 DNA Gel Electrophoresis**

#### **2.1.9.1 10% Polyacrylamide Gel**

A 10% (w/v) polyacrylamide gel was made using: 16.4 mL ddH<sub>2</sub>O, 12 mL 29:1 bis-acrylamide (Severn Biotech, Kidderminster, U.K.), 7.2 mL 5x Tris-Borate-EDTA (TBE) buffer (MP Biomedicals, Stretton, U.K.), 360  $\mu$ l 10% (w/v) ammonium persulfate (APS), and 36  $\mu$ l Tetramethylethylenediamine (TEMED). Samples were loaded into wells with an equal volume of 2x DNA loading buffer (Ambion, Austin TX U.S.A., Cat. No. AM8546G: 95% Formamide, 18 mM EDTA and 0.025% each of SDS,

Xylene Cyanol, and Bromophenol Blue) and a 10 bp DNA ladder (Invitrogen, Cat. No. 10821-015, Figure 2.6 A, 10 – 330 bp). 1x TBE buffer was used as running buffer. Gels were run for 1 hour at 8 Watts using a Consort E832 power pack (Turnhout, Belgium) and stained with ethidium bromide (1 µg/mL).

### **2.1.9.2 1% and 3% Agarose Gel**

0.4 g (1%) or 1.5 g (3%) of agarose was mixed with 50 mL of 1x TBE buffer. Solution was heated in microwave until all agarose had dissolved. Molten agarose was allowed to cool to ~45°C and 2.5 µl of ethidium bromide (10 mg/mL) was added. Mixture was swirled to mix before being poured into tray and allowed to set. Samples were loaded with an equal volume of 2x DNA loading buffer (Ambion) and either a 10 bp (Invitrogen) or a 2-log DNA ladder (New England Biolabs, Cat. No. N3200L, Figure 2.6 B, 0.1 - 10 kb) for 3% and 1% gels respectively. 1x TBE buffer was used as running buffer. Gels were run using a Consort E832 power pack.

### **2.1.10 Protein Gel Electrophoresis Under Denaturing Conditions**

#### **2.1.10.1 Tris-glycine SDS Gel**

A 10-20% (w/v) Tris-HCl gradient gel with a 4% (w/v) stacking gel (Biorad laboratories, Cat. No. 345-0042) was used to run protein samples under denaturing conditions. Gels were run in 1x glycine running buffer with a PageRuler™ prestained protein ladder (Fermentas, St. Leon-Rot Germany, Cat. No. SM0671, Figure 2.6 C) using the Criterion cell system (Biorad laboratories, Cat. No. 165-6001) and a Consort

E832 power pack. The gels were then stained overnight whilst rocking gently with enough coomassie blue staining solution to cover the gel. The gel was then de-stained whilst rocking with de-stain solution until the bands could be visualised.

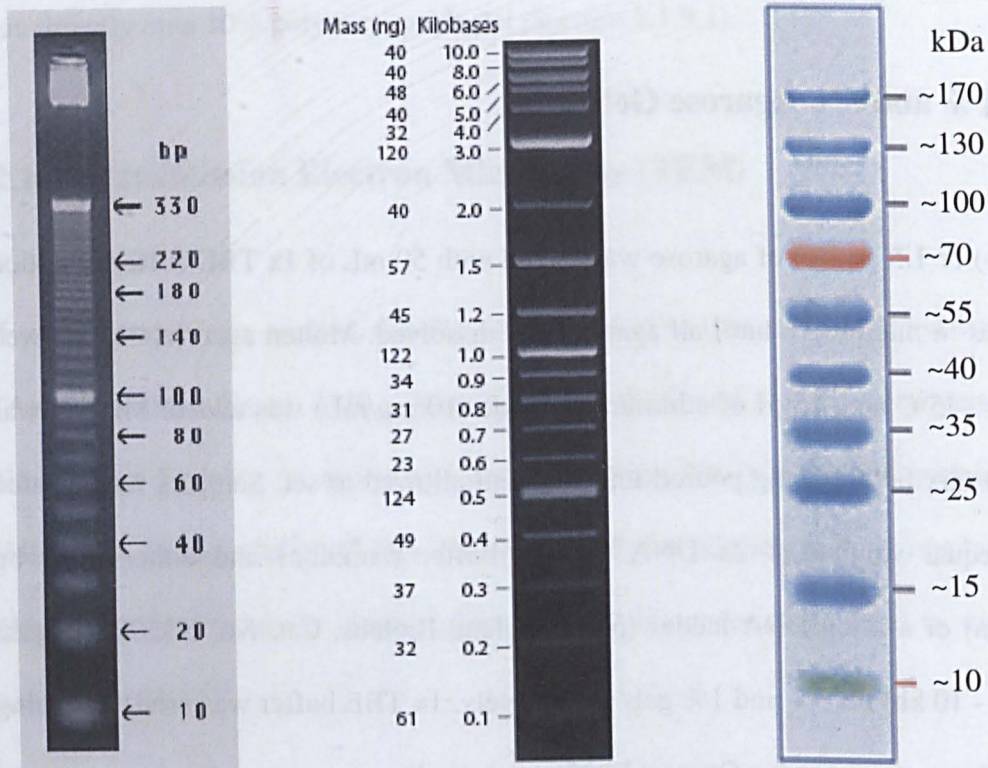


**Figure 2.6. Gel ladders for DNA and proteins.** A) 10 bp ladder image taken from Invitrogen. 10 bp ladder was run on a 4% (w/v) low melting point agarose gel in Tris-acetate (pH 7.6) and stained with ethidium bromide. B) 2-log ladder image taken from New England Biolabs. 2-log ladder was run on a 1% (w/v) agarose gel in TBE. Mass values are for 1  $\mu$ g, i.e. 1  $\mu$ L, of ladder. C) PageRuler™ pre-stained protein ladder image taken from Fermentas. Ladder was run on a 4-20% (w/v) Tris-glycine SDS-PAGE gel.

### 2.1.11 Molecular biology techniques

#### 2.1.11.1 Polymerase Chain Reaction (PCR)

PCR was carried out using Taq DNA polymerase (Invitrogen, Cat. No. 18038-026) which is provided with a 10x buffer (200 mM Tris-HCl pH 8.4 and 500 mM KCl) and 50 mM MgCl<sub>2</sub> solution. One unit of Taq DNA polymerase is defined by Invitrogen as: “incorporating 10 nmol of deoxyribonucleotide into acid-precipitable material in 30 minutes at 74°C. Unit assay conditions: 25 mM TAPS (pH 9.3), 50 mM KCl, 2 mM MgCl<sub>2</sub>, 1 mM DTT, 0.5 mg/mL activated salmon sperm DNA, 0.2 mM dATP, dCTP, dGTP, dTTP”. Primers, provided by MWG-Biotech (Ebersberg, Germany), were spun at max. speed on a table-top centrifuge for 5 minutes to pellet the lyophilised DNA. MWG-Biotech informs you how much buffer is needed to re-suspend the primers so that the concentration is 100 pmole/μL. Primers were re-suspended in EB buffer from the QIAquick PCR purification kit (Qiagen, Cat. No. 28704). Template oligos were re-suspended in the same way but before use diluted 1 in 1000 in ddH<sub>2</sub>O. The 10 mM dNTP mixture (containing 10 mM of dATP, dCTP, dGTP, and dTTP) was created from a 100 mM dNTP set (Invitrogen, Cat. No. 10297-018).

For a single PCR reaction the following was added to a 250 μL PCR tube on ice:

- 2 μL 10x Invitrogen buffer (final concentration 20 mM Tris-HCl pH 8.4, 50 mM KCl),
- 0.6 μL Invitrogen 50 mM MgCl<sub>2</sub> solution (final concentration 1.5 mM),
- 0.2 μL 100 pmole/μL primer 1 (final concentration 1 μM),

## Chapter 2

---

- 0.2  $\mu\text{L}$  100 pmole/ $\mu\text{L}$  primer 2 (final concentration 1  $\mu\text{M}$ ),
- 0.4  $\mu\text{L}$  10 mM dNTP mixture (final concentration 200  $\mu\text{M}$ ),
- 2  $\mu\text{L}$  0.1 pmole/ $\mu\text{L}$  template (final concentration 1 nM),
- 0.2  $\mu\text{L}$  Taq polymerase (1 unit),
- 14.4  $\mu\text{L}$  ddH<sub>2</sub>O (final volume 20  $\mu\text{L}$ ).

When no template was used it was replaced by 2  $\mu\text{L}$  of ddH<sub>2</sub>O. For most PCR reactions a 100  $\mu\text{L}$  master mix, i.e. five PCR reactions, was made and then 20  $\mu\text{L}$  aliquoted into five 250  $\mu\text{L}$  PCR tubes. For 100  $\mu\text{L}$  master mix the following was added to a 1.5 mL Eppendorf tube on ice:

- 10  $\mu\text{L}$  10x Invitrogen buffer,
- 3  $\mu\text{L}$  Invitrogen 50 mM MgCl<sub>2</sub> solution,
- 1  $\mu\text{L}$  100 pmole/ $\mu\text{L}$  primer 1,
- 1  $\mu\text{L}$  100 pmole/ $\mu\text{L}$  primer 2,
- 2  $\mu\text{L}$  10 mM dNTP mixture,
- 10  $\mu\text{L}$  0.1 pmole/ $\mu\text{L}$  template,
- 1  $\mu\text{L}$  Taq polymerase,
- 72  $\mu\text{L}$  ddH<sub>2</sub>O (final volume 100  $\mu\text{L}$ )

The PCR reaction was placed into a thermocycler (Peltier thermal cycler PTC-200, Global Medical Instrumentation Inc., Minneapolis, MN, U.S.A., Cat. No. BC-MJPC200) using the following programme:

- 95°C for 30 seconds,
- followed by 24 cycles of:
  - 95°C for 30 seconds,
  - X°C for 1 minute (the annealing temperature depends on the T<sub>m</sub> of the primers),
  - 72°C for X minutes (1 minute per kb of DNA with 1 minute being the minimum),
- The final step was 68°C for 10 minutes.

Unless otherwise stated, an annealing temperature of 55°C and extension time of 1 minute was used.

### **2.1.11.2 Phenol Chloroform extraction of DNA and ethanol precipitation**

The DNA solution was first made up to 200 µL with ddH<sub>2</sub>O in a 1.5 mL Eppendorf tube. As an example: with a 100 µL PCR reaction, which had been aliquoted into 5 x 20 µL, the 5 reactions were pooled and 100 µL of ddH<sub>2</sub>O added. To the 200 µL of DNA, 400 µL of phenol solution (Sigma-Aldrich, Cat. No. P4557) was added and vortexed for 1 minute before being spun at max speed for 1 minute in a table top centrifuge. This resulted in two phases with the DNA contained in the top phase. The top phase was aspirated with a pipette, with care taken to avoid taking any of the lower phase, and placed into a fresh 1.5 mL tube.

400 µL of chloroform was added to the 200 µL of aspirated DNA and vortexed for 1 minute and spun at max speed for 1 minute. Once again two phases appeared and the

top phase, which contained the DNA, was aspirated to a fresh 1.5 mL tube. The chloroform step was then repeated again to remove any trace of phenol.

To the ~ 200  $\mu$ L of DNA containing solution, 20  $\mu$ L, i.e. 10% (v/v) of original DNA solution, of 3 M sodium acetate was added and vortexed for 30 seconds. Ice cold 100 % (v/v) ethanol was then added and vortexed briefly before the tube was placed at  $-20^{\circ}\text{C}$  overnight to precipitate the DNA. The following day, the tube was spun at  $4^{\circ}\text{C}$  for 20 minutes at max. speed in a table-top centrifuge to pellet the DNA. The ethanol was poured away and 400  $\mu$ L of ice cold 70 % (v/v) ethanol was carefully added and the tube spun again at  $4^{\circ}\text{C}$  for 20 minutes at max speed in a table-top centrifuge. With both centrifugation steps it is important to keep the tube facing the same way so that it is known which side the pellet of DNA is on. The ethanol was removed with a pipette and care taken to keep the pipette tip on the side opposite the DNA pellet. The DNA pellet was re-suspended in 50  $\mu$ L of EB buffer from the QIAquick PCR purification kit (Qiagen, Cat. No. 28704). To remove trace ethanol the tube was placed in a GeneVac EZ-2<sup>plus</sup> (GeneVac, Ipswich, Suffolk, U.K.) for 10 minutes. The amount of DNA was then estimated using a Nanodrop 3300 spectrophotometer (Nanodrop products).

### **2.1.11.3 Insertional PCR**

Insertional PCR is a variation of site directed mutagenesis (Wang, 1999). However, in order to limit primer dimer formation, the two primers are used in two separate site directed mutagenesis reactions before being mixed together to complete the reaction. A QuikChange® Site-directed mutagenesis kit (Agilent Technologies, Stockport, Cheshire, U.K., Cat. No. 200519) was used to perform the insertional PCR. Primer

## Chapter 2

---

design is the same as for site directed mutagenesis: 20 bp overlap of the template DNA both before and after the DNA sequence to be inserted. Primers were ordered from MWG-biotech with High Purity Salt Free (HPSF) purification.

For a single insertional PCR reaction, two separate 250  $\mu\text{L}$  were used. Each contained the following:

5  $\mu\text{L}$  10x buffer (provided with QuikChange® Site-directed mutagenesis kit)

1  $\mu\text{L}$  dNTP solution (provided with QuikChange® Site-directed mutagenesis kit)

1  $\mu\text{L}$  of template DNA (50 to 200 ng of plasmid or RF DNA)

1  $\mu\text{L}$  of 10 pmol/ $\mu\text{L}$  primer (EITHER primer 1 OR primer 2)

42  $\mu\text{L}$  of ddH<sub>2</sub>O

The two reactions, with only differ by which primer is added, were mixed on ice. 0.4  $\mu\text{L}$  (1 unit) of *pfu* polymerase (provided with QuikChange® Site-directed mutagenesis kit) was then added. The two reactions were then placed into a thermocycler (Peltier thermal cycler PTC-200) and the following programme used:

- 95°C for 30 seconds,
- followed by 10 cycles of:
  - 95°C for 30 seconds,
  - 55°C for 1 minute,
  - 68°C for X minutes (1 minute per kb of DNA with 1 minute being the minimum),
- The final step was 68°C for 10 minutes.

Unless otherwise stated, an extension time of 8 minutes was used.

25  $\mu\text{L}$  of each reaction was then taken and mixed together (so that a single PCR tube contained 25  $\mu\text{L}$  of each reaction) and 0.4  $\mu\text{L}$  of *pfu* polymerase added. The PCR tube was then placed back into the thermocycler and the same programme used. However, the number of cycles was increased to 18. 1  $\mu\text{L}$  (10 units) of *dpn* I (provided with QuikChange® Site-directed mutagenesis kit) was then added to the reaction and incubated at 37°C for 3 hours. *Dpn* I digests methylated DNA and therefore it should only digest the template DNA. 1  $\mu\text{L}$  of the *dpn* I digested insertional PCR reaction was then transformed into 5-alpha F Iq Competent *E.coli* (New England Biolabs, Cat. No. C2992H) as in section 2.1.3.

### 2.1.11.4 Ligation of DNA fragments

100 ng of phage DNA was mixed with 1  $\mu\text{L}$  of restricted PCR product (concentration was irrelevant) and 1  $\mu\text{L}$  (3 Units) of T4 DNA ligase (Promega, Cat. No. M1801). 1  $\mu\text{L}$  of buffer (provided with ligase) was added and the final volume made up to 10  $\mu\text{L}$  with ddH<sub>2</sub>O in a 1.5 mL Eppendorf tube. The sample was then incubated at room temperature for 3 hours. 3  $\mu\text{L}$  of the ligated DNA was then transformed into 5-alpha F Iq Competent *E.coli* (New England Biolabs, Cat. No. C2992H) as in section 2.1.3.

## 2.2 Specific Methods for Chapter 3

### 2.2.1 Creation of the microphage plasmid (pMicro)

The packaging signal (PS) was amplified from the F1 origin (4894-5349) of the vector pET26-b (Novagen, Cat. No. 69862-3) using step1for and step1rev primers (Table 2.1) which flanked the 91bp PS. The PCR, and subsequent purification was carried out as described in section 2.1.11.1.

**Table 2.1 A list of the primers used in creating the microphage plasmid pMicro.**

Primer	Sequence 5'-3'
Step1for	ATGCACGCGCCCTGTAGCGG
Step1rev	ATGCGGAGCGGGCGCTAGG
Step2for	AACACTCAACCCTATCTCGGGCAAGCTTGGACGCGCCCTGTAGCGGGCGCA
Step2rev	TCCCCGAAAAGTGCCACCTGTCCGATCCCGGGAGCGGGCGCTAGGGCGCT
Step3for	ACTGCCATCGCCCTGATAGAC
Step3rev	ACTGTTCCAGTTTGGAAACAAGAG
Step4for	CGCCCGCTCCCGGGATCGGAATTCCGGCCATCGCCCTGATAGACG
Step4rev	TCCCCGAAAAGTGCCACCTGAGACGTTTTCCAGTTTGGAAACAAGAGT
Microamplifyfor	ATCGGATCCAGACGTTTTCCAGTTTGG
Microamplifyrev	ATGCTCTAGACCATCGCCCTGATAGAC
pJetfor	CGACTCACTATAGGGAGAGAGGCC
pJetrev	GAAGAACATCGATTTTCCATGGCAG

The PCR fragment from step 1 was then used as the template to produce the primers for insertional PCR of the PS into the pET26-b vector. PCR was carried out with the step 1 PCR fragment as the template and Step2for and Step2rev primers; these primers overlap the step 1 fragment and add 20 bp at the 5' and 3' ends which is complementary to

## Chapter 2

---

pET26-b. This PCR fragment was then used as the primer for insertional PCR (section 2.1.11.3), using pET26-b as the template, in order to insert the PS downstream of the origin of replication and create the plasmid pET26-bPS

A truncated origin of replication, lacking 29 bp from domain B, was amplified from pET26-b using Step3for and Step3rev primers using PCR (section 2.1.11.1). As before, this fragment was then used as the template for PCR using Step4for and Step4rev primers resulting in a fragment that contained overlaps that were complementary for pET26-bPS. This PCR fragment was then used as the primer for insertional PCR (section 2.1.11.3) with pET26-bPS as the template, in order to insert the truncated origin of replication downstream of the PS and create the plasmid pM1.

The 310 bp microphage cassette was then PCR amplified (section 2.1.11.1) from pM1 using microamplifyfor and microamplifyrev (Table 2.1). This fragment was then cloned into the pJET1.2 vector (Fermentas) using the CloneJet™ PCR cloning kit (Fermentas, Cat. No. K1232) following the method provided to produce pMicro. Briefly, the PCR fragment was blunted and then ligated into the pJET1.2 vector between the Xho1 and Xba1 sites (Figure 2.7). The pJET1.2 vector is pre-cut before use to interrupt the *eco47IR* gene. Upon ligation, if no PCR product is present to continue to interrupt the gene, the gene becomes active and is lethal to the *E.coli* host: thus only pJET1.2 vectors containing the PCR insert allow the *E.coli* to grow, making selection of the correct clone simple. pMicro was sequenced using the pJET1.2 forward sequencing primer (pJetfor) and pJET1.2 reverse sequencing primer (pJetrev) (Fermentas Cat. No. K1232) to confirm microphage cassette was present.

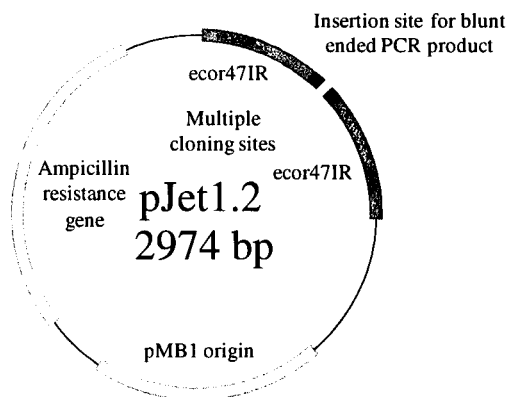


**Figure 2.7. Vector Map of pJET1.2.** Adapted from Fermentas.

### 2.2.2 Creation of longer microphage cassette (pMicroKan)

Kanamycin resistance gene was PCR amplified (section 2.1.11.1) from pET-26b (Novagen) using KanforecoR1 (ATCGGAATTCAGGCGGTGCTACAGAG) and KanrevcoR1 (ATCGGAATTCATATGTATCCGCTCATGAAT). pMicro and the amplified kanamycin resistance gene were cut with EcoR1 (New England Biolabs, R0101) and ligated together (section 2.1.11.4) to create pMicroKan. pJetfor and pJetrev were used for sequencing reactions to confirm insertion of the kanamycin resistance gene.

### 2.2.3 Creation of the helper plasmid pM13CP

The chloramphenicol resistance gene was PCR amplified (section 2.1.11.1) from the plasmid pACYC184 using the primers pACYC184camfor and pACYC184camrev (Table 2.2). M13KE (New England Biolabs) was PCR amplified using Expand high Fidelity PCR system (Roche, Cat. No. 11732641001) and the two outward facing primers M13MLu1for and M13MLu1rev (Table 2.2); this amplifies the entire M13KE

## Chapter 2

genome, terminating with MluI sites. The protocol for this PCR amplification was provided with the kit. The amplified M13KE genome and chloramphenicol resistance gene were cut with MluI (New England Biolabs, R0198L) and ligated together (section 2.1.11.4) to create M13C.

**Table 2.2 A list of the primers used in creating the helper plasmid M13CP.**

Primer	Sequence 5'-3'
M13MLu1for	TTGATGACGCGTCCTATTGGTAAAAAATGAGCTG
M13MLu1rev	TTGATGACGCGTCCGAAATCGGCAAATCC
pACYC184camfor	TTGATGACGCGTGTCCGAATTTCTGCCATTC
pACYC184camrev	TTGATGACGCGTCAATAAATACCTGTGAC
M13cpfor	TGATTTCCATGGACGCGTGTCCGAATTTCTGCCATTCATCC
M13cprev	CCACACCCATGGCGCTTAATGCGCCGCTACAGGGCGCGTACT
p15afor	TATCGCCATGGGCGCTAGCGGAGTG
p15arev	TATCGCCATGGACAACCTTATATCGTATGGGGC
M13CPseq1	AATGCTACTACTATTAGTAGAATTG
M13CPseq2	GTATTCCTAAATCTCAACTGATG
M13CPseq3	CTTAACTCCCTGCAAG
M13CPseq4	GTTACTCAAGGCACTGACC
M13CPseq5	GAAAGACAGCCGATTATTG
M13CPseq6	GGTAATTCAAATGAAATTG
M13CPseq7	CTGACCGCCTCACCTCTGTTTTATC
M13CPseq8	GCTGCACCGGTGCGTCAG
M13CPseq9	CGTTTTTCAGAGCAAGAGATTAC
M13CPseq10	CAAGAATGTGAATAAAGGCCG
M13CPseq11	CATATTGATGGTGATTTGACTG

The p15a bacterial origin was amplified from pACYC184 using the p15afor and p15arev primers (Table 2.2). M13C was amplified using the Expand high Fidelity PCR system (Roche, Cat. No. 11732641001) and the two outward facing primers M13cpfor and M13cprev (Table 2.2). This amplified the entire M13c genome minus the intergenic

region that contains the M13 origin of replication. Both PCR fragments were cut with NcoI (New England Biolabs, Cat. No. R0193L) and ligated together (section 2.1.11.4) to create the bacterial plasmid M13CP. The entire M13CP plasmid was then sequenced using M13CPseq1-11 (Table 2.2).

### **2.2.4 Production of shorter length phage particles using M13KO7**

pMicro, pMicroKan and the phagemid pLitmus28i (New England Biolabs, Cat. No. N3528S) were each transformed (section 2.1.3) into DH5- $\alpha$  F' I<sup>q</sup> *E.coli* (New England Biolabs, Cat. No. C2992H) and grown overnight on LB agar plates containing ampicillin and tetracycline at 37°C. The next day a single colony was picked and grown overnight at 37°C in 10 mL SB medium with ampicillin and tetracycline with vigorous shaking (250 rpm). 1 mL of the overnight culture was then added to 100 mL of SB medium in a 500 mL conical flask containing ampicillin and tetracycline and grown until slightly turbid (OD<sub>600</sub> ~ 0.05, typically 1 hour) at 37°C with vigorous shaking. 100  $\mu$ L of M13KO7 was added (New England Biolabs, N0315S) to a final concentration of  $1 \times 10^9$  pfu and grown for a further 2 hours at which point kanamycin was added (70  $\mu$ g/mL) and the culture grown overnight at 37°C with vigorous shaking. When growing M13KO7 the same protocol was carried out but with DH5- $\alpha$  F' I<sup>q</sup> *E.coli* containing no plasmid. Controls were also grown in same manner with DH5- $\alpha$  F' I<sup>q</sup> *E.coli*, pMicro, pMicroKan and pLitmus28i only but with no addition of M13KO7 or kanamycin.

### 2.2.5 Production of shorter length phage particles using M13CP

pMicro, pMicroKan and the phagemid pLitmus28i (New England Biolabs, Cat. No. N3528S) were each transformed (section 2.1.3) into DH5- $\alpha$  F' I<sup>q</sup> *E.coli* and grown overnight on LB agar plates containing ampicillin at 37°C. The next day a single colony was picked and grown overnight at 37°C in SB medium with ampicillin with vigorous shaking (250 rpm). Cells were then made chemically competent (section 2.1.2) and transformed (section 2.1.3) with M13CP and grown overnight on LB agar plates containing ampicillin and chloramphenicol at 37°C (DH5- $\alpha$  F' I<sup>q</sup> *E.coli* was also transformed with M13CP only to act as a control). To produce the shorter phage particles a single colony was grown overnight in 100 mL of SB medium containing ampicillin and chloramphenicol at 37°C and vigorous shaking. Controls were also grown in same manner with DH5- $\alpha$  F' I<sup>q</sup> *E.coli*, M13CP, pMicro, pMicroKan and pLitmus28i only.

### 2.2.6 Purification of shorter phage particles

Purification of shorter length phage particles followed a modification of the Yamamoto, *et al.* (1970) and Speckthrie, *et al.* (1992) methods. The overnight cell culture was centrifuged at 10,000 x g for 10 minutes to pellet the cells. The supernatant was removed and added to a fresh centrifuge tube containing 15 g PEG 8000 (GE Healthcare) and 2.922 g NaCl for a final concentration of 15 % (w/v) PEG and 0.5 M NaCl. Supernatant was mixed thoroughly by 100 inversions and then left overnight at 4°C to precipitate the phage particles. Phage were pelleted by centrifugation at 10,000 x g for 1 hour. Supernatant was removed and centrifuge tubes inverted for 10 minutes to

allow remaining liquid to drain away. Pellet was re-suspended thoroughly in 100 mL PBS pH 7.4. PEG/NaCl purification was then repeated as above and the pellet re-suspended in 1 mL PBS pH 7.4.

### **2.2.7 Caesium chloride purification of shorter length phage particles**

PEG precipitated shorter length phage particles were occasionally further purified on a CsCl gradient (section 2.1.5.2) and dialysed against three changes of PBS, pH 7.4, buffer using a 100 kDa molecular weight cut off, cellulose ester, dialysis membrane (Spectra/Por, Cat. No. 131408).

### **2.2.8 Linear sucrose density ultracentrifugation of shorter length phage particles**

1 mL of PEG precipitated shorter length phage particles was loaded onto a 30-60% linear sucrose gradient (section 2.1.5.3). Samples were then spun at 30,000 rpm for 18 hours before being fractionated (section 2.1.5.4). Peaks containing the relevant phage were collected and PBS added to bring the fraction up to 10 mL. The phage were then PEG precipitated (15% PEG-8000, 0.5 M NaCl) and spun at 10,000 rpm for 1 hour. Phage pellets were re-suspended in 500  $\mu$ L of PBS pH 7.4.

### **2.2.9 Size exclusion chromatography of shorter length phage particles**

Phage samples (up to 250  $\mu$ l maximum) in PBS were applied to a Tricorn™ column (1 cm diameter, 25 mL volume, 30 cm bed height) packed with superose 6™ (column was

purchased pre-packaged from GE healthcare: Superose 6 10/300 GL, Cat. No. 17-5172-01). Superose 6 is a highly cross-linked agarose matrix with a protein separation range of  $5 \times 10^3$ - $5 \times 10^6$  Da and an exclusion limit of  $4 \times 10^7$  Da. An ÄKTAexplorer™ (GE healthcare) using the UNICORN software was used to control and monitor the column. The column was first equilibrated with PBS pH 7.4 overnight at a flow rate of 0.1 mL/min. The samples were applied under a flow rate of 0.5 mL/min and eluted with 1.5 times the column volume of PBS. 1 mL fractions were continuously collected in 1.5 mL Eppendorf tubes. The absorbance at 260 nm and 280 nm were monitored using the monitor UV-900 included with the ÄKTAexplorer™. 5  $\mu$ L of each fraction was used for TEM (section 2.1.8).

### **2.2.10 Titering of shorter length phage particles**

10  $\mu$ L of phage were serially diluted to  $10^{-4}$  and  $10^{-6}$  in 90  $\mu$ L 2xYT medium or used directly from the stock solution. 10  $\mu$ L of each was then mixed with 90  $\mu$ L of an overnight growth of ER2738 *E.coli* (New England Biolabs, Cat. No. E4104S) and mixed briefly. 10  $\mu$ L was then plated onto LB agar plates containing either ampicillin, kanamycin, chloramphenicol, or a mixture of the three. The plates were then grown overnight at 37°C. The number of colonies were counted the following day.

### **2.2.11 Measurement of shorter length phage particle length by TEM**

10  $\mu$ L of phage were serially diluted to  $10^{-4}$  and  $10^{-6}$  in 90  $\mu$ L of ddH<sub>2</sub>O. 5  $\mu$ L was then viewed using TEM (2.1.8). Images were taken at a magnification of x20000. Ten images for each phage particle were taken at arbitrary positions upon the grid in order to

## Chapter 2

---

get a representative cross-reference of phage particles. The images were used to obtain an average length of each phage particle using ImageJ, version 1.43u (Abramoff, 2004). From each of the ten images, 50 phage particles were measured using imageJ to get an average length from 500 particles. Lengths were measured using the point selection tool which had been calibrated with the TEM scale bar.

### 2.3 Specific Methods for Chapter 4

#### 2.3.1 Insertion of selenocysteine into *gIII*

The selenocysteine containing peptide (S A R V U H G P S V A G L H Q S A, where U is selenocysteine) was inserted into position 1 of the mature pIII coat protein between the Acc65 I and Eag I sites located in *gIII* of the commercial strain M13KE (New England Biolabs, Cat. No. N0316S). Cutting of the M13KE genome using the Acc65 I and Eag I restriction enzymes results in the removal of part of the leader sequence (V P F Y S H S) - needed for correct localisation of pIII to the cell membrane (Clackson, 2004) - along with the first amino acid (alanine) of the mature pIII coat protein. Therefore these amino acids, along with the selenocysteine sequence, were inserted: the full inserted peptide sequence was V P F Y S H S S A R V U H G P S V A G L H Q S A.

The DNA sequence corresponding to the selenocysteine containing sequence (V P F Y S H S S A R V U H G P S V A G L H Q S A) was PCR amplified (section 2.1.11.1) using overlapping DNA primers (Biotinfor 5'- ATC GGG TAC CTT TCT ATT CTC ACT CTA GCG CTC GTG TCT GAC ACG GC -3', Biotinrev 5'- ATC GCG GCC GAT TGG TGC AGA CCT GCA ACC GAT GGG CCG TGT CAG ACA C -3').

PCR products were then purified using the QIAquick PCR purification kit (Qiagen, Cat. No. 28704) and the entire eluate (typically 25 µL) was cut with 6 µL (60 units) each of Acc65 I and Eag I (New England Biolabs, Cat. No. R0599L and R0505L respectively) using 9 µL buffer 3 and 0.9 µL BSA (provided with the enzymes) and made up to 90 µL

## Chapter 2

---

with ddH<sub>2</sub>O. The mixture was then split into three 30 μL aliquots and dispensed into 0.25 mL PCR tubes. They were then incubated at 37°C for 4 hours before recombining the three aliquots and mixing with 110 μL of ddH<sub>2</sub>O (for a total of 200 μL) and the sample phenol:chloroform purified and ethanol precipitated (section 2.1.11.2).

M13KO7 and M13KE RF DNA were purified from 10 mL of overnight culture in 2xYT medium containing 5-alpha F<sup>'</sup> *E.coli* (New England Biolabs, Cat. No. C2992H) infected with either M13KO7 or M13KE phage. The phage DNA was purified from the *E.coli* using the QIAprep spin miniprep kit (Qiagen, Cat. No. 27106). As with the selenocysteine PCR product, the entire eluate (typically 25 μL) was cut with *Acc65 I* and *Eag I*. The 90 μL of cut DNA was then purified using the QIAquick PCR purification kit. The entire eluate (typically 25 μL) was then treated with 15 μL (15 Units) of shrimp alkaline phosphatase (Promega, Cat. No. M8201), 9 μL of 10 x buffer (provided with the phosphatase) and made up to a final volume of 90 μL with ddH<sub>2</sub>O. This enzyme removes the phosphate groups from the 5' terminus of the DNA which prevents the DNA from being re-ligated when treated with a ligase. The mixture was then split into three 30 μL aliquots and dispensed into 0.25 mL PCR tubes. They were then incubated at 37°C for 1 hour before recombining the three aliquots and mixing with 110 μL of ddH<sub>2</sub>O (for a total of 200 μL) and the sample phenol:chloroform purified and ethanol precipitated (section 2.1.11.2)

The restricted and purified phage RF DNA (either M13KE or M13KO7) and selenocysteine PCR DNA were ligated together (section 2.1.11.4). 2 μL of the ligated sample was then transformed (section 2.1.3) into 50 μL of chemically competent 5-alpha F<sup>'</sup> *E.coli* (New England Biolabs, Cat. No. C2992H) and plated on LB agar

plates containing tetracycline and 2  $\mu$ M sodium selenite (Sigma-Aldrich, Cat. No. S9133). The sodium selenite was essential since clones containing selenocysteine would not grow without it present. The plates were then incubated overnight at 37°C.

The following day, 14 plaques were picked for each phage (M13KE and M13KO7) and colony PCR carried out (section 2.1.7) using seq-g3-for (5'-CAC CTC GAA AGC AAG CTG ATA AAC -3') and seq-g3-rev (5'- GAC AAC CCT CAT AGT TAG CGT AAC G -3'). 10 successful clones were sent for sequencing using the seq-g3-rev primer and a single clone containing the correct sequence was used in further experiments. M13KE containing selenocysteine was termed M13pIIISel and M13KO7 containing selenocysteine was termed M13KO7pIIISel.

### **2.3.2 Production of selenocysteine containing phage**

M13pIIISel and M13KO7pIIISel RF DNA was transformed into 5-alpha *F'*<sup>tr</sup> *E.coli* and plated onto tetracycline, sodium selenite LB agar plates using top agar and overnight *E.coli* stock (section 2.1.3) and incubated overnight at 37°C. Phage stocks were then grown and purified as in section 2.1.5.1 but with 2  $\mu$ M sodium selenite supplement in the growth medium. Phage particles were then CsCl purified (section 2.1.5.2).

### **2.3.3 Production of microphage containing selenocysteine**

Microphage containing selenocysteine were produced and purified as in sections 2.2.2 and 2.2.6. However, M13KO7pIIISel was used instead of M13KO7.

### 2.3.4 Creation and production of pIII cysteine mutant

The cysteine at position 7 of the mature pIII coat protein (A E T V E S C) was substituted with a glycine via a single nucleotide substitution (T to G at position 1650 of the M13KE genome). This was done using the QuikChange™ site directed mutagenesis kit (Stratagene, Cat. No. 200519) which uses the high fidelity *pfu* polymerase. Mutagenesis was carried out as in kit instructions using 100 ng of M13KE RF DNA as the template. The mutagenesis product was digested for 3 hours with *dpn* I before being transformed into NEB 5-alpha F' *I*<sup>h</sup> Competent *E. Coli* (New England Biolabs, Cat. No. C2992H). The primers used were pIIIremovalfor (5'- CTG TTG AAA GTG GTT TAG CAA AAT CCC ATA C -3') and pIIIremovalrev (5'- GTA TGG GAT TTT GCT AAA CCA CTT TCA ACA G -3'). Successfully created mutants were grown and purified as in section 2.1.5.1 and then stored at 4°C.

### 2.3.5 Binding of M13pIIISel and wild-type M13 to gold nanoparticles

$10^{12}$  virions/mL of M13pIIISel or wild-type M13 in 100  $\mu$ L PBS buffer pH 7.4 were mixed with citrate stabilised 5 nm or 10 nm gold nanoparticles (Ted Pella via Agar scientific, the U.K. distributor, Cat. No. 15703-20. 15702-20). The gold nanoparticles were supplied in water with trace amounts of citrate, tannic acid and potassium carbonate (precise amounts unknown). The 10 nm gold nanoparticles came as a monodisperse solution at a concentration of  $5.7 \times 10^{12}$  particles/mL whilst the 5 nm were supplied at a concentration of  $5 \times 10^{13}$  particles/mL. The phage and gold nanoparticles were vortexed briefly in a 1.5 mL Eppendorf tube and then rolled overnight at room temperature.

### 2.3.6 Binding of M13pIIISeI and wild-type M13 to quantum dots

Quantum dots were purchased from Invitrogen where they are sold under the trade name of Qdot® Nanocrystals. Qdot ITK™ amino (PEG) quantum dots (8 µM solution supplied in borate buffer pH 8.3) were purchased that have a fluorescence emission wavelength at 525 nm (Cat No. Q21541MP) and 800 nm (Cat. No. Q21571MP). There are a number of differences between these quantum dots (Table 2.3).

**Table 2.3. Dimensions and composition of Qdot® nanocrystals.** Core/Shell diameter size was measured by TEM. Core/Shell/Polymer size and Core/Shell/Polymer/PEG size relates to the hydrodynamic size of the quantum dots as measured by size exclusion chromatography. Sizes were determined by retention times relative to a standard curve of protein standards. PEG layer size relates to the difference in Core/Shell/Polymer size and Core/Shell/Polymer/PEG size. Information provided by Invitrogen upon request.

Name	Core/Shell composition	Core/Shell size (nm)	Core/Shell/Polymer size (nm)	Core/Shell/Polymer/PEG size (nm)	PEG layer size (nm)
Qdot 525	CdSe/ZnS	3 to 4	12	13	1
Qdot 545	CdSe/ZnS	Approx. 4	13	14	1
Qdot 565	CdSe/ZnS	4.6	14	15	1
Qdot 585	CdSe/ZnS	5.3	15	16	1
Qdot 605	CdSe/ZnS	Ellipsoid: 4 x 9.4	16	16	Unknown
Qdot 625	CdSe/ZnS	8.1	Approx. 17	Approx. 16 to 20	Unknown
Qdot 655	CdSe/ZnS	Ellipsoid: 6 x 12	18	20	2
Qdot 705	CdSeTe/ZnS	Ellipsoid: 6 x 12	18.5	20.5	2
Qdot 800	CdSeTe/ZnS	Ellipsoid: 6 x 12	19	21	2

Qdots consist of a nanocrystal (the core) made of either cadmium selenide (CdSe) or cadmium seleno-telluride (CdSeTe) surrounded by zinc sulphide (the shell). This is then further encased within a polymer (propriety information) and a PEG layer to make the Qdot soluble in water (Figure 2.8)

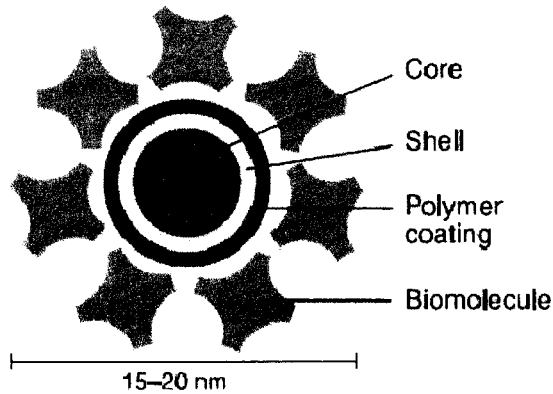


**Figure 2.8. The Qdot quantum dot from Invitrogen.** The diagram was taken from Invitrogen and shows the main structural elements of the Qdot; they are drawn roughly to scale relative to one another.

The Qdots were functionalised with sulfo-SMCC (Sulfosuccinimidyl-4-(*N*-maleimidomethyl)cyclohexane-1-carboxylate). Sulfo-SMCC is a water soluble compound that contains an amine reactive NHS-ester (*N*-hydroxysuccinimide) at one end and a sulfhydryl-reactive maleimide group at the other end (Figure 2.9).

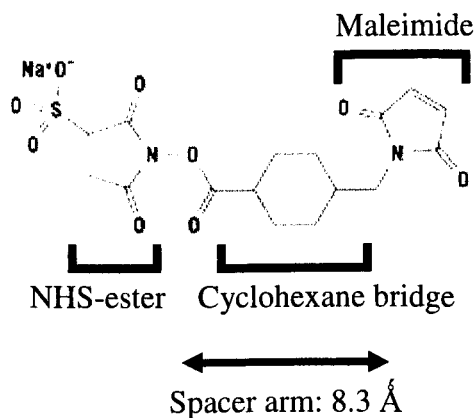


**Figure 2.9. The structure of sulfo-SMCC** (Sulfosuccinimidyl-4-(*N*-maleimidomethyl)cyclohexane-1-carboxylate). Molecular weight is 436.37. Image was taken from Thermo scientific Pierce Protein Research Products.

## Chapter 2

---

Since maleimide hydrolyses rapidly in water, sulfo-SMCC was always used fresh: to achieve this it was purchased as the pre-weight format (Thermo scientific Pierce Protein Research Products, Cat. No. 22622) where 2 mg of sulfo-SMCC come pre-weighed and sealed. The following protocol was adapted from that provided by Evident Technologies for their EviTag quantum dots. 2 mg of sulfo-SMCC (using the pre-weighed format) was mixed with 400  $\mu\text{L}$  50 mM sodium phosphate buffer pH 7.4. Typically it was found that sulfo-SMCC dissolved poorly; therefore, after 5 minutes of vigorous vortexing, 200  $\mu\text{L}$  of the cloudy mixture was added to 62.5  $\mu\text{L}$  8  $\mu\text{M}$  Qdot (525 nm or 800 nm) and 137.5  $\mu\text{L}$  50 mM sodium phosphate pH 7.4 (final volume 400  $\mu\text{L}$ ) in a 1.5 mL Eppendorf tube. The mixture was vortexed briefly and then left to stand at room temperature for 1 hour with brief vortexing every 15 minutes. Excess sulfo-SMCC was removed using a PD-10 desalting column (PD-10, GE Healthcare product number: 17-0851-01).

The PD-10 column was equilibrated with 25 mL of conjugation buffer (100 mM sodium phosphate buffer pH 7.2, 1mM EDTA). The 400  $\mu\text{L}$  Qdot/sulfo-SMCC mixture was loaded on the top of the PD-10 column and allowed to enter the column. 2.1 mL of conjugation buffer was then added on to the column and allowed to enter. It is important to allow the Qdots to enter the column before adding the 2.1 mL of conjugation buffer. The Qdots were then eluted from the column using 3.5 mL of conjugation buffer. In the case of 525 nm Qdot, they can be followed using UV light, whereas 800 nm can be followed with the naked eye as a brown band moving through the column. Typically the quantum dots eluted in a 1 mL fraction (a 16 fold dilution of the quantum dot stock). This gave a maleimide-functionalised Qdot solution of 500 nM (confirmed by spectrometry) in conjugation buffer.

100  $\mu\text{L}$  of  $10^{12}$  virions/mL phage (M13pIIISel or wild-type) were mixed with varying amounts of 500 nM maleimide-functionalised Qdot solution in a 1.5 mL Eppendorf tube and vortexed briefly before rolling overnight at room temperature.

### **2.3.7 Purification of phage:nanoparticle complexes on a linear sucrose gradient**

A 12 mL 30-60% linear sucrose gradient was prepared as in section 2.1.5.3. Phage mixed with nanoparticles (as in 2.3.4 and 2.3.5) were loaded onto the top of the gradient and spun at 18500 rpm using a SW40Ti rotor (Beckman Coulter, Cat. No. 331302) and the Optima L-XP ultracentrifuge overnight (typically 18 hours). The gradient was then fractionated using a gradient fractionator (section 2.1.5.4).

### **2.3.8 Purification of higher order structures using size exclusion chromatography**

An ÄKTAexplorer™ (GE healthcare) using the UNICORN software was used to control and monitor the column. A 90 cm (length) x 1.5 cm (width) column (volume ~150 mL) was filled with Sephacryl S-1000SF (superfine), commercially available from GE healthcare (Fairfield, Connecticut, U.S.A.), and equilibrated overnight with PBS pH 7.4. Phage:nanoparticle solutions (1 mL maximum) were applied under a flow rate of 0.5 mL/min and eluted with 1.5 times the column volume of PBS. 15 mL fractions were continuously collected in 15 mL falcon tubes. The absorbance at 260 nm and 280 nm were monitored using the monitor UV-900 included with the ÄKTAexplorer™. 5  $\mu\text{L}$  of each fraction was used for TEM (section 2.1.8). For small-scale experiments, a

GenElute™ spin column (Sigma-Aldrich, Cat. No. 5-6500) was used. 200 µL of sephacryl S-1000SF was loaded onto the column and washed three times with H<sub>2</sub>O by adding 400 µL of ddH<sub>2</sub>O and spinning the column on a table top centrifuge at 5000 xg for 5 minutes. This was then followed by a single 400 µL wash of PBS pH 7.4. Samples were then loaded onto the column and spun at 5000 xg for 5 minutes.

### **2.3.9 Fabrication of microphage higher order structures**

100 µL (concentration unknown) of M13pIIISel microphage produced as in 2.3.3 was mixed with 100 µL of citrate stabilised 10 nm gold nanoparticles in a 1.5 mL Eppendorf tube and incubated overnight with rolling at room temperature.

### 2.4 Specific Methods for Chapter 5

#### 2.4.1 Creation of pCGMTpIXHisACIDap and pCGMTpIXHisFOS

The DNA sequences corresponding to the HisACID (HHHHHHAQLEKEL QALEKELAQLEWENQALEKELAQLQSGGGSG) and HisFOS (HHHHHHL NDTLQAETDQLEDEKSALQTEIANLLNEKEKLEFIL AAHLQSGGGSG) peptides were PCR amplified (section 2.1.11.1) using overlapping DNA primers ACIDfor (ATC GAA GCT TCA CCA CCA CCA CCA CCA CGC GCA GCT GGA AAA AGA ACT TCA GGC GCT G), ACIDtemplate (GAA AAA GAA CTT CAG GCG CTG GAA AAA GAA CTG GCG CAG CTG GAA TGG GAA AAC CAG GCG), and ACIDrev (CGA TCT GCA GCT GCG CCA GTT CTT TTT CCA GCG CCT GGT TTT CCC A) for HisACID. For HisFOS the overlapping DNA primers FOSfor (ATC GAA GCT TCA CCA CCA CCA CCA CCA CCT GAC CGA TAC CCT GCA AGC GGA AAC CGA TCA), FOSTemplate (GCA GGC GGA AAC CGA TCA GCT GGA AGA TGA AAA AAG CGC GCT GCA AAC CGA AAT TGC GAA CCT GCT GAA AGA AA) and FOSrev (CGA TCT GCA GAT GCG CCG CCA GAA TAA ATT CCA GTT TTT CTT TTT CTT TCA GCA GGT TCG) were used.

The PCR products were then inserted into the HindIII and PstI sites of pCGMT-1b (kindly provided by Dr Bin Zhou, The Scripps Research Institute, La Jolla, CA, U.S.A.) using the method described in section 2.3.1. However HindIII (New England Biolabs, Cat. No. R0104L) and PstI (New England Biolabs, Cat. No. R0140L) were used instead of Acc65 I and Eag I and pCGMT-1b used instead of M13KE RF DNA. After transformation (section 2.1.3) into *E.coli* ER2738, 5 colonies of

pCGMTpIXHisACIDap and pCGMTpIXHisFOS were picked and sent for sequencing using pCGMTSEQFOR (AGG AAG CGG AAG AGC GCC CA).

### **2.4.2 Production of M13pIXHisACIDap and M13pIXHisFOS phage**

A single colony of either pCGMTpIXHisACIDap or pCGMTpIXHisFOS was picked and grown overnight at 37°C, 220 rpm, in 10 mL SB medium containing tetracycline, carbenicillin and 2% (w/v) glucose. The following day, 10 mL of the overnight culture was diluted into 1 L of SB medium, in a 5 L conical flask, containing tetracycline, carbenicillin and 2% (w/v) glucose. The culture was then grown at 37°C, 220 rpm, for ~3 hours until an OD<sub>600</sub> between 0.5-0.7 was reached. The 1 L of culture was then poured into a 6 L conical flask containing 4 L of SB medium. The following was added to the 5 L of diluted culture: tetracycline, carbenicillin, IPTG (final concentration 1 mM) and M13KO7 (final concentration 4 x 10<sup>8</sup> pfu/mL: New England Biolabs, Cat. No. N0315S). The 5 L culture was swirled gently to mix and left to stand at room temperature for 30 minutes and then incubated at 30°C, 220 rpm, for 2 hours. Kanamycin was then added and the 5 L culture divided into 5 x 1 L in 2 L flasks. The 5 flasks were then incubated at 30°C, 220 rpm, overnight. The phage were then PEG/NaCl purified as in section 2.1.5.1. Purified phage from the 5 L culture were pooled and re-suspended in 5 mL of Tris-HCl buffer.

### **2.4.3 Purification of M13pIXHisACIDap and M13pIXHisFOS phage**

M13pIXHisACIDap and M13pIXHisFOS phage were purified using a 5 mL HisTrap™ HP column (GE Healthcare, Cat. No. 17-5247-01). These are pre-packed with Ni

Sepharose High Performance resin charged with Ni<sup>2+</sup>. An ÄKTAexplorer™ (GE healthcare) using the UNICORN software was used to control and monitor the column. The column was first equilibrated with 3 column volumes (15 mL) of Tris-HCl buffer at a flow rate of 1 mL/min. The 5 mL of purified phage were then loaded onto the column at a flow rate of 0.5 mL/min using Tris-HCl running buffer. 3 column volumes were used to wash the column of any phage bound non-specificly. Elution of the bound phage was carried out at a flow rate of 1 mL/min using Tris-HCl buffer containing 400 mM imidazole (Sigma Aldrich, Cat. No. I0125). The concentration was increased from 0 mM (0%) so that at 40 mL the concentration of imidazole was 400 mM (100%). The column was then washed for a further 6 column volumes (30 mL) with Tris-HCl, 400 mM imidazole (100%). 1 mL fractions were continuously collected in 1.5 mL Eppendorf tubes. The absorbance at 260 nm and 280 nm were monitored using the monitor UV-900 included with the ÄKTAexplorer™. Fractions from 5 – 30 mL (which were found to contain the phage) were pooled and PEG/NaCl precipitated as in section 2.1.5.1. Purified phage were re-suspended in 1 mL PBS pH 7.5.

### **2.4.4 Creation and production of M13pIIIACIDap phage**

The DNA sequence corresponding to the ACIDap peptide (AQLEKELQALEKELAQL EWENQALEKELAQLQSGGGSG) was PCR amplified (section 2.1.11.1) using overlapping DNA primers pIIIACIDrev (ATC GCG GCC GAG CTT CCT CCT CCC TGC GCC AGT TCT TTT TCC AGC GCC TGG TTT TCC C), ACIDtemplate (section 2.4.1) and pIIIACIDfor (ATC TGG TAC CTT TCT ATT CTC ACT CTG CGC AGC TGG AAA AAG AAC TGC AG). The PCR products were then inserted into the Acc65 I and Eag I sites of M13KE using the method described in section 2.3.1. 5 colonies were

picked and sequenced with Seq-g3-for (section 2.1.7). One of the phage containing the correct sequence was used for further experiments and termed M13pIIIACID. M13pIIIACID was grown and purified as in section 2.1.5.1 and then further purified using caesium chloride as in section 2.1.5.2.

### **2.4.5 HPLC of ACIDap and BASEap peptides**

HPLC was performed on a Dionex (Sunnyvale, CA. U.S.A.) HPLC machine consisting of: P680 HPLC pump, ASI-100 Automated Sample Injection and PDA-100 photodiode (deuterium lamp was used) and controlled using the Dionex Chromeleon™ version 6.5 software. A 250 x 4.6 mm Zorbax C-18 silica gel with dimethyl-n-octadecyl silane column (Agilent Technologies, Santa Clara, CA. U.S.A.) was used with a C-18 guard cartridge (Phenomenex, Torrance, CA., USA, Cat. No. 880952-702). Two running buffers were used: Running buffer A was 5% (v/v) acetonitrile, 0.1% (v/v) trifluoroacetic acid (TFA) and B was 90% (v/v) acetonitrile, 0.06% (v/v) TFA in H<sub>2</sub>O. The buffers were 0.22 µm filter sterilised and degassed before use. Column was equilibrated overnight with buffer A at a flow rate of 0.1 mL/min. Peptides were re-suspended in 200 µL Tris-HCl buffer (final peptide concentration was 25 mg/mL) and loaded onto the column at a flow rate of 0.5 mL/min. 0.5 mL fractions were then collected in 1.5 mL Eppendorf tubes.

### **2.4.6 Circular dichroism (CD) spectroscopy of ACIDap and BASEap peptides**

CD was performed using a Jasco J715 Spectropolarimeter (Jasco, Great Dunmow, Essex, U. K.). 300  $\mu$ L of a 0.2 mg/mL solution of ACIDap or BASEap in PBS pH 7.4 were used. To measure the two peptides combined, 150  $\mu$ L of each solution were mixed in a 1.5 mL Eppendorf tube for 30 seconds before the sample was placed into the machine. The following parameters were used. Absorbance range: 190 nm to 260 nm, Data pitch: 0.2 nm, Scanning mode: continuous, Scanning speed: 50 nm/min, Response: 1, Band width: 1, Accumulate: 9.

### **2.4.7 Surface Plasmon Resonance (SPR) analysis**

SPR was performed using a Biacore 3000 (GE Healthcare) and carried out at room temperature. Sensor chips containing a bare gold surface (GE Healthcare, Cat. No. BR-1005-42) were used for experimental work. BASEap (AQLKKKLQANKKKLAQLKW KLQALKKKLAQGGGSC) was immobilised using gold-thiol chemistry in PBS pH 7.4 running buffer. All samples were in PBS pH 7.4 and injections carried out at a flow rate of 10  $\mu$ L/min. 50  $\mu$ L of 0.15 mg/mL of the control peptide and BASEap was injected across flow cell 2 and 3 respectively. Flow cell 1 was used as a bare gold surface control. PBS pH 7.4 buffer was then passed over the flow cells overnight at a flow rate of 10  $\mu$ L/min to obtain a stable baseline. 50  $\mu$ L of 1 mg/mL of ACIDap was then injected across the flow cells. For the phage samples the phage were PEG/NaCl precipitated and resuspended in running buffer so that the final concentration was  $10^{11}$  virions/mL. 40  $\mu$ L of each phage was then injected across the flow cells at a flow rate of

10  $\mu\text{L}/\text{min}$ . Kinetic data was obtained using the BIAevaluation software, version 3.2 (GE Healthcare). A 1:1 kinetic binding model was used to fit the SPR sensograms.

### **2.4.8 Dual Polarisation Interferometry (DPI) analysis**

DPI was performed using an AnaLight Bio200 optical evanescent DPI machine (Farfield Group Ltd., Manchester Airport, UK) connected to a microfluidics cell consisting of a Rheodyne HPLC injector valve and an external pump (Harvard Apparatus, PHD2000) which was used to control the flow of liquid through the DPI machine. All experiments were performed at 20 °C as controlled by the AnaLight Bio200 thermal control system (able to control temperature to within  $\pm 0.002^\circ\text{C}$ ). Unmodified AnaChip™ were used for experimental work (Farfield Group Ltd, Cat. No. 2007-110c). These are dual sample well silicon oxynitride sensor chips with negatively charged hydroxyl surface chemistry. Before experiments were carried out the sensor chips were piranha cleaned (section 2.5.4.1) and then immersed in a 4% (v/v) solution of mercaptotrimethoxysilane in isopropyl alcohol (IPA) for 18 h, followed by thorough rinsing in IPA. This gave the sensor chip waveguides a thiol exposed surface. The phase response of the sensor chip, and the PBS pH 7.4 running buffer, was then calibrated as follows (Johnson, 2008): PBS pH 7.4, was passed over both sensor sample wells at a flow rate of 50  $\mu\text{L}/\text{min}$  until a steady baseline was reached (~2 hours). This was followed by an 80% (v/v) ethanol/water solution injected over both waveguides for 2 min before reverting to PBS. 150  $\mu\text{L}$  of deionized water was then injected over both sample wells for 2 min before returning again to PBS.

## Chapter 2

---

BASEap (AQLKKKLQANKKKLAQLKWKLQALKKKLAQGGGSC) and a HPLC purified control peptide (SLDTLAEQLDPSANNVLSC: kindly provided by Dr Steve Johnson) were then immobilised onto the sample wells; sample well 1 with BASE and sample well 2 with the control peptide. This was done by injecting 150  $\mu\text{L}$  of 10 mM copper (II) chlorate solution twice over both sample wells. The copper (II) is reduced by the thiol surface to copper (I) which in turn can then be used to bind to the thiol group within a cysteine. 600  $\mu\text{L}$  of 1 mg/mL BASEap was then injected across sample well 1 at a flow rate of 20  $\mu\text{L}/\text{min}$ . This was followed by ~5 minutes of PBS running buffer at a flow rate of 20  $\mu\text{L}/\text{min}$ . The procedure was repeated to immobilise the control peptide onto sample well 2. The flow rate was then increased to 50  $\mu\text{L}/\text{min}$  for ~5 minutes to remove any unbound material. To study the ACIDap/BASEap interaction, the sensor chip was exposed to the ACIDap peptide (AQLKELQALEKELAQLEWENQALEKELAQ). The ACIDap peptide (1 mg/mL) was injected over sample well 1 and 2 at a flow rate of 20  $\mu\text{L}/\text{min}$  before returning to PBS running buffer and increasing the flow rate to 50  $\mu\text{L}/\text{min}$ .

### 2.5 Specific Methods for Chapter 6

#### 2.5.1 Display of tyrosine on pVIII

Tyrosine was inserted into position 4 of the major coat protein of pVIII via a single nucleotide substitution: G to T at position 1379 of the M13KE genome. Substitution was done using site directed mutagenesis with D to YpVIIIfor (TTC GCT GCT GAG GGT TAC GAT CCC GCA AAA G) and D to YpVIIIrev (CTT TTG CGG GAT CGT AAC CCT CAG CAG CGA A) with a QuikChange™ site directed mutagenesis kit (Stratagene, Cat. No. 200519) which uses the high fidelity *pfu* polymerase. Mutagenesis was carried out as in kit instructions using 100 ng of M13KE RF DNA as the template. Mutagenesis product was digested for 3 hours with *dpn* I before being transformed into NEB 5-alpha F'T<sup>+</sup> Competent *E. Coli* (New England Biolabs, Cat. No. C2992H). The transformation reaction was plated onto agar plates containing tetracycline using top agar and overnight *E.coli* culture as in section 2.1.3. The plates were then incubated overnight at 37°C. The following day, 10 plaques were picked and grown overnight at 37°C in 10 mL of 2xYT medium containing tetracycline. RF DNA was then purified from the cultures using a QIAprep spin miniprep kit (Qiagen, Cat. No. 27106). The 10 clones were then sent for sequencing; 8 were found to contain the correct mutation. One clone (termed M13Y) was used for further experiments.

M13Y RF DNA was transformed into chemically competent ER2738 (section 2.1.3) and then phage produced as in section 2.1.5.1. The phage were further purified on a caesium chloride gradient (section 2.1.5.2) and dialysed against three changes of PBS

buffer using a 100 kDa molecular weight cut off, cellulose ester, dialysis membrane (Spectra/Por, Cat. No. 131408).

### **2.5.2 Fabrication of gold coated phage in solution**

10  $\mu\text{L}$  of M13Y phage (and as controls 10  $\mu\text{L}$  of wild-type phage and 10  $\mu\text{L}$  of PBS pH 7.4), at a concentration of  $\sim 1 \times 10^{13}$  virions/ mL was added to 100  $\mu\text{L}$  of 6 mM gold salt (99.99% chloroauric acid/ gold (III) chloride solution which is supplied in approx. 2.9 M HCl: Cat. No. 484385) in a 1.5 mL Eppendorf tube and left for 1, 10, 30 and 60 minutes at room temperature. Samples were also left overnight and for 2 days at room temperature.

### **2.5.3 Deposition of M13Y onto carbon and incubation with gold salt**

5  $\mu\text{L}$  of M13Y, wild-type phage (at a concentration of  $5 \times 10^{10}$  virions in 20  $\mu\text{L}$  ddH<sub>2</sub>O) or ddH<sub>2</sub>O was applied directly to charged ultra-thin carbon-coated copper grids (Agar Scientific, Essex, U.K.). After 1 minute the liquid was removed carefully with filter paper. 10  $\mu\text{L}$  of 1 mM gold salt was added to the grid and left for 1 minute, 10 minutes, 30 minutes and 1 hour. The grids were placed in a humidity chamber (a petri dish with a moist cloth covering the bottom). The gold salt was then removed carefully with filter paper and the grid washed with 50  $\mu\text{L}$  of ddH<sub>2</sub>O. The grids viewed using a Philips CM10 or Jeol 1200EX transmission electron microscope at 80 keV.

### 2.5.4 Attempts to deposit gold on M13 adsorbed to SiO<sub>2</sub> surface

#### 2.5.4.1 Piranha cleaning of SiO<sub>2</sub> surface

1 cm<sup>2</sup> SiO<sub>2</sub> chips were prepared from a single sheet of SiO<sub>2</sub> (Compart Technology Ltd, Peterborough, U. K.). Piranha solution was prepared in a 100 mL beaker with 21 mL 95-97% sulphuric acid (Cat. No. 30743) and 9 mL of 35 wt. % in H<sub>2</sub>O fresh hydrogen peroxide (Cat. No. 349887). Piranha solution is very corrosive and it is important to carry out piranha cleaning in a fume hood and wear the necessary face mask, gloves and apron. Only ceramic tweezers should be used for transferring SiO<sub>2</sub> chips in and out of the piranha solution; any other material will corrode. Upon mixing, the solution should smoke slightly and the beaker becomes hot to the touch. SiO<sub>2</sub> chips were placed into the piranha solution for 10 minutes with the surface where sample was to be placed facing up. The chips should form bubbles on their surface. If not then the hydrogen peroxide is inactive and fresh hydrogen peroxide should be used. The SiO<sub>2</sub> chips were then moved to 50 mL of ddH<sub>2</sub>O in a 100 mL beaker and sonicated (Fisherbrand FB11020) for 5 minutes. During this time the piranha solution was poured away and the beaker washed thoroughly with ddH<sub>2</sub>O and dried with N<sub>2</sub>. This beaker was then filled with 30 mL 100% (v/v) isopropanol (Fisher Scientific, Cat. No. P/7500/PC17). The SiO<sub>2</sub> chips were transferred to the beaker containing isopropanol and sonicated for 5 minutes. The chips were then removed from the isopropanol and dried for ~30 seconds using a nitrogen spray gun. The SiO<sub>2</sub> chips were placed in a humid chamber, sealed with parafilm® (Alphalaboratories, Cat. No. WS5000-10), and aged overnight in a fume hood at room temperature.

### **2.5.4.2 Adsorption of M13 particles to SiO<sub>2</sub> surface and incubation with gold salt**

$5 \times 10^{10}$  virions, in 20  $\mu\text{L}$  ddH<sub>2</sub>O, of either M13Y or wild-type M13 were deposited on a piranha cleaned SiO<sub>2</sub> chip (section 2.5.4.1) for 30 minutes in a humidity chamber. Unbound phage were then washed off using distilled water, sprayed on from an angle at a constant stream from a bottle. The chip was then dried (from same angle as water) using a nitrogen spray gun until dry. Ensuring the angle is the same for the water and drying steps ensures that the phage are aligned in the same direction. 20  $\mu\text{L}$  of gold salt, between 1 and 6 mM, (or 1 mM hydrochloric acid) was then placed onto the chip and left for a specified time at room temperature in a humid chamber to stop evaporation. The SiO<sub>2</sub> chip was then washed and dried as above. Samples were viewed via atomic force microscopy (section 2.5.4).

### **2.5.5 AFM (Atomic Force Microscopy)**

AFM was carried out in tapping mode in air using a Veeco Dimension 3100 AFM. For scanning of M13 particles, the tip amplitude was adjusted so that the tip tapped as lightly as possible on the phage: i.e. amplitude was reduced until tip lost contact with surface and then the amplitude was increased until tip regained contact. Any harder tapping tended to result in no virus particle being observed.

### 2.5.6 Scanning Electron Microscopy of gold nanowires

M13 phage particles were incubated with gold salt as in section 2.5.4.2. The samples were then examined using a LEO 1530 Gemini FEGSEM with Oxford Instruments INCA 350 EDX system.

### 2.5.7 Conductivity measurements

M13 phage particles were incubated with gold salt as in section 2.5.4.2 on a SiO<sub>2</sub> surface with pre-fabricated gold crosses on (kindly fabricated by Dr Steve Johnson). To do this a 2 x 2 cm SiO<sub>2</sub> layer was piranha cleaned as in section 2.5.4.1. A 300 nm thick Poly(methyl methacrylate) (PMMA) layer was then spin coated onto the SiO<sub>2</sub> layer. A Raith 50 Electron Beam Lithography machine (Raith, Dortmund, Germany) was used to pattern 10 x 10 μm cross-hairs. The SiO<sub>2</sub> layer was then incubated in a 3:1 mixture of methyl isobutyl ketone for 70 seconds to dissolve the irradiated PMMA. An electron beam evaporator (Oerlikon, Pfäffikon, Switzerland) was then used to deposit a 150 nm thick layer of gold onto the SiO<sub>2</sub> layer. Finally, the SiO<sub>2</sub> layer was incubated in 100% (v/v) acetone overnight to lift off remaining PMMA. After the M13 phage particles had been deposited onto the SiO<sub>2</sub> layer and incubated with gold salt an AFM image was taken. The gold deposition process was then repeated using the AFM image to align the Raith 50 Electron Beam Lithography machine to pattern the electrodes at the ends of phage particles.

# Chapter 3

---

## The Microphage

This Chapter describes the work carried out to investigate using the 50 nm long microphage to produce bespoke length phage particles. The methods to purify these short phage were also investigated.

### 3.1 Introduction

#### 3.1.1 The Microphage

Wild-type M13 bacteriophage are approximately 1  $\mu\text{m}$  long with a diameter of 6 nm (Lee, 2002). The length of the phage particle is dictated by the size of the single stranded DNA genome of the phage. Increasing the length of the DNA strand results in an increase in length of the virion particle (Zinder, 1982). The opposite is also true: by deleting some of the DNA genome it is possible to create a smaller phage particle (Specthrie, 1992). The explanation for the link between DNA strand length and the length of the phage particle is the role played by the positively charged C-terminus on the pVIII coat protein in negating the ssDNA's negatively charged backbone (Hunter, 1988). On average each pVIII protein interacts with 2.3 nucleotides. It is therefore a physical link between the number of nucleotides and the number of pVIII proteins.

Whether there is an ultimate limit for the length of encapsulated DNA is unknown, although it has been observed, both in the literature (Lopez, 1983, Bradley, 1964, Caro, 1966, Marvin, 1963) and in this present study, that double and triple length phage do occur within a typical wild-type phage population. It has been shown that these dimer and trimer phage contain multiple phage DNA strands (Lopez, 1983), i.e. a trimer contains three distinct strands of wild-type length ssDNA. It is thought that this occurs when the pIII/pVI complex fails to “cap” the phage as it extrudes through the viral pore and so other ssDNA phage strands are encapsulated before a successful capping event (Lopez, 1983). Using pIII, pIX, pVI and pVII amber mutations, Lopez *et al.* (1983) produced phage with more than three ssDNA strands; although they failed to report the length of the longest of

these phage. However, the study does highlight that very large phage can be produced, with large amounts of DNA contained within. Obviously, the longer the phage, the higher the chance of shearing, as noted within Lopez *et al.*(1983), which perhaps explains why the phage genome is very economical with coding capacity and only encapsulates the amount of genomic information that is needed to replicate.

Using genetic engineering it is relatively easy to increase the length of the genome, and the intergenic region (IG) has been shown to be highly tolerant of DNA insertion (Herrmann, 1980), with up to 12 kb having been inserted in this way. In fact, the phage genome DNA sequence is irrelevant for the production of phage particles. All that is needed is the M13 origin of replication, which contains the packaging signal (PS) which is an invariant loop containing a 32 bp palindromic sequence (Shen, 1979, Lopez, 1983).

When a bacterial plasmid contains an M13 origin it is termed a phagemid. Transforming the phagemid into an F+ strain of *E.coli*, which is then super-infected with an infective phage particle (a helper phage), results in an ssDNA copy of the phagemid being encapsulated in a phage capsid. The explanation for this is that the viral proteins produced by the RF DNA of the helper phage recognize the phagemid M13 origin and act upon it as if it were a wild-type M13 origin. A huge variety of phagemids have been produced for scientific research (Alting-Mees, 1989, Gao, 2002, Krebber, 1997). Large numbers of the encapsulated phagemid can be produced allowing for large quantities, a few milligrams per milliliter (Vieira, 1987), of phagemid ssDNA to be isolated. DNA that has been cloned into the phagemid can then be sequenced (Short, 1988, Dotto, 1981)

## Chapter 3

---

As discussed above, it is relatively easy to create long phage particles. However, it is far more difficult to create a shorter phage particle since the filamentous phage are very economical with their genome, with all the viral genes closely packed together. Therefore removing enough DNA to create a significantly shorter phage particle requires the removal of the genes needed for the production of the phage proteins. Since each of the 11 genes is vital for phage particle production, the removal of any of them results in the loss of production of viable phage particles.

This does not mean that shorter phage cannot be propagated. It is a well characterized phenomenon that shorter phage particles are produced during phage growth in *E.coli* culture after repeated passages (Griffith, 1974). The more passages that are done with the phage, the larger the population of shorter phage produced (Horiuchi, 1983). These shorter phages, or miniphages, are typically 100 to 500 nm in length but are otherwise morphologically identical to wild-type phage (Griffith, 1974, Hewitt, 1975). The minimum length of these miniphage may be an artifact of the purification method used in the studies (see below). These phage only propagate in the presence of full-length phage (Hewitt, 1975), and even appear to have an advantage over full-length phage with regard to encapsulation (Griffith, 1974). Within the DNA packaged by miniphage it was found that the origin of replication was always present.

Specthrie *et al.* (1992) took this knowledge and showed that an even shorter “microphage” could be produced by creating a plasmid, termed pLS7, that synthesized a 221 base long piece of ssDNA containing only the M13 packaging signal. This 221 base ssDNA fragment leads to the production of a phage particle 45-50 nm long (Figure 3.1). At 50 nm long, it is half the length of the 100 nm long miniphage described by Griffith *et*

*al.* (1974). However, as mentioned above this may be due to the purification method used. Both of the original studies (Griffith, 1974, Hewitt, 1975) used a concentration of polyethylene glycol (PEG) concentration of between 4 and 10% w/v. PEG is used to “crowd” the phage out of solution, resulting in phage precipitates which can be pelleted. Specthrie, *et al.* had to use 15% w/v PEG in order to precipitate the 50 nm long microphage. Therefore, phage <100 nm may well be produced by multiple passages of wild-type infected *E.coli*, but they would not be purified by the methods used. Griffith and Hewitt highlight this weakness of their studies within their papers.

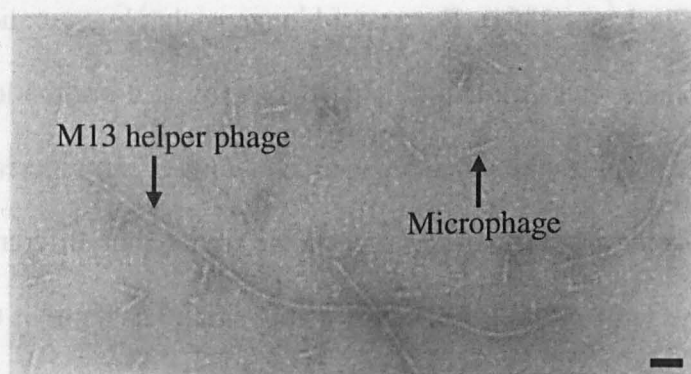


**Figure 3.1.** An electron micrograph of microphage particles. Taken from Specthrie, *et al.*, (1992). Scale bar equals 50 nm.

In order to create pLS7 (Specthrie, 1992) a functioning M13 viral origin of replication was placed upstream of the packaging signal (PS). A truncated (29 bases are deleted) M13 origin acts as a terminator of single strand DNA synthesis downstream of the PS. In between these two components is the packaging signal itself (Figure 3.2). The PS is needed for efficient encapsulation of the single stranded DNA by viral coat proteins (Clackson, 2004). By transfecting an *E.coli* cell containing pLS7 with a helper phage, a full-length phage which acts to provide all the proteins needed for encapsulation,

microphage particles can be produced. However, only 1- 3% of the phage population, by mass, was found to be microphage, the remainder consisted of helper phage.

Spethrie, *et al.* determined how small a phage particle could be produced. However, their work has an obvious application for M13 bacteriophage in respect for its use in bionanotechnology, i.e. the ability to control the length of a phage particle in order to produce a nanowire of a desired length. By inserting DNA into either the Hind III or EcoRI site of the microphage cassette (Figure 3.2) it should be possible to produce a phage particle longer than 50 nm, and this increase should be proportional to the amount of inserted DNA (Clackson, 2004). For many bionanotechnology applications the wild-type M13 bacteriophage, at 1  $\mu\text{m}$ , is too long. The ability to tailor the length of the M13 particle to a specific purpose has a great appeal and would greatly increase the versatility of the M13 phage for bionanotechnology. It could be argued that different size phagemids could be used for the same purpose. However, a very small phagemid is typically 1000 bp long, resulting in a phage particle of around 200 nm; therefore the microphage cassette is the only way to make phage particles smaller than 200 nm.

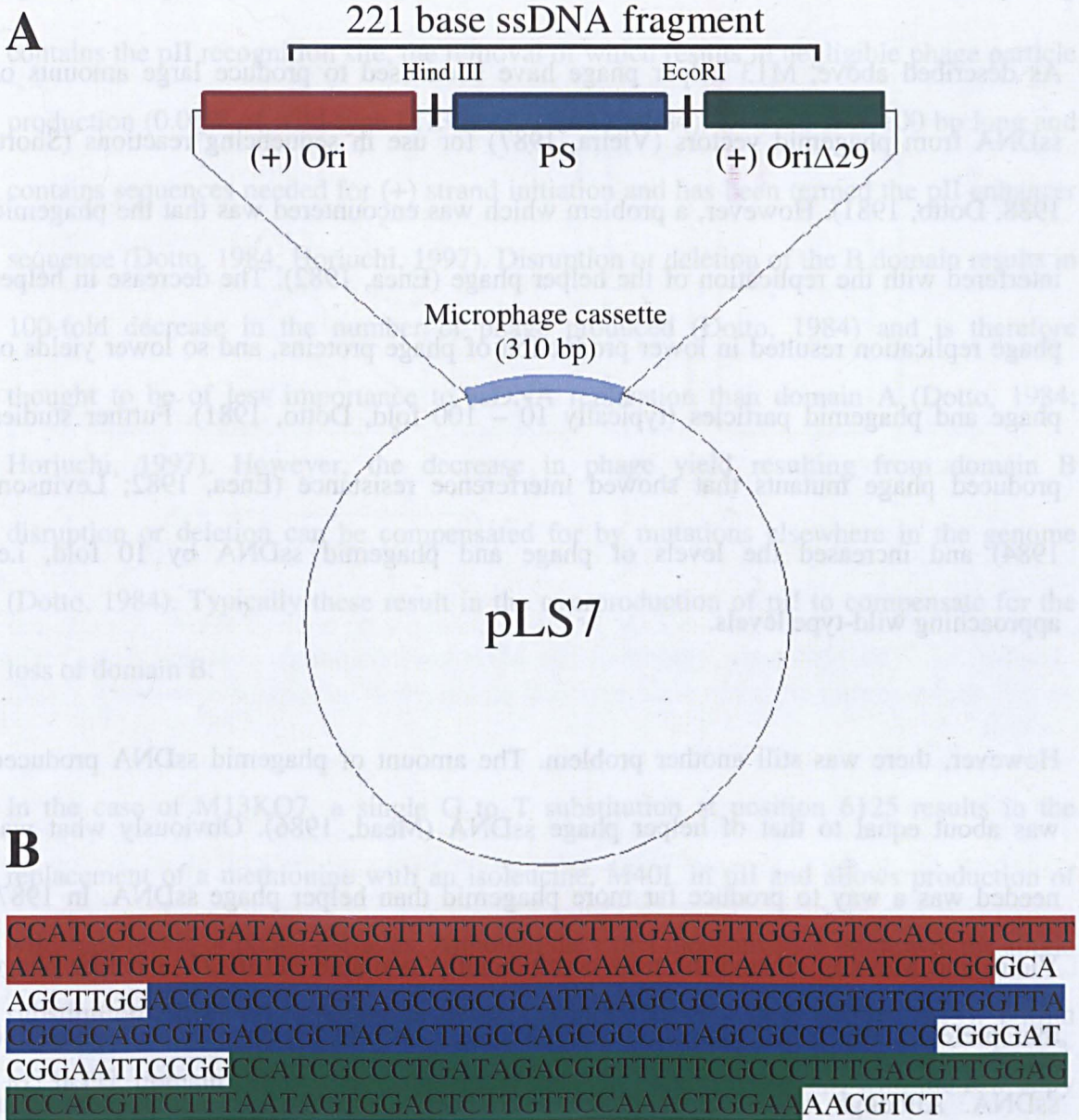


**Figure 3.2. The structure of the microphage cassette.** Diagram showing the structure of the microphage cassette situated within the pLS7 plasmid (A) created by Specthrie, *et al.*, (1992). Shows: origin of replication (+) Ori; packaging signal (PS); and (+) Ori $\Delta$ 29, which acts as ssDNA synthesis terminator. B shows the DNA sequence of the microphage cassette, with the sequences highlighted: (+) Ori (red); PS (blue); and (+) Ori $\Delta$ 29 (green). Adapted from Specthrie *et al.* (1992).

### 3.1.2 The Helper phage M13KO7

As described above, M13 helper phage have been used to produce large amounts of ssDNA from phagemid vectors (Vieira, 1987) for use in sequencing reactions (Short, 1988, Dotto, 1981). However, a problem which was encountered was that the phagemid interfered with the replication of the helper phage (Enea, 1982). The decrease in helper phage replication resulted in lower production of phage proteins, and so lower yields of phage and phagemid particles (typically 10 – 100 fold, Dotto, 1981). Further studies produced phage mutants that showed interference resistance (Enea, 1982; Levinson, 1984) and increased the levels of phage and phagemid ssDNA by 10 fold, i.e. approaching wild-type levels.

However, there was still another problem. The amount of phagemid ssDNA produced was about equal to that of helper phage ssDNA (Mead, 1986). Obviously what was needed was a way to produce far more phagemid than helper phage ssDNA. In 1987, Vieira and Messing created the now commercially available M13KO7: a helper phage that preferentially packs phagemid ssDNA and results in higher yields of phagemid ssDNA. Although other helper phage have been created which show preferential packaging, such as those described in Specthrie *et al.* (1992), M13KO7 is still the most widely used.

Gene II of the M13 bacteriophage produces a protein (pII) that creates a site-specific nick in the (+) strand of the RF dsDNA (Figure 3.3) within the origin of replication and so initiates the rolling circle replication of both ds and ssDNA. It also acts to terminate ssDNA synthesis by cleaving the displaced (+) strand (at the same site) and ligating the

two ends to form the circular strand of ssDNA. The 140 bp (+) strand origin of DNA synthesis (Figure 3.3) can be divided into two domains. Domain A which at 40 bp long contains the pII recognition site, the removal of which results in negligible phage particle production (0.01% of wild-type M13 levels, Dotto, 1984). Domain B is 100 bp long and contains sequences needed for (+) strand initiation and has been termed the pII enhancer sequence (Dotto, 1984; Horiuchi, 1997). Disruption or deletion of the B domain results in 100-fold decrease in the number of phage produced (Dotto, 1984) and is therefore thought to be of less importance to ssDNA replication than domain A (Dotto, 1984; Horiuchi, 1997). However, the decrease in phage yield resulting from domain B disruption or deletion can be compensated for by mutations elsewhere in the genome (Dotto, 1984). Typically these result in the overproduction of pII to compensate for the loss of domain B.

In the case of M13KO7, a single G to T substitution at position 6125 results in the replacement of a methionine with an isoleucine, M40I, in pII and allows production of wild-type levels of phage particles. Although the exact mechanism is unknown, the single substitution allows pII to recognize domain A in the absence of B (Dotto, 1984). Within M13KO7, domain B has been displaced at the Ava I site (Figure 3.3) with the low copy number bacterial origin of replication p15a and a kanamycin resistance gene. The p15a origin of replication allows M13KO7 to replicate within the cell independently of viral proteins, specifically pII. This means the phage can continue to express the correct levels of viral proteins for the production of ssDNA when in the presence of phagemid DNA, which as explained earlier, interferes with the helper phage DNA and lowers the expression of viral proteins. The kanamycin gene permits the for selection of the helper

phage, thus only allowing *E.coli* cells super-infected with the helper phage to grow, increasing the yield of encapsulated phagemid DNA (Vieira, 1987).

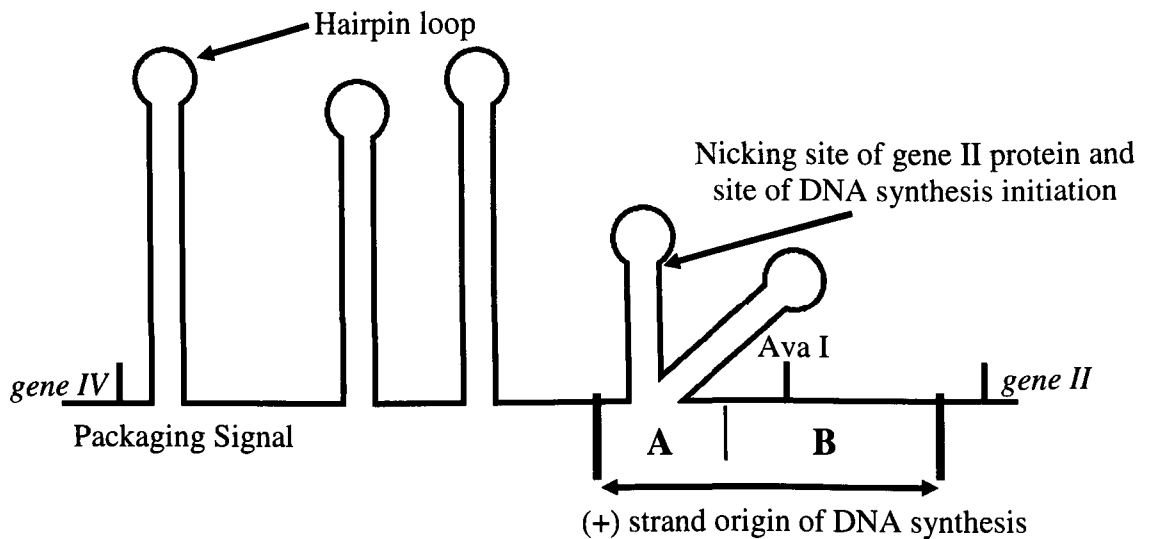


**Figure 3.3. The intergenic region of the M13 bacteriophage.** Adapted from Vieira, (1987).

Although the methionine to isoleucine substitution allows pII recognition of domain A at wild-type efficiency, when a phagemid is present within the cell with a fully wild-type origin of replication, the pII protein preferentially binds to the wild-type origin (Vieira, 1987). This results in the phagemid ssDNA being packaged instead of the helper phage DNA (Vieira, 1987) and leads to higher yields of phagemid ssDNA, e.g.  $>10^{11}$  colony forming units (cfu) compared to  $10^{10}$  cfu when using a wild-type helper phage. Although the phagemid DNA is preferentially packaged, some M13KO7 DNA is also packaged and this therefore results in a heterogeneous population of phage.

### 3.1.3 The Helper Plasmid

When Specthrie *et al.* (1992) produced the microphage they used a helper phage which resulted in 1-3% of the mass of phage produced being microphage. Further purification was used to purify a homogenous population of microphage, i.e. 15% w/v PEG, in order to remove the helper phage downstream. Although these techniques are straightforward, a simpler method to create a homogenous population of microphage is to remove the helper phage altogether from the production of microphage.

In 2006, Chasteen *et al.* at the Los Alamos National Laboratory in the U.S.A produced the plasmid pM13CP, or as they described it: “an M13 based helper plasmid” (Chasteen, 2006). They were attempting to overcome the same issue of helper phage contamination. At its most basic, it is merely an evolution of the M13KO7 helper phage. Instead of an interrupted origin of replication, and a compensatory mutation, they completely removed the viral origin of replication (Figure 3.4) and replaced it with the p15a origin of replication. The p15a origin is a low copy number bacterial origin of replication and plasmids containing the p15a origin are typically present at 10-15 copies per *E.coli* cell. As with M13KO7, the p15a origin allows for the viral plasmid to produce all the viral coat proteins. However, the lack of any viral origin of replication, specifically the packaging signal, results in no M13CP ssDNA being encapsulated (Chasteen, 2006) and so only phagemid ssDNA is packaged into phage particles. The yield was also found to be equivalent to M13KO7, thus making the M13CP helper plasmid an ideal replacement of the M13KO7 helper phage.

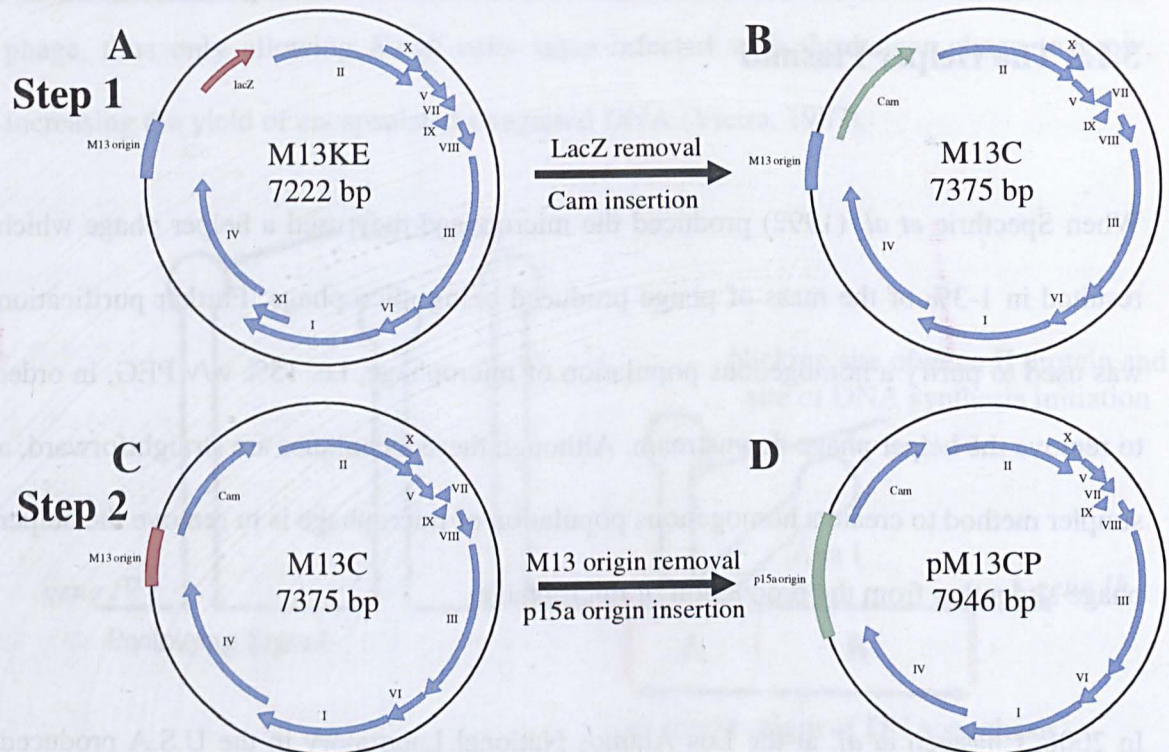


**Figure 3.4. Schematic of method used to create pM13CP.** Red indicates deletion of DNA whilst green indicates the addition of DNA. To create M13CP the *lacZ* gene was deleted (A) and replaced with a chloramphenicol resistance (*cam*) gene (B). The M13 origin was then deleted (C) and replaced with the p15a bacterial origin of replication (D).

### 3.1.4 Aims of the work described within this Chapter

1. To re-create the microphage plasmid and produce microphage using the M13KO7 helper phage
2. To re-create the M13CP helper plasmid and investigate its use in producing a homogenous population of microphage.
3. To investigate alternating the length of the microphage DNA cassette to produce different length phage.

## 3.2 Results and Discussion

### 3.2.1 Creation of microphage

The pMicro cassette (Spechthrie, 1992) was recreated and inserted into the pJet1.2 vector (purchased from Fermentas, York, U.K.): a high copy number vector containing the pMB1 bacterial origin of replication (Figure 3.5 A).

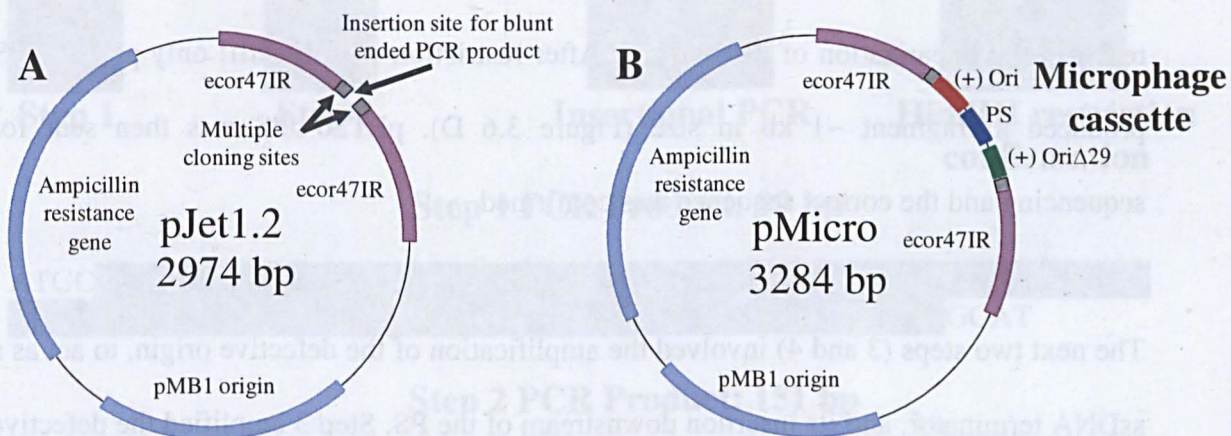


**Figure 3.5. Maps of the pJet1.2 (A) and pMicro (B) vectors.**

The creation of the microphage cassette involved four steps (Chapter 2, Table 2.1 lists the primers involved). Step 1 involved amplifying the packaging signal (PS), to create a 99 bp long fragment from pET26-b (Figure 3.6 A); this was followed by step 2 which involved further amplification of the PS fragment to add 25 bp flanking sequences either side of the PS that were complementary to pET26-b (Figure 3.6 B).

The DNA fragment from step 2 was then directly used as a primer for insertional PCR, which is a variation of site directed mutagenesis (Wang, 1999). Insertional PCR was performed to insert the PS downstream of the M13 origin of replication found in the

## Chapter 3

---

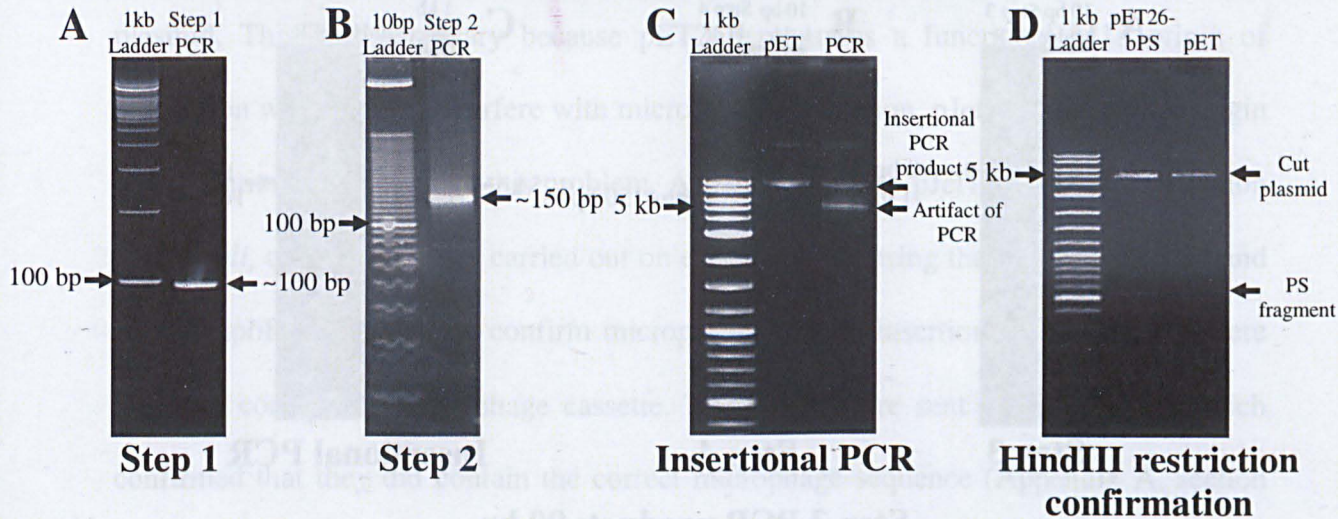
pET26-b vector. Figure 3.6 C shows that mutagenesis was successful due to the formation of an insertional PCR product. After transformation of the insertional PCR product, one colony was found. This was picked and cultured and the plasmid DNA (termed pET26-bPS) purified. To confirm that the PS had been successfully inserted into pET26-b, pET26-bPS and pET26-b were cut with the restriction enzyme HindIII. The microphage cassette contains a single HindIII site (Figure 3.6). Successful creation of pET26-bPS will result in two HindIII sites present within the plasmid compared to the single HindIII site present in pET26-b. Therefore restriction of pET26-bPS with HindIII should release a fragment of ~ 1kb, whilst restriction of pET26-b with HindIII should result in the linearization of the plasmid. After restriction with HindIII only pET26-bPS produced a fragment ~1 kb in size (Figure 3.6 D). pET26-bPS was then sent for sequencing and the correct sequence was confirmed.

The next two steps (3 and 4) involved the amplification of the defective origin, to act as a ssDNA terminator, and its insertion downstream of the PS. Step 3 amplified the defective origin from pET26-b to produce a 90 bp fragment (Figure 3.7 A). This was then amplified further with the step 4 primers to put pET26-bPS complementary overlaps onto the 90 bp fragment to produce a 136 bp fragment (Figure 3.7 B). The 136 bp fragment from step 4 was then used as the primer in insertional PCR with pET26-bPS as the template. After PCR a product was present (Figure 3.7 C) indicating that the reaction was successful. When transformed it gave a large number of colonies, ten of which were picked and used for sequencing. Eight of these confirmed the creation of the desired sequence (Appendix A, section 1.0). One was carried forward for further experiments and was termed pM1.

Microphage cassette

```

(+) Ori CCATCGCCCTGATAGACGGTTTTTCGCCCTTTGACGTTGGAGTCCACGTTCTTT
AATAGTGGACTCTTGTTCCAAACTGGAACAACACTCAACCCTATCTCGG GCA
PS AGCTTGGACGCGCCCTGTAGCGGGCGCATTAAAGCGCGGCGGGTGTGGTGGTTA
CGCGCAGCGTGACCGCTACACTTGCCAGCGCCCTAGCGCCCGCTCC CGGGAT
(+) Ori M13 CGGAATTCCGG CCATCGCCCTGATAGACGGTTTTTCGCCCTTTGACGTTGGAG
TCCACGTTCTTTAATAGTGGACTCTTGTTCCAAACTGGA AACGTCT
    
```



Step 1 PCR Product: 99 bp

```

ATGCACGCGCCCTGTAGCGGGCGCATTAAAGCGCGGCGGGTGTGGTGGTTACGC
GCAGCGTGACCGCTACACTTGCCAGCGCCCTAGCGCCCGCTCCGCAT
    
```

Step 2 PCR Product: 151 bp

Complementary to pET26-b vector HindIII site

```

AACACTCAACCCTATCTCGGGCAAGCTTGGACGCGCCCTGTAGCGGCGCATT
AAGCGCGGCGGGTGTGGTGGTTACGCGCAGCGTGACCGCTACACTTGCCAGC
GCCCTAGCGCCCGCTCCCGGGATCGGACAGGTGGCACTTTTCGGGGA
    
```

Complementary to pET26-b vector

Insertional PCR

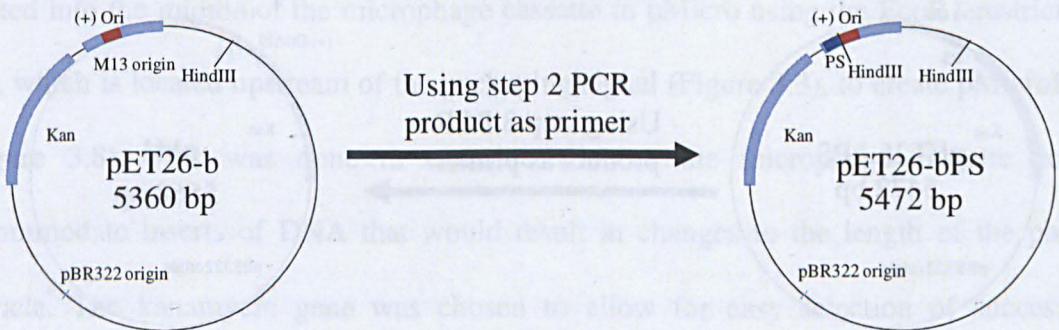
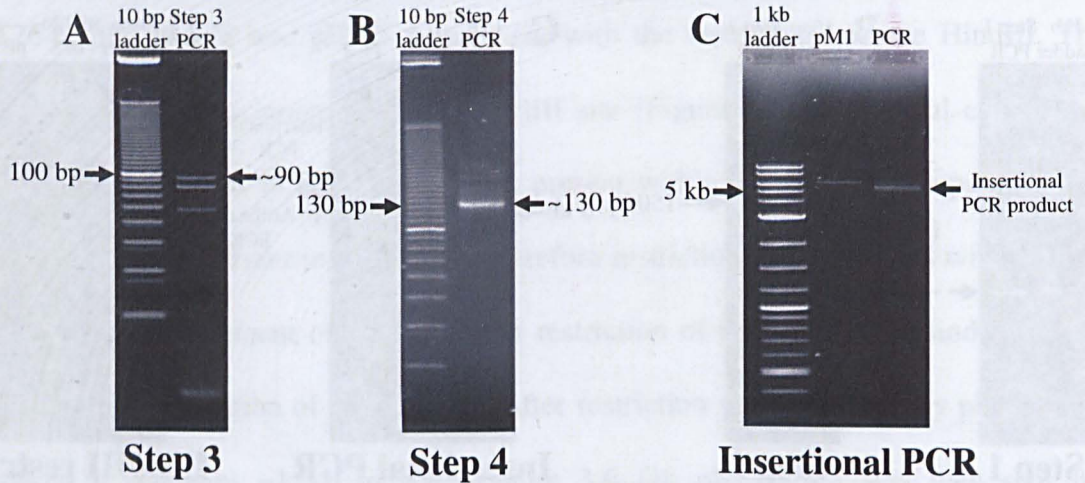


Figure 3.6. Insertion of packaging signal (PS) into the pET26-b vector. Shows 0.8% (w/v) agarose gels run at 120 V for 1.5 hours and stained with ethidium bromide.

**Microphage cassette**

```

(+) Ori CCATCGCCCTGATAGACGGTTTTTCGCCCTTTGACGTTGGAGTCCACGTTCTTT
AATAGTGGACTCTTGTTCCAAACCTGGAACAACACTCAACCCTATCTCGG GCA
AGCTTGG ACGCGCCCTGTAGCGGCGCATTAAAGCGCGGGCGGGTGTGGTGGTTA
CGCGCAGCGTGACCGCTACACTTGCCAGCGCCCTAGCGCCCCGCTCCCGGGAT
(+) OriΔ29 CGGAATTCCGG CCATCGCCCTGATAGACGGTTTTTCGCCCTTTGACGTTGGAG
TCCACGTTCTTTAATAGTGGACTCTTGTTCCAAACCTGGA AACGTCT
    
```



**Step 3 PCR product: 90 bp**

```

ATCG CCATCGCCCTGATAGACGGTTTTTCGCCCTTTGACGTTGGAGTCCACGT
TCTTTAATAGTGGACTCTTGTTCCAAACCTGGAATGAC
    
```

**Step 4 PCR product: 136 bp**

Complementary to pM1 vector

```

CGCCCCGCTCCCGGGATCGGAATTCCGG CCATCGCCCTGATAGACGGTTTTTCG
CCCTTTGACGTTGGAGTCCACGTTCTTTAATAGTGGACTCTTGTTCCAAACCTG
GAA AACGTCTCAGGTGGCACTTTTCGGGGA
    
```

Complementary to pM1 vector

**Insertional PCR**

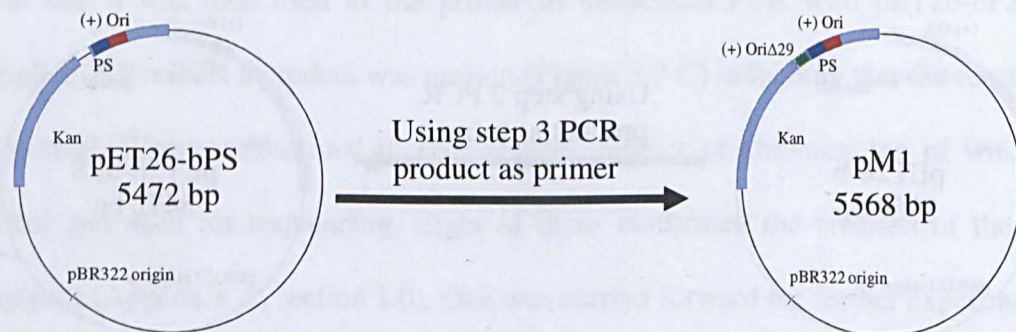


**Figure 3.7. Insertion of defective origin, (+) Ori $\Delta$ 29, into the pET26-bPS vector.**

Shows 0.8% (w/v) agarose gels run at 120 V for 1.5 hours and stained with EtBr

The microphage cassette, created in Step 4 (pM1), was then amplified using the Microamplifyfor and Microamplifyrev primers (Chapter 2, Table 2.1) which flank the 310 bp microphage cassette. This was then ligated into the pJet1.2 plasmid (Fermentas), a pre-cut plasmid with blunt ends and allows for simple insertion of PCR fragments into the plasmid. This was necessary because pET26-b contains a functional M13 origin of replication which would interfere with microphage production. pJet1.2 has no viral origin of replication and so avoids this problem. After ligation into pJet1.2, and transformation into *E.coli*, colony PCR was carried out on eight colonies using the Microamplifyfor and Microamplifyrev primers to confirm microphage cassette insertion. Four plasmids were found to contain the microphage cassette. These four were sent for sequencing which confirmed that they did contain the correct microphage sequence (Appendix A, section 2.0). Of these four, only one was carried forward for further experiments and was termed pMicro (Figure 3.5 B).

### 3.2.2 Creation of pMicroKan

A kanamycin resistance gene (1165 bp) was PCR amplified using the KanforecoR1 and Kanrevecor1 primers from pET26-b (Novagen). The kanamycin resistance gene was ligated into the middle of the microphage cassette in pMicro using the EcoR1 restriction site, which is located upstream of the packaging signal (Figure 3.3), to create pMicroKan (Figure 3.8). This was done to examine whether the microphage cassette could accommodate inserts of DNA that would result in changes to the length of the phage particle. The kanamycin gene was chosen to allow for easy selection of successful mutants that carried the correct insert. Ten colonies that grew on LB agar plates containing kanamycin were sequenced to confirm that the microphage cassette sequence

was correct and contained the kanamycin resistance gene in the correct position. One was used in further experiments and was termed pMicroKan (Appendix A, section 3.0).

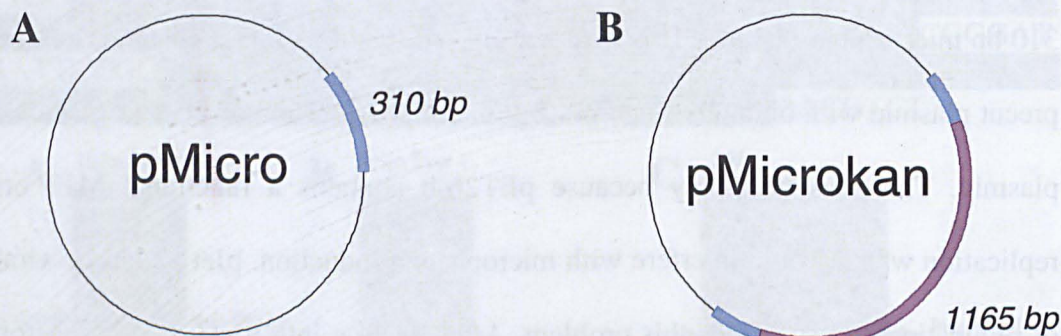


**Figure 3.8. Controlling the length of phage particles.** The plasmid pMicro (A) can be used as a scaffold to vary the length of phage. By inserting DNA into the 310 bp microphage cassette it is possible to control the length of the phage particles. In this case, a kanamycin gene was inserted to produce pMicroKan (B).

### 3.2.3 Creation of the pM13CP helper plasmid

Following the original paper (Chasteen, 2006), the *lacZ* gene and multiple cloning site (MCS), present in commercial strains of M13, were removed from M13KE (New England Biolabs) by PCR amplification using a high fidelity polymerase and the outward facing primers M13Mlu1for and M13Mlurev. These primers flanked the *lacZ* gene and MCS and resulted in a PCR fragment ~7 kb in length (Figure 3.9 A) which lacked the *lacZ* gene and MCS with Mlu1 restriction enzyme sites at either end. A chloramphenicol resistance gene (Figure 3.9 B) was then amplified from pACYC184 (New England Biolabs) using the primers pACYC184camfor and pACYC184camrev which resulted in a PCR fragment ~1 kb in length with Mlu1 restriction enzyme sites at either end. The chloramphenicol resistance gene was then ligated into the Mlu1 sites to produce a functional M13 bacteriophage (M13C) with chloramphenicol resistance.

The viral M13 origin of replication was then replaced by the low copy number p15a origin of replication by once again amplifying M13C with a high fidelity polymerase and the outward facing primers M13cpfor and M13cprev which produced a PCR fragment of ~8 kb in length (Figure 3.9 C) with Nco1 restriction sites at either end. The outward facing primers flanked the M13 origin of replication, resulting in this region being absent from the PCR fragment.

The p15a origin of replication (Figure 3.9 C) was amplified from pACYC184 using the primers p15afor and p15arev and then cloned into the Nco1 sites of the 8 kb M13C PCR fragment producing pM13CP. The low copy number bacterial origin of replication (p15a) was used in the original paper so that pM13CP mimicked the RF DNA form of the viral genome (Chasteen, 2006). There are 10-15 copies of RF DNA per cell, which is a similar copy number to a plasmid containing the p15a origin. By using this origin, a bacterial plasmid was produced lacking the M13 origin of replication and reported to produce all the proteins needed for phage assembly without packaging itself (Chasteen, 2006). pM13CP was then fully sequenced (Appendix A, section 4.0) and five silent mutations were found (highlighted in Appendix A, section 4.0).

### **3.2.4 Production of shorter phage using the helper plasmid pM13CP**

pMicro was first transformed into *E.coli* ER2738. A single colony was then grown, competent cells produced, and transformed with pM13CP so that a colony of *E.coli* contained pMicro and pM13CP. After growing overnight in a rich medium containing chloramphenicol and carbenicillin, the phage particles were purified using 15% w/v PEG and 0.5 M NaCl.

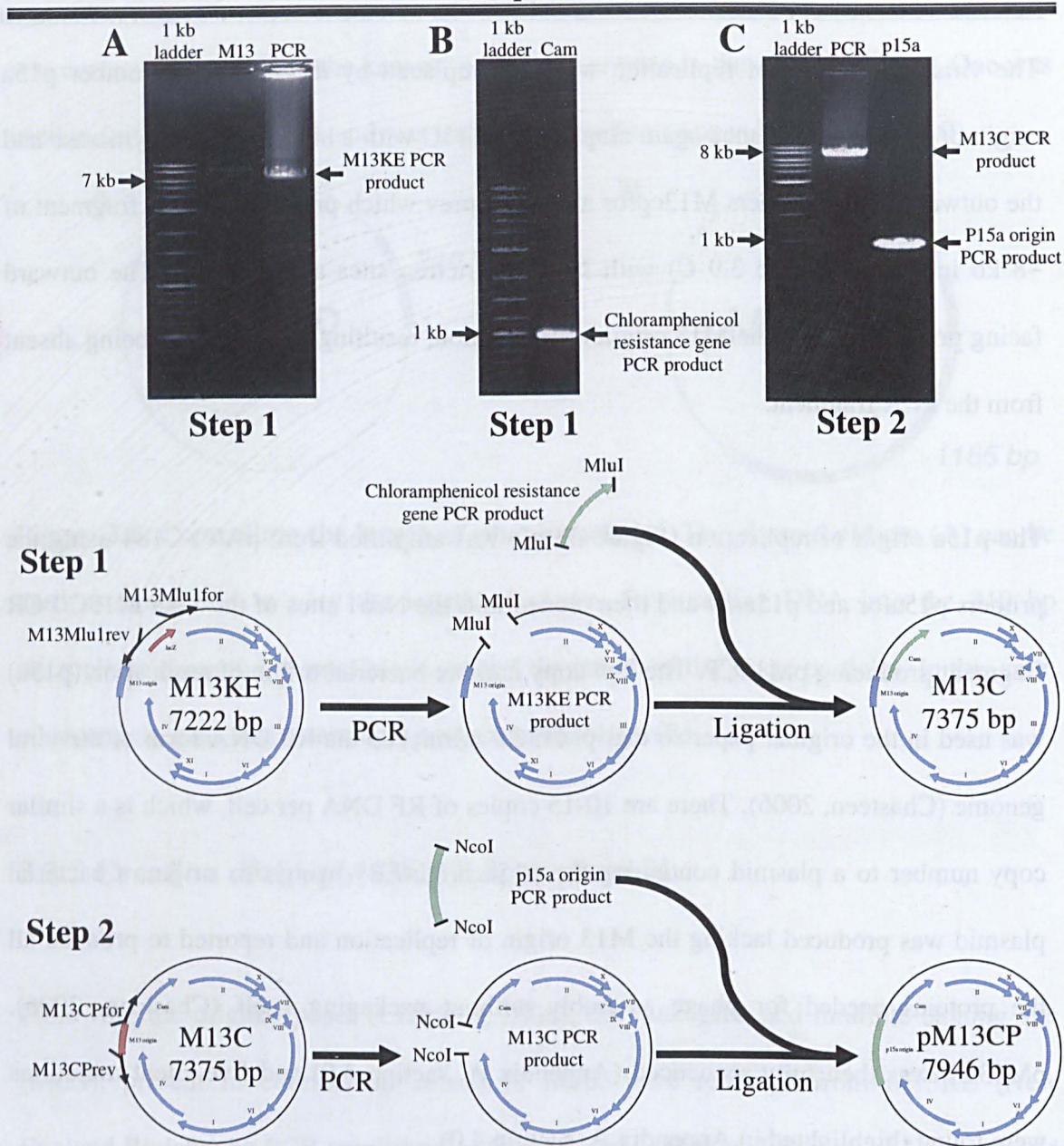


**Figure 3.9. Creation of pM13CP helper plasmid.** Shows 0.8% (w/v) agarose gels run at 120 V for 1.5 hours and stained with ethidium bromide.

Examination of the purified microphage with transmission electron microscopy (TEM) showed that only microphage particles were present (Figure 3.10 A). No wild-type length phage were seen. To confirm that the M13CP plasmid was not being packaged into phage particles an experiment from the original paper was repeated (Chasteen, 2006). M13CP was co-transformed with the commercial phagemid pLitmus28i. This phagemid

contains both a bacterial and an M13 origin of replication. Therefore when M13 assembly proteins are present, the pLitmus28i phagemid should be packaged. This was done so that phage concentrations could be titered since the microphage cassette is unable to replicate inside an *E.coli* cell and contains no antibiotic resistance gene.

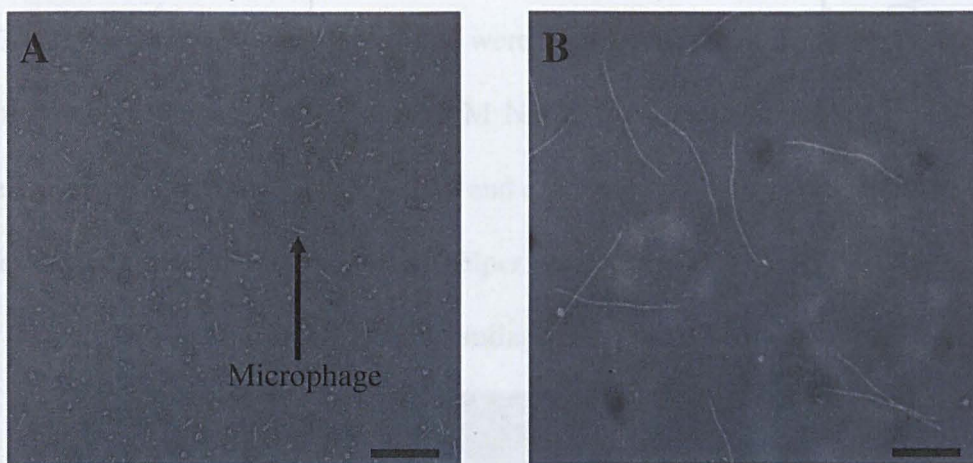


**Figure 3.10.** Phage produced using pM13CP and pMicro (A) and pLitmus 28i (B).

Scale bar equals 200 nm.

*E.coli* containing either, pM13CP, pLitmus28i, both pM13CP and pLitmus28i, or no plasmid, were grown overnight and phage particles PEG precipitated and re-suspended in 1 mL of PBS. 10  $\mu$ L of each sample was mixed with *E.coli* for one hour before being spread on agar plates containing either ampicillin or chloramphenicol. After incubation overnight at 37°C the number of colonies on each plate was counted (Figure 3.11). Only samples originating from *E.coli* containing both plasmids produced colonies and grew only on the ampicillin plates. These results indicate that the M13CP plasmid was behaving as expected, i.e. that it was unable to package itself into a phage particle and could only produce phage particles when a plasmid containing the M13 origin of replication was present. This was further confirmed by electron microscopy where only phage particles approximately 400 nm long, the predicted length of phage particles

encapsulating pLitmus28i, were seen in the sample originating from cells containing both the plasmids (Figure 3.10 B). Once again no wild-type length phage were observed.

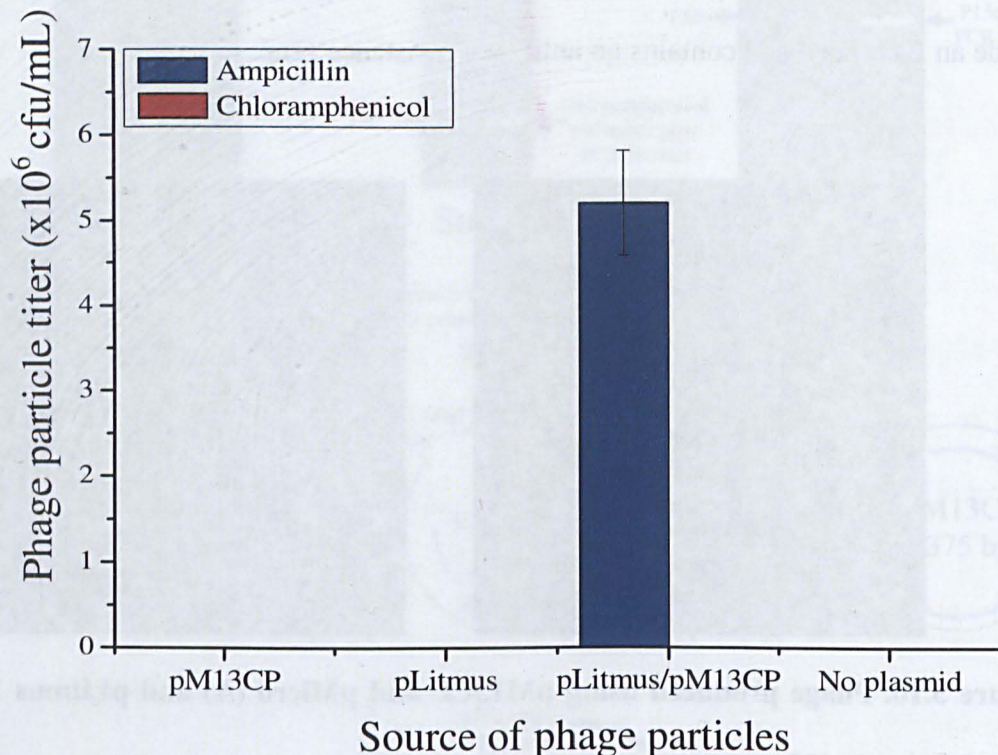


**Figure 3.11. Titer of pLitmus28i and pM13CP.** Results an average of 3 titers. Error bar shows standard deviation.

However, the phage titer was very low ( $\sim 5 \times 10^6$  cfu/mL). The original paper (Chasteen, 2006) states that titer levels using pM13CP were equivalent to those using the M13KO7 helper phage ( $\sim 10^{11}$  cfu/mL). No satisfactory explanation can be given for such a wide discrepancy in phage titer. With no sequence data available for the original pM13CP plasmid it is impossible to compare the plasmid produced in this study with the original. It may be that their plasmid contains a beneficial mutation that increases phage titer.

The amount of phage produced by pM13CP in this study was too low to allow for further experiments; therefore pM13CP was not used to create any further phage particles.

### 3.2.5 Production of shorter phage using the helper phage M13KO7

Since M13CP failed to work to expectations, the M13KO7 helper plasmid was used to produce different length phage. Therefore a colony of *E.coli* ER2738 containing pMicro was grown until early log phase, super-infected with the commercial helper phage M13KO7 and grown overnight. The phage were then purified from the supernatant by precipitation with 15% (w/v) PEG and 0.5 M NaCl. Upon centrifugation a small pellet was observed. This was resuspended in PBS and a sample was viewed using TEM. It was found that the sample contained a mix of helper phage (Figure 3.12 B) and 50 nm long particles (Figure 3.12 A), morphologically similar to the helper phage.

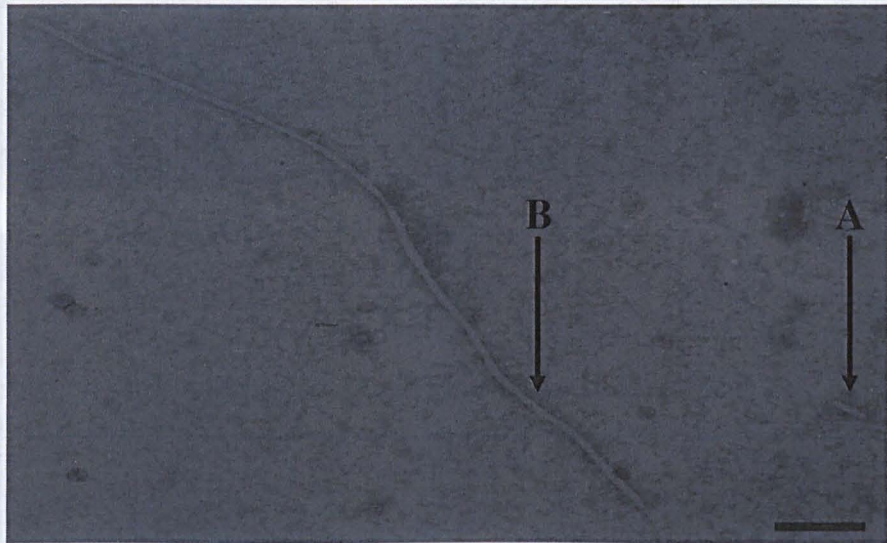


**Figure 3.12. Production of microphage.** A representative electron micrograph of microphage (A) produced by the super-infection of *E.coli* containing pMicro with M13KO7 helper phage (B). Due to the insertion of the chloramphenicol resistance gene and p15a origin of replication the M13KO7 phage are ~1350 nm long. Scale bar equals 100 nm.

### 3.2.6 Production of different length phage and purification

Using the same method as in 3.3.5 two other shorter phage particles were produced. This was done using pMicroKan (1324 bases) and the commercial phagemid pLitmus28i (2832 bases). pLitmus28i was chosen as a cheaply available phagemid control. pLitmus28i contains an ampicillin resistance gene and since the entire phagemid is encapsulated to produce phage it could be used to measure phage titers. After production of the shorter phage particles, including M13KO7 helper phage, and PEG purification (15% PEG, 0.5 M NaCl) the phage were further purified on a linear sucrose gradient (Figure 3.13) in order to separate the shorter phage from the M13KO7 helper phage.

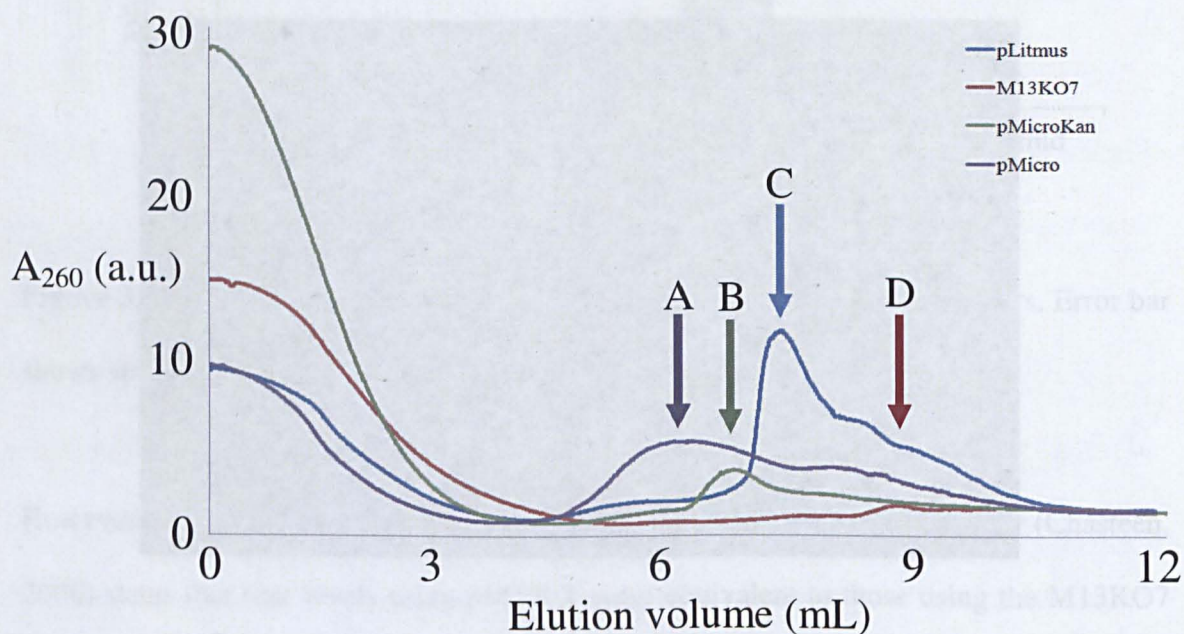


**Figure 3.13. Linear sucrose gradient fractionation of different length phage particles.** 100 ml of overnight culture of *E.coli* containing the different length phage particle plasmids, super-infected with M13KO7, were precipitated with 15% (w/v) PEG, 0.5 M NaCl and resuspended in 500  $\mu$ L PBS. The 500  $\mu$ l was then loaded on top of a 12 mL 30-60% (w/v) linear sucrose density gradient and centrifuged for 20 hours at 18500 rpm. The gradients were then fractionated and the absorbance at 260 nm recorded.

## Chapter 3

It was observed that each phage particle sedimented different distances into the sucrose gradient (Figure 3.12). pMicroKan, pLitmus28i and M13KO7 gave relatively sharp peaks (B, C and D, respectively). pMicro gave a very broad peak (A). Each peak was collected and a sample viewed under TEM (Figure 3.14). Each peak contained a homogenous population of phage (Figure 3.17). Most importantly, the shorter phage particle peaks (pMicro, pMicroKan and pLitmus28i) contained no helper phage.

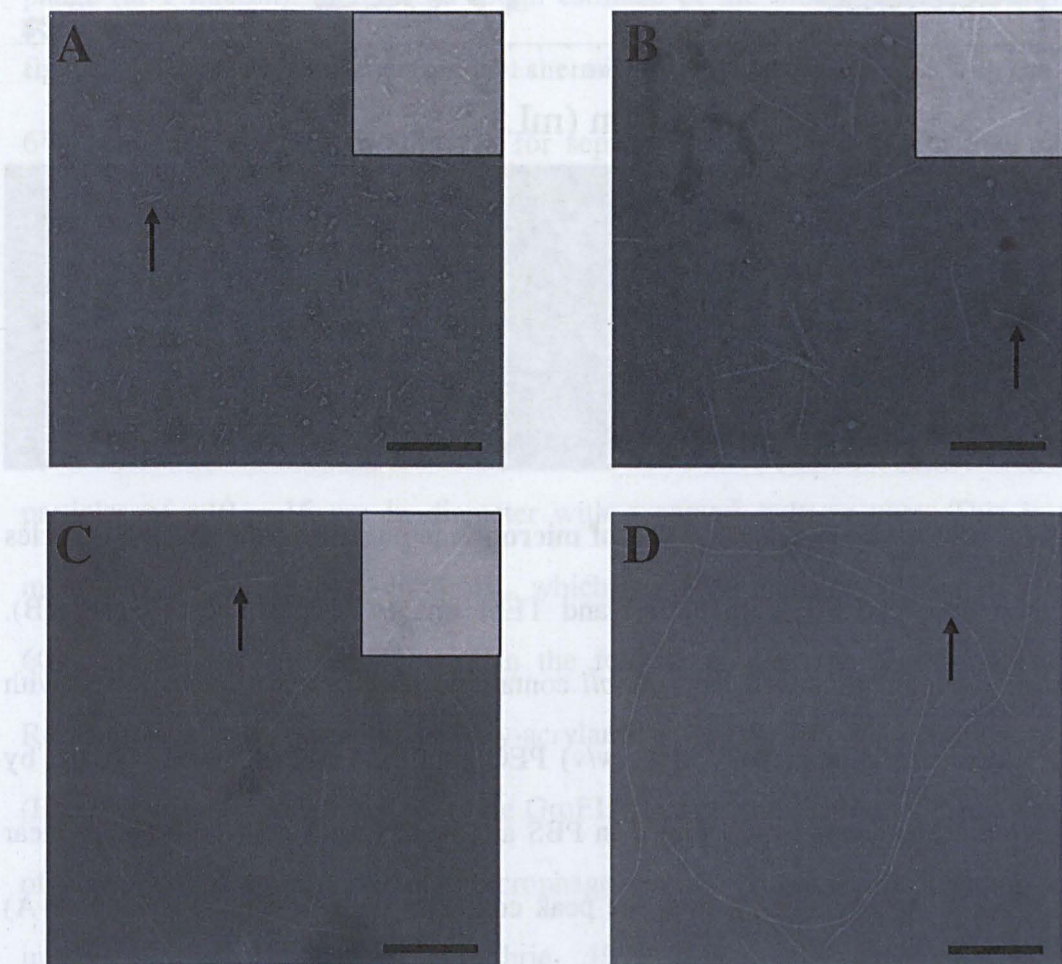


**Figure 3.14. Transmission electron micrographs of gradient fractionated phage particles; pMicro (A); pMicroKan (B); pLitmus (C); and M13KO7 helper phage (D).** Scale bar equals 200 nm. Arrows highlight phage particles. A to C inset show image at same scale but at higher contrast and brightness.

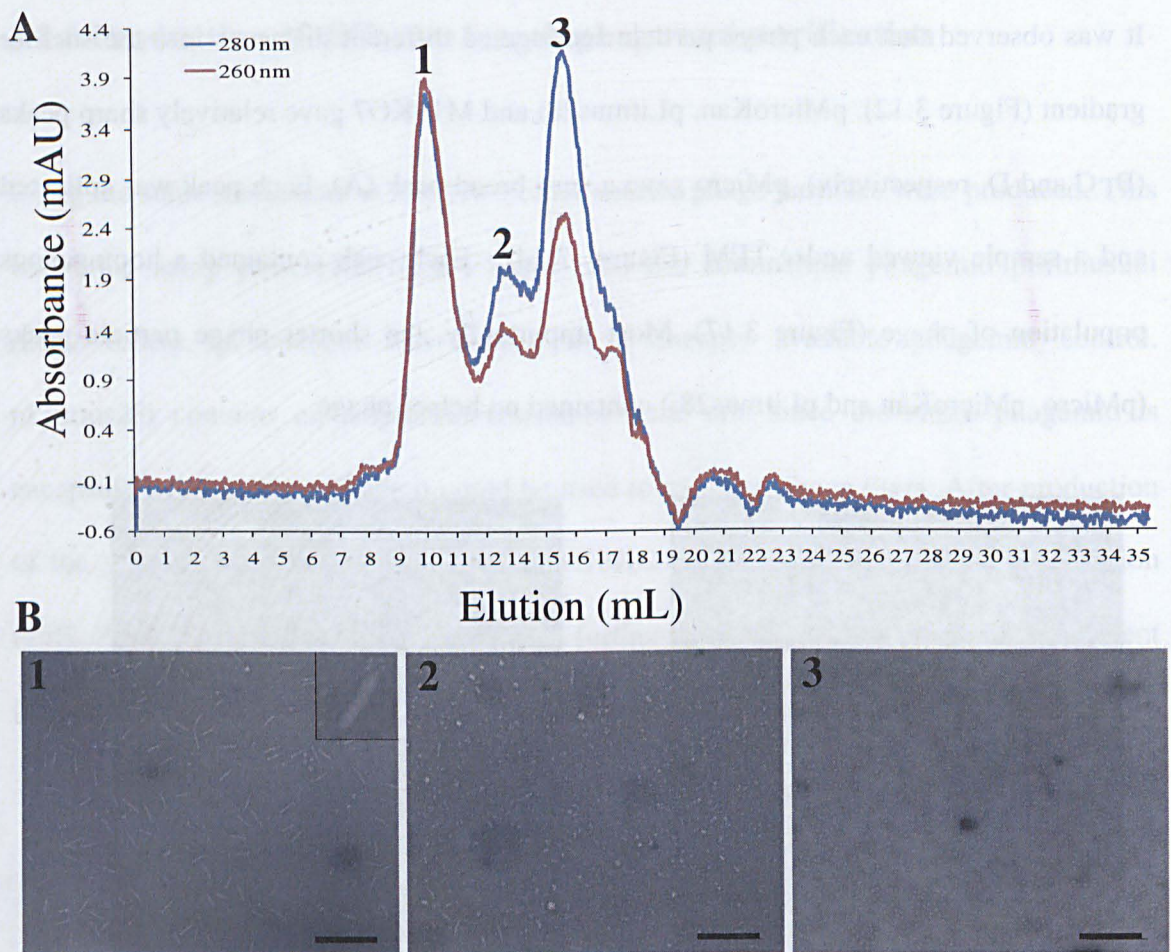


**Figure 3.15. Size exclusion purification of microphage particles.** Microphage particles applied to a Superose 6™ column (A) and TEM images of peaks 1, 2 and 3 (B). Microphage particles, produced from *E.coli* containing pMicro and super-infected with M13KO7, were precipitated with 15% (w/v) PEG-8000, 0.5 M NaCl and pelleted by centrifugation. These were re-suspended in PBS and loaded onto a 30-60% (w/v) linear sucrose gradient. After centrifugation, the peak containing microphage (Figure 3.13 A) was collected and dialyzed against PBS. Phage were then PEG precipitated and re-suspended in 500  $\mu$ L of PBS. 10  $\mu$ L was then loaded onto a Tricorn™ column (1 cm diameter, 25 mL volume, 30 cm bed height) packed with Superose 6™ (protein separation range of  $5 \times 10^3$  -  $5 \times 10^6$  Da). The column buffer (PBS) was run at a flow rate of 0.5 mL/min and absorbance measured at 260 and 280 nm. 35 1 mL fractions were collected. 5  $\mu$ L of each fraction was viewed using TEM. Scale bar equals 200 nm.

## Chapter 3

---

As a final step of purification, the microphage from the sucrose gradient were fractionated by gel filtration on a Superose 6™ column (GE Healthcare, Little Chalfont, U.K.). The molecular weight of a wild-type M13 particle is  $12 \times 10^6$  Da (Berkowitz, 1980; Ling, 2004). This is outside the fraction range of a Superose 6™ column, which has a range of  $5 \times 10^3$  to  $5 \times 10^6$  Da, and so the phage would be eluted in the column void volume. At 50 nm, the microphage is approximately 20 times shorter than the wild-type phage (at 1 micron), therefore a rough estimate of the molecular weight provides the figure of  $0.6 \times 10^6$  Da, indicating that the microphage should interact with the Superose 6™ column and therefore allowing for separation. Applying the purified microphage sample to the column resulted in three peaks (labeled 1 to 3 in Figure 3.15 A).

Examination of these peaks showed that the first peak contained a pure fraction of microphage (Figure 3.15 B 1). The third peak (Figure 3.15 B 3) contained spherical particles of ~10 – 15 nm in diameter with a central hole or pore. This is a similar morphology to the chaperonin GroEL, which is a dual-ringed tetradecamer comprised of 60 kDa subunits and is involved in the folding of proteins (Zeilstra-Ryalls, 1991). Running peak 3 on a denaturing poly-acrylamide gel revealed a single band at ~60 kDa (Figure 3.16), which is the size of the GroEL subunit, and further indicates the presence of GroEL in the sucrose purified microphage sample. Examination of the original TEM image of the microphage (Specthrie, 1992, Figure 3.1) indicates that GroEL contamination of the microphage particle has always been an issue. The second peak (Figure 3.15 B 2) appeared to be a mix of GroEL, microphage and irregular structures, most likely aggregated protein.

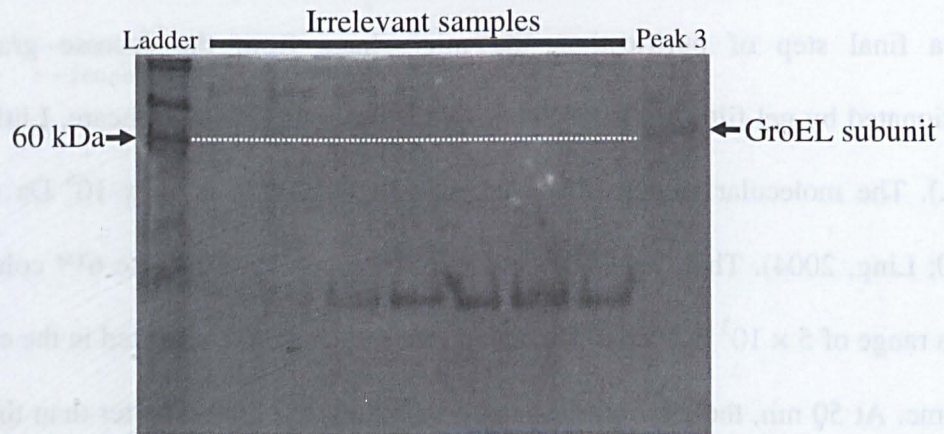


**Figure 3.16. Denaturing PAGE analysis of GroEL.** Peak 3 from Figure 3.15 was run on a 10% (v/v) denaturing poly-acrylamide gel. Gel was run for 2 hours at 8 W and stained with coomassie blue.

### 3.2.7 Examination of shorter phage particles

The shorter phage all exhibited similar morphology to wild-type phage (Figure 3.14); with pIII molecules clearly present on the microphage after purification (see Figure 3.15 B1 inset). Since there is a linear relationship between the length of ssDNA and the length of the phage (Specthrie, 1992), populations homogenous in length should be produced by pMicro, pMicroKan and pLitmus28i after purification from helper phage. Therefore 500 individual phage particles, from each purified phage peak on the sucrose gradient (Figure 3.13 A to D), were measured using ImageJ (Abramoff, 2004) to ascertain the homogeneity of the population (Figure 3.17). The result clearly shows that the shorter phage particles (pMicro and pMicroKan) have less homogeneity than the longer pLitmus28i phage. However, this has probably arisen from measuring errors. Figure 3.17 also highlights a result which differs to that of the original microphage paper (Specthrie, 1992). Within the microphage they produced, two distinct populations were observed at 45.5 and 50.5 nm. However, within this study, those populations were not observed

(Figure 3.17) with only a single population between 46 and 49 nm: a result more in agreement with the theoretical length of 49 nm. Whether this is an important result or down to different measurement methods or degradation of their phage particles is difficult to ascertain.

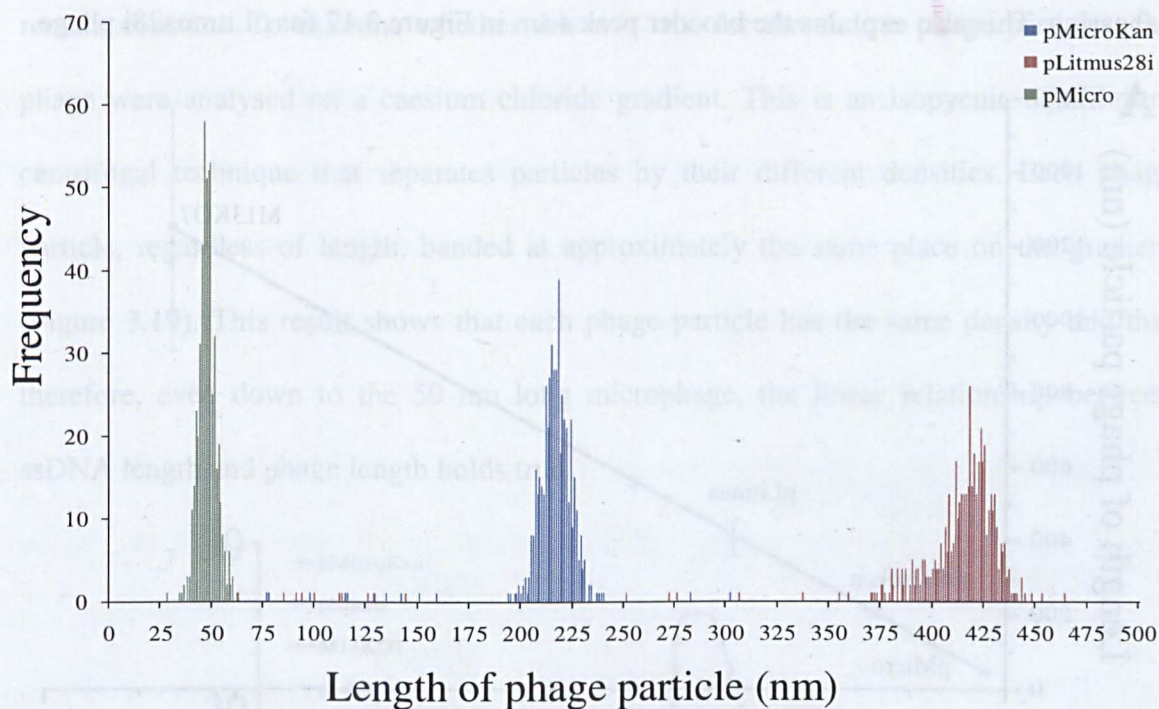


**Figure 3.17. Homogeneity of shorter phage particle populations.** 500 individual particles were measured from phage produced from pMicro, pLitmus28i and pMicroKan using M13KO7 helper phage and purified on a 30-60% (w/v) linear sucrose gradient to remove M13KO7. These samples were not gel purified. Phage particles were measured using ImageJ (see Chapter 2, section 2.2.11).

The different phage particles produced showed the expected length dependency with the amount of DNA being packaged (Figure 3.18 A). As the phage length increased the phage population also showed greater length variance, e.g. M13KO7 has a wide range of lengths (Figure 3.18 A). There are two reasons for this variance. The first is that longer phage are produced by the natural phenomenon of incorrect pIII/pVI capping of mature

phage particles (Griffith, 1974) resulting in the phage particle not detaching from the *E. coli* cell and so allowing for a second or third M13 genome to enter the phage particle before successful capping. The second is that shorter phage are likely to result from shearing during purification. The longer the phage particle, the more the likelihood of shearing. This also explains the broader peak seen in Figure 3.17 for pLitmus28i phage.

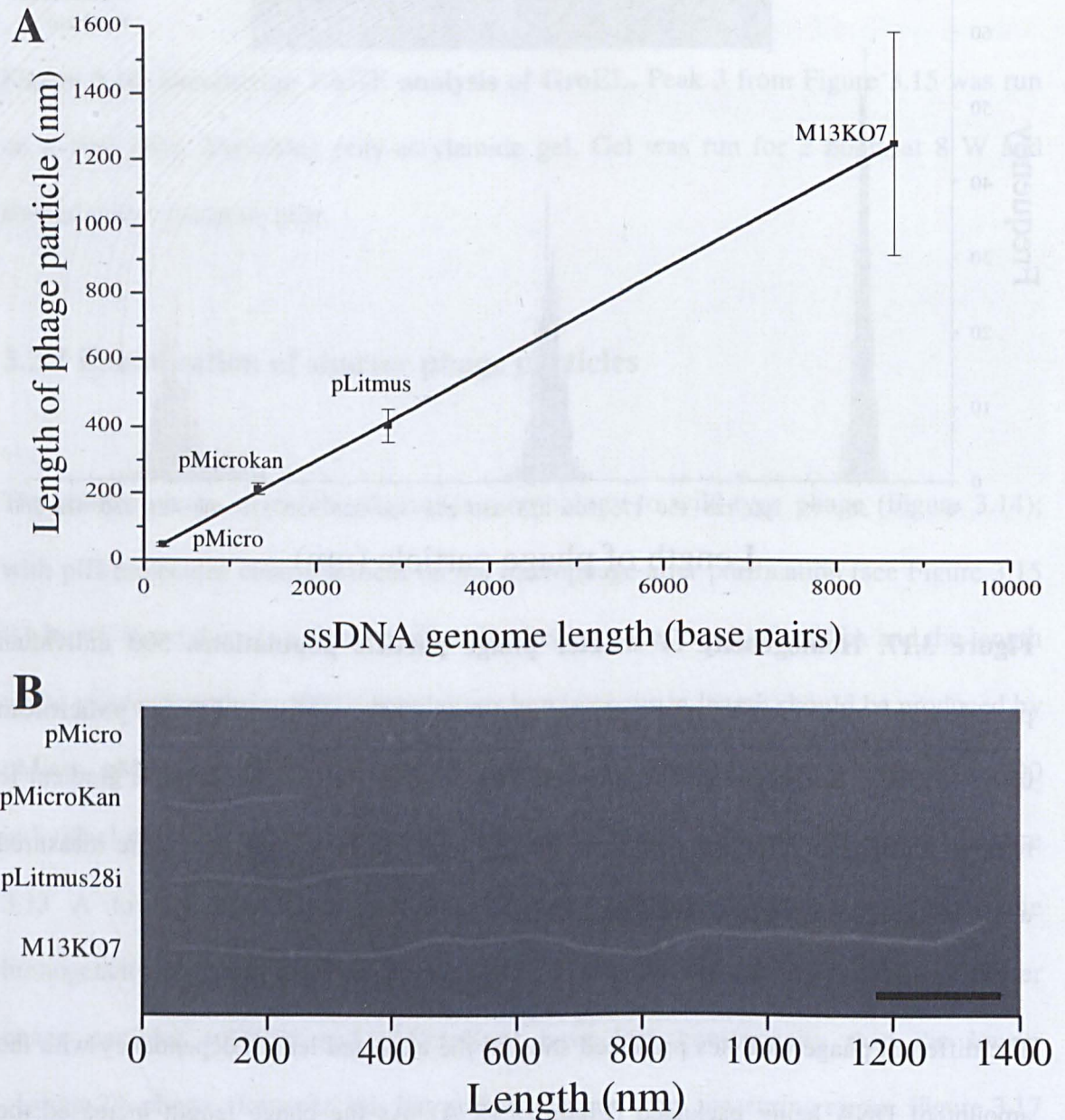


**Figure 3.18. The length of different phage particles.** A graph showing the relationship between the length of phage particles and the length of the ssDNA genome (A) with the error bars showing standard deviation (N = 500). B shows representative images of each

phage particle where the phage have been aligned from separate images using Adobe Photoshop™. Scale bar equals 200 nm.

The linear relationship between the length of ssDNA and length of phage particle should result in each phage particle having the same density, since the mass/unit length should remain constant. To examine whether this was true for the shorter phage particles, the phage were analysed on a caesium chloride gradient. This is an isopycnic equilibrium centrifugal technique that separates particles by their different densities. Each phage particle, regardless of length, banded at approximately the same place on the gradient (Figure 3.19). This result shows that each phage particle has the same density and that therefore, even down to the 50 nm long microphage, the linear relationship between ssDNA length and phage length holds true.

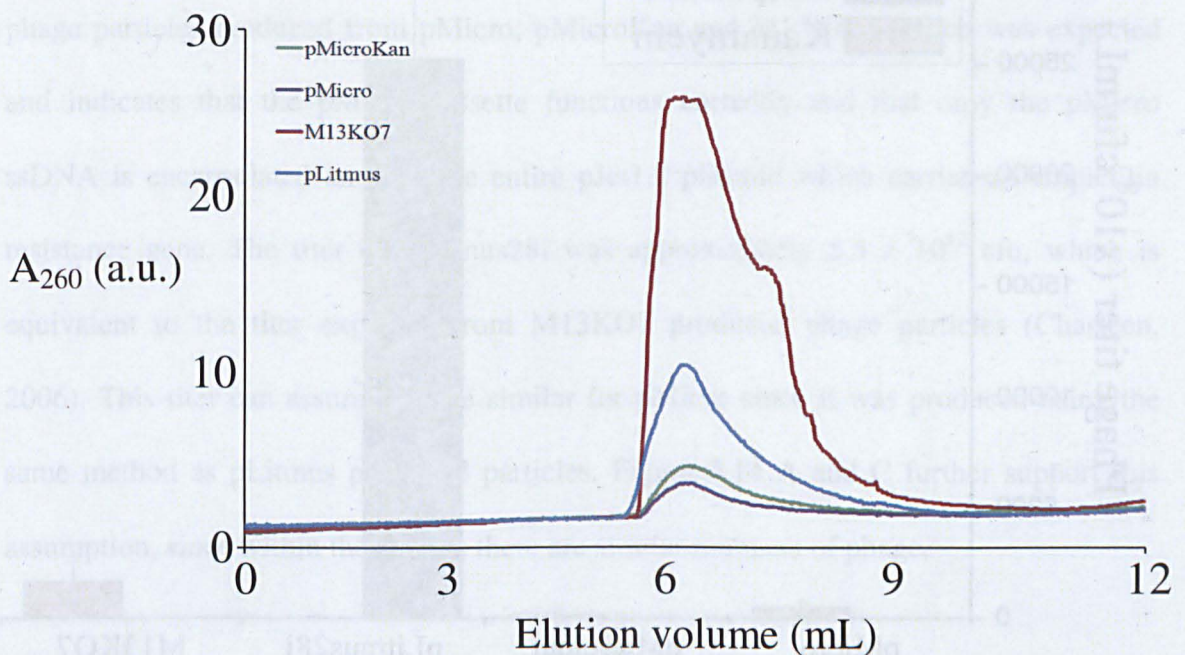


**Figure 3.19. CsCl gradient of different length phage particles.** 100 ml of overnight culture of *E.coli* containing the different length phage particle plasmids and super-infected with M13KO7, were precipitated with 15% (w/v) PEG-8000, 0.5 M NaCl and pelleted by centrifugation. These were re-suspended in 500  $\mu$ l PBS. The 500  $\mu$ l was then

loaded onto a 12 mL 30% CsCl gradient and centrifuged for 60 hours at 30000 rpm. The gradients were then fractionated and the absorbance at 260 nm recorded.

The number of phage particles produced from the microphage cassette when super-infected with M13KO7 was then investigated. Since the pMicro cassette produces only a short piece of ssDNA, that is not infectious, it is impossible to titer. Therefore the titer of the pLitmus28i was used as an indication of pMicro titer. Since pLitmus28i is a bacterial plasmid, after transfection into *E.coli* it can replicate and produce ampicillin resistant *E.coli* colonies (the resistance gene located on pLitmus28i). This method results in a titer given in colony forming units (cfu/mL).

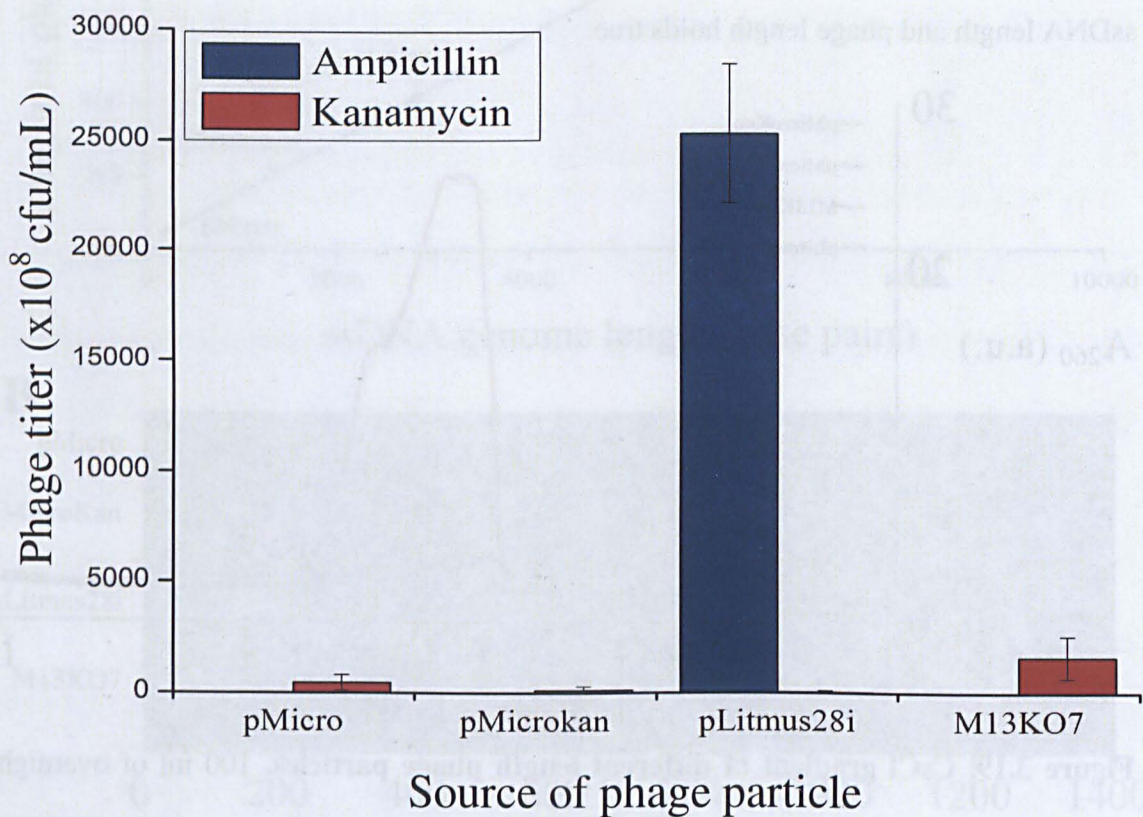


**Figure 3.20. Titer of different length phage.** Purified phage particles (15% PEG w/v, 0.5 M NaCl) were serially diluted to  $10^6$  or used from stock. They were then mixed with *E.coli* ER2738 expressing F-pili for one hour and then plated onto agar plates containing

ampicillin or kanamycin and incubated overnight at 37°C. Colonies were then counted on each plate.

Therefore after the initial 15% PEG (w/v), 0.5 M NaCl purification, the phage were titered to quantify the yield of each respective phage particle (Figure 3.20). The titer was carried out by mixing the purified phage particles with *E.coli* and then plating on agar plates containing ampicillin or kanamycin. Packaged pLitmus would provide ampicillin resistance whilst packaged M13KO7 would provide kanamycin resistance. Packaged pMicro and pMicrokan would provide no antibiotic resistance.

The results show (Figure 3.20) that no colonies were observed on ampicillin plates for phage particles produced from pMicro, pMicroKan and M13KO7; which was expected and indicates that the pMicro cassette functions correctly and that only the pMicro ssDNA is encapsulated and not the entire pJet1.2 plasmid which carries an ampicillin resistance gene. The titer of pLitmus28i was approximately  $2.5 \times 10^{12}$  cfu, which is equivalent to the titer expected from M13KO7 produced phage particles (Chasteen, 2006). This titer can assumed to be similar for pMicro since it was produced using the same method as pLitmus packaged particles. Figure 3.14 A and C further support this assumption, since within the images there are similar numbers of phage.

### 3.3 Conclusions and Future Work

At 50 nm long, the microphage is the shortest known M13 particle. It is this small size that makes it an attractive tool in bionanotechnology. The M13 bacteriophage has already been utilized for various nano-scale devices; e.g. a lithium ion battery (Lee, 2009);

## Chapter 3

---

various metal and semi-conducting nanowires (Flynn, 2003; Mao, 2003); and for the production of simple higher order structures (Nam, 2004). However, each of these devices has had to use wild-type M13 and were therefore restricted to a particle that was a micron in length. The result of this restriction was that each nanoscale device had a minimum length which could potentially inhibit these devices' applications, e.g. all nanowires created using M13 are a micron in length which limits the number of wires that could be deposited on a surface.

To date, no-one has exploited the microphage. The work described in this Chapter shows that the microphage can act as a blueprint for the bespoke creation of M13 particles; where the length of each M13 particle can be controlled in a predictable and rational manner. By using the pMicro cassette and inserting pre-determined lengths of DNA, then any desired length phage, greater than 50 nm long, can be produced. In this case, the insertion of a kanamycin resistance gene resulted in a ~214 nm long phage particle where the amount of DNA inserted showed a linear relationship with the length of the phage particle produced. Further investigation needs to be carried out to study whether this linear relationship continues when longer pieces of DNA are inserted into the microphage cassette.

It is possible that the microphage has not been used due to its difficulty in purification, and discussions with other academics indicates this may be the case (personal communication). The need for a 15% (w/v) PEG purification step results in the precipitation of DNA and other unwanted proteins that normally, with regard to wild-type M13 purification, would not be an issue. The work here has shown that performing a straight forward sucrose density gradient step followed by size exclusion chromatography

## Chapter 3

---

results in a pure microphage population with a yield of  $2.5 \times 10^{12}$  cfu: roughly analogous to wild-type phage titers.

In the future it would be interesting to attempt the combination of the pMicro plasmid with the helper plasmid (pM13CP) created by Chasteen, *et al.* (2006) to investigate whether the plasmid they created produces higher phage titers. If so then it would be a better way to produce the microphage. Using helper phage is less desirable since you first need to produce the helper phage which takes time and resources, and also when growing the microphage it is necessary to allow the *E.coli* host to attain the log phase of growth before adding the helper phage. By using the helper plasmid these time consuming aspects of microphage production would be eliminated. It is also possible to envisage a single plasmid being utilized by cloning the microphage cassette into the helper plasmid. Different length phage could then be created by adding DNA to this single plasmid and therefore resulting in a library of plasmids that each produces a different length phage particle. These could then easily be transformed into an *E.coli* host to produce the different phage.

**This page is intentionally blank**

# Chapter 4

---

## Fabrication of Higher Order Structures

This Chapter describes the work carried out to fabricate higher order structures using wild-type length phage and microphage. It also describes the attempts to purify these higher order structures.

### 4.1 Introduction

#### 4.1.1 The importance of new fabrication techniques

Since the 1970s the number of transistors on a chip has approximately doubled every two years. This is known as Moore's law (Moore, 1965) named after the co-founder of Intel, Gordon Moore, who predicted the rate of development in a 1965 paper in *Electronics* magazine. From millimetres across, transistors can now be fabricated that are just 50 nm in size. This rapid rate of miniaturization has been possible due to the photolithography fabrication technique (Figure 4.1).

Photolithography uses light shone through a transparent material, termed a mask, onto a material (photo-resist) that undergoes a chemical change upon exposure to the light. The mask contains the pattern of the transistor by blacking out certain areas. This blocks the light and therefore the pattern is imprinted onto the photo-resist. Various etching and material deposition steps are then used to remove the patterned photo-resist and create the transistor.

Photolithography's strength lies in its ability to print large numbers of transistors on a small area in a very reproducible manner, i.e. although only one transistor is shown in Figure 4.1, by using sophisticated masks large numbers of transistors can be patterned at the same time. However, the fundamental limitation with photolithography is the light source (Berkowski, 2005). The size of the fabricated features, i.e. the distance between the electrodes of the transistor is dictated by the wavelength of the light (Lin, 1986).

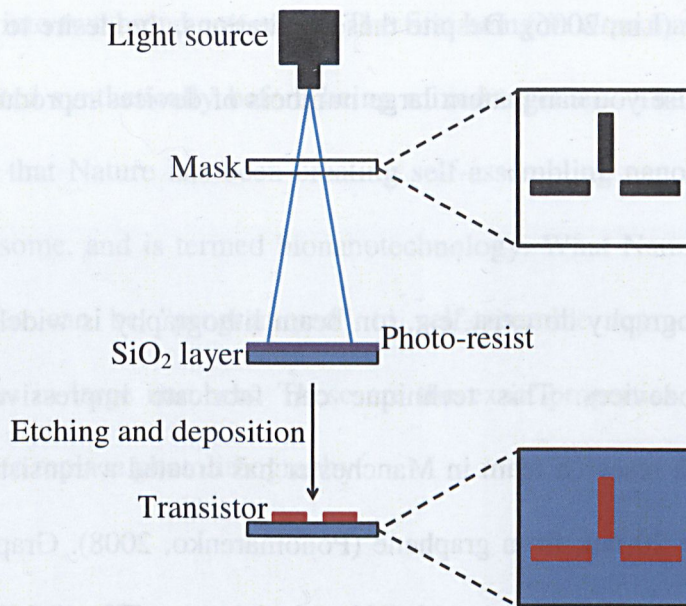


**Figure 4.1. Photolithography.** A diagram showing the important steps involved in the fabrication of a transistor using photolithography.

Current commercial photolithography machines use deep ultraviolet light which contain wavelengths of 193 - 248 nm, allowing the generation of feature sizes down to ~35 nm (Arnold, 2007). Creating structures smaller than 50 nm is becoming increasingly difficult (Brunner, 2003). The difficulties are present throughout the entire process. For creating structures below 50 nm, the mask and the mirrors required for orientating the beam to the photo-resist need to be of far higher quality. Likewise, the photo-resist needs to be changed to decrease its absorption so the scattered light doesn't affect the surrounding photo-resist (Lin, 2006). There is a large amount of research being undertaken to push photolithography further, e.g. moving to extreme UV (EUV) with a wavelength of 13.5 nm. However, using EUV produces new challenges. EUV is absorbed by all matter (Lin, 2006). Therefore all the components e.g. mask, lens, mirrors etc, must all be defect free. The patterning must also be carried out in a vacuum. The result of these considerations is that EUV is very expensive compared to traditional

193 nm photolithography (Lin, 2006). Despite these limitations, the desire to stay with photolithography is because you can pattern large numbers of devices reproducibly in a short space of time.

Alternatives to photolithography do exist, e.g. ion beam lithography is widely used in research to create nanodevices. This technique can fabricate impressively small structures. For example, a research team in Manchester has created a transistor, where the structures were under 20 nm, from graphene (Ponomarenko, 2008). Graphene is a sheet of carbon atoms arranged in a honey-comb lattice structure. The thickness of the graphene is a single carbon atom. They carved all the features of the transistor from the graphene using an electron beam, including the central island and the electrodes surrounding it. However, although these techniques can produce very small devices, they are not industrially viable due to the mechanism by which they operate. Ion beam lithography uses an electron beam to pattern a material. It is inherently slow in creating a device since it has to draw each component individually and cannot pattern large numbers of them simultaneously. Therefore, if a new technique is to replace photolithography in the next generation of transistors it is going to have similar properties to it; namely, it must be able to produce large numbers of devices quickly and reproducibly.

### **4.1.2 Self-assembly of molecular transistors**

Rather than patterning a surface, another method may be to design molecules that self-assemble into a transistor when mixed together. This is called a 'bottom up' approach to fabrication (with lithography being a 'top down' example). Self-assembly can be further

divided into two broad categories. The first being *in vitro* manufacture where molecules are created synthetically before being mixed together. The other category recognises the fact that Nature has been creating self-assembling nanodevices for millennia, e.g. the ribosome, and is termed bionanotechnology. What Nature shows is that biological molecules can be “programmed” to self-assemble reproducibly into higher order structures in large numbers. These are the exact properties that are needed for a new method to replace photolithography.

### **4.1.3 Viral self-assembly into higher order structures**

The use of viruses to create higher order structures is a relatively novel field. As discussed in Chapter 1, the M13 bacteriophage can be modified at the genetic level to display small peptides on its surface. Harnessing this property has led to the self-assembly of M13 particles into discrete architectures in an effort to create scaffolds for nanoscale devices. An example of this has been the display, on M13, of an anti-streptavidin peptide on pIII (SWDPYSHLLQHPQ) and a hexahistidine peptide on pIX (i.e. on the opposite end of the phage). This mutant phage, displaying the two peptides, was mixed with a “linker molecule” consisting of streptavidin conjugated with nickel-nitrilotriacetic acid, which binds tightly to hexahistidine. By controlling the stoichiometry of the phage and the linker it was possible to create a nano-ring (Figure 1.9, Chapter 1) from individual phage (Nam, 2004). These nano-rings have the potential to act as scaffolds in the nucleation of various inorganic materials by using pVIII displayed peptides. Within the original paper they highlight the potential of nucleating a magnetic material to create a magnetic nano-ring that could function as a memory device (Zhu, 2000). Aside from the nano-ring, it was found that by altering the

stoichiometry, so that there were 10 mutant phage per linker, radial (Figure 4.2 A) and linear (Figure 4.2 B) structures were created.

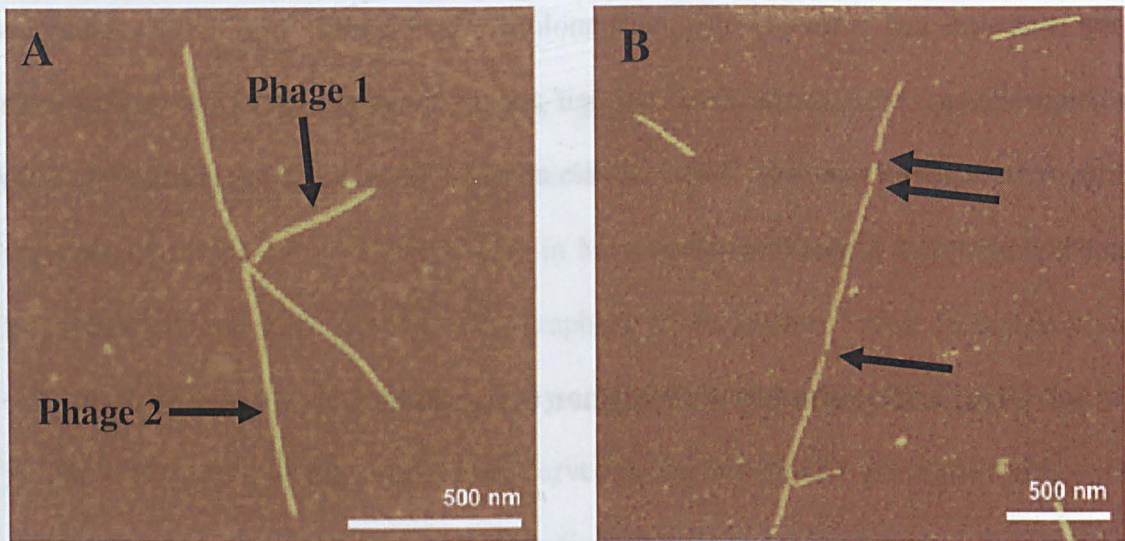


**Figure 4.2. AFM images of M13 bacteriophage higher order structures.** M13 bacteriophage were created displaying an anti-streptavidin peptide on the minor coat protein pIII and a hexahistidine peptide on pIX. The mutant phage were mixed with a streptavidin conjugated with nickel-nitrilotriacetic acid linker molecule at a ratio of 10:1. Taken from Nam, (2004).

The AFM images given as evidence (Figure 4.2 A and B) for the existence of these radial and linear higher order structures are, however, less than convincing. Neither AFM image is particularly conclusive with most of the phage having a broken appearance (highlighted by arrows in Figure 4.2 B). A more worrying aspect is the large degree of variability in length of the phage particles (Phage 1 and 2 in Figure 4.2 B). The phage were produced using the typical phagemid and helper phage system (Chapter 1, section 1.7.1) and within the paper it is claimed that the phagemid particles vary in length from 300 to 600 nm. As shown in Chapter 3 (Chapter 3, Figure 3.17), although phagemid systems do produce some variation in phage length, it is not usually as

extreme as seen in Figure 4.2. It is more likely that the phage used by Nam, *et al.* were sheared during the purification process. Assuming that higher order structures can be created using this method, the lack of homogeneity in the phage length would make them difficult to use. For instance, attempting to get them to self-assemble onto pre-fabricated electrodes would be very difficult since the lengths would change for every higher order structure.

Further work has been done with the anti-streptavidin peptide by the same group. By combining this peptide on pIII with a gold nanoparticle binding peptide (VSGSSPDS) on pVIII further higher order structures have been created (Figure 4.3; Huang, 2005). By mixing these phage with streptavidin coated 15 nm gold nanoparticles it was possible to see phage bound to the particles and in some cases multiple phage bound to a single particle. By then adding 5 nm gold nanoparticles, which bound specifically to the gold nanoparticle binding peptide, it was possible to coat the phage with the gold nanoparticles.

However, once again the images given to demonstrate these higher order structures are not convincing. Examining the structure consisting of three phage (Figure 4.3 B) it appears more likely that there is one phage bound to the 15 nm gold nanoparticle and then another phage intercepting it (I have highlighted these phage in red in Figure 4.3 C). The other figures are similarly ambiguous with no further data to back up the TEM images. A further major flaw with using the gold nanoparticles in this instance to create nanowires is that upon enhancement of the gold nanoparticles, i.e. using the nanoparticles as “seeds” for further deposition of gold to create continuous and current conducting nanowires, the various nanowires would fuse at the point where they

intersect therefore creating an amorphous gold area with no use as a nanodevice. As with the previous paper from the group (Nam, 2004) no further mention is made to these higher order structures and no further papers have been published regarding them.

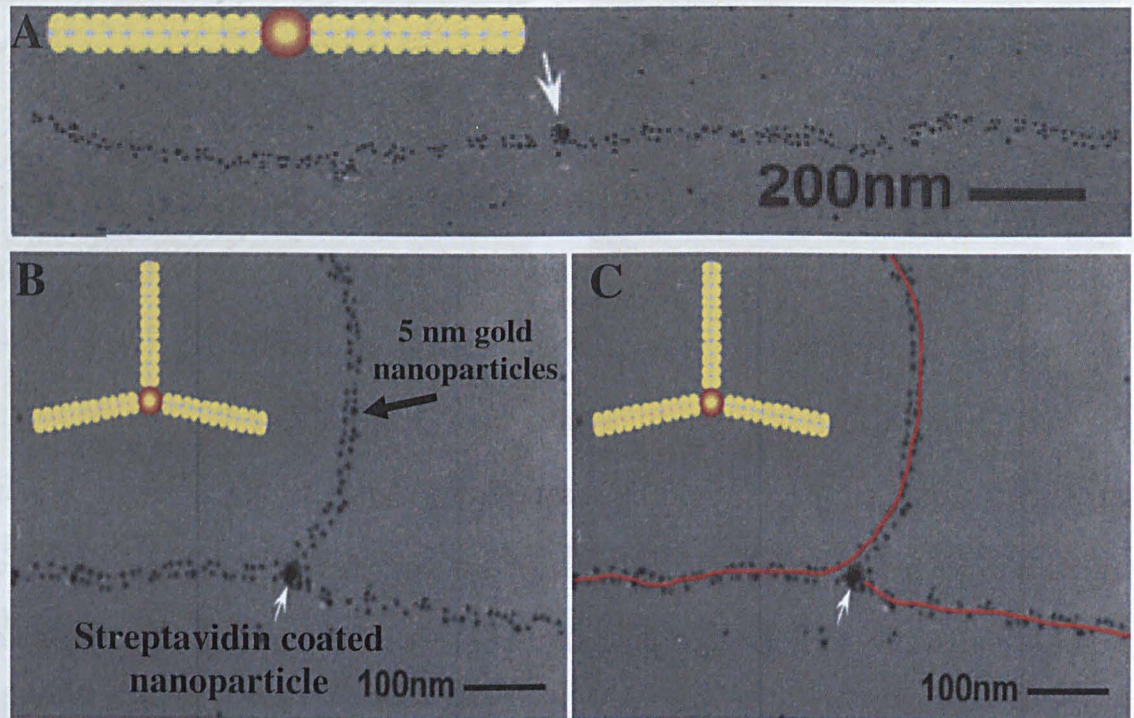


**Figure 4.3. Gold coated M13 bacteriophage higher order structures.** M13 bacteriophage displaying an anti-streptavidin peptide on the pIII coat protein were mixed with streptavidin coated 15 nm gold nanoparticles. **A** shows two phage bound to a single nanoparticle. **B** shows three phage bound to a gold nanoparticle. **C** shows the same image as **B** but with two phage highlighted in red. Taken from Huang, 2005.

It therefore seems feasible that distinct higher order structures using the M13 bacteriophage can be created, although the evidence in the literature is not convincing (Nam, 2004; Huang, 2005). The challenge appears to be finding a way to create homogenous higher order structures that is reproducible, and then purify them.

### 4.1.4 Selenocysteine

Selenocysteine is the 21<sup>st</sup> genetically encoded amino acid, first identified in 1986 (Chambers, 1986 and Zinoni, 1986). It is an analogue of cysteine except the sulphur atom is replaced with a selenium atom. It is one of only two genetically encoded amino acids that fall outside of the 20 standard amino acids; the other being pyrrolysine which is found only in methanogenic archaea and bacteria species (Atkins, 2002). In contrast, selenocysteine has been found in every domain in life, from simple bacteria to humans (Fischer, 2007). Selenocysteine containing proteins are more common in higher eukaryotes (Johansson, 2005).

Almost all of the proteins that have been identified containing selenocysteine (called selenoproteins) are enzymes involved in the catalysis of oxidation/reduction reactions (Bock, 1991). An example is glutathione peroxidase, an enzyme which reduces free hydrogen peroxide to water and so protecting the cell from oxidative damage (Flohe, 1973). Selenocysteine, although chemically similar to cysteine, has a number of unique properties including high electrophilicity (Stadtman, 1996) and a low pKa (5.2 vs 8.3 for cysteine – Huber, 1967). The consequence of the low pKa is that at physiological pH, the selenol group is mainly in its anionic selenolate form whilst the thiol group of the cysteine is protonated. The result of this is that at ~pH 7, selenocysteine is ~10 times more reactive than cysteine (Sandman, 2000, Johansson, 2005) and it remains reactive down to pH 5.2 (Sandman, 2000).

Perhaps the most interesting aspect of selenocysteine (and also pyrrolysine) is their incorporation into proteins. There are 64 possible triplet codons using the four nucleic

acid bases. 61 of these are used for the incorporation of the twenty standard amino acids and three act as a terminator of protein synthesis, i.e. stop codons. It is the opal stop codon (TGA/UGA) that is utilised for selenocysteine incorporation.

The incorporation of selenocysteine requires four gene products (Bock 1991). The first gene, *SelC*, encodes a unique tRNA molecule associated with selenocysteine known as tRNA<sup>Sec</sup>. The tRNA<sup>Sec</sup> molecule has evolved to have a different primary and secondary structure to the standard tRNAs. It has a longer acceptor stem and variable arm, and has base substitutions at several positions which are conserved amongst the other standard tRNAs (Bock, 1991, and Schon, 1989). tRNA<sup>Sec</sup> is initially synthesised containing a seryl residue (Ser-tRNA) which is then converted to a selenocysteinyl moiety (Sec-tRNA) by the enzyme selenocysteine synthase (*SelA* product). The synthase uses selenomonophosphate (synthesised from a sodium selenite source and ATP by the *SelD* gene product selenophosphate synthetase) as the selenium donor (Bock, 1991, Fischer, 2007).

Incorporation of tRNA<sup>Sec</sup> into the opal stop codon requires the *SelB* gene product and a 38 nucleotide long hairpin stem loop contained within the mRNA of the selenoprotein known as the “SElenoCysteine Insertion Sequence” (SECIS) element (Figure 4.4, Bock, 1991). Within prokaryotes the SECIS element is located immediately downstream of the opal stop codon (Sandman, 2003), whereas it can be located further away in eukaryotes. This aspect makes expressing eukaryotic selenoproteins in *E.coli* problematic. The SECIS element's function is to recruit the *SelB* gene product to the ribosome where it catalyses selenocysteine insertion into the opal stop codon using

tRNA<sup>Sec</sup> and GTP (Johansson, 2005): The exact mechanism of these events is still not known in detail (Fischer, 2007).

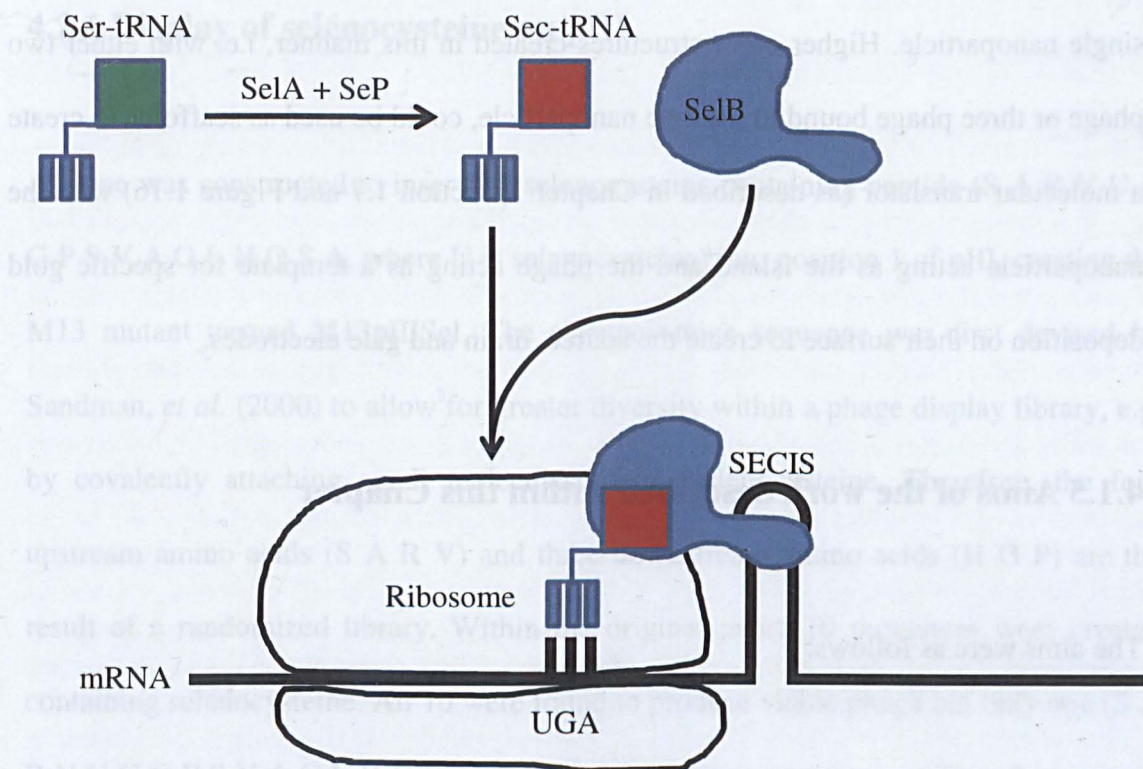


**Figure 4.4. Incorporation of selenocysteine into the opal stop codon in prokaryotes.**

In 2000, Sandman *et al.*, working for New England Biolabs, inserted selenocysteine into position 1 of the M13 pIII coat protein. Their aim was to increase the diversity of phage display libraries by allowing specific targeting of the selenocysteine with small molecules using thiol-like (selenol) chemistry, i.e. iodoacetyl or maleimide chemistry. The specificity of the selenocysteine targeting was needed because of the endogenous M13 cysteines. pIX, pVI and pVII all have one cysteine, whilst pIII has 8 and pVIII has none. To date, this mutant phage has only been used to tag the M13 bacteriophage with biotin. Khalil, *et al.* have used this method to tether the M13 molecule to a streptavidin-coated bead, allowing for stretching experiments to be performed to measure the persistence length of the M13 particle (Khalil, 2007).

However, there is no reason why the selenocysteine residue, when displayed on pIII, cannot react specifically with spherical gold nanoparticles or maleimide-coated quantum dots to create higher order structures where multiple phage are bound to a single nanoparticle. Higher order structures created in this manner, i.e. with either two phage or three phage bound to a single nanoparticle, could be used as scaffolds to create a molecular transistor (as described in Chapter 1, section 1.7 and Figure 1.16) with the nanoparticle acting as the island and the phage acting as a template for specific gold deposition on their surface to create the source, drain and gate electrodes.

### **4.1.5 Aims of the work described within this Chapter**

The aims were as follows:

1. To reproduce pIII selenocysteine displaying phage (M13pIIISel).
2. To fabricate higher order structures using M13pIIISel and bind gold nanoparticles and quantum dots specifically to the selenocysteine amino acid.
3. To purify the higher order structures.
4. To fabricate higher order structures using microphage.

### 4.2 Results and Discussion

#### 4.2.1 Display of selenocysteine on pIII

A clone was constructed to insert the selenocysteine containing peptide (S A R V U H G P S V A G L H Q S A, where U is selenocysteine) into position 1 of pIII, creating the M13 mutant termed M13pIIISel. The selenocysteine sequence was first devised by Sandman, *et al.* (2000) to allow for greater diversity within a phage display library, e.g. by covalently attaching small molecules to the selenocysteine. Therefore, the four upstream amino acids (S A R V) and three downstream amino acids (H G P) are the result of a randomized library. Within the original paper 10 sequences were created containing selenocysteine. All 10 were found to produce viable phage but only one (S A R V U H G P S V A G L H Q S A) was used for further experiments. Therefore instead of S A R V H G P any arbitrary amino acids could be used or perhaps removed altogether. Since the selenocysteine containing peptide had been shown to react successfully with small molecules (Sandman, 2000) it was decided to use the same sequence within this study. The remaining downstream amino acids (S V A G L H Q S A) are far more restricted since the DNA sequence encoding these amino acids creates the SECIS element needed for selenocysteine incorporation.

To create M13pIIISel, PCR amplification was carried out using the overlapping primers Biotinfor and Biotinrev (Chapter 2, section 2.3.1) to produce a product ~70 bp in length (Figure 4.5 A). This was cloned into *gIII* between the *Acc65 I* and *Eag I* sites of M13KE (New England Biolabs, Ipswich, MA, U.S.A.). This corresponds to position 1 of the mature pIII protein (Figure 4.5 B). Therefore selenocysteine was displayed at position 5

of the altered pIII. The ligation reaction was transformed into *E.coli* and plated onto agar containing 2  $\mu$ M sodium selenite (explained in section 4.2.2). Ten colonies were then picked and sequenced which confirmed that they contained the selenocysteine sequence. One was carried forward for further experiments and was termed M13pIIISel (Appendix B, section 1.0).

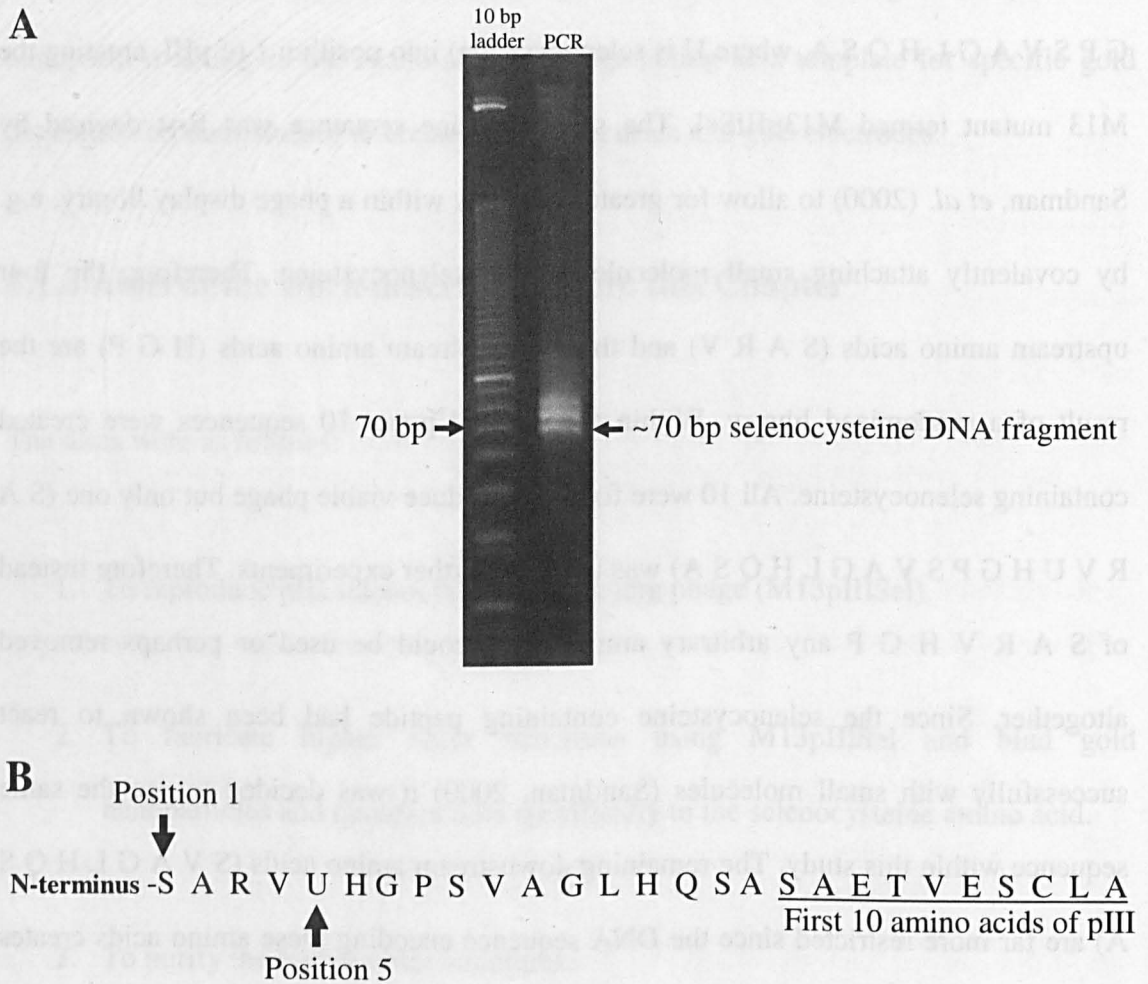


**Figure 4.5. Amplification of DNA fragment encoding for selenocysteine containing peptide.** Shows 0.8 % w/v agarose gel run at 120 V for 1 hour and stained with ethidium bromide (A). The DNA fragment was created by PCR amplification using biotinfor and biotinrev primers. B shows the position of the selenocysteine (U) containing peptide within the mature pIII protein of the M13pIIISel phage.

### 4.2.2 Incorporation of selenocysteine into M13pIIISel

Production of selenocysteine containing proteins requires the addition of 2  $\mu\text{M}$  sodium selenite (Sandman, 2000) to a culture of *E.coli*. The sodium selenite acts as a source of selenium atoms for the SelA protein (Figure 4.4). This extra selenium is added to ensure that enough selenocysteine is produced by the *E.coli* cells to be incorporated by the phage displaying selenocysteine. When the *E.coli* cell has insufficient selenocysteine, or there is incorrect incorporation, the ribosome reads the selenocysteine codon as a stop codon and so terminates protein synthesis. This aspect of selenocysteine insertion acts as an in-built control. Since the selenocysteine containing peptide was cloned into position 1 of pIII, it should mean that if selenocysteine is not incorporated into pIII then the rest of the pIII protein should not be produced. pIII is needed for successful phage assembly (Clackson, 2004), and therefore any pIII particles incorporated into a M13pIIISel particle must contain selenocysteine. Therefore any viable phage should also contain selenocysteine. It was found that when M13pIIISel replicative form (RF) DNA was transformed into *E.coli* and plated on agar plates lacking any sodium selenite supplement that no plaques were observed. When 2  $\mu\text{M}$  sodium selenite was added the transfection efficiency was equivalent to that of wild-type M13KE DNA ( $\sim 1 \times 10^8$  plaques/ng of DNA).

### 4.2.3 Titer of M13pIIISel

The display of peptides on pIII has been reported to lower phage titer (Loset, 2008). The addition of 2  $\mu\text{M}$  sodium selenite to produce M13pIIISel may also affect titer, although this was not discussed in Sandman *et al.* (2000). To examine the effect of sodium

selenite on infectivity, the RF DNA of M13pIIISel and wild-type was transformed into *E.coli* and plated on agar containing 2  $\mu$ M sodium selenite. The plaques of M13pIIISel were observed to be approximately half the size of wild-type phage plaques. This is consistent with a lower infectivity (Petrenko, 2000). M13pIIISel and wild-type M13 phage were grown in 1 L of *E.coli* cultured in super-broth (SB) medium supplemented with 2  $\mu$ M sodium selenite and then PEG purified. Using an average of five 1 L cultures, the M13pIIISel phage were found to have a lower titer than wild-type M13 ( $\sim 2 \times 10^9$  pfu/mL vs  $\sim 4 \times 10^{12}$  pfu/mL). The absorbance at 269 nm of the phage stocks were also used to calculate the number of phage particles within the solution (Chapter 2 section 2.1.6.2). The absorbances suggested values of  $\sim 20 \times 10^{13}$  virions/mL for M13pIIISel compared to  $\sim 3 \times 10^{13}$  virions/mL for wild-type phage. The observation that during PEG purification that M13pIIISel produced more precipitate than wild-type indicates that the virions/mL values are correct.

Obviously there is a large discrepancy between the pfu/mL and virions/mL values. The likely reason for the differences is that display of peptides on pIII decreases infectivity (Loiset, 2008) and the titer is a direct measurement of phage infectivity. The presence of the selenocysteine containing peptide therefore appears to have an adverse affect on the function of pIII. However, to produce the phage particles, a single plaque of the phage was added to an overnight culture of *E.coli* which had been diluted 1 in 100 within the SB medium, i.e. 10 mL of *E.coli* within 1 L of SB. Therefore if infectivity is adversely affected by the insertion of the peptide within pIII then one would expect the infection of the *E.coli* to be slower for M13pIIISel than wild-type and so fewer phage particles produced. However, the virions/mL values indicate that the selenocysteine containing peptide increases the number of phage particles produced. A suitable explanation for the

increase in phage numbers cannot be provided. However, these differences between pfu/mL and virions/mL highlight the difficulty in relying on phage titer to determine phage particle numbers. For the work described in this Chapter I decided that the virions/mL values would be used since the M13pIIISel particles must contain pIII molecules displaying selenocysteine (section 4.2.2).

### **4.2.4 Fabrication of higher order structures with gold nanoparticles**

As described in Chapter 1, a molecular transistor is made of three electrodes (source, drain and gate) surrounding an island. Preferably the island should consist of a semi-conducting material, allowing for greater control and use of the transistor at room temperature. However, a purely metallic island can also be used, although these are restricted by needing extremely low temperatures to operate (Yamaguchi, 2010). Therefore in this study, two types of nanoparticle were examined as possible islands: gold nanoparticles and semi-conducting quantum dots. Although gold nanoparticles would be a disadvantage in the final device, they are cheaper and therefore they were used initially to establish reaction conditions and so on.

100  $\mu\text{L}$  of  $1 \times 10^{12}$  virions/mL M13pIIISel phage were mixed with sodium citrate stabilised 10 nm gold nanoparticles (GNP10nm/cit) at a ratio of 35 phage particles per gold nanoparticle. Sodium citrate is a commonly used stabilising agent which also acts as the reducing agent in the formation of the gold nanoparticles. It adsorbs onto the surface of the nanoparticles, leading to a net negative charge that repels nanoparticles from one another and stops aggregation.

## Chapter 4

---

A set of conditions were established for the mixing and purification of the GNP10nm/cit and phage structures. The mixture was incubated overnight at room temperature and loaded onto a 12 mL 30-60% w/v linear sucrose gradient. The tubes were then centrifuged at 18500 rpm for 18 hours at 4°C before being fractionated whilst measuring the absorbance at 260 nm. These conditions were used for all the linear sucrose gradient experiments discussed in this chapter and are described as sucrose purification.

Sucrose purification of M13pIIISel particles only (with no GNP10nm/cit present) showed that the phage migrated principally as a single band (Figure 4.6 A) through the gradient. When only GNP10nm/cit were sucrose purified, they were observed to form a red pellet at the bottom of the tube (the same colour as the nanoparticle solution). When M13pIIISel and GNP10nm/cit were mixed, two peaks were observed (Figure 4.6 A and B). Examination of peaks A and B with TEM revealed that peak A consisted of phage only (Figure 4.6 C) whilst B contained phage (the vast majority were 2 to 4 phage) bound to single gold nanoparticles (Figure 4.6 D-F). Importantly, gold nanoparticles were never seen at both ends of a phage particle, suggesting that the gold nanoparticles only bound to the selenocysteine displayed on pIII.

Gold nanoparticles are very dense and it is unsurprising that they pellet to the bottom of the centrifuge tube. In an attempt to stop the gold nanoparticles from forming a pellet a 70% w/v sucrose cushion was used for a single experiment. A cushion is commonly used to stop a sample pelleting. A 30-60% w/v linear sucrose gradient was created with a 1 mL 70% w/v cushion at the bottom. 500 µL of ~ 10 nM GNP10nm/cit were then loaded onto the sucrose gradient and centrifuged at 18500 rpm for 18 hours at 4°C. However, it was observed that the gold nanoparticles still pelleted.

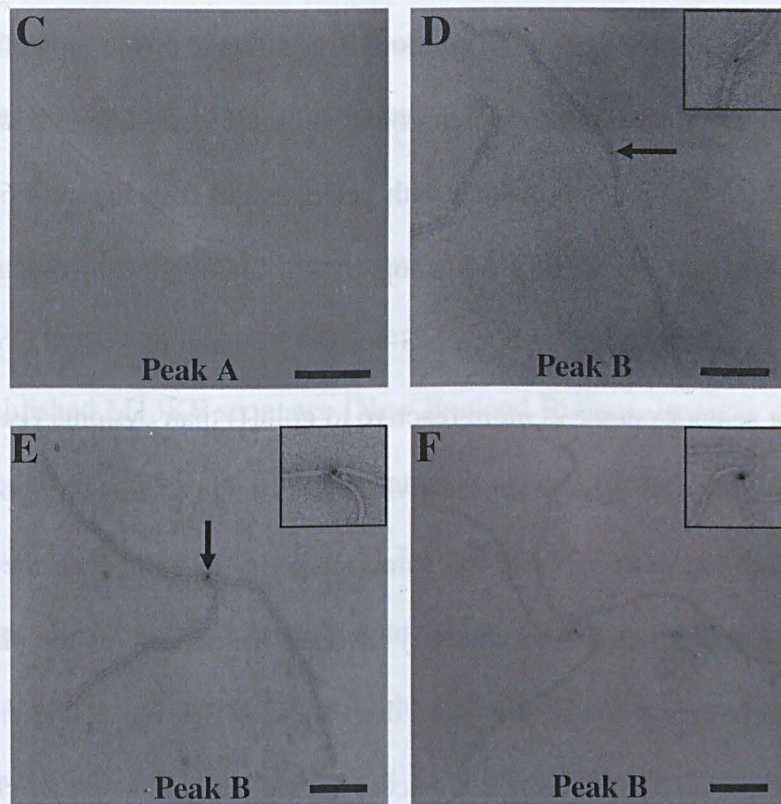
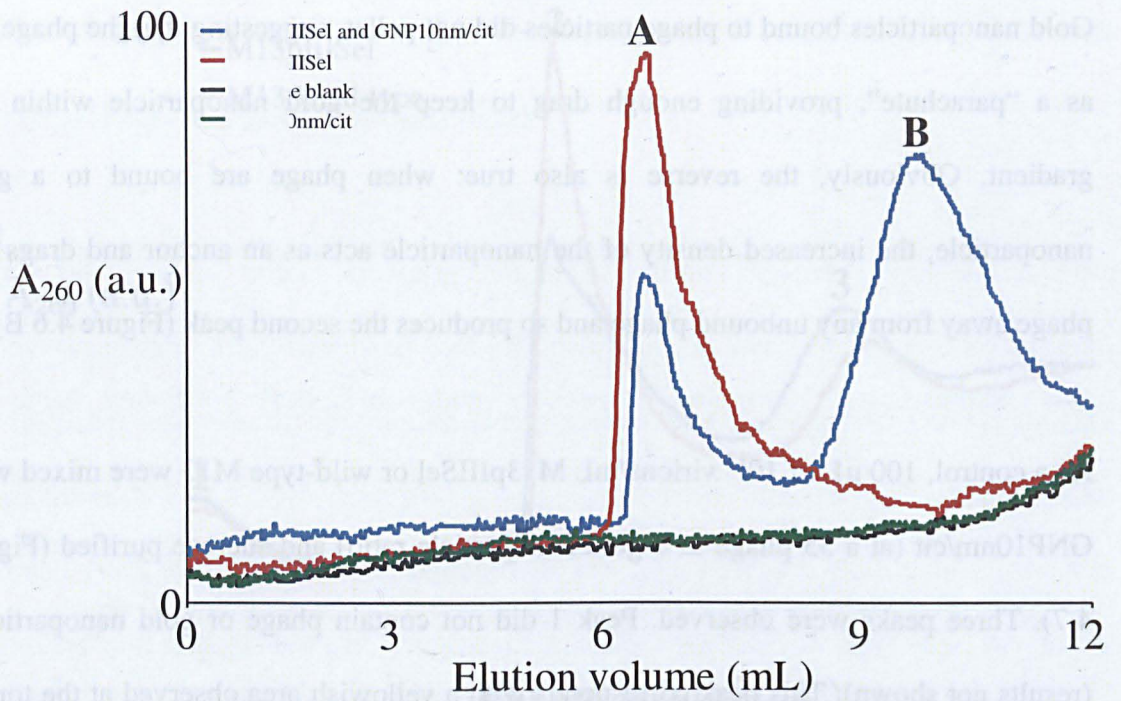


**Figure 4.6. Linear sucrose gradient purification of M13pIISel phage particles bound to gold nanoparticles. C-F show TEM images of phage higher order structures found in peak A and B. Scale bar equals 200 nm. Arrows highlight gold nanoparticles.**

Gold nanoparticles bound to phage particles did not pellet, suggesting that the phage act as a “parachute”, providing enough drag to keep the gold nanoparticle within the gradient. Obviously, the reverse is also true: when phage are bound to a gold nanoparticle, the increased density of the nanoparticle acts as an anchor and drags the phage away from any unbound phage and so produces the second peak (Figure 4.6 B).

As a control, 100  $\mu\text{L}$  of  $10^{12}$  virions/mL M13pIIISel or wild-type M13 were mixed with GNP10nm/cit (at a 35 phage to 1 gold nanoparticle ratio) and sucrose purified (Figure 4.7). Three peaks were observed. Peak 1 did not contain phage or gold nanoparticles (results not shown). This peak corresponds with a yellowish area observed at the top of the gradient after centrifugation. The colour suggests that this is the buffer that the gold nanoparticles are suspended in which contains tannic acid: a solute with a yellowish colour. Peaks 2 and 3 corresponded with peaks A and B in Figure 4.6. Unexpectedly, wild-type M13 also bound to gold nanoparticles, although with much less efficiency than with M13pIIISel phage, i.e. peak 3 was ~40% smaller for wild-type. It has been reported that selenocysteine is more reactive to gold(I) than cysteine (Isab, 1994) and so selenocysteine may also be more reactive than cysteine to metallic gold. If, however, selenocysteine and cysteine have the same reactivity to gold, then the presence of ~5 copies of selenocysteine would naturally increase the affinity of the phage particle for the gold nanoparticles. What this result does show is that out of the eight endogenous pIII cysteines, one or more of them are accessible to the gold nanoparticle.

The most obvious candidate cysteine to investigate is located at position 7 of the mature pIII coat protein nearest the N-terminus (A E T V E S C). It was thought that removal of this cysteine might decrease phage viability. Therefore M13C (Chapter 3), a wild-type

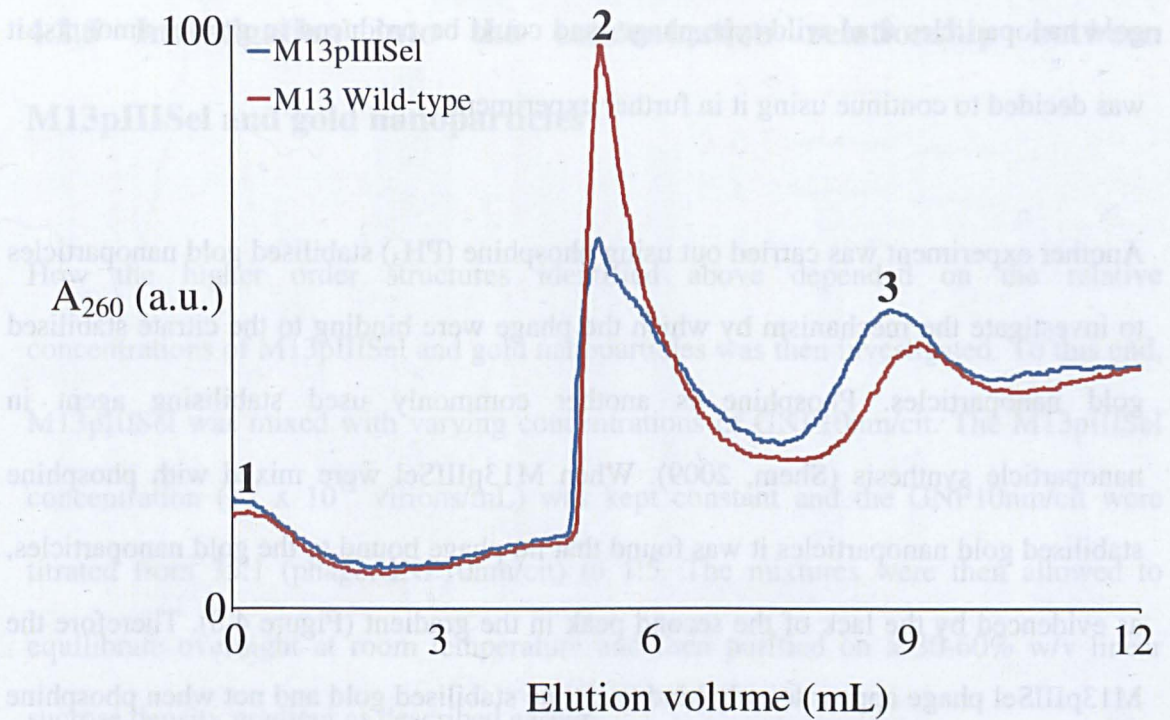


**Figure 4.7. Linear sucrose gradient purification of M13pIIISel and wild-type M13 phage particles bound to gold nanoparticles.**

phage containing a chloramphenicol resistance gene to allow for selection, was used to create a pIII (C7G) mutant. This was achieved by substituting T by a G at position 1650 of the published M13KE sequence (New England Biolabs, Ipswich, MA, U.S.A.). The substitution was done by site directed mutagenesis using the primers pIIIremovalfor and pIIIremovalrev (Chapter 2, section 2.3.4). After mutagenesis the clones were transformed into *E.coli* and plated onto agar plates containing chloramphenicol. Ten colonies were then picked and sequenced which confirmed that they all contained the desired sequence. One was carried forward for further experiments and was termed M13pIIIC (Appendix B, section 2.0). However, all attempts to produce M13pIIIC phage failed. Therefore, it appears that removal of the Cys7 makes the phage non-viable. No further work was carried out to ascertain which naturally occurring cysteine is accessible to the gold nanoparticle. Since M13pIIISel was more efficient at binding to

gold nanoparticles than wild-type phage, and could be produced in greater amounts, it was decided to continue using it in further experiments.

Another experiment was carried out using phosphine ( $\text{PH}_3$ ) stabilised gold nanoparticles to investigate the mechanism by which the phage were binding to the citrate stabilised gold nanoparticles. Phosphine is another commonly used stabilising agent in nanoparticle synthesis (Shem, 2009). When M13pIIISel were mixed with phosphine stabilised gold nanoparticles it was found that no phage bound to the gold nanoparticles, as evidenced by the lack of the second peak in the gradient (Figure 4.8). Therefore the M13pIIISel phage appear to only bind to citrate stabilised gold and not when phosphine is used. This may suggest that the phage are interacting with the citrate instead of the gold. However, no reports of citrate interacting with cysteine or selenocysteine have been published. It is therefore more likely that the citrate is more easily displaced than the phosphine, allowing direct interaction with the gold surface.

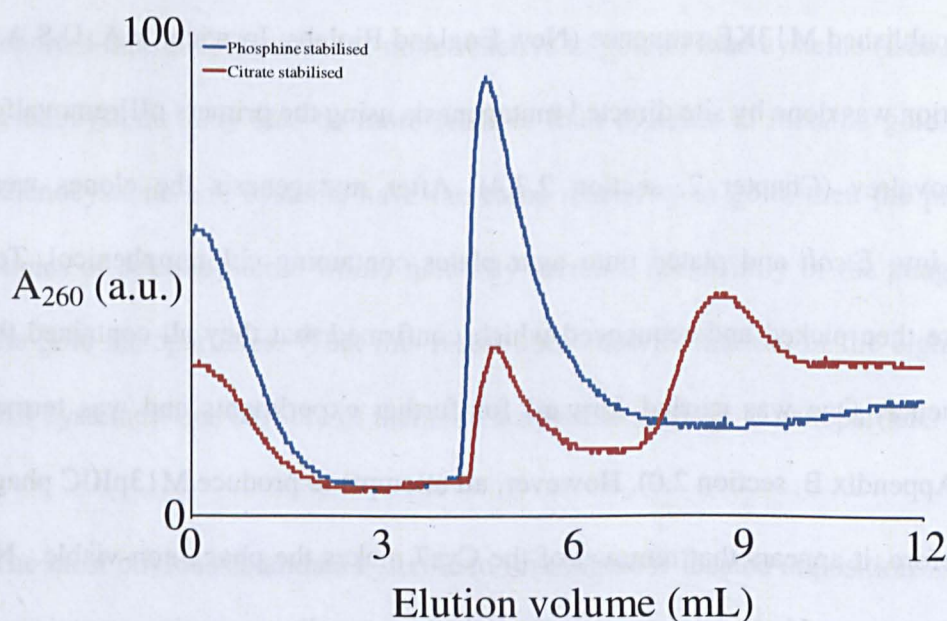


**Figure 4.8. Linear sucrose gradient purification of M13pIIISel and phosphine stabilised gold nanoparticles.**

### 4.2.5 Investigation into the concentration relationship between M13pIIISel and gold nanoparticles

How the higher order structures identified above depended on the relative concentrations of M13pIIISel and gold nanoparticles was then investigated. To this end, M13pIIISel was mixed with varying concentrations of GNP10nm/cit. The M13pIIISel concentration ( $\sim 1 \times 10^{12}$  virions/mL) was kept constant and the GNP10nm/cit were titrated from 35:1 (phage:GNP10nm/cit) to 1:5. The mixtures were then allowed to equilibrate overnight at room temperature and then purified on a 30-60% w/v linear sucrose density gradient as described earlier.

Upon fractionation four peaks were observed (Figure 4.9). The first three peaks (1-3 Figure 4.9) migrated similarly to peaks observed in earlier experiments (Figure 4.7). Peak 4 (Figure 4.9) was not present in earlier experiments where high phage to GNP10nm/cit ratios were used. As the ratio decreased, peak 4 increased. Only at ratios of 3.5:1 and below was peak 4 substantial.

Peak 1 once again corresponded to the buffer GNP10nm/cit were suspended in. This conclusion is further supported by the increasing size of peak 1 as more gold was used, cf. 35:1 and 1:5 samples.

Peak 2 (Figure 4.9) contained single phage particles only. The size of the peak decreased at lower phage: GNP10nm/cit ratios, and was completely absent in the 1:5 sample (the grey line in Figure 4.9 A).

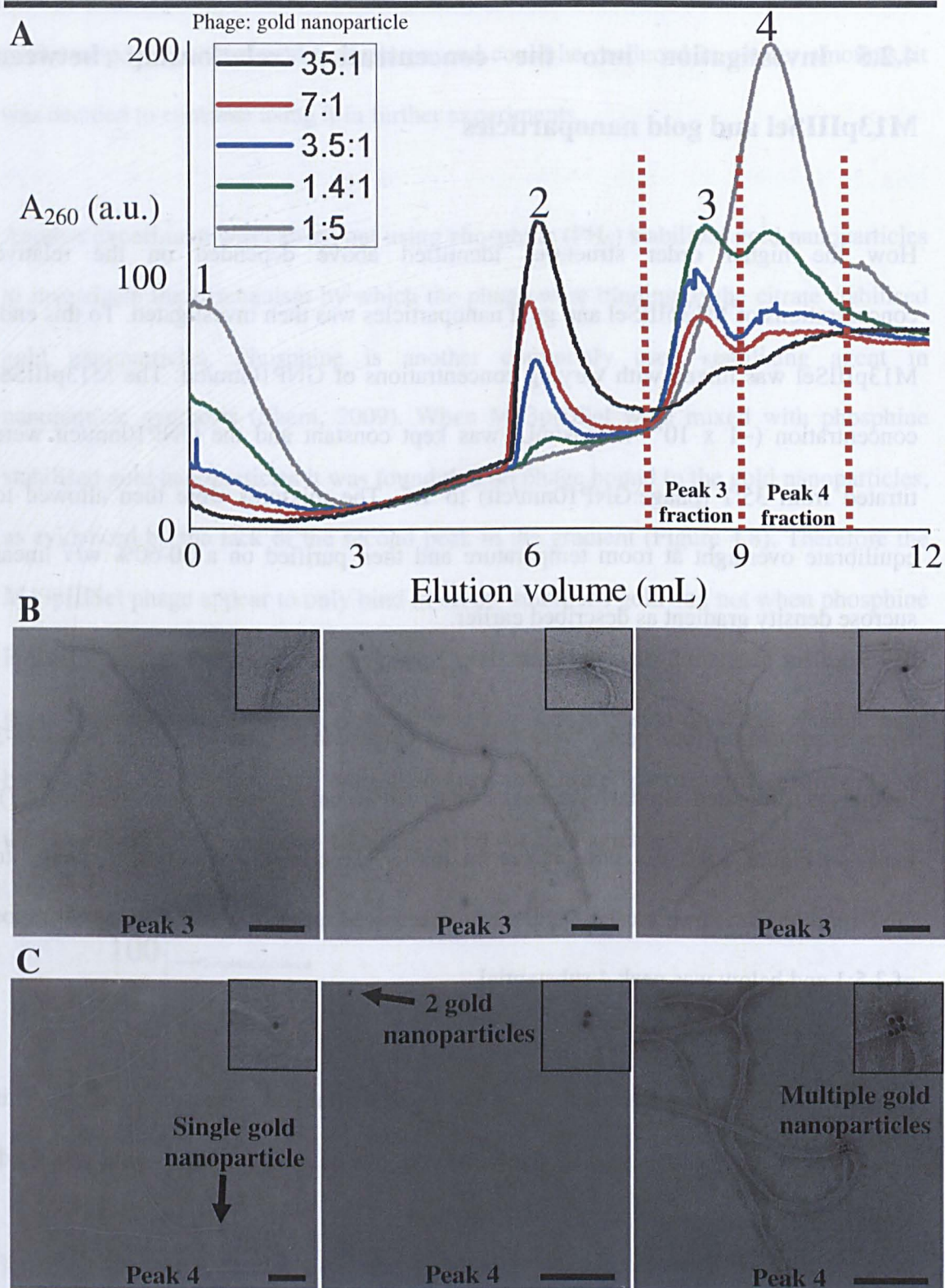


**Figure 4.9.** Concentration dependence of M13pIIISeI and GNP10nm/cit in fabricating higher order structures. Mixtures were purified on a 30-60% w/v linear sucrose gradient and fractionated at 260 nm. Scale bar equals 200 nm.

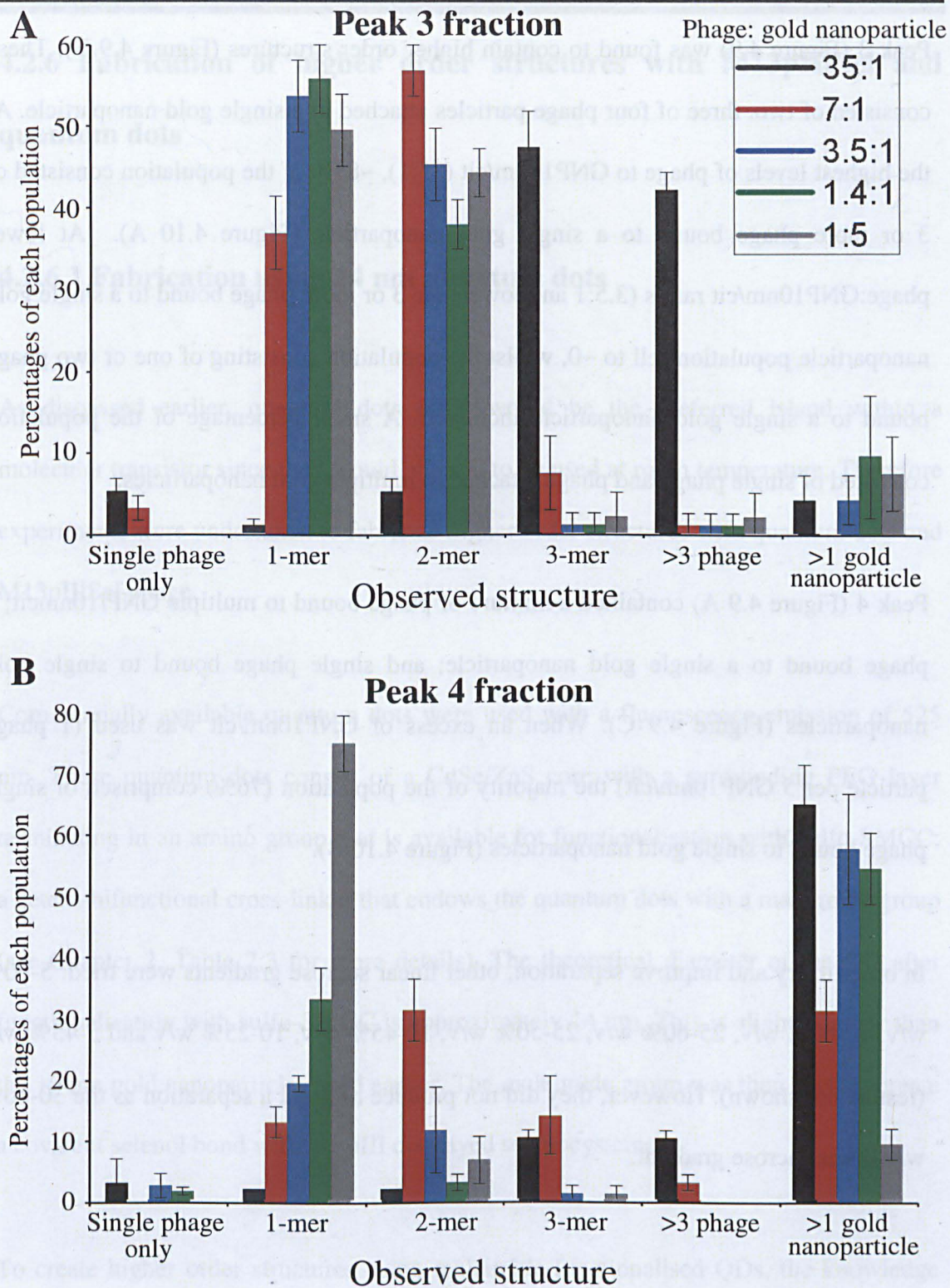


**Figure 4.10. Quantitation of sucrose purified higher order structures.** Shows the number of higher order structures found in peak 3 of Figure 4.9 (A) and peak 4 of Figure 4.9 (B). Peaks 3 and 4 were collected as 1 mL fractions from three different experiments (highlighted in Figure 4.9 A) and the number of structures counted using TEM ( $n = 50$  for each fraction).

Peak 3 (Figure 4.9) was found to contain higher order structures (Figure 4.9 B). These consisted of two, three or four phage particles attached to a single gold nanoparticle. At the highest levels of phage to GNP10nm/cit (35:1), ~85% of the population consisted of 3 or more phage bound to a single gold nanoparticle (Figure 4.10 A). At lower phage:GNP10nm/cit ratios (3.5:1 and lower) the 3 or more phage bound to a single gold nanoparticle population fell to ~0, whilst the population consisting of one or two phage bound to a single gold nanoparticle increased. A small percentage of the population consisted of single phage and phage attached to multiple gold nanoparticles.

Peak 4 (Figure 4.9 A) contained a mixture of phage bound to multiple GNP/10nmcit; 2 phage bound to a single gold nanoparticle; and single phage bound to single gold nanoparticles (Figure 4.9 C). When an excess of GNP10nm/cit was used (1 phage particle per 5 GNP10nm/cit) the majority of the population (76%) comprised of single phage bound to single gold nanoparticles (Figure 4.10 B).

In order to try and improve separation, other linear sucrose gradients were tried: 5-60% w/v, 10-60% w/v, 25-60% w/v, 25-50% w/v, 10-45% w/v, 10-25% w/v and 5-45% w/v (results not shown). However, they did not produce as good a separation as the 30-60% w/v linear sucrose gradient.

### **4.2.6 Fabrication of higher order structures with M13pIIISel and quantum dots**

#### **4.2.6.1 Fabrication using 14 nm quantum dots**

As discussed earlier, quantum dots (QD) would be the preferred island within a molecular transistor since they would allow it to be used at room temperature. Therefore experiments were undertaken to fabricate higher order structures with quantum dots and M13pIIISel phage.

Commercially available quantum dots were used with a fluorescence emission of 525 nm. These quantum dots consist of a CdSe/ZnS core with a surrounding PEG layer terminating in an amino group that is available for functionalisation with sulfo-SMCC; a hetero-bifunctional cross-linker that endows the quantum dots with a maleimide group (see Chapter 2, Table 2.3 for more details). The theoretical diameter of the QD after functionalisation with sulfo-SMCC is approximately 14 nm. This is slightly larger than the 10 nm gold nanoparticles used earlier. The maleimide group was then used to create a covalent selenol bond with the pIII displayed selenocysteine.

To create higher order structures using maleimide-functionalised QDs, the knowledge gained from working with GNP10nm/cit was used. 100  $\mu\text{L}$  of M13pIIISel ( $\sim 1 \times 10^{12}$  virions/mL) was mixed with freshly created maleimide functionalised QDs (maleimide hydrolyses very quickly in aqueous solutions at pH 7.5 and therefore cannot be stored successfully) at different ratios of phage to QD (from 35 phage per QD to 1 phage to 5 QD). Once again, the concentration of M13pIIISel was kept constant whilst increasing

that of the QDs. The mixtures were then allowed to equilibrate overnight and analysed on a 30-60% w/v linear sucrose gradient (the same set of conditions was used as above in section 4.2.4) A very different result was obtained (Figure 4.11 A) compared with gold nanoparticles (Figure 4.9).

Peak 1 contained no phage or quantum dots (Figure 4.11 A). This peak had no colour but is likely to be the buffer that the quantum dots were suspended in. Peak 2 contained quantum dots only (Figure 4.11 B) and peak 3 contained what appeared to be a mixture of single phage only and higher order structures (Figure 4.11 C-E), although the contrast of the images was poor. However, there was no separate higher order structure peak. Measuring the emission of the peaks at 525 nm (results not shown) showed that QDs were present in peaks 2 and 3. The presence of QDs in peak 3 may explain the rising absorbance seen as the amount of QDs increased since the quantum dots have a high absorbance at 260 nm, cf. 35:1 to 1:5 ratios in Figure 4.11.

Although the phage may have been binding to the QDs (although the results are less than convincing) the result shows that a linear sucrose gradient does not separate phage bound to QD from unbound phage. The reason for this is the molecular weight of the 525 nm emission QD. Unlike GNP10nm/cit, QDs don't pellet at the bottom of the tube but instead migrate above the phage. Therefore the QDs don't have enough mass to drag the bound phage away from the unbound phage.

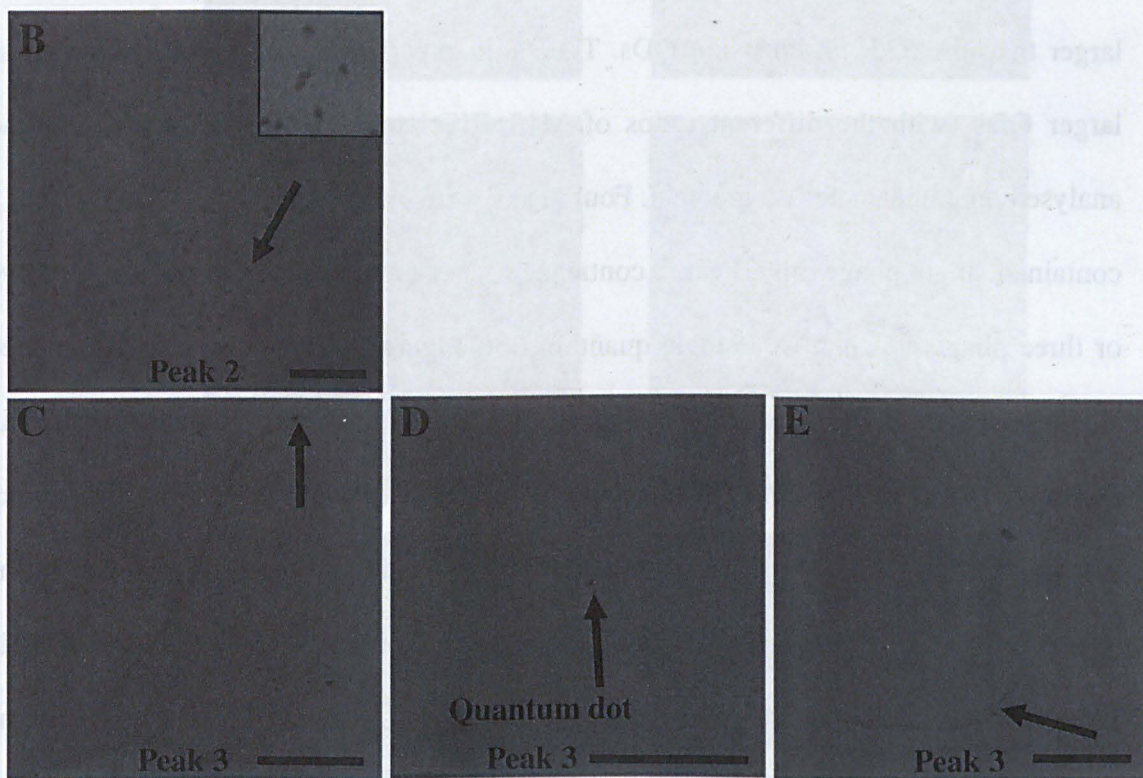
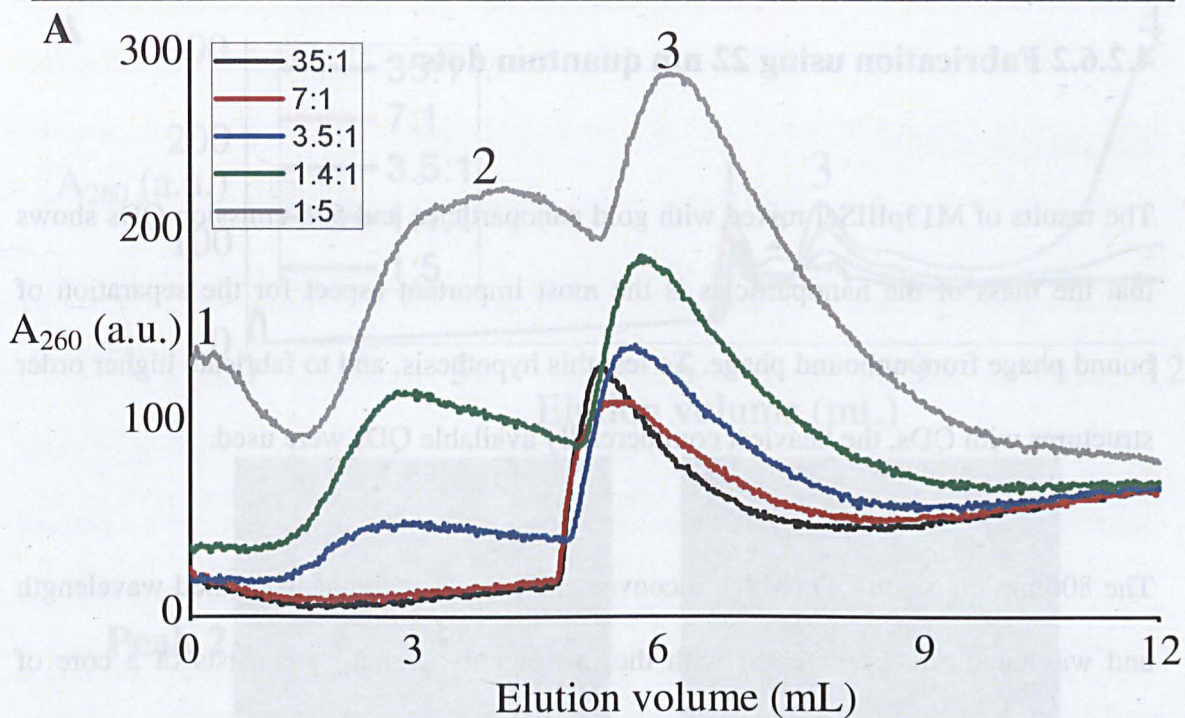


**Figure 4.11. Fabrication of higher order structures using M13pIIISeI phage and 525 nm emission QDs.** Purified using 30-60% linear sucrose gradient (A). Scale bar equals 200 nm. Arrows highlight quantum dots.

### 4.2.6.2 Fabrication using 22 nm quantum dots

The results of M13pIIISel mixed with gold nanoparticles and 525 emission QDs shows that the mass of the nanoparticles is the most important aspect for the separation of bound phage from unbound phage. To test this hypothesis, and to fabricate higher order structures with QDs, the heaviest commercially available QDs were used.

The 800 nm emission QD (which inconveniently emits at the near-infrared wavelength and was unable to be detected with the instruments available) consists of a core of CdTeSe/ZnS and when functionalised with maleimide has a diameter of 22 nm, i.e. 64% larger than the 525 nm emission QDs. The same experiment was repeated with these larger QDs (with the different ratios of M13pIIISel to 800 nm emission QDs) and analysed on a linear sucrose gradient. Four peaks were observed (Figure 4.12 A). Peak 1 contained single phage only. Peak 2 contained higher order structures consisting of two or three phage attached to a single quantum dot (Figure 4.12, B-E). Peak 3 contained single phage attached to 1 or 2 QDs (Figure 4.12, F and G). Peak 4 contained QDs only and shows that the 800 nm emission QDs, whilst heavier than the 525 nm QDs, were still lighter than the 10 nm gold nanoparticles. This difference in mass resulted in the peaks being far closer together (when compared to M13pIIISel and GNP10nm/cit in Figure 4.9) and therefore there were high levels of cross contamination between the peaks.

Therefore, even with the heaviest QDs available, using linear sucrose gradients still didn't provide ideal separation of higher order structures from unbound phage and phage bound to a single QD.

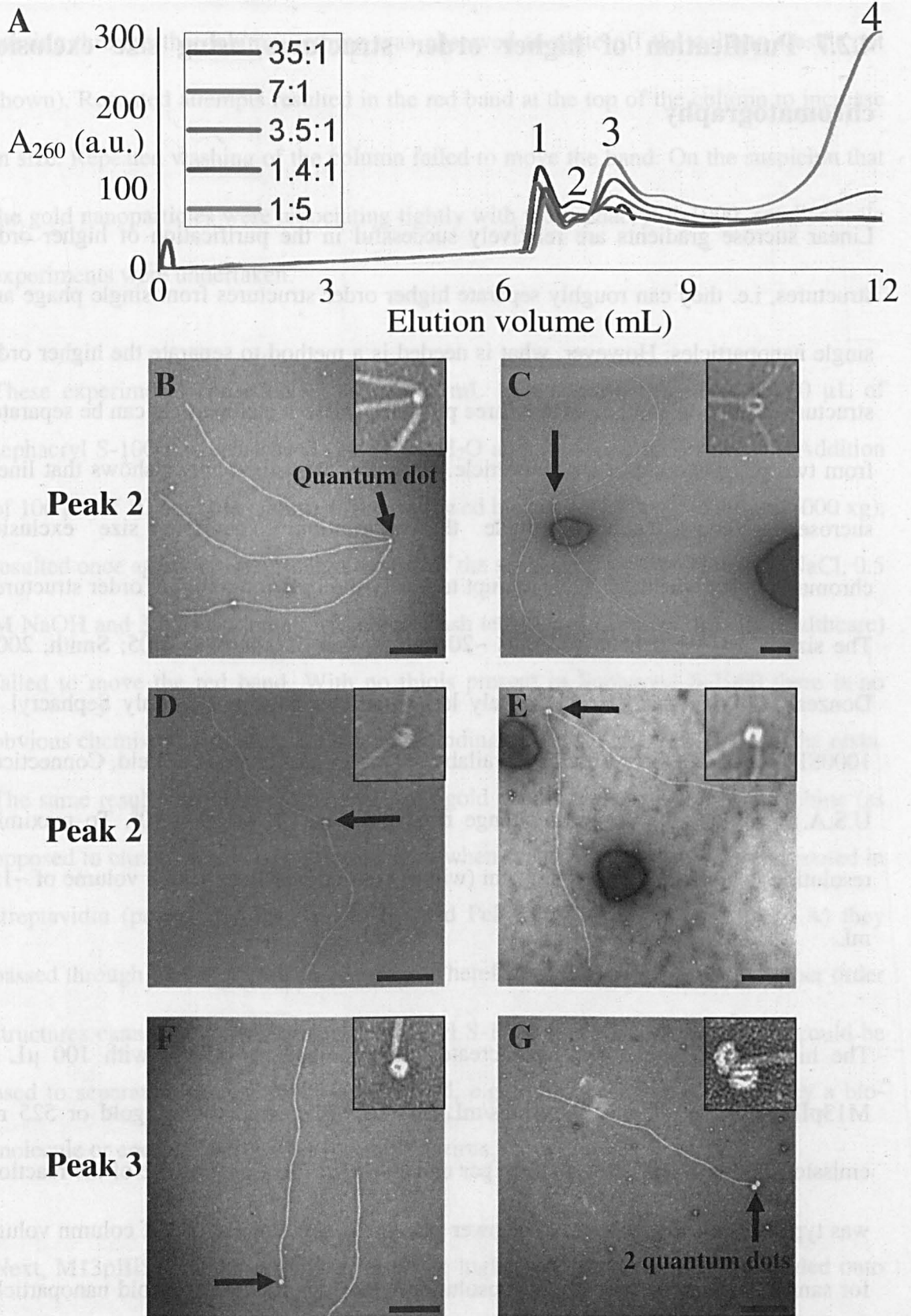


**Figure 4.12.** Fabrication of higher order structures using M13pIIISeI phage and 800 nm emission QDs. Purified on a 30-60% linear sucrose gradient (A). Scale bar equals 200 nm. B, E, F and G taken on CCD camera.

### 4.2.7 Purification of higher order structures using size exclusion chromatography

Linear sucrose gradients are relatively successful in the purification of higher order structures, i.e. they can roughly separate higher order structures from single phage and single nanoparticles. However, what is needed is a method to separate the higher order structures from one another so that three phage bound to a nanoparticle can be separated from two phage bound to a nanoparticle. The work described above shows that linear sucrose gradients cannot provide that resolution. Therefore size exclusion chromatography was used in an attempt to purify the individual higher order structures. The size of M13 has been given as ~20 megadalton (Zakharova, 2005; Smith, 2005, Donzeau, 2006), which is a relatively large particle. At  $2 \times 10^7$ , only Sephacryl S-1000SF (superfine), commercially available from GE healthcare (Fairfield, Connecticut, U.S.A.), provides the separation range needed:  $\sim 5 \times 10^5$  to  $\sim 5 \times 10^8$ . To maximise resolution, a 90 cm (length) x 1.5 cm (width) column was used with a volume of ~150 mL.

The higher order structures were created as described previously with 100  $\mu$ L of M13pIIISel phage ( $1 \times 10^{12}$  virions/mL) mixed with nanoparticles, gold or 525 nm emission QD, at a ratio of 1.4 phage per nanoparticle. The final volume of the reactions was typically 200  $\mu$ L, which is far lower than the recommended 1% of column volume for sample loading to have a good resolution. Once again, since the gold nanoparticles were cheaper than the QDs, the gold nanoparticle higher order structures were ran first on the column. Upon loading of the gold nanoparticles and phage it was observed that a red band appeared at the top of the column. After 1.5 column volumes to elute anything

passing through the column nothing was observed to elute off the column (result not shown). Repeated attempts resulted in the red band at the top of the column to increase in size. Repeated washing of the column failed to move the band. On the suspicion that the gold nanoparticles were associating tightly with the sephacryl S-1000, smaller scale experiments were undertaken.

These experiments consisted of using a 1 mL spin column loaded with 200  $\mu$ L of sephacryl S-1000, which was washed with H<sub>2</sub>O and then PBS buffer pH 7.2. Addition of 100  $\mu$ L of 10 nm gold nanoparticles, followed by low speed centrifugation (5000  $\times$ g), resulted once again in a red band at the top of the sephacryl. Washes with 5 M NaCl, 0.5 M NaOH and 30% isopropanol (standard wash techniques provided by GE Healthcare) failed to move the red band. With no thiols present in Sephacryl S-1000 there is no obvious chemistry to account for the tight binding of the gold nanoparticles to the resin. The same result was obtained when 10 nm gold nanoparticles coated in phosphine (as opposed to citrate) were used. Interestingly, when the gold nanoparticles were coated in streptavidin (provided commercially by Ted Pella, Redding, California, U.S.A) they passed through the resin with no retention. Therefore although phage: gold higher order structures cannot be purified using Sephacryl S-1000 it appears that the resin could be used to separate coated gold from bare gold, e.g. gold nanoparticles coated by a bio-molecule or encapsulated within a spherical virus.

Next, M13pIIISeI mixed with QDs to create higher order structures, were loaded onto the 90 cm column. The column was then eluted with 1.5 column volumes (~225 mL) and 15 mL fractions collected whilst measuring absorbance at 280 nm (Figure 4.13 A). Three main peaks were observed. The counting of different structures within each

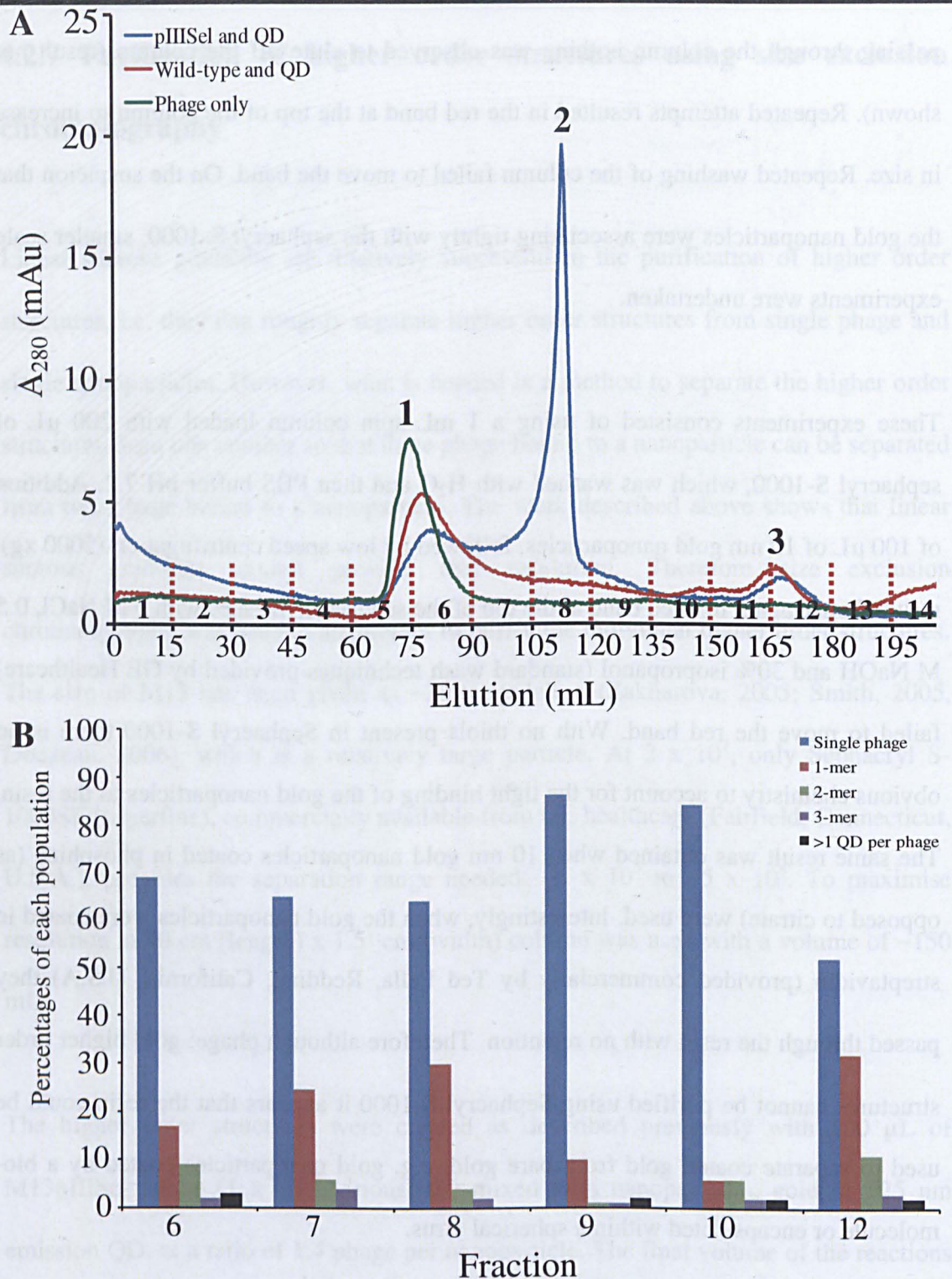


**Figure 4.13. Purification of higher order structures using size exclusion chromatography.** M13pIIISeI were mixed with maleimide functionalised 525 nm emission QDs. Mixture loaded onto a 150 mL Sephacryl S-1000SF resin column and eluted with 1.5 column volumes (A). The eluate was collected as 15 mL fractions (shown by red lines) and number of structures counted using TEM,  $n = 100$  (B).

fraction (Figure 4.13 B),  $n = 100$ , shows that although there are discrete peaks, none of them appear to relate to any distinct structure. All of the peaks contain a majority of single phage with some higher order structures mixed in. Although it is not possible to identify any specific structures to account for peaks 1 and 2, peak 3 contained countless QDs. Disappointingly, size exclusion also failed to purify higher order structures. In fact it performed worse than linear sucrose gradients.

### 4.2.8 Fabrication of higher order structures using microphage

The work described above has shown that higher order structures can be created using the M13 bacteriophage. However, since the length of the M13 phage particle is  $1\ \mu\text{m}$ , it means that when two phage are attached to a nanoparticle that the entire device is  $2\ \mu\text{m}$  in size. With regards to a transistor, it is the distance between the source and drain electrodes that is important. Since the phage are to be used as scaffolds for the deposition of gold to create the electrodes, then the distance between the electrodes will be the size of the quantum dot, i.e. 14 or 22 nm. Therefore the  $2\ \mu\text{m}$  length will not affect this important aspect. However, the size limits the number of the transistors that could be deposited on a surface. They are also very flexible with a persistence length of  $\sim 1.3\ \mu\text{m}$  (Khalil, 2007). This flexibility increases the chance that the phage particles attached to the nanoparticle will overlay upon each other; making the device useless.

The microphage (Chapter 3), at 50 nm in length, would be an ideal way to decrease the size of the higher order structures. Microphage<sup>III</sup>Sel were therefore produced using M13KO7 helper phage displaying selenocysteine on pIII (M13KO7p<sup>III</sup>Sel). Using M13KO7p<sup>III</sup>Sel resulted in microphage<sup>III</sup>Sel displaying selenocysteine on pIII.

MicrophageIII<sub>Sel</sub> were then purified using PEG/NaCl followed by Superose 6 size exclusion chromatography and resuspended in PBS pH 7.4. The specific amount of microphageIII<sub>Sel</sub> is difficult to define since, as discussed in Chapter 3, the microphage cannot be titered. It was also found that the peak at 269, used to calculate virions/ mL, shifts towards 260 nm.

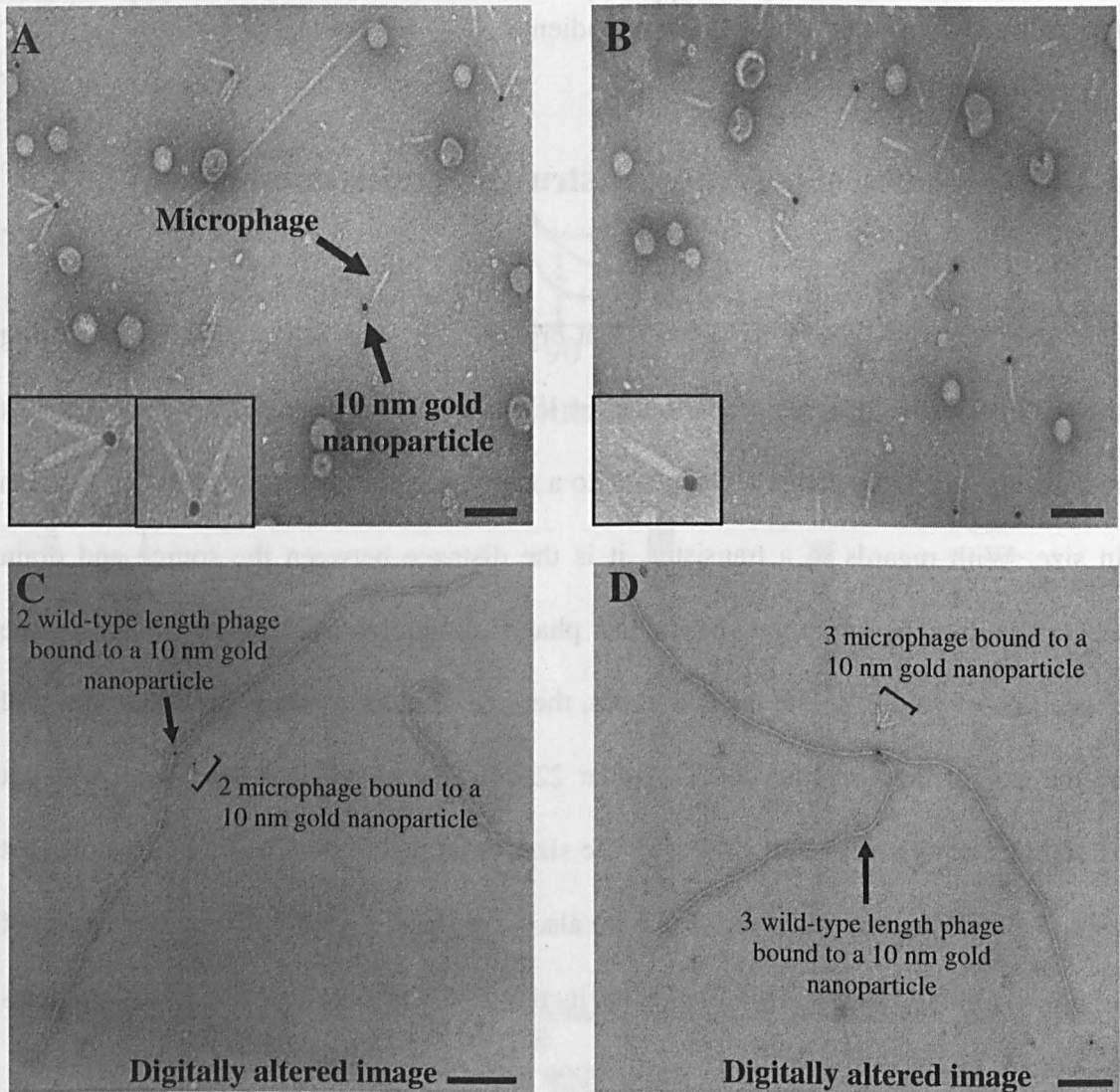


**Figure 4.14. Higher order structures using microphageIII<sub>Sel</sub>.** Microphage displaying selenocysteine on pIII were mixed with citrate stabilised 10 nm gold nanoparticles (A and B). C and D have been digitally altered using Adobe Photoshop™ to compare the higher order microphage structures with higher order structures created with wild-type length (~1µm) M13pIII<sub>Sel</sub> phage. Scale bar equals 200 nm.

The microphageIIISeI solution was measured at the following absorbances; 260 nm: 1.130; 269 nm: 0.975; 280 nm: 0.664; 320 nm: 0.009. The  $Abs_{269}$  value was used to calculate the number of microphageIIISeI particles (with a genome size of 221 bases):  $\sim 25 \times 10^{16}$  virions/mL. A very high value relative to typical phage yields.

Although the number of microphageIIISeI particles was unknown, 100  $\mu$ L of the microphageoIIISeI solution was mixed with 100  $\mu$ L of GNP10nm/cit and equilibrated overnight at room temperature. Due to time constraints no purification was attempted. However, some of the mixture was placed on a carbon coated TEM grid. The same structures were observed (Figure 4.14 A and B) as with wild-type length M13pIIISeI with two and three microphageIIISeI bound to a single gold nanoparticle (inset Figure 4.14 A) along with single microphageIIISeI bound to single gold nanoparticles (inset Figure 4.14 B). When compared with wild-type length higher order structures (Figure 4.14 C and D) it becomes clear how much smaller the microphageIIISeI higher order structures are. At  $\sim 100$  nm in size, they are  $\sim 20$  times smaller.

### 4.3 Conclusions and Future Work

The main aim of the work described within this chapter was to fabricate higher order structures. This aim was achieved by engineering M13 bacteriophage to display a highly reactive selenocysteine on pIII which would preferentially form a covalent bond with a nanoparticle. A secondary aim was to try and purify these structures from unbound reactants. As has been shown, the M13 bacteriophage can self-assemble into higher order structures with multiple phage capable of binding to a single gold nanoparticle or

quantum dot. The creation of higher order structures with M13 bacteriophage has been investigated before by Huang, *et al.* (2005). They created an M13 bacteriophage displaying a streptavidin-binding peptide on pIII and mixed it with gold nanoparticles and quantum dots coated in streptavidin. Although the original publication produced higher order structures, of two and three phage bound to a nanoparticle, the results were not convincing (Figure 4.3). The work in this chapter is far more definitive with many more examples of higher order structures being fabricated. The method used to create the higher order structures was also different. The use of a covalent selenol bond, instead of a streptavidin bond, to attach the phage to the nanoparticles, should result in far more stable structures being fabricated. The use of selenocysteine also allows for easier fabrication of higher order structures with different nanoparticles. Instead of having to attach a streptavidin to a nanoparticle, the selenocysteine can be used with just the nanoparticle. Future work could involve fabricating higher order structures with different nanoparticles, e.g. a magnetic nanoparticle.

A weakness within this study is the differences between the pfu/mL and virions/mL values. For this study I decided to use the virions/mL values since I was more interested in the number of phage particles. However, if that assumption is wrong, then all comparisons between M13pIIISel and M13 wild-type are called into question. This finding of differences between pfu/mL and virions/mL also calls into question the results of previous studies on M13pIIISel (Sandman, 2000) since pfu/mL values were used.

The observation that gold nanoparticles and quantum dots only bind to one end of the M13 particle strongly indicates that it is the selenocysteine that is forming the bond.

However, it was also observed that wild-type phage can also bind to gold nanoparticles, indicating that there is an accessible cysteine within the pIII molecule. Obviously this is an area of future work to ascertain which cysteine (of the eight within pIII) this is and to investigate if it can be removed without affecting phage yield. However, since none of the cysteines at the other end of the phage (within pIX and pVII) appear accessible to the nanoparticles then it may not be an issue for the future fabrication of higher order structures.

With regard to purifying the higher order structures there was less success, with linear sucrose gradients able to purify the structures away from reactants, e.g. single phage and nanoparticles, but unable to separate the individual structures. There also appeared to be a trade off between the purity of the purified higher order structures and the yield. Using a large excess of phage to gold nanoparticles, e.g. 35 phage per gold nanoparticle, provided a sample that comprised ~88% of higher order structures (2 or more phage bound to a single gold nanoparticle). However, the size of the peak containing the higher order structures (Peak 3 Figure 4.9) was smaller than the peaks found with other phage to gold ratios, indicating that the yield is low. Whereas using a small excess of phage, e.g. 7 phage per gold nanoparticle, results in a higher yield but lower purity of higher order structures: ~60% of the population.

Future work needs to find a method that can purify the individual higher order structures, e.g. two phage bound to a single nanoparticle from three phage bound to a single nanoparticle. Due to the flexibility of the phage it is unlikely that this will be possible with many purification techniques, e.g. agarose electrophoresis and size

## Chapter 4

---

exclusion chromatography, optimised for globular proteins of regular size. This problem may be overcome by using the microphage.

As has been shown, the microphage can be used to display selenocysteine and fabricate higher order structures with two or three microphage bound to a single nanoparticle. By using microphagepIIISeI it has been possible to miniaturise the higher order structures created within this study by 20 times to just 100 nm across. Due to their smaller size, they appear to be more rigid and therefore it may be possible to purify these higher order structures using caesium chloride or agarose gel electrophoresis. Future work would ideally focus on purifying these smaller structures instead of the larger ones.

# Chapter 5

---

## Phage Particle Attachment to a Gold Surface

The work described within this Chapter investigates whether the coiled-coil ACID:BASE pair can be used to anchor M13 phage particles to a surface.

## 5.1 Introduction

### 5.1.1 Coiled-coils

A coiled-coil forms when two or more amphipathic alpha helices twist around one another to form a stable, yet reversible (O'Shea, 1993), left-handed super-coil (Figure 5.1; O'Shea, 1992). Coiled-coils are known to form dimeric, trimeric and up to octomeric structures (Burkhard, 2001; Kohn, 1998). The coiled-coil structure motif is found in a large number of proteins: ~2 to 5% of all known proteins contain coiled-coils (Wolf, 1997), where the motif mediates the oligomerisation of protein subunits (Burkhard, 2001). Leucine zippers are well characterised coiled-coils, e.g. the yeast transcriptional factor GCN4 (Figure 5.1), which bind to DNA and act as transcription factors (O'Shea, 1992). However, coiled-coils are also involved in a wide range of other cellular functions, e.g. the creation of the cytoskeleton (Herrmann, 1999) whereby coiled-coils form the building blocks of the cytoskeletal filaments.

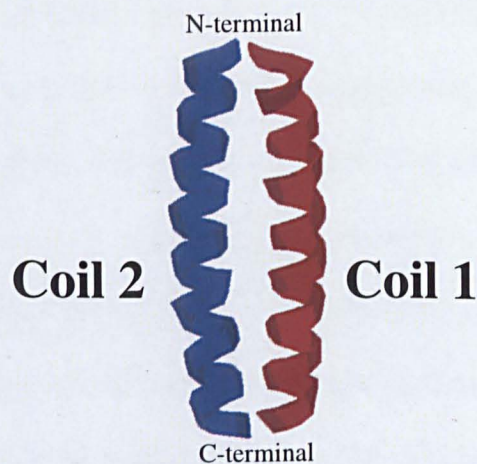


**Figure 5.1. Structure of a coiled-coil.** The x-ray crystal structure of the leucine zipper GCN4 in a parallel orientation, at 1.8 Å resolution, PDB accession code 2zta. O'Shea, *et al.* (1991).

Coiled-coils typically consist of a repeated pattern of 7 amino acids, where the residues are conventionally labelled “abcdefg” (Figure 5.2 A), termed a heptad repeat: a coiled-coil can contain between 2 to 200 repeats (Burkhard, 2000; Kohn, 1997). The heptad is repeated every 2 turns of the coil (Landschulz, 1988), and the interactions between the amino acids of the heptad repeat are vital to the structure of the super-coil. Coiled-coils have been termed “peptide Velcro” (O’Shea, 1993) since the amino acids at positions “a” and “d”, at the core of the super-coil, overlap one another, much like Velcro, forming interactions that stabilise the super-coil.

The amino acids at positions “a” and “d” are hydrophobic, e.g. leucine, alanine or isoleucine, which interact to create the hydrophobic core of the coiled-coil. This hydrophobic core is the main element that stabilises the super-coil. Amino acids at positions “b”, “c” and “f” play little role in the super-coil, although they must be hydrophilic (Graddis, 1993) since they are solvent exposed. The amino acids at positions “e” and “g” are charged and are commonly found to be glutamic acid or lysine. The charge of these amino acids dictates whether a homo- or hetero-dimer is formed (Figure 5.2 B; Shuermann, 1991). When the amino acid residues at “e” and “g” are oppositely charged then a homodimer is preferred, e.g. a positively charged lysine at “e” and a negatively charged glutamic acid at “g”. The oppositely charged residues of the coil mean that homodimer formation would result in favourable electrostatic interactions, e.g. positive charge to negative charge. Likewise, when the amino acid residues at “e” and “g” have similar charge then a heterodimer is preferred due to electrostatic repulsion between the charged amino acids.

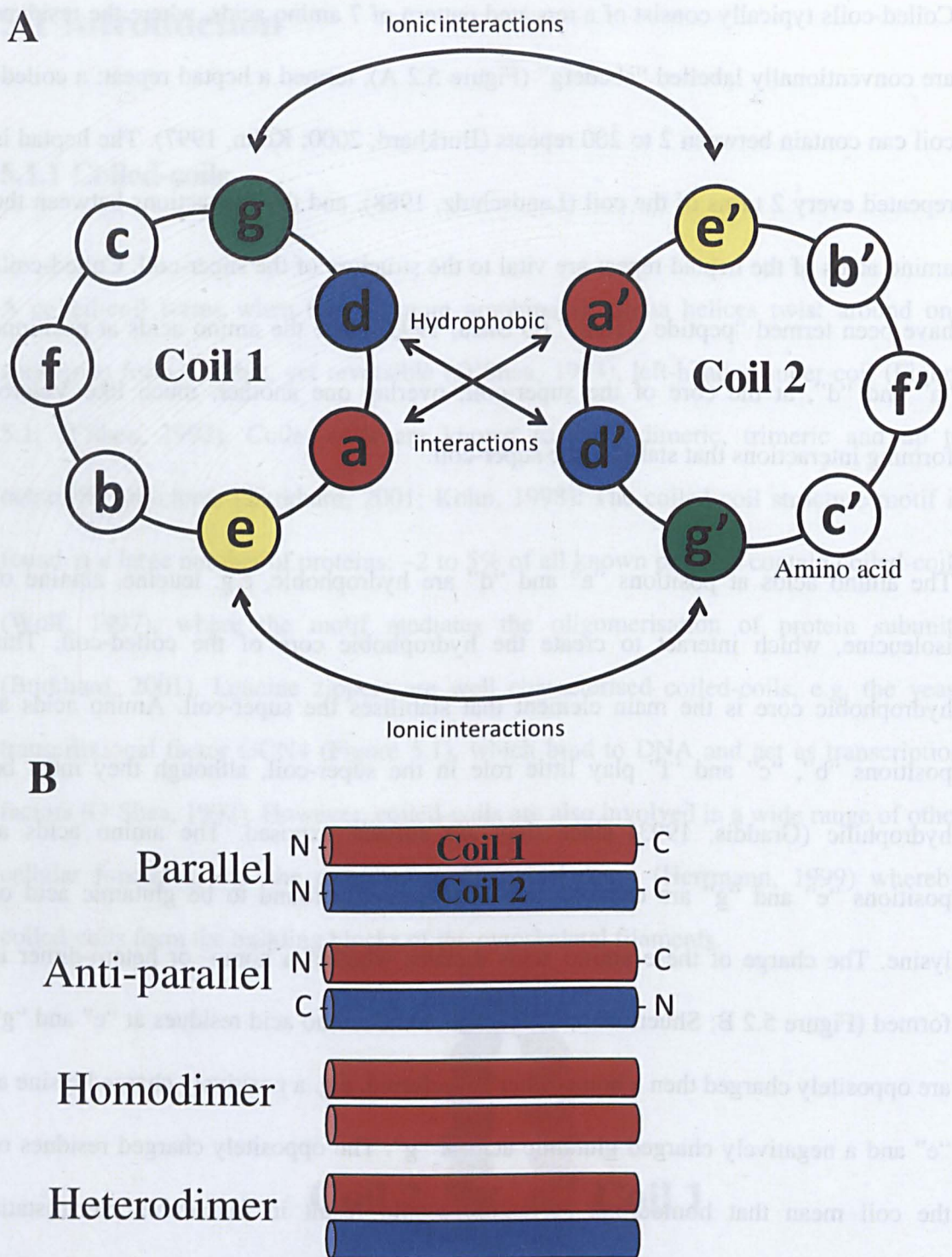


**Figure 5.2. Schematic showing coiled-coil interactions.** A shows helical wheels of the coiled-coils with the view shown looking along the super-coil axis. a – g represent the 7 amino acids that make up the coiled-coil heptad repeat. B shows the different orientations that coiled-coils can have.

The knowledge of the different roles that each amino acid has within a heptad means that coiled-coil pairs have been designed *in silico*. Perhaps the most well known being the ACID:BASE leucine zipper pair designed by O'Shea, *et al.* (1993). This pair of coils are identical except at positions "e" and "g" (Figure 5.3 A) with glutamic acid (E) present at positions "e" and "g" within the ACID peptide. Whilst at the same positions within BASE there is a lysine (K) residue. The result of this is that heterodimers are the pre-dominant species due to the electrostatic attraction of the oppositely charged glutamic acid and lysine residues. In the presence of BASE, ACID has a  $10^5$ -fold preference for heterodimers over homodimers (O'Shea, 1993). An asparagine residue (N) was placed within the third heptad repeat at position 14 of ACID and BASE (Figure 5.3 A). The polar residue stabilises the coiled-coil into the parallel orientation (Figure 5.2 B) via a hydrogen bond between the asparagine residues of ACID and BASE (O'Shea, 1991; O'Shea 1993). By moving the asparagine residues it was possible to create ACID:BASE coiled-coils that favoured the anti-parallel (ap) orientation (Oakley, 1998): termed ACIDap and BASEap (Figure 5.3 B). Within the anti-parallel orientation the amino acids at position "a" of ACID interact with those at position "d" of BASE.

The ACIDap:BASEap pair has been utilised to create multimeric M13 phage nanostructures (Figure 5.3 D; Sweeney, 2006). The ACIDap leucine zipper was displayed on pIII whilst its complementary partner, BASEap, was displayed on the opposite end of the phage particle on pIX (Figure 5.3 C). A phagemid system (Chapter 1, Figure 1.6 A) was used to accomplish the pIII and pIX display resulting in one ACIDap/BASEap pair displayed per phage particle.

A

**Parallel**

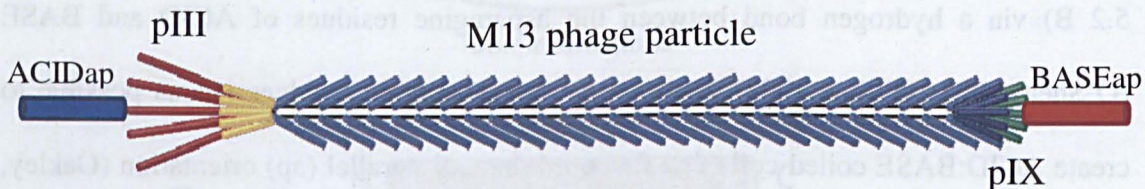
b c d e f g a b c d e f g a b c d e f g a b c d e f g a b c  
 ACID: N-AQLEKELQALEKENNAQLEWE LQALEK ELAQ-C  
 BASE: N-AQLKKKLQALKKKNAQLKWKLQALKKKLAQ-C  
 b' c' d' e' f' g' a' b' c'

B

**Anti-parallel**

b c d e f g a b c d e f g a b c d e f g a b c d e f g a b c  
 ACIDap: N-AQLEKE LQALEKEL AQLEWENNQALEKE LAQ-C  
 BASEap: C-QAL KKKLAQLKWKLQALKKKNAQLKKKLQA-N  
 c' b' a' g' f' e' d' c' b'

C



D

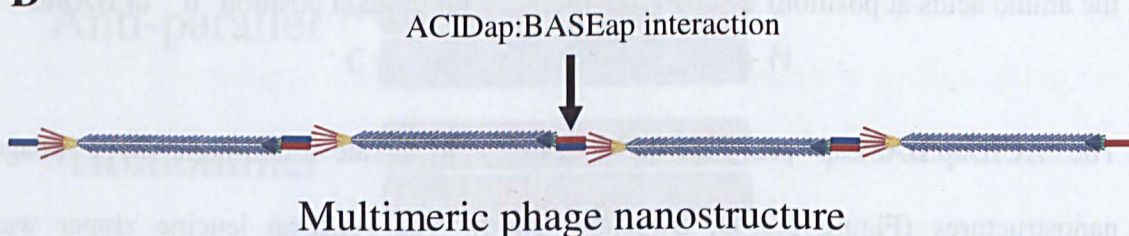


**Figure 5.3. The ACID:BASE leucine zipper pair.** Shows the sequence of ACID and BASE to create parallel (A) and anti-parallel (B) coiled-coils. C shows a schematic of the structure of the M13 phage particle created by Sweeney, et al. (2006), whilst D shows how the phage bound to one another.

Long filaments, the aforementioned multimeric phage nanostructures, were created by mixing these altered phage together: on average, ~8 phage particles were joined end to end via the ACIDap/BASEap interactions. However, in some instances ~30 phage particles were observed to have formed a 15  $\mu\text{m}$  long filament (Sweeney, 2006). This result suggests that the ACIDap/BASEap pair can be displayed upon the M13 phage particle and retain their function.

### 5.1.2 Attachment of M13 phage particles to a surface

The work of Sweeney, et al. (2006) raises the possibility that their use of the ACIDap/BASEap leucine zippers on M13 can be extended to attach an M13 particle to a gold surface (Figure 5.4 A). The work described within this chapter addresses this possibility. The rationale was as follows: firstly, display the ACIDap peptide on pIII and pIX of the M13 phage particle. The BASEap peptide would then be immobilised onto a gold surface using a cysteine-containing linker sequence (GGGSC) that had been added to the C-terminus of the peptide. By washing the M13 phage particle displaying the ACIDap over the gold surface the two coils would interact, forming the coiled-coil, and so anchoring the phage particle. This anchoring could then be taken further and used for the attachment of the higher order structures created in Chapter 4 to gold electrodes (Figure 5.4 B). Using the ACIDap/BASEap pair to attach the higher order structures to a surface adds another level of self-assembly and means that the structures can be accurately placed onto a surface instead of randomly deposited.

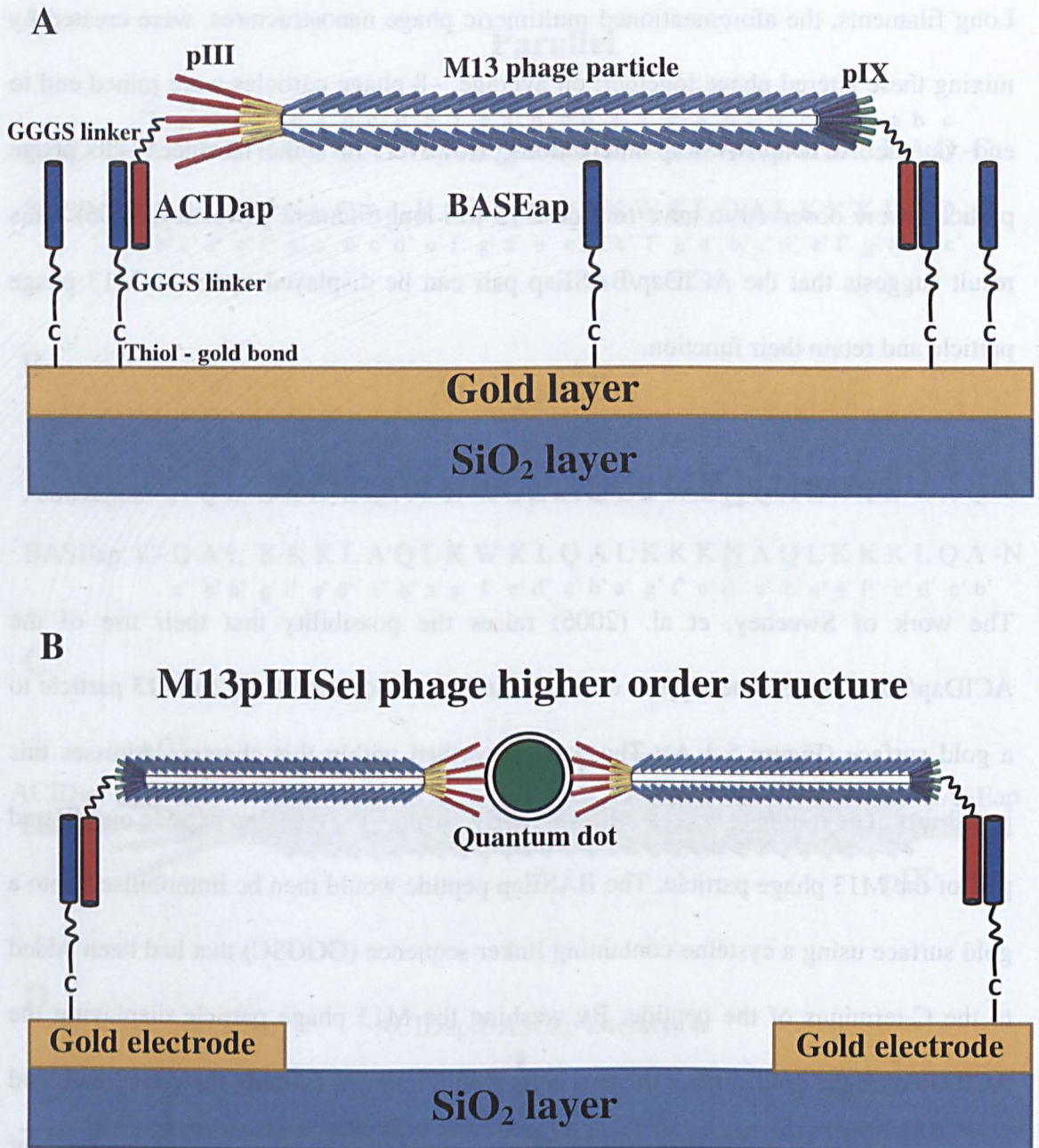


**Figure 5.4. Schematic of M13 phage particle attachment to a gold surface.** The rationale of the work described within this chapter to attach a phage (A) and a higher order structure (B) to a gold surface.

It was expected that the BASEap peptide would retain its function upon immobilisation given that other studies have attached coiled-coils to gold surfaces (Schlizerman, 2010; Stevens, 2004). However, these studies attached pre-formed coiled-coils to gold surfaces, i.e. the coiled-coil was formed in solution and attached to the surface. The coiled-coil, comprised of coils between 24 and 76 amino acids long, contained a C- or N-terminal cysteine residue on one or both of the coils so they could be immobilised onto the gold surface via thiol:gold bonds. A single study has been performed investigating coiled-coil formation on a surface (Johnson, 2005). However, he used 210-355 amino acid long proteins containing coiled-coils to perform the experiments.

### 5.1.3 Aims of the work described within this Chapter

The aims were as follows:

1. To display the ACIDap peptide on pIII and pIX.
2. To immobilise BASEap peptide to a gold surface using a cysteine residue.
3. To investigate the functionality of the BASEap peptide and its ability to interact with its complementary partner, ACIDap, and a phage displayed ACIDap peptide, using Surface Plasmon Resonance (SPR) and Dual Polarisation Interferometry (DPI).

### 5.2 Results and Discussion

#### 5.2.1 Production and purification of ACIDap and BASEap peptides

ACIDap (AQLEKELQALEKELAQLEWENQALEKELAQ) and BASEap (AQLKKKLQANKKKLAQLKWKLQALKKKLAQGGGSC) were purchased from Peptide Protein Research Ltd. (Wickham, Hampshire, U.K.). Peptide Protein Research Ltd. had desalted the peptides using High-Performance Liquid Chromatography (HPLC) and analysed them using mass spectrometry which confirmed they were the correct sequence. However, further HPLC purification was carried out once the peptides had arrived.

Each peptide was HPLC purified using a reverse phase C18-silica Zorbax ODS (dimethyl-n-octadecyl silane) column (Agilent Technologies, Santa Clara, CA, U.S.A.). The absorbance at 280 nm of the sample was measured and the peaks fractionated (Figure 5.5). Both samples were relatively pure with a single large peak (Figure 5.5 A and B). However, the BASEap sample gave a trailing peak (Figure 5.5 A) which suggested that larger peptides were present. The tail of this peak was also collected (Fraction 2). These samples were then analysed using mass spectrometry (Micromass Platform II, Waters Corporation, Milford, MA, U.S.A.) which confirmed that the peptides contained within fraction 1 were of the correct size (Appendix C, section 1.0). The tail of the BASEap sample peak was found to contain peptides ~100 Da larger (Appendix C, section 1.0). Therefore only the BASEap fraction 1 was used for further experiments.

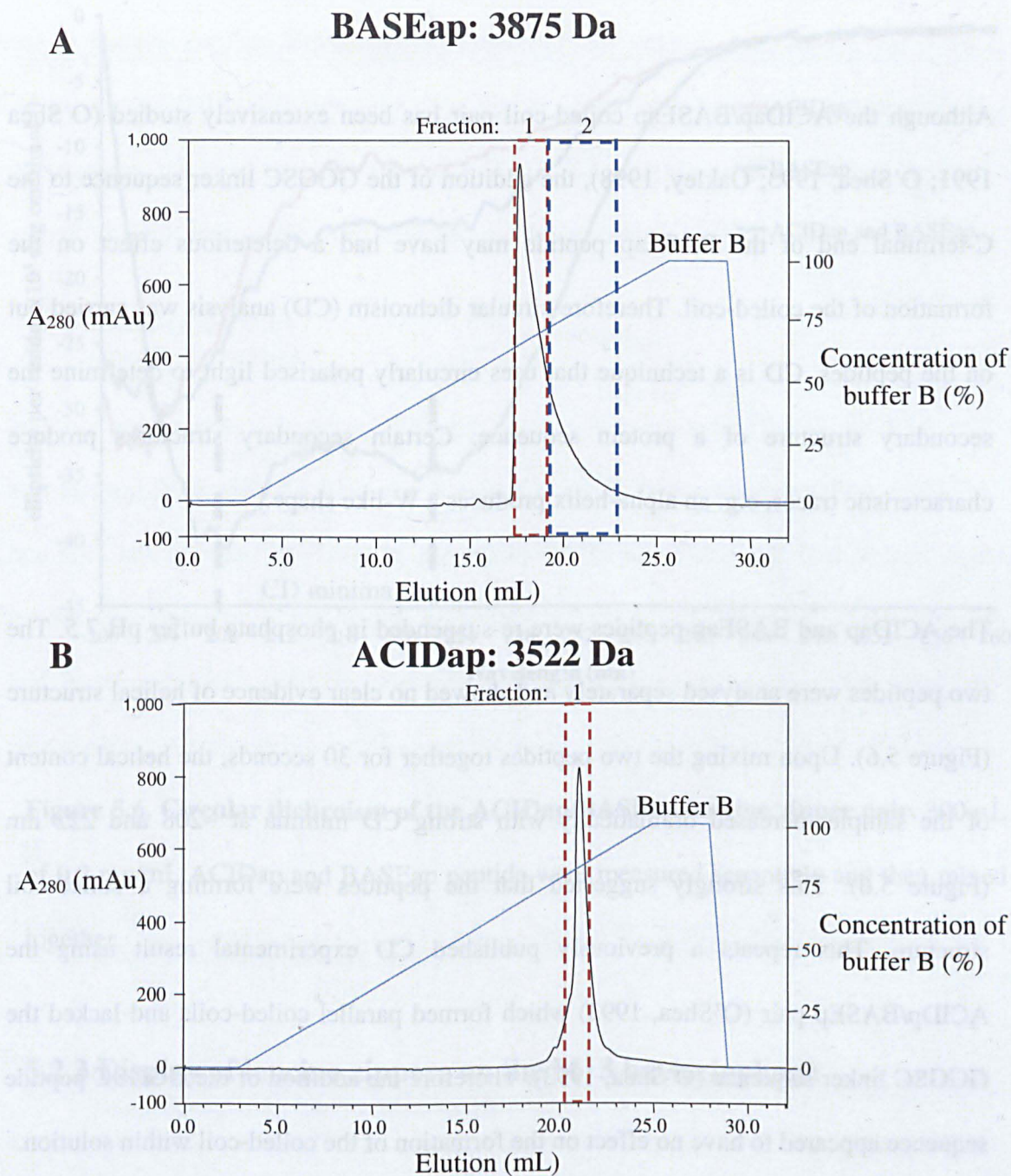


**Figure 5.5. HPLC purification of ACIDap and BASEap peptides.** Purification of 200  $\mu\text{L}$  of 25 mg/mL BASEap (A) and ACIDap (B) peptides using a reverse phase Zorbax ODS column (comprised of C-18 silica gel with dimethyl-n-octadecyl silane). Running buffer A was 5% v/v acetonitrile, 0.1% v/v trifluoroacetic acid (TFA) and B was 90% v/v acetonitrile, 0.06% v/v TFA.

### 5.2.2 Analysis of ACIDap/BASEap coiled-coil formation

Although the ACIDap/BASEap coiled-coil pair has been extensively studied (O'Shea 1991; O'Shea, 1993; Oakley, 1998), the addition of the GGGSC linker sequence to the C-terminal end of the BASEap peptide may have had a deleterious effect on the formation of the coiled-coil. Therefore circular dichroism (CD) analysis was carried out on the peptides. CD is a technique that uses circularly polarised light to determine the secondary structure of a protein sequence. Certain secondary structures produce characteristic traces, e.g. an alpha-helix produces a W-like shape.

The ACIDap and BASEap peptides were re-suspended in phosphate buffer pH 7.5. The two peptides were analysed separately and showed no clear evidence of helical structure (Figure 5.6). Upon mixing the two peptides together for 30 seconds, the helical content of the sample increased dramatically with strong CD minima at ~208 and 222 nm (Figure 5.6). This strongly suggested that the peptides were forming a coiled-coil structure. This repeats a previously published CD experimental result using the ACIDp/BASEp pair (O'Shea, 1993) which formed parallel coiled-coils and lacked the GGGSC linker sequence (O'Shea, 1993). Therefore the addition of the GGGSC peptide sequence appeared to have no effect on the formation of the coiled-coil within solution.

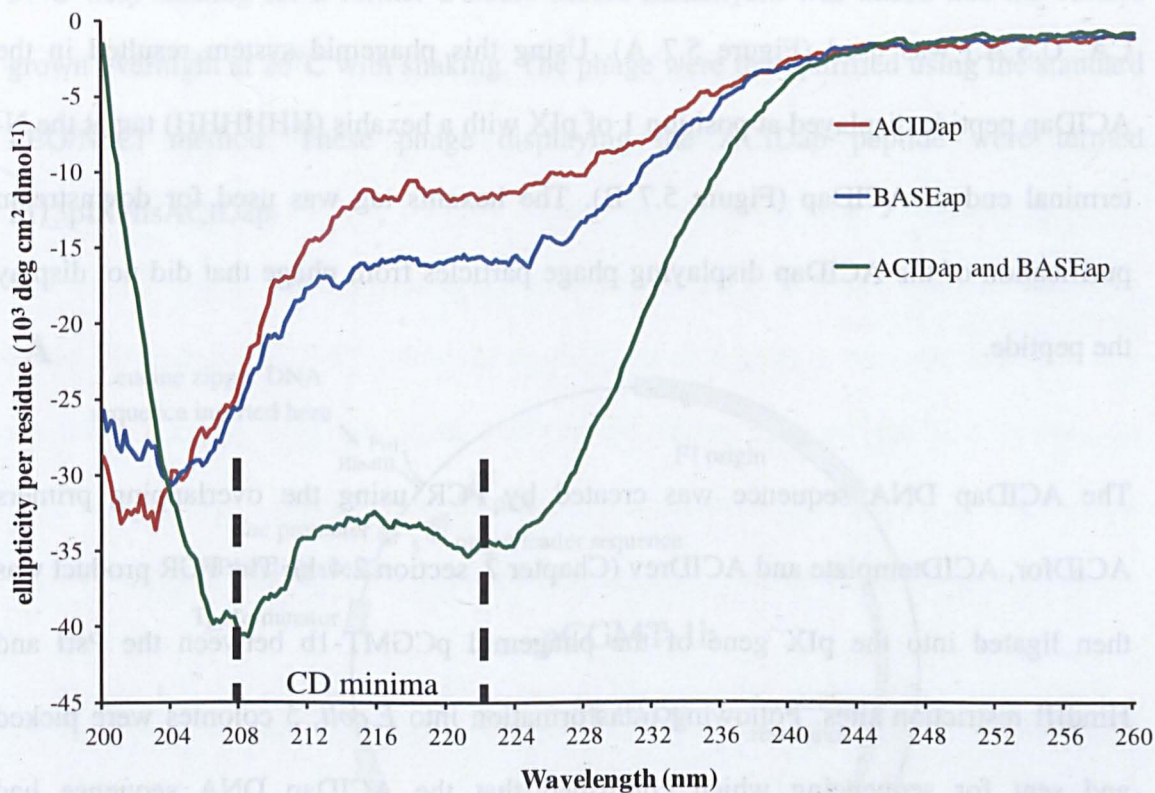


**Figure 5.6. Circular dichroism of the ACIDap/BASEap leucine zipper pair.** 300  $\mu\text{L}$  of 0.2 mg/mL ACIDap and BASEap peptide were measured separately and then mixed together.

### 5.2.3 Display of leucine zippers on the M13 bacteriophage

#### 5.2.3.1 Display of ACIDap on pIX

N-terminal display of peptides on pIX is problematic because the start codon (ATG) of pIX overlaps with the stop codon (TGA) of pVII. The standard practice is to use a phagemid system of display (Chapter 1, section 1.4.1). To this end, the phagemid

pCGMT-1b (kindly provided by Dr Bin Zhou, The Scripps Research Institute, La Jolla, CA, U.S.A.) was used (Figure 5.7 A). Using this phagemid system resulted in the ACIDap peptide displayed at position 1 of pIX with a hexahis (HHHHHH) tag at the N-terminal end of ACIDap (Figure 5.7 B). The hexahis tag was used for downstream purification of the ACIDap displaying phage particles from phage that did not display the peptide.

The ACIDap DNA sequence was created by PCR using the overlapping primers ACIDfor, ACIDtemplate and ACIDrev (Chapter 2, section 2.4.1). The PCR product was then ligated into the pIX gene of the phagemid pCGMT-1b between the PstI and HindIII restriction sites. Following transformation into *E.coli*, 5 colonies were picked and sent for sequencing which confirmed that the ACIDap DNA sequence had successfully been inserted into pIX. One was carried forward for further experiments and termed pCGMTpIXHisACIDap (Appendix C, section 2.0).

### 5.2.3.2 Production and purification of M13pIXHisACID

M13KO7 phage displaying ACIDap on pIX were produced from pCGMTpIXHisACIDap using the method of Gao, *et al.* (2002). 5 L of super-broth medium, inoculated with *E.coli* ER2738 containing pCGMTpIXHisACIDap, were grown to an OD<sub>600</sub> of ~0.5 in the presence of carbenicillin and tetracycline. The pIX gene within pCGMT-1b is under the control of the *lac* promoter. Therefore Isopropyl  $\beta$ -D-1-thiogalactopyranoside (IPTG) was added to a final concentration of 1 mM along with  $1 \times 10^{12}$  pfu/mL of the helper phage M13KO7. The culture was then incubated at

## Chapter 5

37°C with shaking for a further 2 hours before kanamycin was added and the culture grown overnight at 25°C with shaking. The phage were then purified using the standard PEG/NaCl method. These phage displaying the ACIDap peptide were termed M13pIXHisACIDap.

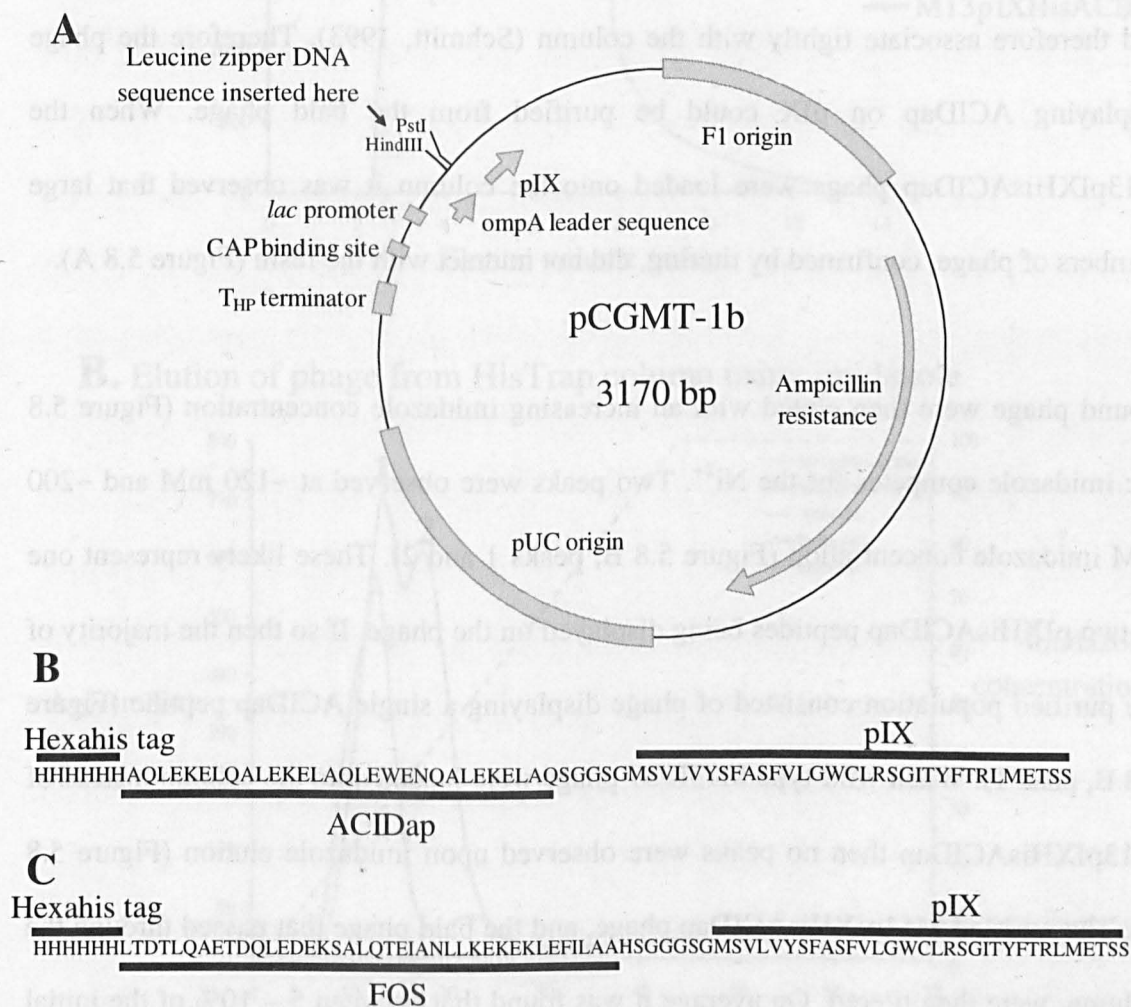


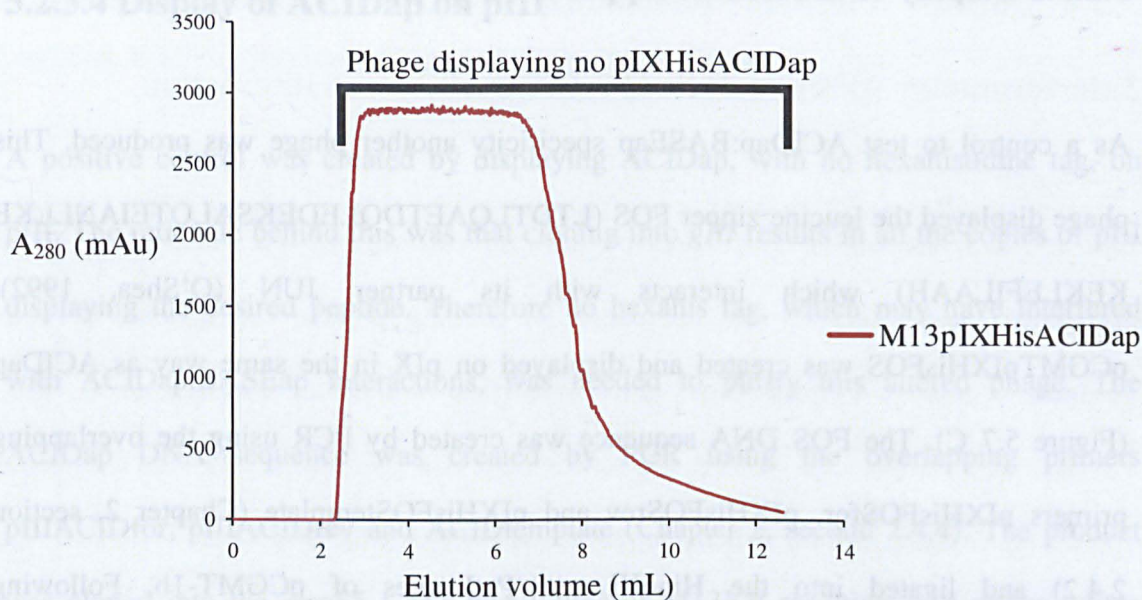
**Figure 5.7. Display of the ACIDap peptide on pIX.** Shows the phagemid pCGMT-1b (A) used to display the ACIDap (B) and FOS (C) peptides on pIX.

The use of phagemid vectors to display peptides typically results in 10% of the phage population displaying the desired peptide (Clackson, 2004). The rest are termed “bald”

since they display no peptide. Therefore the N-terminal hexahis tag was utilised to purify the phage displaying the ACIDap peptide (Figure 5.7 B). The PEG/NaCl purified phage were washed across a HisTrap™ column (GE Healthcare, Little Chalfont, Buckinghamshire, U.K.). These are pre-packed with Ni Sepharose High Performance resin and charged with Ni<sup>2+</sup> ions. Hexahistidine tags have a high affinity for the Ni<sup>2+</sup> and therefore associate tightly with the column (Schmitt, 1993). Therefore the phage displaying ACIDap on pIX could be purified from the bald phage. When the M13pIXHisACIDap phage were loaded onto the column it was observed that large numbers of phage, confirmed by titering, did not interact with the resin (Figure 5.8 A).

Bound phage were then eluted with an increasing imidazole concentration (Figure 5.8 B): imidazole competes for the Ni<sup>2+</sup>. Two peaks were observed at ~120 mM and ~200 mM imidazole concentration (Figure 5.8 B, peaks 1 and 2). These likely represent one or two pIXHisACIDap peptides being displayed on the phage. If so then the majority of the purified population consisted of phage displaying a single ACIDap peptide (Figure 5.8 B, peak 1). When wild-type M13KO7 phage were loaded onto the column instead of M13pIXHisACIDap then no peaks were observed upon imidazole elution (Figure 5.8 B). The purified M13pIXHisACIDap phage, and the bald phage that passed through the column, were then titered. On average it was found that between 5 – 10% of the initial phage population displayed at least one pIXHisACIDap peptide. Mass spectrometry was then attempted upon the phage to determine if ACIDap was present. However, the signal from the major coat protein pVIII, ~2700 copies per phage, dwarfed that of pIX, ~5 copies per phage, so the display of ACIDap could not be confirmed. However, the presence of the hexahis tag, together with the correct DNA sequence of this construct, means that the ACIDap peptide must be present.

### A. Loading of M13pIXHisACIDap on HisTrap column



### B. Elution of phage from HisTrap column using imidazole

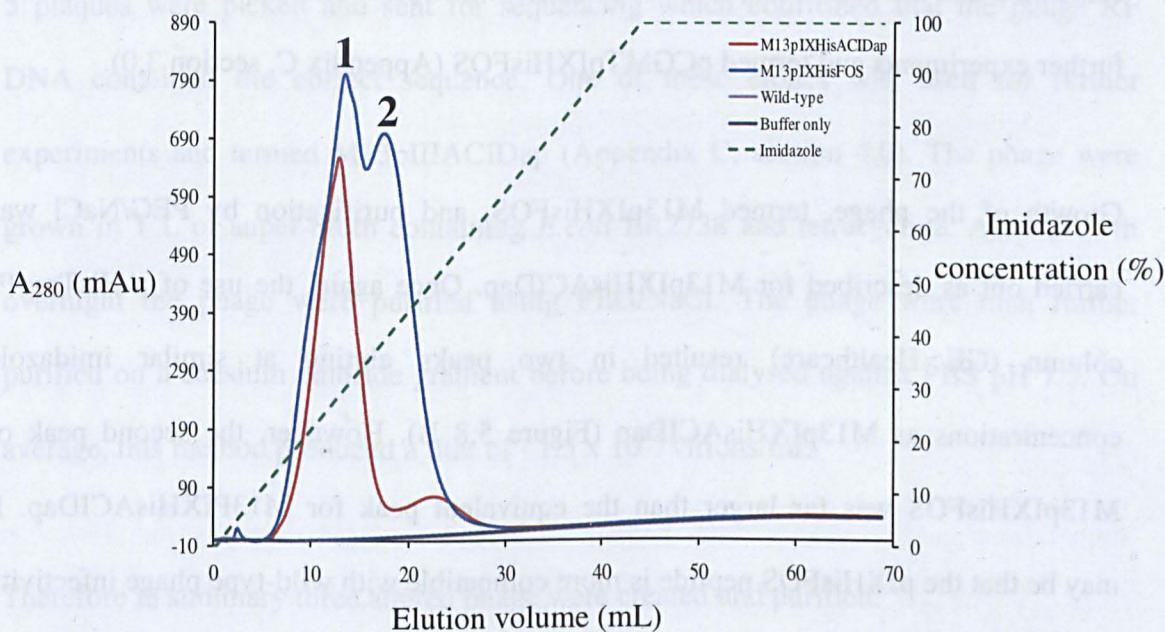


**Figure 5.8.** HisTrap™ column purification of M13pIXHisACIDap and M13pIXHisFOS. PEG/NaCl purified phage were loaded onto a 5 mL HisTrap™ column (A). M13pIXHisFOS loading can be overlaid that of M13pIXHisACIDap. Phage associated with column resin were then eluted with an increasing imidazole concentration (B).

### 5.2.3.3 Display of the leucine zipper FOS on pIX

As a control to test ACIDap:BASEap specificity another phage was produced. This phage displayed the leucine zipper FOS (LTDTLQAETDQLEDEKSALQTEIANLLKE KEKLEFILAAH) which interacts with its partner JUN (O'Shea, 1992). pCGMTpIXHisFOS was created and displayed on pIX in the same way as ACIDap (Figure 5.7 C). The FOS DNA sequence was created by PCR using the overlapping primers pIXHisFOSfor, pIXHisFOSrev and pIXHisFOSemplate (Chapter 2, section 2.4.2) and ligated into the HindIII and PstI sites of pCGMT-1b. Following transformation into *E.coli*, 5 colonies were picked and sent for sequencing which confirmed that the correct sequence been inserted into pIX. One was carried forward for further experiments and termed pCGMTpIXHisFOS (Appendix C, section 3.0).

Growth of the phage, termed M13pIXHisFOS, and purification by PEG/NaCl was carried out as described for M13pIXHisACIDap. Once again, the use of a HisTrap™ column (GE Healthcare) resulted in two peaks eluting at similar imidazole concentrations as M13pIXHisACIDap (Figure 5.8 B). However, the second peak of M13pIXHisFOS was far larger than the equivalent peak for M13pIXHisACIDap. It may be that the pIXHisFOS peptide is more compatible with wild-type phage infectivity than pIXHisACIDap, allowing for more phage to display two peptides. After repeated cultures and purifications it was found that the titer of M13pIXHisFOS was ~10 times that of M13pIXHisACIDap ( $\sim 7 \times 10^{13}$  against  $\sim 0.7 \times 10^{13}$  virions/mL). This further indicates that the pIXHisFOS peptide is more compatible with wild-type phage infectivity than pIXHisACIDap.

### 5.2.3.4 Display of ACIDap on pIII

A positive control was created by displaying ACIDap, with no hexahistidine tag, on pIII. The rationale behind this was that cloning into *gIII* results in all the copies of pIII displaying the desired peptide. Therefore no hexahis tag, which may have interfered with ACIDap:BASEap interactions, was needed to purify this altered phage. The ACIDap DNA sequence was created by PCR using the overlapping primers pIIIACIDfor, pIIIACIDrev and ACIDtemplate (Chapter 2, second 2.4.4). The product was cloned into the Acc65 I and Eag I sites of M13KE resulting in a phage where ACIDap was displayed at position 1 of the pIII protein. After transformation into *E.coli*, 5 plaques were picked and sent for sequencing which confirmed that the phage RF DNA contained the correct sequence. One of these clones was used for further experiments and termed M13pIIIACIDap (Appendix C, section 4.0). The phage were grown in 1 L of super-broth containing *E.coli* ER2738 and tetracycline. After growth overnight the phage were purified using PEG/NaCl. The phage were then further purified on a caesium chloride gradient before being dialysed against PBS pH 7.5. On average, this method produced a titer of  $\sim 1.5 \times 10^{13}$  virions/mL.

Therefore in summary three altered phage were created and purified:

1. M13pIXHisACIDap: displaying HisACIDap on  $\sim 1$  copy of pIX per phage,
2. M13pIXHisFOS: displaying HisFOS on  $\sim 1$  copy of pIX per phage (negative control),
3. M13pIIIACIDap: displaying ACIDap on  $\sim 5$  copies of pIII (positive control).

### 5.2.4 Surface Plasmon Resonance (SPR) and Dual Polarisation Interferometry (DPI) analysis of ACIDap:BASEap interaction

DPI and SPR are similar techniques in that they can both be used to measure mass adsorption onto a surface and are useful in probing peptide interactions. In both methods, a peptide is immobilised onto the surface of a sensor chip (Homola, 1999; Cross, 2003). In the case of SPR the sensor chip is a gold surface to which cysteine containing peptides can be directly immobilised using a thiol:gold bond. With DPI, the immobilisation chemistry is slightly different because the sensor chip is made from silicon oxynitride. To immobilise the peptide the sensor chip must first be functionalised with a silicon reactive heterobifunctional cross-linker which reacts with the silicon and produces exposed thiols to solution. A copper (II) solution is then washed over the sensor chip. The copper is reduced by the exposed thiols to copper (I). This reduced copper is then used to form a covalent bond with the thiol contained within the peptide (Johnson, 2008).

The goal of using the ACIDap:BASEap coiled-coil was to orientate phage displaying the ACIDap peptide onto a surface using an immobilised BASEap peptide. Therefore SPR and DPI were used to investigate whether the ACIDap:BASEap coiled-coil would form when the BASEap peptide was first covalently immobilised on a surface and the ACIDap peptide washed over it. Before continuing it must be noted that although SPR and DPI are powerful techniques that can, when used properly, provide useful data, e.g. association and dissociation kinetics of peptide interactions, within this study the two

techniques were primarily used as a method to detect binding between the ACIDap:BASEap peptides or between phage and BASEap.

**5.2.4.1 SPR analysis of BASEap:ACIDap coiled-coil formation**

SPR and DPI instruments have multiple channel sensor chips: SPR has 4 flow cells and DPI has 2 sample wells (Figure 5.9). The sample well and flow cell are both just channels within the sensor chip upon which experiments can be carried out. The presence of multiple sample wells or flow cells allows for simultaneous experiments to be performed independently of one another on the same sensor chip.

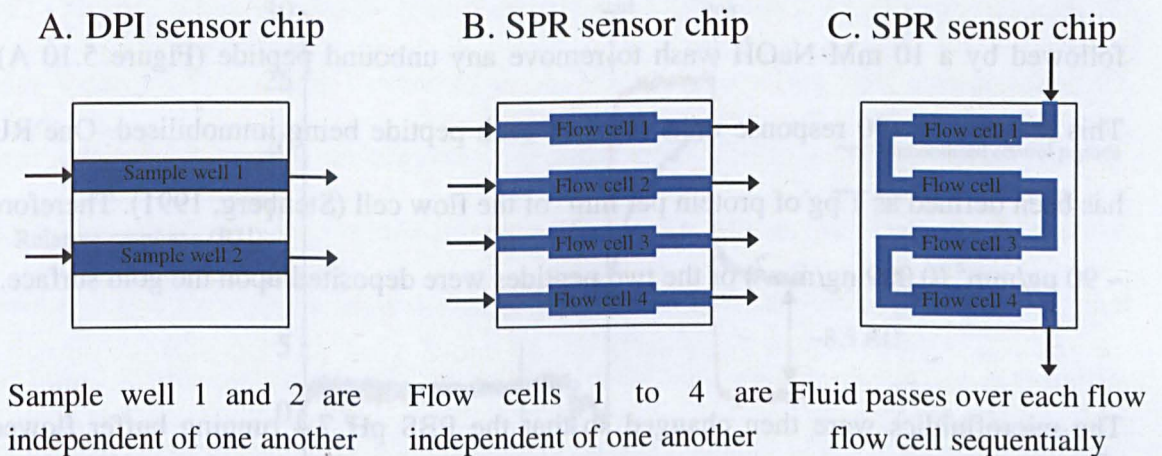


**Figure 5.9. Schematic of DPI and SPR sensor chips.** Shows how the fluid flows (denoted by arrows) through each DPI sample well (A) or SPR flow cell (B and C). In the case of SPR the micro-fluidics can be changed so the flow cells are independent (B), or in series (C), so that a single analyte can be passed over all 4 flow cells.

Although SPR has four channels, only two were used: one to immobilise BASEap and the other to immobilise a control peptide (SLDTLAEQLDPSANNVLSC) which was provided by Dr Steve Johnson (School of Electronic and Electrical Engineering, University of Leeds, U.K.). The control peptide was chosen as it was an unrelated non-leucine zipper peptide that was available within the lab. The SPR microfluidics were configured so that each flow cell was independent of one another (Figure 5.9, B). The control peptide and HPLC purified BASEap were immobilised onto flow cell 2 and 3, respectively, of a bare gold SPR sensor chip. Flow cell 1 and 4 were left as bare gold. Two 50  $\mu\text{L}$  injections of each peptide were performed. Previous studies have shown that gold:thiol bonds are formed within minutes (Lee, 2005). Therefore at a flow rate of 10  $\mu\text{L}/\text{min}$  it was expected that the peptides would be immobilised. These injections were followed by a 10 mM NaOH wash to remove any unbound peptide (Figure 5.10 A). This resulted in  $\sim 90$  response units (RU) of each peptide being immobilised. One RU has been defined as 1 pg of protein per  $\text{mm}^2$  of the flow cell (Stenberg, 1991). Therefore  $\sim 90$   $\text{pg}/\text{mm}^2$  ( $0.009$   $\text{ng}/\text{mm}^2$ ) of the two peptides were deposited upon the gold surface.

The microfluidics were then changed so that the PBS pH 7.4 running buffer flowed sequentially over the flow cells, i.e. 1 then 2 then 3 (Figure 5.9, C), and left overnight to equilibrate with the running buffer at a flow rate of 10  $\mu\text{L}/\text{min}$ . It was observed that the base line changed with an increase to  $\sim 170$  RU before stabilising (Figure 5.10 A). This new value was then used as the base line, i.e. 0 RU, for examining ACIDap interactions with BASEap and the control peptide. 1 mg/mL of ACIDap peptide, in PBS pH 7.4, was injected across the two immobilised peptides (Figure 5.10 B). Although there was no change in response for the control peptide, an increase of  $\sim 8.5$  RU was observed on the flow cell containing immobilised BASEap.

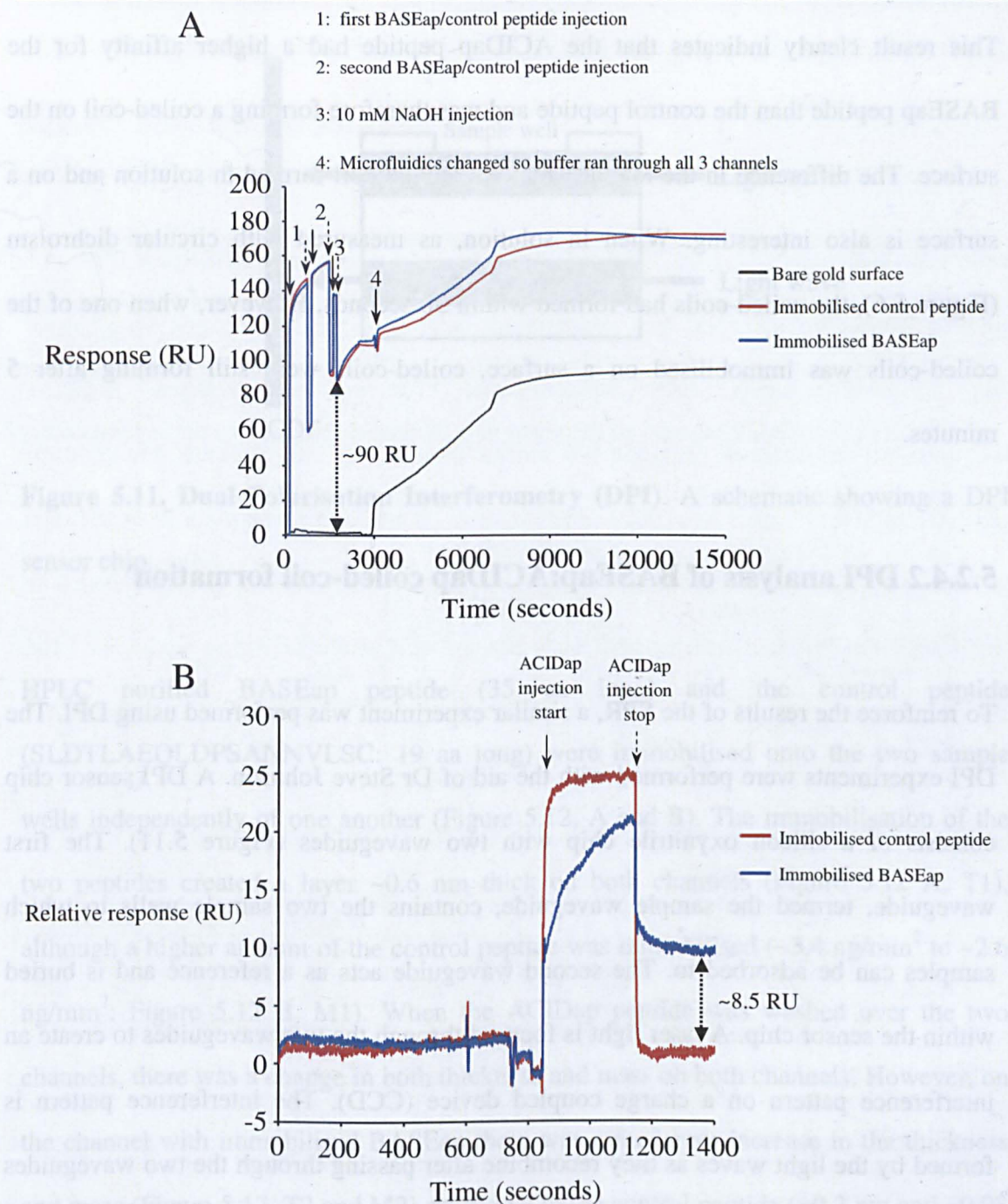


**Figure 5.10. SPR analysis of ACIDap:BASEap interactions.** A) shows a raw sensogram of BASEap and a control peptide immobilised on two separate channels via their thiol group in a PBS pH 7.4 running buffer. B) shows a corrected sensogram, relative to the bare gold surface, of ACIDap washed over the channels to investigate its interactions with the two immobilised peptides. The start and end of sample injections are indicated by solid and hashed arrows, respectively.

This result clearly indicates that the ACIDap peptide had a higher affinity for the BASEap peptide than the control peptide and was therefore forming a coiled-coil on the surface. The difference in the rate at which the coiled-coil formed in solution and on a surface is also interesting. When in solution, as measured with circular dichroism (Figure 5.6), the coiled-coils had formed within 30 seconds. However, when one of the coiled-coils was immobilised on a surface, coiled-coils were still forming after 5 minutes.

### **5.2.4.2 DPI analysis of BASEap:ACIDap coiled-coil formation**

To reinforce the results of the SPR, a similar experiment was performed using DPI. The DPI experiments were performed with the aid of Dr Steve Johnson. A DPI sensor chip consists of a silicon oxynitride chip with two waveguides (Figure 5.11). The first waveguide, termed the sample waveguide, contains the two sample wells to which samples can be adsorbed to. The second waveguide acts as a reference and is buried within the sensor chip. A laser light is focused through the two waveguides to create an interference pattern on a charge coupled device (CCD). The interference pattern is formed by the light waves as they recombine after passing through the two waveguides (Cross, 2003). The adsorption of particles, e.g. proteins, to the sample wells within the sample waveguide alters the optical path length of the light wave as it passes through. By measuring the difference between the light wave passing through the sample waveguide with that of the reference waveguide, which will not interact with the sample, it is possible to obtain accurate measurements of the refractive index and thickness of the adsorbed layer (Cross, 2003).

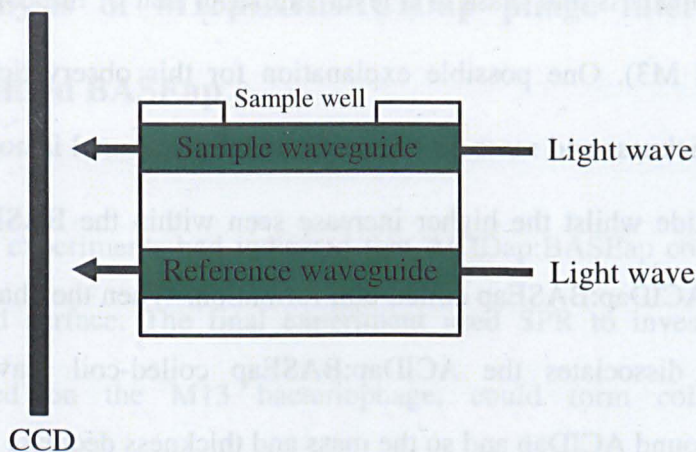


**Figure 5.11. Dual Polarisation Interferometry (DPI).** A schematic showing a DPI sensor chip.

HPLC purified BASEap peptide (35 aa long) and the control peptide (SLDTLAEQLDPSANNVLSC: 19 aa long) were immobilised onto the two sample wells independently of one another (Figure 5.12, A and B). The immobilisation of the two peptides created a layer  $\sim 0.6$  nm thick on both channels (Figure 5.12 A, T1), although a higher amount of the control peptide was immobilised ( $\sim 3.4$  ng/mm<sup>2</sup> to  $\sim 2.6$  ng/mm<sup>2</sup>: Figure 5.12 B, M1). When the ACIDap peptide was washed over the two channels, there was a change in both thickness and mass on both channels. However, on the channel with immobilised BASEap there was a far larger increase in the thickness and mass (Figure 5.12, T2 and M2) compared to the control peptide ( $\sim 0.2$  nm and  $\sim 0.08$  ng/mm<sup>2</sup>).

Previous work has indicated that at high pH the ACID:BASE coiled-coil is unstable, leading to dissociation (O'Shea, 1993). Therefore PBS pH 11.2 was washed over the two channels. Although there was minimal change in thickness and mass with regard to the control peptide, the channel where BASEap was immobilised was observed to

decrease in thickness and mass to a level similar to that of the control peptide (Figure 5.12, T3 and M3). One possible explanation for this observation is that the initial increase in thickness and mass on the control peptide channel is non-specifically bound ACIDap peptide whilst the higher increase seen within the BASEap channel is non-specific and ACIDap:BASEap coiled-coil formation. When the channels are exposed to pH 11.2, it dissociates the ACIDap:BASEap coiled-coil leaving only the non-specifically bound ACIDap and so the mass and thickness decrease to that of the control peptide channel.

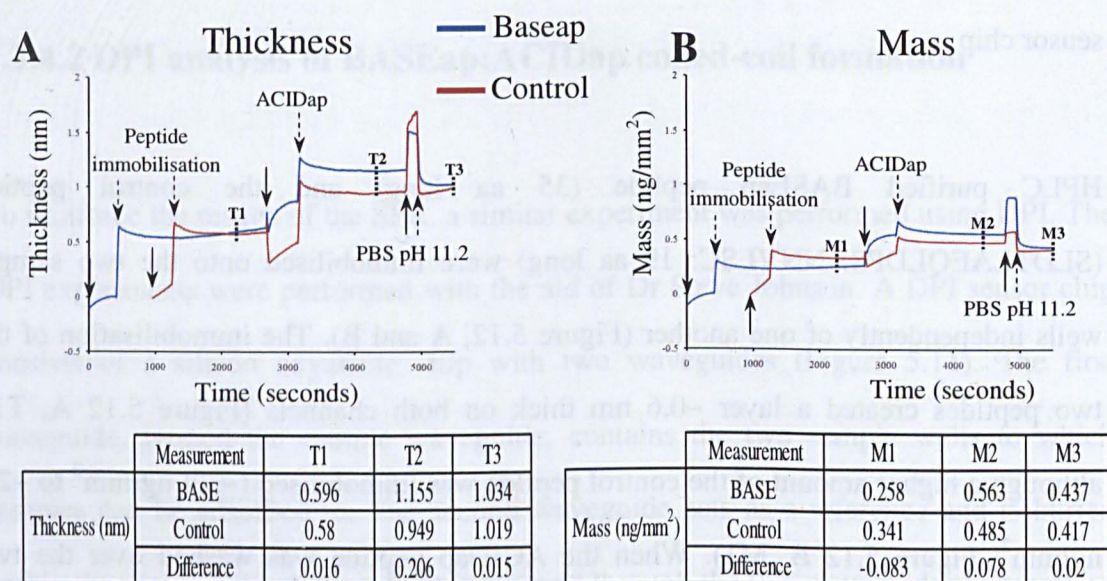


**Figure 5.12. DPI analysis of ACIDap:BASEap interactions.** BASEap (AQLKKKLQANKKKLAQLKWKLQALKKKLAQGGGSC) and a control peptide (SLDTLAEQLDPSANNVLSC) were immobilised on two separate sample wells via their thiol group in a PBS pH 7.4 running buffer. ACIDap was washed over the sample wells to investigate its interactions with the two peptides. A pH 11.2 PBS wash was used to investigate the effect of pH on the ACIDap:BASEap coiled-coil. The thickness (A) and mass (B) were measured and the difference between BASEap and the control peptide were noted at 2200, 4400 and 5610 seconds (T1-T3 and M1-M3). The start and end of sample injections are indicated by solid and hashed arrows, respectively.

### 5.2.5 SPR analysis of M13pIXHisACIDap phage interaction with surface immobilised BASEap

The SPR and DPI experiments had indicated that ACIDap:BASEap coiled-coils were forming on a gold surface. The final experiment used SPR to investigate whether ACIDap, displayed on the M13 bacteriophage, could form coiled-coils with immobilised BASEap and in doing so anchor the phage to the surface. BASEap was injected over a single SPR channel, as in section 5.2.4.1, so that ~90 RU of BASEap was immobilised. 100  $\mu$ L ( $10^{11}$  virions/mL) of M13pIXHisACIDap, M13pIXHisFOS, M13 wild-type and M13pIIIACIDap phage were then injected across the immobilised BASEap peptide (Figure 5.13). M13pIIIACIDap produced the largest response (~450 RU). This larger response was expected since the phage displayed ~5 copies of the ACIDap peptide per phage particle and therefore should have had a greater affinity for BASEap compared to the other phage. M13pIXHisACIDap and M13pIXHisFOS produced similar responses to one another (~350 RU to ~300 RU) although the phage particles displaying pIXHisACIDap did repeatedly, from three repeats of the experiment on separate sensor chips, produce a higher response of ~50 RU. Compared to wild-type, which produced a response of ~100 RU, these two phage showed much higher affinity for BASEap.

The observation that the displayed HisFOS peptide also showed relatively high affinity, compared to wild-type, for the immobilised BASEap may suggest two possibilities. The first is that FOS does show some affinity for BASEap. Although coiled-coil pairs are known to be generally specific to their complementary partner (Newman, 2003), with

regard to the JUN:FOS and ACID:BASE leucine zipper pairs there have been no studies investigating their specificity. However, Sweeney, *et al.* (2006), who created the multimeric phage nanostructures using ACIDap:BASEap displaying phage (Figure 5.3 D), also produced M13 phage particles displaying FOS on pIII and BASEap on pIX. When these phage were mixed together, they failed to form the multimeric phage nanostructures observed with the ACIDap:BASEap displaying phage; although some multiple phage structures were seen. This suggests that FOS and BASEap have a low affinity for one another and do not form coiled-coils.

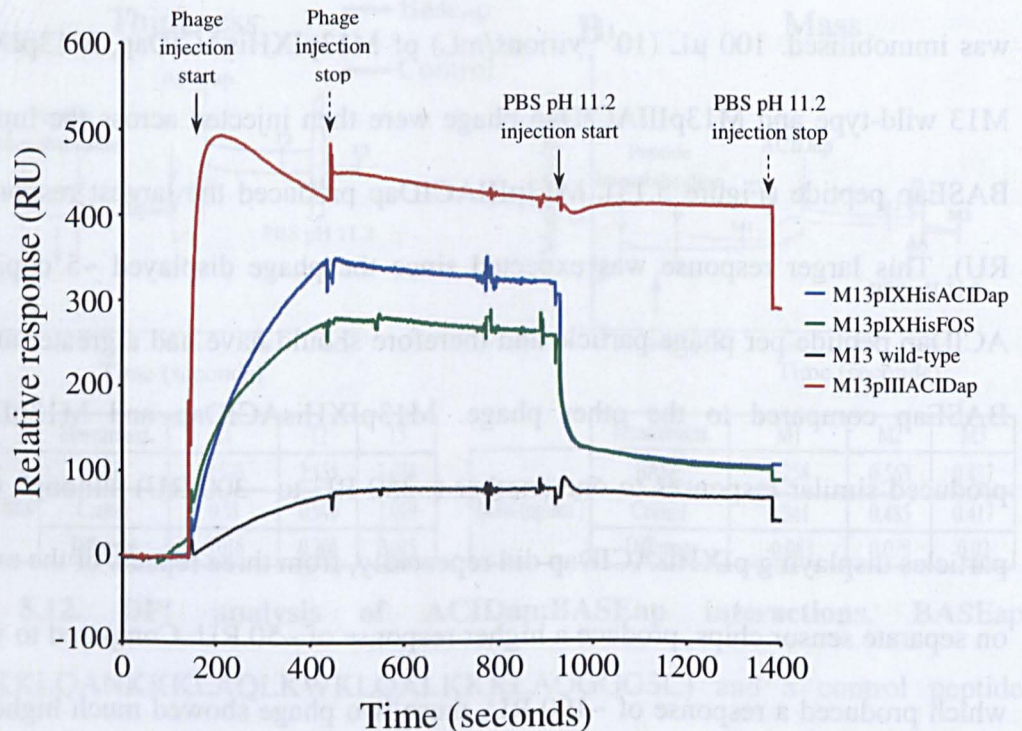


**Figure 5.13. SPR analysis of M13 phage and immobilised BASEap.** Shows a corrected sensorgram, relative to bare gold, where BASEap was immobilised onto a gold surface via its thiol group in a PBS pH 7.4 running buffer. Phage displaying ACIDap or FOS leucine zippers were washed over the immobilised peptide to investigate their interactions. The start and end of sample injections are indicated by solid and hashed arrows, respectively.

The second possibility is that the hexahis tag is interacting with the gold surface of the sensor chip. Histidine containing peptides have been shown to have a high affinity for gold surfaces (Iori, 2008; Peele, 2005). There have also been studies using hexahistidine to attach peptides to an SPR gold surface (Wegner, 2003; Baek, 2004; Ro, 2005). However, none of these studies used a bare gold SPR sensor chip. They all utilised Ni-NTA cross-linkers to immobilise the hexahistidine tags to the gold surface. Whether this was because the hexahistidine tags failed to directly bind the gold surface was not noted.

Once again, a pH 11.2 wash was performed to dissociate the ACIDap:BASEap coiled-coils (Figure 5.13). The increase in pH had no effect on the wild-type and pIIIACIDap phage. This suggests that, as expected, the wild-type phage were bound non-specifically to the BASEap layer. The possibility of the M13pIIIACIDap phage forming 5 coiled-coil interactions, and binding very tightly to the surface, may explain why the phage particles were not dissociated following the pH 11.2 wash. Both M13pIXHisACIDap and M13pIXHisFOS dissociated rapidly upon injection of the pH 11.2 buffer. This supports the notion that M13pIXHisACIDap was forming coiled-coils with the immobilised BASEap. However, it also suggests that the displayed FOS was forming coiled-coils with the BASEap peptide. A

**Table 5.1. Rate and equilibrium constants obtained from sensograms shown in Figures 5.10 B and 5.13.** The standard deviation ( $\pm$ ) is also provided.

	$k_a$ ( $M^{-1} s^{-1}$ )	$k_d$ ( $s^{-1}$ )	$K_A$ (1/M)	$K_D$ (M)	$\chi^2$
ACIDap only	$177 \pm 3.03$	$1.07 \times 10^{-3} \pm 5.07 \times 10^{-5}$	$1.65 \times 10^5$	$6.06 \times 10^{-6}$	0.109
M13pIXHisACIDap	$9.85 \times 10^5 \pm 4.95 \times 10^3$	$1.9 \times 10^{-4} \pm 1.56 \times 10^{-6}$	$5.16 \times 10^9$	$1.94 \times 10^{-10}$	4.24

Basic kinetic fits were done on the sensograms using the BIAevaluation software and a 1:1 binding model (Table 5.1 and Appendix C, section 5). A  $\chi^2$  value less than 10 typically represents an acceptable fit for the sensogram (Biacore, 1997). The dissociation constant ( $K_D$ ) of the parallel conformation of ACID:BASE has been found to be  $3 \times 10^{-8}$  M (O'Shea, 1993). However, this was calculated using circular dichroism measurements at different concentrations of urea. The SPR data within this study found the  $K_D$  of the anti-parallel ACID:BASE coiled-coil to be  $\sim 6 \times 10^{-6}$  M when using free ACIDap and  $\sim 2 \times 10^{-10}$  M when the ACIDap was displayed on the M13 particle. However, whereas the original study used free ACID and BASE (O'Shea, 1993), this study used an immobilised BASEap with the ACIDap peptide free in solution which would be expected to affect ACIDap:BASEap interactions. The higher  $K_D$  observed when the ACIDap was displayed on the M13 phage particle may be a result of multiple ACIDap peptides being available for binding per phage particle, i.e. a phage may display two ACIDap peptides instead of one. It may also be that the M13 coat proteins are interacting with the BASEap peptides, as the M13 wild-type result (Figure 5.13) suggests.

### 5.3 Conclusions and Future Work

The work described within this chapter provides proof of principle that leucine zippers can be displayed on the M13 bacteriophage coat proteins, both pIII and pIX, and used to attach the phage particle to a surface. Currently, nanodevices fabricated using the M13 bacteriophage, e.g. metallic nanowires, are deposited randomly on surfaces. In the

future the coiled-coils could be used as a generic phage anchoring method to attach multiple nanodevices to a pre-fabricated electronic circuit in a targeted manner.

I have shown that the ACIDap leucine zipper could be displayed upon the M13 bacteriophage and then used to anchor the phage particle to a gold surface via the ACIDap:BASEap coiled-coil interaction. To this end phage displaying ACIDap on pIII and pIX were produced. A phage displaying the FOS leucine zipper, whose partner is JUN, was also produced. Since pIX phage display required the use of a phagemid display system an N-terminal hexahis (HHHHHH) tag was also incorporated. The use of this tag allowed for the purification of phage displaying the pIXHisACIDap and pIXHisFOS phage away from wild-type phage.

To immobilise the BASEap peptide onto a gold surface a GGGSC linker sequence was added to the C-terminal. Using circular dichroism (CD) it was shown that the addition of this linker sequence had no detrimental effect on the ACIDap:BASEap coiled-coil formation within solution and the result repeated that of previous CD experiments using ACID:BASE pairs. Using Surface Plasmon Resonance and Dual Polarisation Interferometry it was shown that BASEap could be immobilised onto a gold or silicon oxynitride surface and form coiled-coils with ACIDap. To my knowledge this is the first time that short leucine zippers have been shown to form coiled-coils on a surface when one of the pair was first immobilised on the surface. Further work with SPR showed that ACIDap, displayed on pIII or pIX will form coiled-coils with an immobilised BASEap peptide and so anchor the phage to the surface.

## Chapter 5

---

These experiments need to be taken further in the future and moved onto gold electrodes on a silicon dioxide surface. BASEap would be immobilised on two gold surfaces separated by an SiO<sub>2</sub> layer where there would be no BASEap. Phage displaying pIX and pIII ACIDap could then be washed across and immobilised between the two gold surfaces (Figure 5.4 A). Likewise the same could be done with the higher order structures fabricated in chapter 4 (Figure 5.4 B). With regard to the ACIDap:BASEap coiled-coil the SPR work could be taken further. The kinetic evaluation was basic within this study, e.g. only one concentration of ACIDap was used and the ACIDap:BASEap interaction was not allowed to reach equilibrium. Further work investigating the kinetics of the ACIDap:BASEap coiled-coil formation could be done. Likewise, SPR kinetic experiments could be performed using the JUN:FOS coiled-coil pair. The specificity of the coiled-coils for their partner, i.e. does FOS form a coiled-coil with immobilised BASEap, is an interesting area to explore since if they are specific then this would allow for the use of coiled-coil pairs to self-assemble phage onto different areas of a surface, e.g. one phage displaying ACIDap and another displaying FOS being directed to different areas by their specific partner.

# Chapter 6

---

## Fabrication of Gold-Coated M13 Bacteriophage

This Chapter describes the work carried out attempting to fabricate gold nanowires using M13 phage particles displaying tyrosine on pVIII as scaffolds.

### 6.1 Introduction

#### 6.1.1 Bio-mineralisation of nanoparticles

The process by which biological molecules synthesise inorganic nanoparticles, e.g. silica, metal, etc, is known as bio-mineralisation (Sarıkaya, 2003). Nature exhibits a wide range of mechanisms and applications for bio-mineralisation. Most likely, organisms evolved the ability to produce inorganic nanoparticles in response to metal ions taken up non-specifically from the environment via cationic membrane transport systems (Hu, 2007). Many metal ions are toxic to the cell, such as gold, cadmium, and silver ions (Crookes-Goodson, 2008), and are therefore commonly used as anti-bacterial agents. Algae, plants and bacteria have all evolved detoxification pathways that remove the metal ions from within the cell: either by actively pumping the ions out (Nies, 2003), or by reducing the reactive ions to a relatively inert state, e.g. by the creation of metallic nanoparticles (Silver, 1996). For instance, a silver resistant strain of *Pseudomonas stutzeri*, AG259, when incubated with silver nitrate produces silver nanoparticles with a diameter of 35 to 46 nm, and silver sulphide at the cell surface (Slawson, 1992). In fact, some bacterial strains that are silver resistant are reported to have 25% of their dry weight as accumulated silver nanoparticles at their cell walls (Mandal, 2006). The exact mechanism for the resistance found in *P. stutzeri* is still not fully understood.

Another excellent example is that of the unicellular green alga, *Chlorella vulgaris* (Xie, 2007). It was found that when the algae were incubated with chloroauric acid ( $\text{HAuCl}_4$ ), as a source of gold ions ( $\text{Au}^{3+}$ ), for two days that a variety of nanoparticles were formed

exhibiting a wide range of triangular and hexagonal shapes (Xie, 2007). Further studies identified a 28 kDa protein, called the gold shape-direction protein (GSP), which was responsible for the creation of these nanoparticles (Xie, 2007).

Other organisms have evolved far more exotic and fascinating bio-mineralisation methods. The magnetotactic bacteria, e.g. *Magnetospirillum gryphiswaldense* (Figure 6.1 A), use either ferric ( $\text{Fe}^{3+}$ ) or ferrous ( $\text{Fe}^{2+}$ ) iron that has been taken up from the surrounding area to create magnetic iron nanoparticles (Komeili, 2007). Although the mechanism is not fully understood, it is thought that the iron-storage protein ferritin plays a lead role. Ferritin, which is associated with an intracellular membrane complex known as the magnetosome, quickly co-precipitates the ferric and ferrous irons to produce magnetite, or sometimes greigite (depending on the species), nanoparticles. These 30 – 50 nm nanoparticles are contained within the magnetosome, which is itself linked to the cell via the cytoskeleton (Figure 6.1 B).

The magnetotactic bacterium uses the nanoparticles to align the cell relative to a magnetic field. The field causes the magnetic nanoparticles to line up which in turn forces the magnetosome into alignment. The magnetosome is linked to the cytoskeleton and so the cell can sense these changes and adjust its position appropriately. The theory behind the evolution of this system is complex and still disputed. These bacteria are typically aquatic micro-aerophiles, i.e. their metabolism functions best at low oxygen concentrations, and so they inhabit the oxic-anoxic transition zone which is found at the sediment/water interface (Stolz, 1993). It is thought that the bacteria use the magnetosome to reach the oxic-anoxic transition zone. However, the mechanism by which the bacteria achieve this is still being researched.

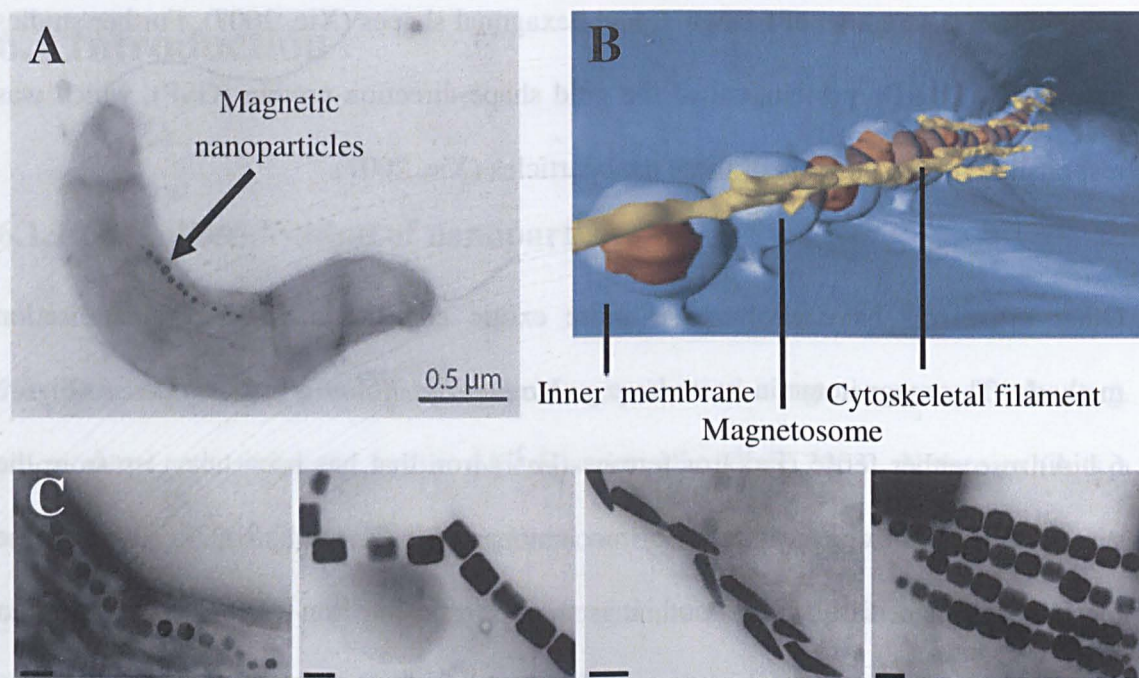


**Figure 6.1. The magnetotactic bacteria.** (A) A transmission electron microscope image of the magnetotactic bacterium *Magnetospirillum gryphiswaldense*. (B) A diagram showing the structure of the magnetosome within the bacterium. (C) Various morphologies and organisation of magnetosomes from different magnetotactic bacteria. (A) and (C) are taken from Schüler, (1999) and B adapted from Komeili, (2007). Scale bar in (C) equal to 100 nm.

Perhaps the most fascinating aspect of the magnetotactic bacteria is that different species produce a plethora of diverse morphological crystalline nanoparticles and organise them differently within the magnetosome (Figure 6.1 C). The morphology of these nanoparticles is under genetic control and their fabrication occurs under ambient conditions (Schüler, 1999). This ability of organisms to reproducibly create nanoparticles under ambient conditions using genetically controlled proteins is what attracts engineers and scientists to bio-mineralisation and is a recurring theme through different studies.

### 6.1.2 Amino acid reduction of metal salts

Gold nanoparticles are typically created by the reduction of gold salts ( $\text{Au}^{3+}$ ) in an organic solvent, e.g. toluene (Brust, 1994; Daniel, 2004). The reaction is typically done using a strong reducing agent, such as sodium borohydride ( $\text{NaBH}_4$ ) or citrate and is carried out in the presence of a so-called capping agent. Capping agents are typically a molecule such as citrate (Turkevich, 1951), various polymers, or bio-macromolecules (Mirkin, 1996), that act to stabilise the nanoparticles. Citrate is the most commonly used since it acts as both the reducing and capping agent. However, left over reagents, such as un-reacted citrate, need to be removed so that downstream applications of the nanoparticles are unaffected. All this must also be done at high temperature meaning that the creation of gold nanoparticles is very energy intensive. Nature works in ambient conditions and is less energy intensive. Therefore using Nature to fabricate nanoparticles has attracted a lot of attention in recent years. One area of attention has been in the ability of amino acids to act as nucleating and reducing agents (Sarıkaya, 2003; Tamerler, 2009).

Many of these metal nucleating peptides have been identified using M13 phage display libraries and bio-panning (Flynn, 2003; Lee, 2002; Mao, 2003; Mao, 2004; Nam, 2010).

In all of the studies the metal binding peptide is used to either bind to existing nanoparticles or bind to metal ions. The metal ions are then reduced with a strong reducing agent, e.g. sodium borohydride, onto the surface of the peptide. This, however, leads to a large amount of background material: either unbound nanoparticles or reduced metal un-associated with the peptides. None of the peptides actively reduce the metal ions, e.g.  $\text{Au}^{3+}$ , to metal nanoparticles.

## Chapter 6

Relatively few groups have researched the metal salt reduction properties of single amino acids, repeats of these amino acids and peptides: with only a handful of papers being published. It has been shown that tyrosine (Zhou, 2001), tryptophan (Selvakannan, 2004) and aspartic acid (Mandal, 2002) all act as metal ion reducing agents. Tyrosine plays an important role as an electron transfer agent in photosystem II (the first protein complex in the light dependent reactions of photosynthesis; Barber, 2008; Barry, 1990) as well as in various enzymes, such as galactose oxidase (Firbank, 2004; Whittaker, 1990). More recently, it has been shown that this electron transfer mechanism can be used to reduce gold metal salts ( $\text{Au}^{3+}$ ) to metallic gold (Zhou, 2001; Selvakannan, 2004; Slocik, 2005 and Si, 2006). The proposed mechanism of tyrosine reduction of gold is depicted below in Figure 6.2.

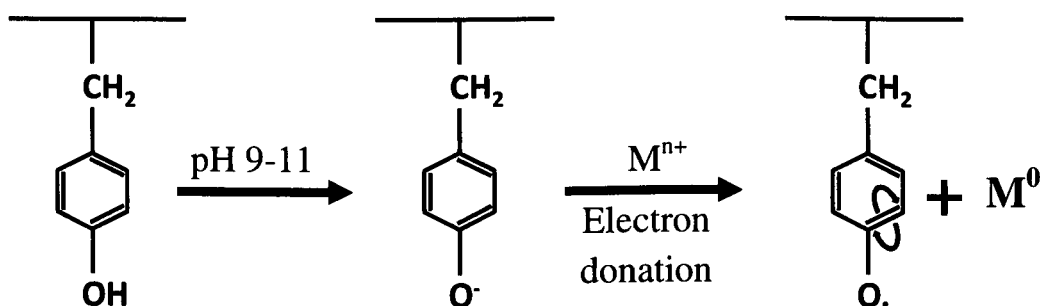


**Figure 6.2.** Cartoon showing a proposed mechanism of metal reduction by tyrosine. Adapted from Si, 2006.

It has been claimed that tyrosine (Y) is implicated in the reduction of gold salt by the spherical Cowpea Chlorotic Mottle Virus (CCMV; Slocik, 2005). Each CCMV coat protein, 180 make up the viral capsid (Liepold, 2005), has four endogenous tyrosine residues in close proximity to the C-terminus, which extends from the surface of the virus into solution (Speir, 1995). When CCMV was mixed with  $\text{HAuCl}_4$ , metallic gold ( $\text{Au}^0$ ) was quickly formed. Measurement of the tyrosine fluorescence emission at 352

nm showed that it was quickly quenched. This was used as evidence that the tyrosine was donating its electron for the reduction of the gold ions and being oxidised and so losing its fluorescence. However, gold nanoparticles are able to quench fluorescent molecules (Schneider, 2006; Dulkeith, 2002). The possibility that this was occurring instead of the oxidation of the tyrosine was not discussed. However, studies using peptides have further indicated the metal ion reducing properties of tyrosine (Slocik, 2004; Si, 2006). These studies took YYY peptides and mixed them with  $\text{HAuCl}_4$ . As with CCMV, gold nanoparticles were rapidly formed, typically 20 nm in size (Si, 2006).

As the work described in Chapter 5 has shown, it is possible to bind M13 particles to a specific surface using leucine zipper interactions. This raises the possibility that phage bound to a quantum dot or gold nanoparticle (see Chapter 4) could be positioned between two gold electrodes. This could be achieved by displaying a leucine zipper at the end of the phage (Chapter 5) and depositing its complementary partner onto the gold electrode. When the higher order structure, with phage displaying leucine zippers, was washed over the gold surface, the leucine zippers would interact and therefore position the higher order structure between the two gold electrodes. The phage would then be used as scaffolds for metal deposition (Chapter 1, Figure 1.16). This self-assembled structure could then act as a simple molecular transistor.

It is likely that if the phage were coated with a metal in solution that the leucine zipper's affinity for its complementary partner would be destroyed. Likewise, attachment of the phage to the surface first followed by metal deposition using a reducing agent, such as sodium borohydride, would result in large amounts of background. This background would negatively affect any electrical characteristics of the nano-device. Therefore a

preferable method would be to attach the phage to the surface first and then use the phage as the reducing agent to limit the deposition of metal to the phage only and minimize background.

Therefore the rationale behind the work described within this chapter was that phage could be deposited onto a surface to replicate phage self-assembling onto a surface using leucine zippers. Then a tyrosine residue displayed on pVIII of the M13 particle could be used as the reducing agent of gold ions to minimize background metal deposition.

### **6.1.3 Aims of the work described within this Chapter**

The aims were as follows:

1. To display tyrosine on the major coat protein pVIII of the M13 bacteriophage.
2. To deposit phage onto a silicon dioxide surface.
3. To use the tyrosine displaying phage to examine its reduction of gold specifically onto the M13 bacteriophage.
4. To characterise the composition and electrical properties of the gold nanowires.

## 6.2 Results and Discussion

### 6.2.1 Display of tyrosine on pVIII

The wild-type M13 pVIII coat protein contains two endogenous tyrosine (Y) residues at positions 21 and 24 (Chapter 1, Figure 1.10). They are located within the hydrophobic region, and are not thought to be solvent exposed (Vos, 2009; Overman, 1995; Matsuno, 1998). The first six amino acids of the pVIII coat protein are, however, thought to be solvent exposed (Vos, 2009). Therefore to display a solvent exposed tyrosine residue on the pVIII coat protein, the aspartic acid (D) residue at position 4 of the mature pVIII coat protein was replaced with a tyrosine (Y) residue. This was achieved via a G to T substitution at position 1379 of the M13KE sequence (New England Biolabs, Ipswich, MA, U.S.A.) by site-directed mutagenesis with the D to YpVIIIfor and D to YpVIIIrev primers (Chapter 2, section 2.5.1) using M13KE RF DNA as the template. The site-directed mutagenesis product was transformed into *E.coli*, and ten colonies picked and sent for sequencing which confirmed that they contained the correct mutation.

One of these mutants (Appendix D, section 1.0) was carried forward for further experiments and termed M13Y. Phage produced from this clone carry a tyrosine residue on all ~2700 copies of pVIII. When grown in *E.coli* the M13Y phage produced an equivalent titer to wild-type M13 phage and had a similar morphology under TEM analysis to wild-type M13.

### 6.2.2 Fabrication of gold coated phage in solution

The rationale for using tyrosine was to allow for *in situ* reduction of gold onto the M13 phage particle after the phage had been deposited onto a surface. However, before starting surface experiments, the reduction capabilities of the M13Y phage in solution were investigated. M13Y was grown and purified using a caesium chloride gradient to remove possible reducing agents produced by the cell. Titrations were carried out using differing amounts of M13Y or wild-type M13 against 1 mM chloroauric acid ( $\text{HAuCl}_4$ ): from hereon in chloroauric acid will be called gold salt. Likewise, titrations were carried out of differing concentrations of gold salt against  $10 \mu\text{L}$  of  $10^{13}$  virions/mL of M13Y or wild-type M13.  $5 \mu\text{L}$  of each reaction was then taken and placed on a carbon coated TEM grid for 10 seconds before being washed in water. No stain was used. The result for both titrations with M13Y was the same (Figure 6.3 A) with large aggregates of filamentous structures present. There was no obvious difference between M13Y and wild-type M13 (Figure 6.3 B). The filamentous structures had an amorphous grey appearance to them with no obvious fine detail (Figure 6.3 A inset). As mentioned, the aggregates were present in all the reactions: no single phage particles were observed.

Whenever large concentrations of phage, i.e.  $50$  and  $100 \mu\text{L}$  of M13Y phage, were mixed with gold salt then within 30 seconds of mixing there appeared a single grey dust-like particle within the solution. The diameter of the dust-like particle was between  $0.5$ - $2$  mm and increased in size the higher the concentration of M13Y phage. The dust-like particle only appeared when M13Y phage was used, i.e. it did not appear when wild-type M13 phage or no phage were used. The dust-like particle stayed suspended within the solution but would settle at the bottom of the tube after leaving overnight.

However, it could easily be moved from the bottom of the tube with a single flick. Vigorous vortexing of the tube led to fragmentation of the dust-like particle into numerous smaller particles. Further vortexing made no difference. Examination of the dust-like particle in TEM showed the same aggregates as described previously (Figure 6.3 A and B).

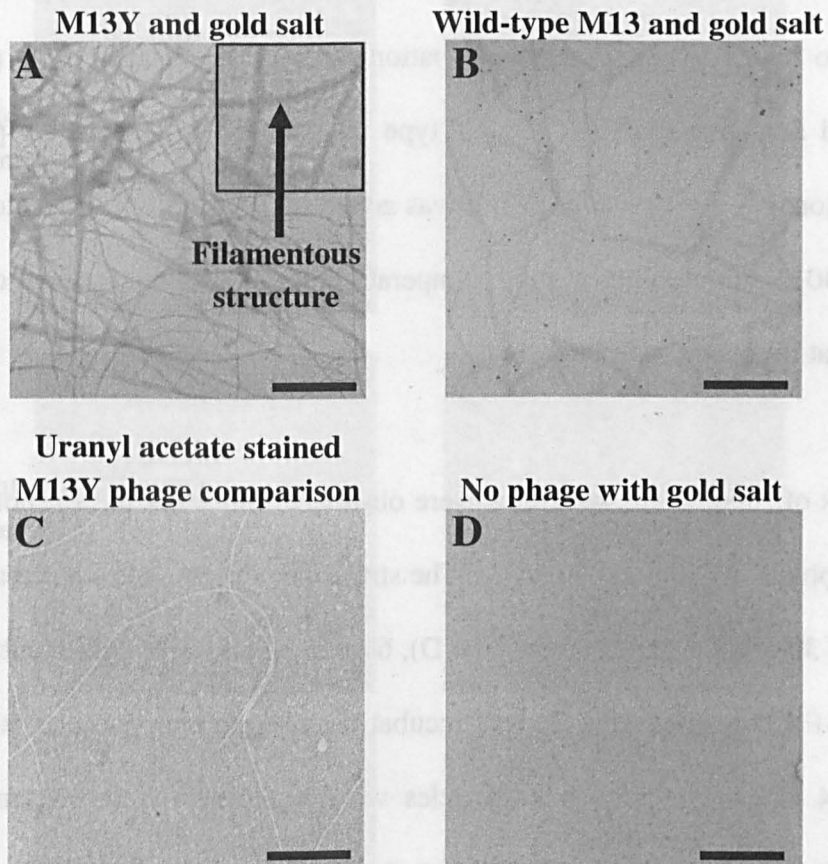


**Figure 6.3. A TEM image of M13 phage mixed with gold salt overnight in solution.** Specifically, 100  $\mu\text{L}$  of M13Y (A) or wild-type M13 (B) phage ( $\sim 1 \times 10^{13}$  virions/mL) suspended in PBS pH 7.4 was added to 100  $\mu\text{L}$  of 1 mM chloroauric acid ( $\text{HAuCl}_4$ ) and mixed briefly and incubated overnight. D shows the same reaction with 100  $\mu\text{L}$  PBS instead of M13. C shows M13Y phage stained with uranyl acetate and no gold salt present. 5  $\mu\text{L}$  of each reaction was then taken and placed on a carbon coated TEM grid for 10 seconds before being washed in water. Scale bar equals 200 nm.

## Chapter 6

---

When the same experiment was carried out, but with no M13Y phage, none of the structures were observed (Figure 6.3 D). This suggests that the filamentous structures observed were M13Y phage. The fact that they can be seen using TEM indicates that the phage were coated with some electron dense material. The obvious candidate for this would be reduced gold. If gold was being deposited onto the M13Y phage it was concentration independent since the results were the same for titrations of M13Y to gold and gold to M13Y. Therefore the incubation time was investigated. 10  $\mu\text{L}$  of M13Y phage (and as controls 10  $\mu\text{L}$  of wild-type phage and 10  $\mu\text{L}$  of PBS pH 7.4), at a concentration of  $\sim 1 \times 10^{13}$  virions/ mL was added to 100  $\mu\text{L}$  of 6 mM gold salt and left for 1, 10, 30 and 60 minutes at room temperature. Samples were also left overnight and for 2 days at room temperature.

Aggregates of filamentous structures were observed after 1 minute for both M13Y and wild-type phage (Figure 6.4 A and B). The structures did not alter in appearance for the 10 minute, 30 minute (Figure 6.4 C and D), 60 minute and overnight incubation (Figure 6.4 E and F). However, after 2 days incubation discrete nanoparticles were observed (Figure 6.4 G and H). The nanoparticles were ordered in a similar manner to the filamentous structures seen in earlier time points. This suggests that the nanoparticles were forming along the length of the phage particles. The only difference between M13Y and wild-type phage was that the nanoparticles on the M13Y phage were smaller (an average diameter of  $4.2 \text{ nm} \pm 1.6$  compared to  $9.2 \text{ nm} \pm 7.7$ ,  $n = 50$ ). There also appeared a large number of background nanoparticles (highlighted with an arrow in Figure 6.4 G inset). When no phage were present no nanoparticles were seen (result the same as Figure 6.3 D). This indicates either that the nanoparticles formed on the phage and proceeded to dissociate into the solution, or the phage solution contained *E.coli* cell

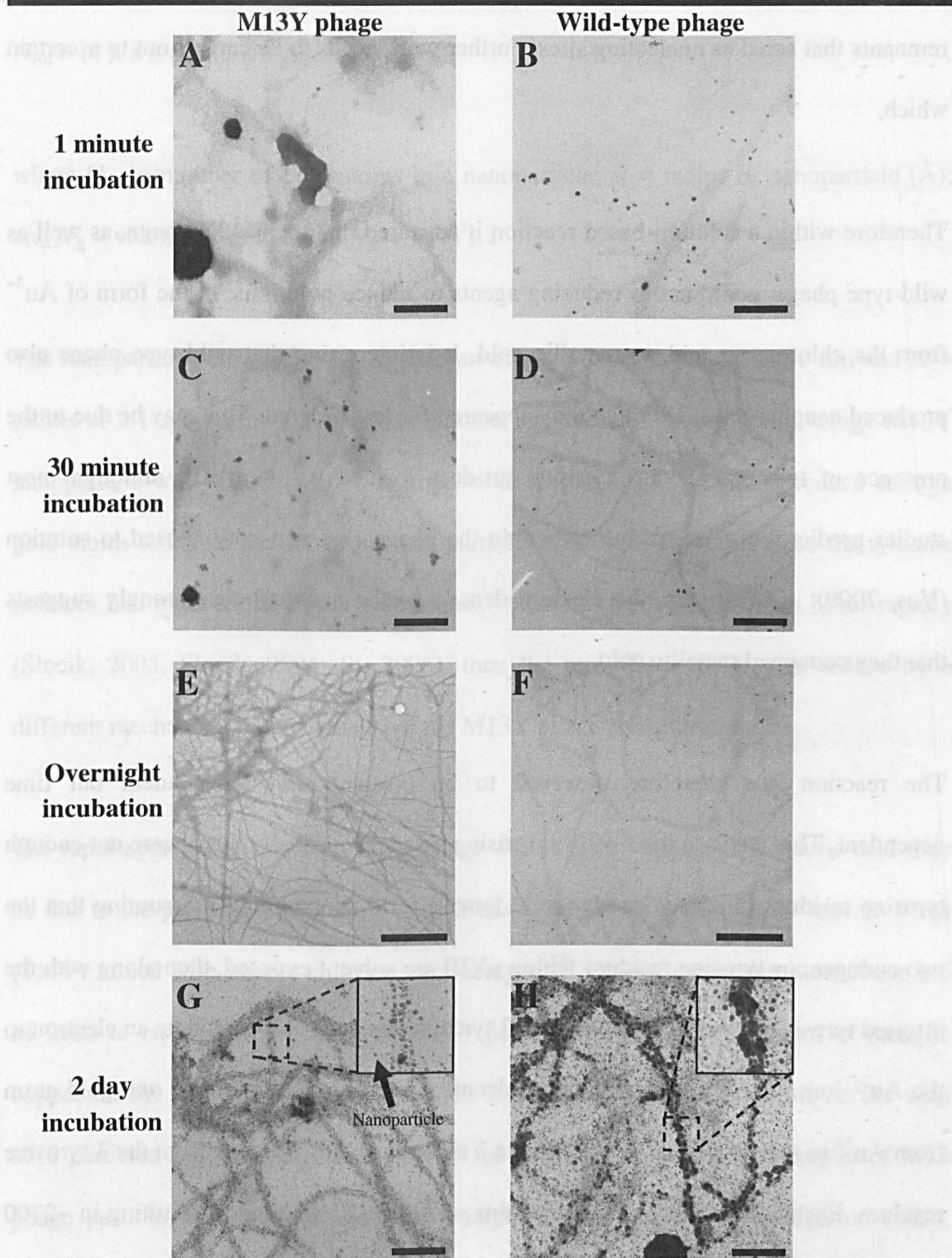


**Figure 6.4.** Time course of M13Y and wild-type phage mixed with gold salt. TEM images of 10  $\mu\text{L}$  of M13Y or wild-type phage ( $\sim 1 \times 10^{13}$  virions/mL) added to 100  $\mu\text{L}$  of 6 mM chloroauric acid and left for 1 minute (A and B), 30 minutes (C and D), overnight (E and F) and two days (G and H). Scale bar equals 200 nm.

## Chapter 6

---

remnants that acted as nucleating sites. Further work needs to be carried out to ascertain which.

Therefore within a solution-based reaction it appeared that the M13Y phage, as well as wild-type phage, could act as reducing agents to reduce gold ions, in the form of  $\text{Au}^{3+}$  from the chloroauric acid, to metallic gold. It is interesting that wild-type phage also produced nanoparticles; although they appeared far less ordered. This may be due to the presence of two endogenous tyrosine residues located within pVIII; although most studies predict that they are buried within the phage coat and not exposed to solution (Vos, 2009). Once again, the electron density of the nanoparticles strongly suggests that they contained metallic gold.

The reaction was therefore observed to be concentration independent but time dependent. This result is not overly surprising since theoretically there were not enough tyrosine residues to reduce enough gold ions to form nanoparticles. Assuming that the two endogenous tyrosine residues within pVIII are solvent exposed, then along with the inserted tyrosine, it means that there are 3 tyrosine residues able to donate an electron to the  $\text{Au}^{3+}$  ions. Therefore each pVIII molecule can theoretically reduce one gold atom from  $\text{Au}^{3+}$  to metallic gold ( $\text{Au}^0$ ), with the 3 electrons being donated from the 3 tyrosine residues. Each M13 phage particle contains ~2700 pVIII molecules, resulting in ~2700 metallic gold atoms.

The following equation (Cseh, 2007) was used to calculate the number of gold atoms within the gold nanoparticles:

$$N_{\text{Au}} = (4 \times \pi \times R^3) / (3 \times V_g)$$

where  $N_{\text{Au}}$  = number of gold atoms in a nanoparticle;  $R$  = radius of nanoparticle ( $\text{\AA}$ ); and  $V_g$  = volume of gold atom ( $V_g = 17 \text{\AA}^3$ ).

The nanoparticles formed by M13Y had an average diameter of  $4.2 \pm 1.6$  nm and so a radius of  $2.1 \pm 0.8$  nm. Therefore the number of gold atoms within an average M13Y nanoparticle was  $\sim 2300$ . So it was impossible for the M13Y phage to reduce enough gold atoms to create the numerous nanoparticles observed. Therefore once the tyrosine residues had reduced the initial gold atoms, which has been measured to occur rapidly (Slocik, 2005, Slocik, 2004; Si, 2006), then the rest of the gold must reduce by a different mechanism independently of the M13Y phage concentration.

The rapid aggregation seen when the phage were mixed with the chloroauric acid may be due to the presence of the  $\text{Au}^{3+}$  ions. It has been shown that Tobacco Mosaic Virus (TMV) mixed with copper chloride, producing  $\text{Cu}^{2+}$  ions, at a concentration above 0.5 M leads to rapid aggregation of the TMV particles along with deposition of metallic copper on the TMV particles (Lee, 2006). Perhaps a similar mechanism occurs with M13 particles and  $\text{Au}^{3+}$  ions. A review of the literature shows many examples of M13 phage particles mixed with positively charged atoms leading to aggregation (Nam, 2006; Reiss, 2004 and Soo-Kwan, 2006). However, Lee *et al.* (2006), found that when the concentration of  $\text{CuCl}_2$  was lower than 0.5 M that no copper deposition occurred upon the TMV particles. It therefore appears that solution reduction of metal salts is a “catch-22” situation. Metal reduction on phage particles may only occur at concentrations of metal ions that cause aggregation.

### 6.2.3 Deposition of M13Y onto carbon and patterning with gold

For electronic measurements of any gold-coated phage, the ideal surface would be SiO<sub>2</sub> due to its insulating properties. However, it was unknown whether phage would deposit onto an SiO<sub>2</sub> surface successfully. Additionally, phage deposited on SiO<sub>2</sub> could only be viewed using atomic force microscopy (AFM) which provides less detail than TEM. Therefore I decided to deposit M13Y phage onto a charged, carbon-coated TEM grid to initially carry out surface gold reduction experiments before moving onto SiO<sub>2</sub> surfaces. 5  $\mu$ L of M13Y and wild-type ( $1 \times 10^{10}$  virions/mL) phage were placed onto an ultra-violet charged, carbon-coated, copper TEM grid. The phage were left for 1 minute on the grid to allow for adsorption of the particles to the surface. Excess liquid was then removed using filter paper.

A 10  $\mu$ L drop of 1 mM chloroauric acid (HAuCl<sub>4</sub>) was then placed onto the grid for different times (Figure 6.5 A-C) before being washed off with distilled water. After 1 minute (Figure 6.5 A) nanoparticles, ~4 nm across, formed along the phage particle, and these increased in size in a time-dependent fashion (Figures 6.5 B and C). The shape and electron density strongly indicated that the nanoparticles consisted of gold. Occasionally after 1 hour of incubation with 1 mM HAuCl<sub>4</sub> large background aggregates were observed. Once again, wild-type phage also produced similar structures to M13Y with similar incubation times (Figure 6.5 D).

The main difference between the solution and surface based exposure of M13Y to chloroauric acid was the lack of aggregation when done on the surface. Since all the phage were deposited separately from one another, they could interact with the

chloroauric acid without aggregation. Therefore the initial rationale of phage deposition before gold reduction appeared to be correct. The other difference between solution and surface was the speed that nanoparticles were formed. With the solution based reaction it took 2 days for nanoparticles to form. This is contrasted with nanoparticle formation after 1 minute when the phage were present upon a surface.

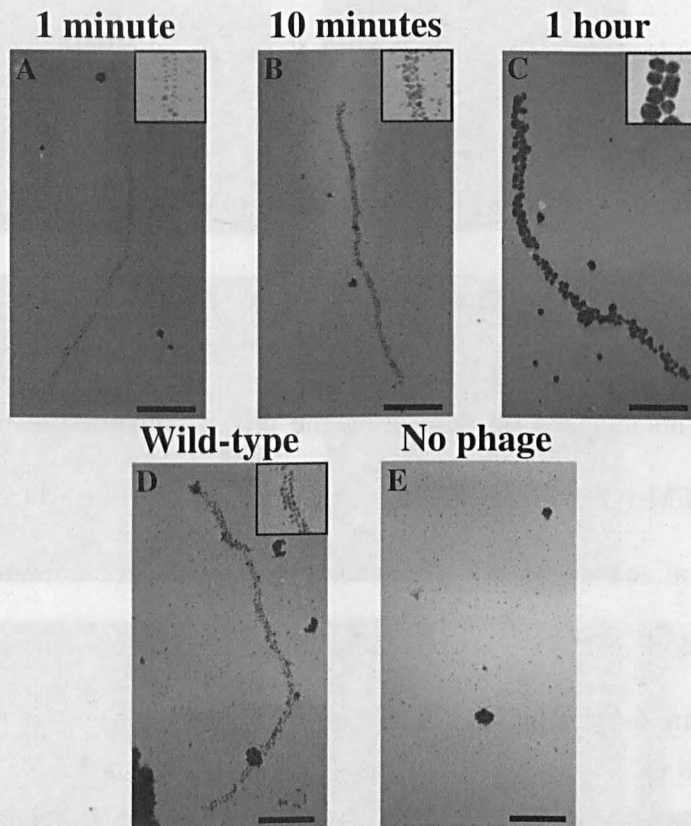


**Figure 6.5. Phage particles on a carbon surface exposed to gold salt.** M13Y phage deposited on a carbon-coated, copper TEM grid incubated with 1 mM  $\text{HAuCl}_4$  for 1 minute (A), 10 minutes (B) and 1 hour (C) in a humid chamber. Wild-type was incubated for 10 minutes with 1 mM  $\text{HAuCl}_4$  (D). A carbon-coated grid with no phage was incubated with 1 mM  $\text{HAuCl}_4$  for 1 hour (E). Scale bar equals 200 nm.

### 6.2.4 Attempts to deposit gold on M13 adsorbed to SiO<sub>2</sub> surface

Since it appeared that the system was working on carbon surfaces, the experiments were moved onto a silicon dioxide surface. As explained above, the SiO<sub>2</sub> surface was necessary because any future electrical characterisation of the nanowires, or a nanodevice, would have to be done on a silicon surface. Therefore silicon surfaces (Compart Technology Ltd, Peterborough, U. K.) were prepared by cleaning 1 cm<sup>2</sup> SiO<sub>2</sub> chips with piranha solution. Piranha solution is a mixture of sulphuric acid and hydrogen peroxide (3:1) which etches the silicon, removing any debris, and producing a clean surface for deposition.

Initial experiments focused on depositing the phage onto the cleaned surface. It was found, using AFM (Chapter 2, section 2.5.5) that aging the surface overnight (whilst keeping it in a sealed humidity chamber to limit dust contamination) at room temperature before adding the phage resulted in a high concentration of phage deposition (Figure 6.6 A and B).

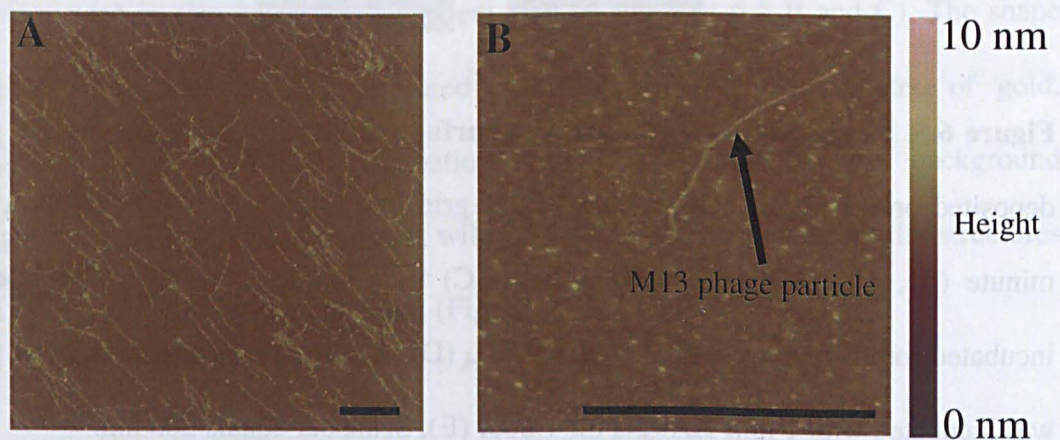


**Figure 6.6.** M13 bacteriophage particles adsorbed to SiO<sub>2</sub> surface. M13Y phage on piranha cleaned SiO<sub>2</sub> (A, B). Surfaces viewed with AFM. Scale bar equals 1 μm.

Phage failed to deposit on freshly cleaned silicon surfaces, perhaps due to the charge of the surface which changed from a net negative charge (which would be expected to repel the negatively charged phage particle) to a net neutral charge as it aged.

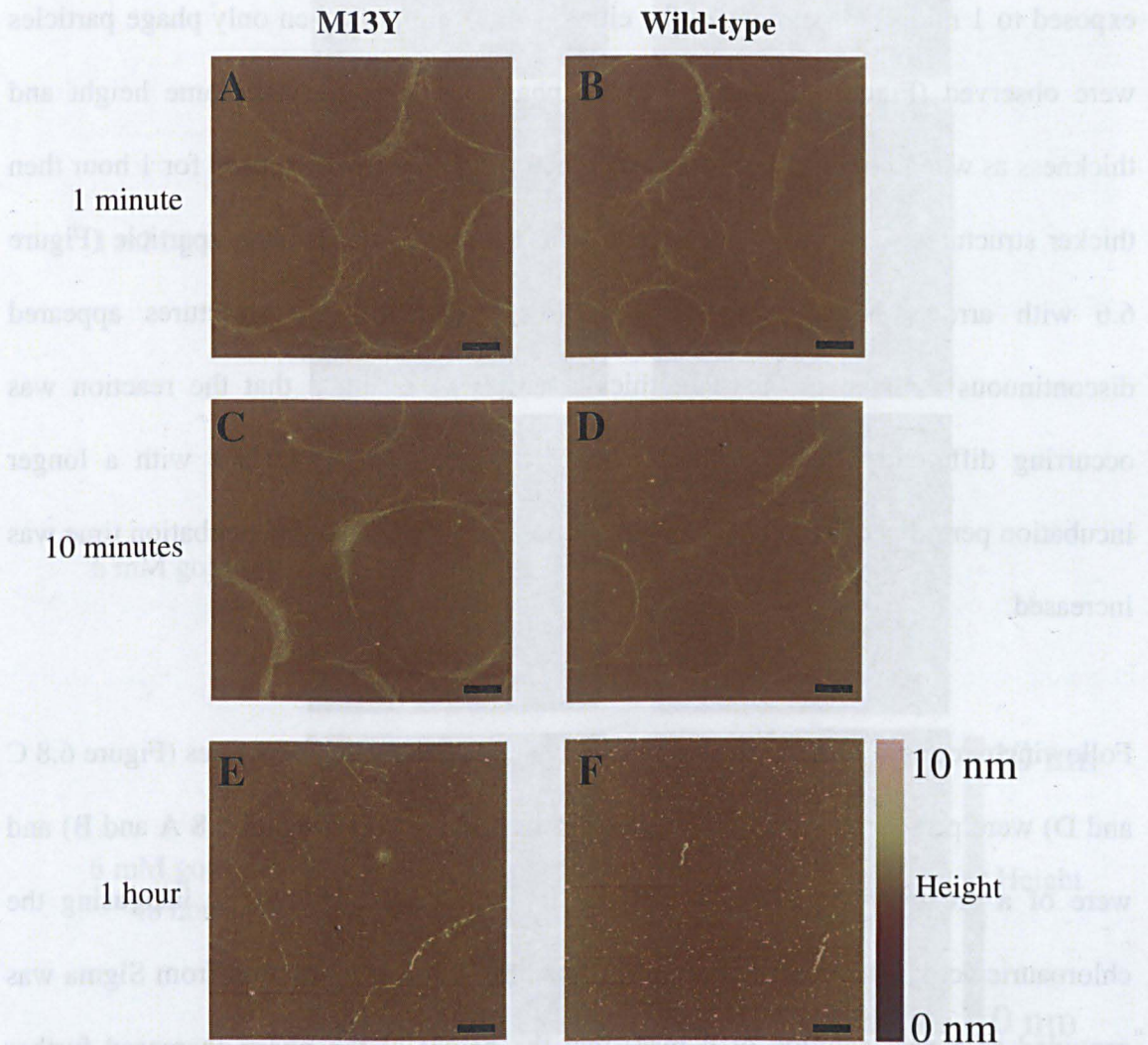


**Figure 6.7. M13 phage particles adsorbed to  $\text{SiO}_2$  and incubated with gold salt for different times.** AFM image showing M13Y and wild-type phage exposed to a solution of 1 mM chloroauric acid ( $\text{HAuCl}_4$ ) for 1 minute, 10 minutes and 1 hour. Scale equals 1  $\mu\text{m}$ .

Once it was found that virions could be deposited onto a bare SiO<sub>2</sub> surface, the next step was to investigate whether the tyrosine displayed on pVIII of M13Y, and the endogenous tyrosines of wild-type M13, could reduce gold from solution to coat the virus particle. When silicon surfaces covered in M13Y, or wild-type, phage were exposed to 1 mM chloroauric acid for either 1 or 10 minutes then only phage particles were observed (Figure 6.7 A-D), i.e. the phage particles had the same height and thickness as when no gold salt was used. When the phage were exposed for 1 hour then thicker structures were seen with a greater height than a single phage particle (Figure 6.6 with arrows highlighting the structures). However, the structures appeared discontinuous with an inconsistent thickness. It was assumed that the reaction was occurring differently on the silicon surface than the carbon surface with a longer incubation period needed to result in gold deposition. Therefore the incubation time was increased.

Following overnight incubation, it was observed that phage-like structures (Figure 6.8 C and D) were present which appeared thicker than phage only (Figure 6.8 A and B) and were of a greater height (Figure 6.9 A). It was also found that by increasing the chloroauric acid concentration to 6 mM (the chloroauric acid solution from Sigma was provided as a neat solution of 6 mM) that the height of the phage increased further (Figure 6.8 E and F; Figure 6.9 A). It is interesting that the width of the particles decreased when the phage were exposed to 1 mM chloroauric acid, compared to just phage on the surface, and then increased again when exposed to 6 mM (Figure 6.9 B). This is because AFM lacks the resolution to discern the width of objects smaller than its tip, which is typically 20 to 50 nm in size (Decossas, 2001). Therefore width measurements are often inaccurate.

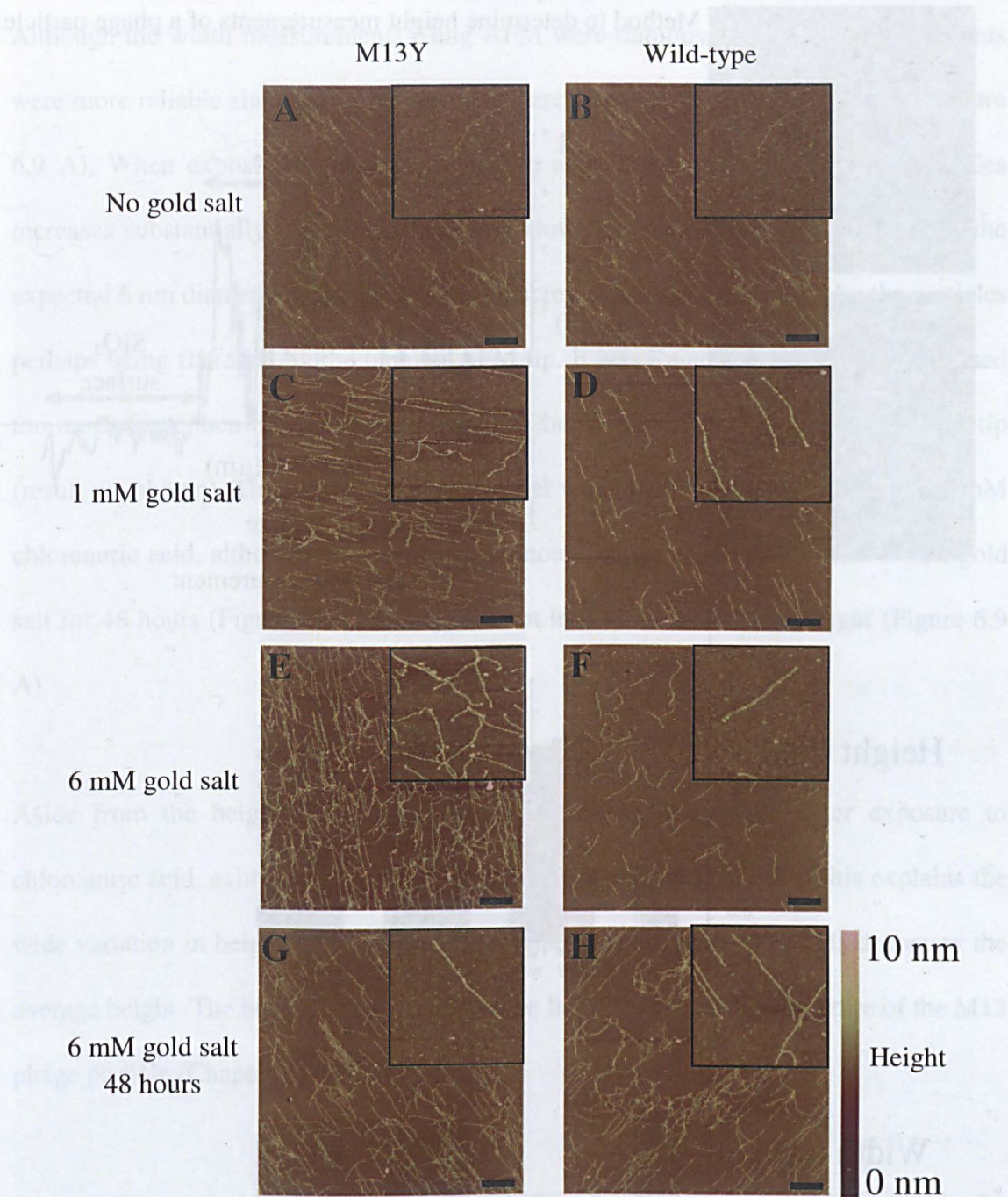


**Figure 6.8. M13 bacteriophage particles adsorbed to SiO<sub>2</sub> surface and incubated with varying amounts of gold salt.** Phage on piranha cleaned SiO<sub>2</sub> (A, B) and 1 mM (C, D) or 6 mM (E, F) HAuCl<sub>4</sub>. Surfaces viewed with AFM. Scale bar equals 1 μm.

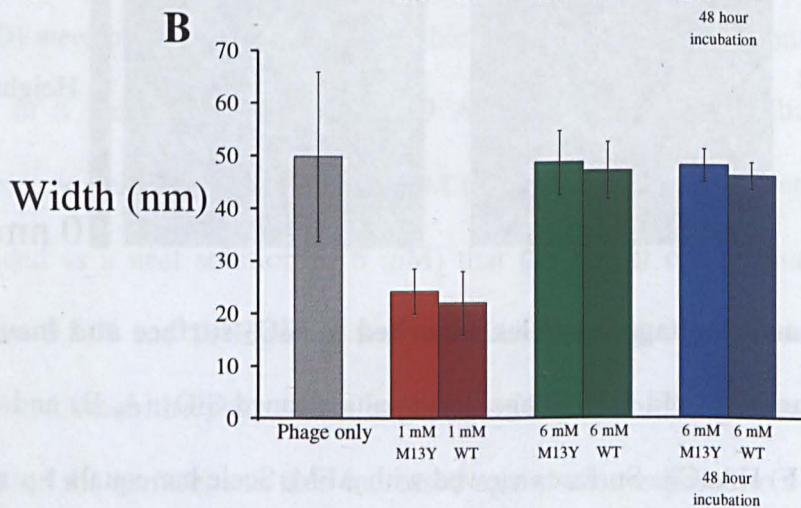
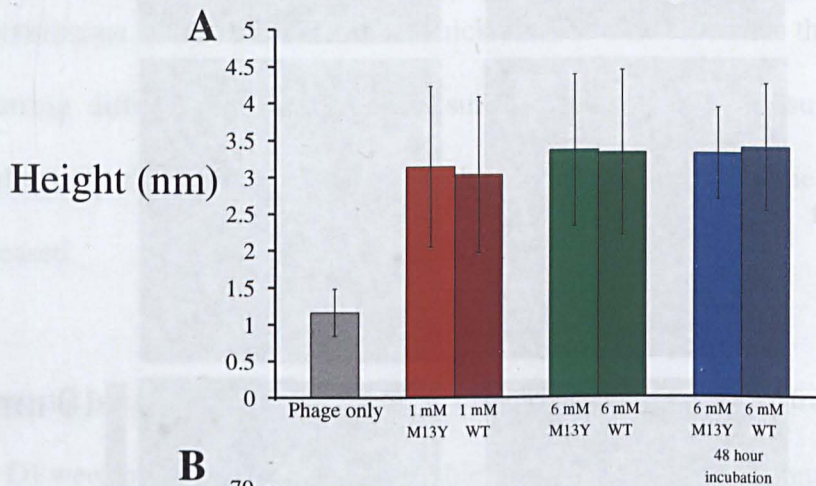
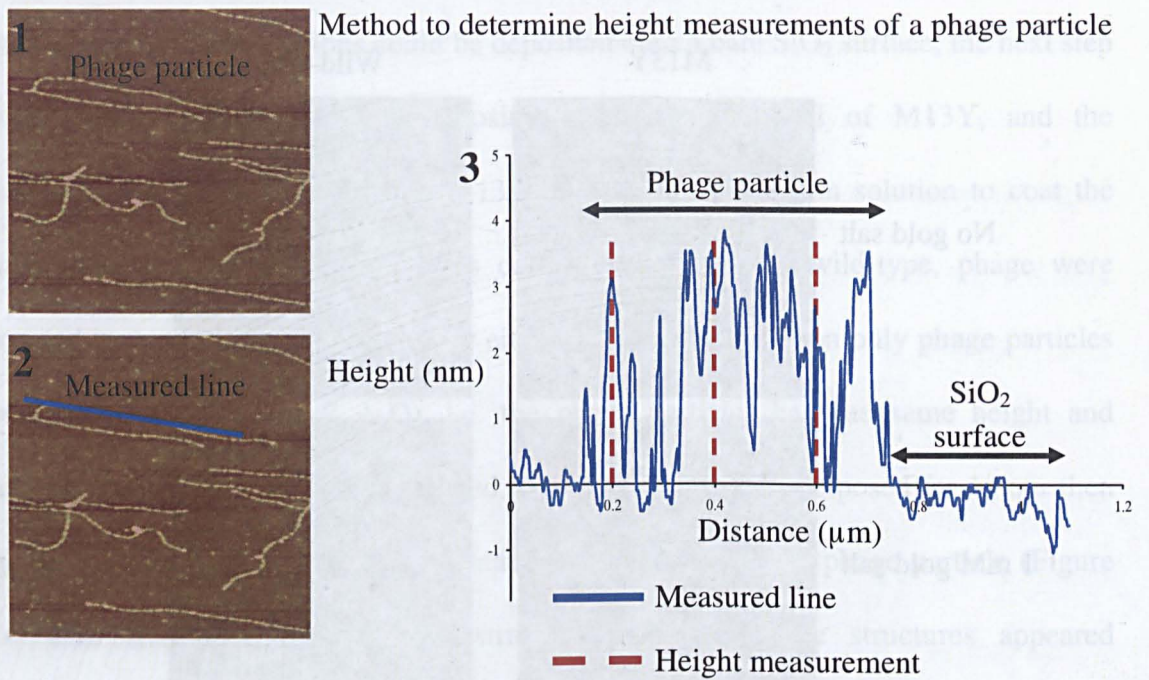


**Figure 6.9. Height and width measurement of M13Y particles.** Average phage particle heights and widths, after gold salt incubation, were measured from 100 phage particles using AFM (steps 1 to 3). Error bars show standard deviation.

Although the width measurements using AFM were dubious, the height measurements were more reliable since these measurements are largely independent of tip size (Figure 6.9 A). When exposed to 1 mM chloroauric acid, the height of the phage particles increases substantially from 1 nm to 3 nm. However, these values are lower than the expected 6 nm diameter of the phage. This discrepancy can be explained by the particles perhaps being flattened by the tapping AFM tip. It was found that when the AFM used too much force then no phage were seen, i.e. they were completely flattened by the tip (result not shown). The height increased further when the phage were exposed to 6 mM chloroauric acid, although only by a small amount. Further incubation with 6 mM gold salt for 48 hours (Figure 6.8 G and H) did not lead to an increase in height (Figure 6.9 A).

Aside from the height differences it was found that the phage, after exposure to chloroauric acid, exhibited a bead-like structure (Figure 6.8 D and F). This explains the wide variation in height (Figure 6.9 A) since the gaps between the beads decreases the average height. The bead-like structure may be linked to the helical structure of the M13 phage particle (Chapter 1, section 1.5).

A control was carried out to ascertain whether the morphological changes, i.e. the changes in height of the phage particles, associated with the gold salt were because of the gold ions being reduced or due to the low pH of the chloroauric acid solution:  $\text{HAuCl}_4$  solution is provided in dilute hydrochloric acid, pH ~3. M13Y phage (adsorbed to  $\text{SiO}_2$  surface) were exposed to 1 mM hydrochloric acid pH 3 (Figure 6.10). After overnight incubation the phage particles appeared degraded (highlighted with arrows)

with none of the bead-like structure or height changes seen when 1 mM chloroauric acid was used. Therefore the morphological changes appear specific to chloroauric acid.

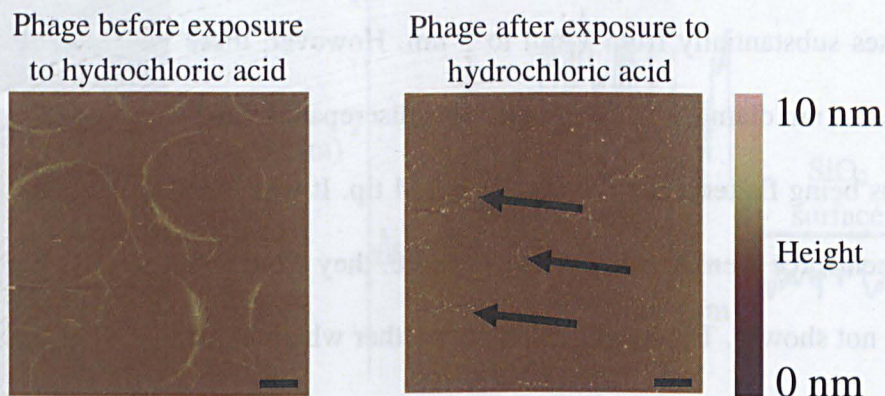


**Figure 6.10. M13Y phage on SiO<sub>2</sub> surface exposed to dilute hydrochloric acid.**

M13Y phage were deposited on a silicon dioxide surface and exposed to 1 mM hydrochloric acid, pH 3, overnight. Surfaces viewed with AFM. Scale bar equals 1  $\mu\text{m}$

The morphological changes observed when M13Y was incubated with chloroauric acid indicated that some material had coated the phage particles. Once again the results strongly indicated that the material was gold. To confirm that gold was coating the M13 particles, scanning electron microscopy (SEM) was carried out. Gold is very electron dense and so it was expected that the gold coated phage particles would be very easily seen with an SEM (despite their small size). Therefore a silicon dioxide surface was prepared with M13Y phage and exposed to 6 mM chloroauric acid overnight (Figure 6.11 A). This produced similar structures to those seen before (Figure 6.8 E). When the surface was viewed using the SEM, no phage shaped structures were seen (Figure 6.11 B), indicating that no gold was present. This was further confirmed using energy-dispersive X-ray spectroscopy (EDX), which is a technique that allows a user to determine the elemental composition of a sample within an SEM. EDX showed that no

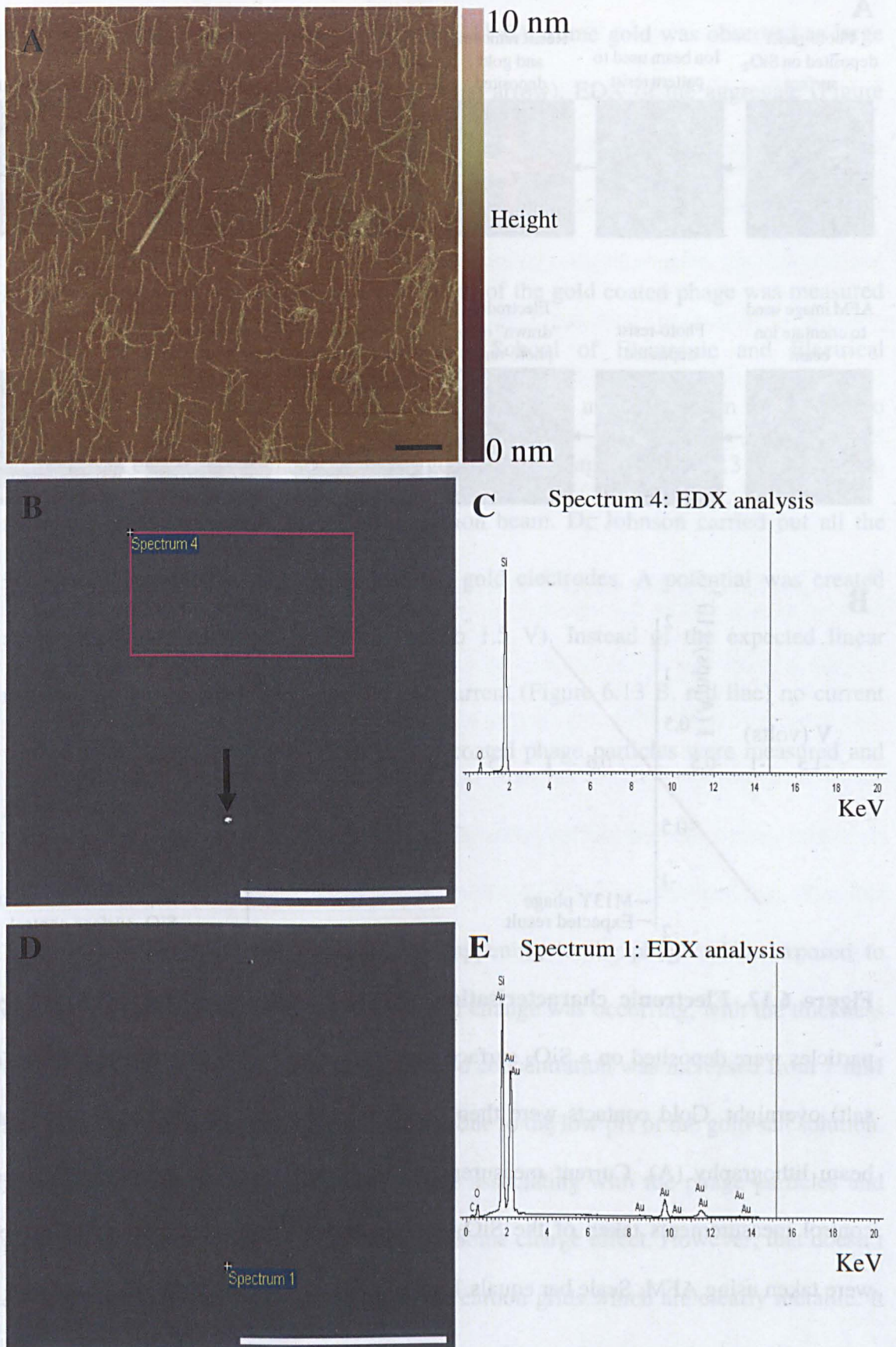


**Figure 6.11. Scanning electron microscopy of M13Y phage exposed to 6 mM gold salt on a SiO<sub>2</sub> surface. AFM scale bar equals 1 μm; SEM scale bar equals 100 μm.**

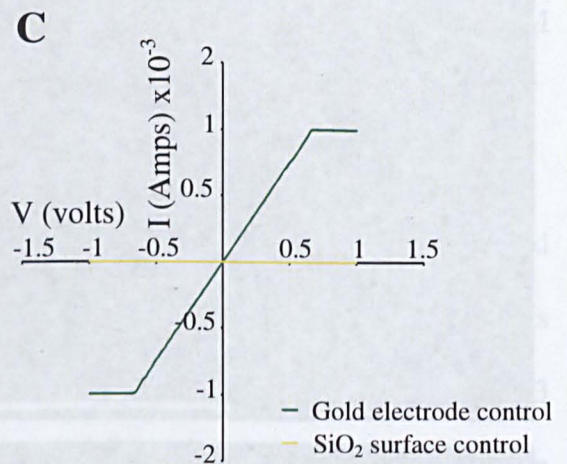
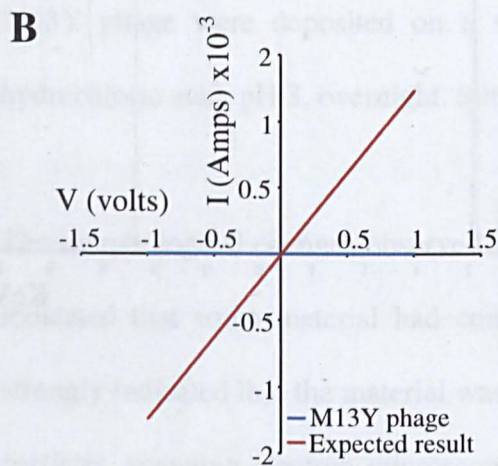
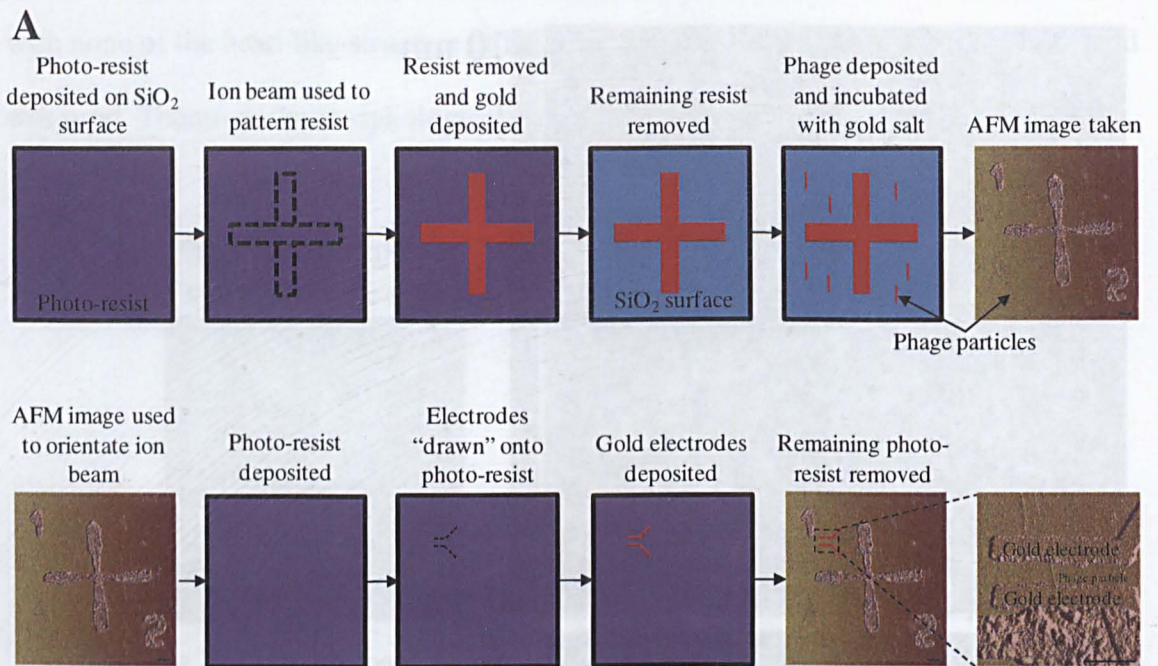


**Figure 6.12. Electronic characterisation of M13Y phage particles.** M13Y phage particles were deposited on a  $\text{SiO}_2$  surface and exposed to 6 mM chloroauric acid (gold salt) overnight. Gold contacts were then drawn over the ends of the phage using ion beam lithography (A). Current measurements were then taken of the phage (B) and control measurements taken of the  $\text{SiO}_2$  surface and the gold electrodes (C). Images were taken using AFM. Scale bar equals 1  $\mu\text{m}$ .

## Chapter 6

---

gold was present within the sample (Figure 6.11 C). Some gold was observed as large aggregates (Figure 6.11 B, highlighted with an arrow). EDX of the aggregate (Figure 6.11 E) showed that it was made of gold.

Further to this work, the electrical conductivity of the gold coated phage was measured with the assistance of Dr Steve Johnson (School of Electronic and Electrical Engineering, University of Leeds). This was achieved by using ion beam lithography to “draw” gold electrodes to the ends of the gold coated phage (Figure 6.13 A) using pre-fabricated gold cross-hairs to orientate the ion beam. Dr Johnson carried out all the lithography involved in the creation of the gold electrodes. A potential was created across the gold coated phage (from -1.5 to 1.5 V). Instead of the expected linear relationship between applied potential and current (Figure 6.13 B, red line) no current was observed (Figure 6.13 B, blue line). 5 coated phage particles were measured and none were conducting.

It is very difficult to explain what was happening to the phage when exposed to chloroauric acid. Clearly some morphological change was occurring, with the thickness of the phage increasing as the chloroauric acid concentration was increased from 1 mM to 6 mM. The morphological change was not due to the low pH of the gold salt solution. It is possible that the gold ions ( $\text{Au}^{3+}$ ) were associating with the phage particles and producing the structures seen with AFM via some charge effect. However, that doesn't explain the structures seen with TEM on the carbon grids which are clearly metallic. It may be that the carbon-coated copper grid is somehow acting as a reducing agent.

Other alternatives may be that the gold layer was too small to be seen by SEM and EDX. Within SEM, the electron beam passes a certain distance into the surface, e.g. SiO<sub>2</sub>. It may be that the electrons bouncing back from the SiO<sub>2</sub> surface are dwarfing those from the gold atoms coating the phage. However, this is unlikely. With regards to the conductivity measurements, the gold coating may consist of nanoparticles, as seen with the TEM results (Figure 6.4). These nanoparticles may be too far apart to allow for conductivity. Once again, this is unlikely since the TEM results indicate the nanoparticles are close enough together.

### 6.3 Conclusions and Future Work

The work described within this chapter has shown that tyrosine can be displayed on the major coat protein pVIII. Initial experiments in solution suggest that the M13Y and wild-type phage particles reduce gold ions from solution into metallic gold. However, the rapid appearance of a dust-like particle when using M13Y suggests that the extra displayed tyrosine does increase the gold reduction properties of the phage. Likewise, the appearance of the dust-like particle suggests that tyrosine is acting as the reducing agent of gold or plays a prevalent role. It is thought that the two endogenous pVIII tyrosines are not solvent exposed (Vos, 2009). However the gold reducing properties of wild-type M13 suggests that at pH 3, the pH at which the reduction was carried out at, that the endogenous tyrosine residues are solvent exposed. Further work with different pH gold salt solutions is needed to investigate this.

## Chapter 6

---

Work on a carbon surface showed that both M13Y and wild-type phage reduce the gold at a far quicker rate than in solution. TEM analysis showed that there was no real difference between the nanoparticles on M13Y and wild-type. This was further supported by work on a silicon dioxide surface, where M13Y and wild-type particles appeared at the same after gold salt incubation. Although the structures observed in solution and on the carbon surfaces appear to be gold based on their electron density, further EDX needs to be carried out to support this. However, the EDX and conductivity measurements on the structures fabricated on the SiO<sub>2</sub> surface showed that no gold was present, which contradicts the observations of TEM and AFM.

Therefore the final conclusion must be that although phage can reduce gold in solution or on a carbon surface, that when adsorbed onto an SiO<sub>2</sub> surface that there is no gold reduction.

Regardless of whether M13Y was reducing gold from solution, the rationale behind using tyrosine still stands. By using the phage particle to reduce gold it would allow for the M13 particle to be orientated onto a surface and have gold specifically reduced onto the phage particles and so avoiding background gold deposition. Therefore a method using tyrosine (or something similar) still appears to be the best route. One such method could involve using lysine which has an amine side chain. There is a lysine at position 8 of the mature pVIII coat protein which could be targeted with gold nanoparticles displaying an amine reactive crosslinker.

**This page is intentionally blank**

# Chapter 7

---

## General Conclusions

The overall aim of the work described within this thesis was to fabricate a self-assembling molecular transistor using the M13 bacteriophage. Although this was not achieved, there was significant progress towards the final objective.

### 7.1 Conclusions from Chapter 3

For practical bionanotechnology applications the M13 bacteriophage is too long. At ~1  $\mu\text{m}$  in length and highly flexible, it is difficult to envisage the phage particle predictably depositing onto a surface so that it can be incorporated into an existing circuit. Likewise, an M13 bacteriophage fabricated transistor would be 2 microns in diameter. With a computer chip, the more transistors that can be packed into a given area, the faster the calculations of the computer chip. The size of the M13 bacteriophage transistor would limit the number that could be deposited onto a surface.

Therefore the work described within Chapter 3 used existing technologies to create, and purify, bespoke length phage particles. The microphage cassette, developed by Specthrie, *et al.* (1992), which produces a 50 nm long phage particle, was used as the starting point to create longer phage particles. A kanamycin gene (1165 bp) was inserted into the microphage cassette which in turn produced a phage particle ~200 nm in length. The relationship between the length of inserted DNA and the length of the phage particle showed a linear relationship, which suggests that in the future, phage of a pre-designed length can be produced. A relatively simple protocol was also established to purify these different length phage from wild-type length phage to produce a homologous population. This involved linear sucrose gradient purification followed by size exclusion chromatography. Using this purification technique regularly produced

yields of  $2.5 \times 10^{12}$  cfu from 1 L *E.coli* cultures, which is roughly analogous to wild-type phage titers.

### 7.2 Conclusions from Chapter 4

The work described within Chapter 4 attempted to create the scaffold of the molecular transistor. The aim was to fabricate, and purify, 2 or 3 phage particles self-assembled around a nanoparticle. M13 bacteriophage were created that displayed selenocysteine (Sel) on the minor coat protein pIII. Although the M13pIIISel phage were found to have a lower infectivity than wild-type M13 ( $\sim 2 \times 10^9$  pfu/mL vs  $\sim 4 \times 10^{12}$  pfu/mL), they produced more virion particles ( $\sim 20 \times 10^{13}$  virions/mL vs  $\sim 3 \times 10^{13}$  virions/mL). The M13pIIISel phage were mixed with either 10 nm gold nanoparticles or maleimide functionalised quantum dots. It was found that the phage self-assembled into a variety of higher order structures: from 2 to 4 phage bound to a single nanoparticle.

However, purification of separate higher order structures, e.g. 3 phage per nanoparticle, was problematic. Using linear sucrose density gradients it was possible to purify the higher order structures away from unbound phage and free nanoparticles. However it was not possible to purify the separate higher order structures. Finally, the 50 nm long microphage particles, displaying pIIISel were used to self-assemble higher order structures of two or three microphage per gold nanoparticle. Therefore although purification is still an issue, and needs to be resolved in the future, the work described within this Chapter has shown that the molecular transistor scaffold can be created from self-assembling phage.

### 7.3 Conclusions from Chapter 5

Although a self-assembled molecular transistor could potentially be a useful nanodevice, with no way to place it specifically within a pre-fabricated circuit it would be of limited use. Therefore the work described within this Chapter addressed this issue by using the coiled-coil pair of leucine zippers ACID and BASE. ACID was displayed on pIX of the M13 bacteriophage. SPR was then used to show that the displayed ACID peptide could be used to anchor the phage onto a gold surface via an immobilised BASE peptide. It is envisaged that with the self-assembled molecular transistor that selenocysteine would be displayed on pIII, to direct the phage to the nanoparticles, and ACID displayed on pIX to target the transistor to a designated area on a surface.

In the process of anchoring the phage to a surface the work within this Chapter showed, for the first time, that small coiled-coils can form on a surface when one of the pair is first immobilised. It also showed that other coiled-coils can be displayed on pIX. In this case it was FOS, which is part of the FOS:JUN coiled-coil pair. Although FOS showed some affinity for the immobilised BASE peptide, it was still lower than the affinity of ACID for BASE. This result raises the possibility of using phage displaying different coiled-coil pairs, i.e. one phage displaying FOS and the other displaying ACID, to simultaneously target those phage to different areas of a surface. Therefore different nanodevices could be fabricated and specifically deposited onto different areas of a surface. Further work could be carried out to investigate the kinetics of the ACIDap:BASEap coiled-coil formation on the gold surface of the SPR chip. Also, the immobilisation of the JUN coiled-coil could be investigated so that M13 phage particles displaying its partner FOS could be anchored to the gold surface.

### 7.4 Conclusions from Chapter 6

The aim of this Chapter was to use the M13 bacteriophage to nucleate metallic gold from solution to create gold nanowires using a displayed tyrosine on pVIII. Within the self-assembled transistor, these gold nanowires would act as the source, drain, and gate electrode and so complete the nanodevice. A tyrosine residue was successfully inserted into position 4 of the pVIII coat protein with no effect on phage titer. Tyrosine was used as it has previously been shown to actively reduce gold salt ( $\text{Au}^{3+}$ ), from solution to metallic gold, when displayed on spherical virus particles and peptides.

Within solution it was observed that the phage reduced the gold salt to metallic gold. However, both the tyrosine displaying phage and wild-type phage reduced gold. Wild-type pVIII has two endogenous tyrosine residues which have been predicated to be inaccessible to solvent (Vos, 2009). This result suggests that in fact they are solvent exposed at pH 3. The addition of the extra tyrosine did have some effect. It was observed that the tyrosine displaying phage, in high concentrations, rapidly aggregated when exposed to gold salt creating grey dust-like particles. Wild-type phage did not produce similar particles. When the phage were deposited onto a carbon surface and then exposed to gold salt it was found that the reduction reaction was far more rapid (minutes instead of hours). Once again, wild-type also reduced gold. These results suggest that the display of an additional tyrosine appears to have had little effect on the gold reducing properties of the phage.

The reactions were then moved to  $\text{SiO}_2$  surfaces. It was found by AFM that exposure of the phage to gold salt resulted in the phage particles increasing in height (~3 nm vs 1

nm). This suggested that gold was being reduced onto the phage particles. However, SEM and EDX measurements of the particles showed that no gold was present. Gold electrodes were then “drawn” to the ends of the particles to carry out electrical measurements. However it was found that the particles were non-conducting. Therefore although within solution and on carbon surfaces the phage (both displaying tyrosine and wild-type) will reduce gold, that on an SiO<sub>2</sub> surface the chemistry does not work. Further work needs to be carried out to find a method to deposit gold onto the phage particles.

### **7.5 Closing remarks**

Although the final aim of a self-assembling transistor was not realised, a large bulk of the work towards that aim has been achieved within this study. Specifically, the scaffold of the transistor was self-assembled from 1 µm and 50 nm long phage particles displaying selenocysteine. Also, a method was devised that would allow these scaffolds to be targeted to a surface. The only aspect that is lacking is the deposition of gold onto the scaffold to finish the self-assembling transistor and make it into a complete nanodevice. If this can be accomplished in the future then all the different features could be incorporated to fabricate the self-assembling transistor.

# References

---

## References

---

- Abramoff, M. D., Magelhaes, P. J., Ram, S. J.** (2004). Image Processing with ImageJ. *Biophotonics International* **11**, 36-42.
- Alberts, B., Frey, L. and Delius, H.** (1972). Isolation and characterization of gene 5 protein of filamentous bacterial viruses. *Journal of Molecular Biology* **68**, 139-152.
- Altting-Mees, M. A. and Short, J. M.** (1989). pBluescript II: gene mapping vectors. *Nucleic Acids Research* **17**, 9494.
- Arnold, W. H., Dusa, M. V. and Finders, J.** (2007). Metrology challenges of double exposure and double patterning. *Proceedings of SPIE* **6518**, 651-802.
- Atkins, F. J. and Gesteland, R.** (2002). The 22nd Amino Acid. *Science* **296**, 1409-1410.
- Baek, S.-H., Shin, Y-B., Kim, M-G., Ro, H-S., Kim, E-K. and Chung, B. H.** (2004). Surface Plasmon Resonance Imaging Analysis of Hexahistidine-tagged Protein on the Gold Thin Film Coated with a Calix Crown Derivative. *Biotechnology and Bioprocess Engineering* **9**, 143-146.
- Barber, J.** (2008). Crystal Structure of the Oxygen-Evolving Complex of Photosystem II. *Inorganic Chemistry* **47**, 1700-1710.
- Barrett, O. P. T. and Chin, J. W.** (2010). Evolved orthogonal ribosome purification for in vitro characterization. *Nucleic Acids Research* **38**, 2682-2691.

## References

---

- Barry, B. A., El-Deeb, M. K., Sandusky, P. O. and Babcock, G. T.** (1990). Tyrosine radicals in photosystem II and related model compounds. Characterization by isotopic labeling and EPR spectroscopy. *Journal of Biological Chemistry* **265**, 20139-20143.
- Bassindale, A. R., Codina-Barrios, A., Frascione, N., and Taylor, P. G.** (2007). An improved phage display methodology for inorganic nanoparticle fabrication. *Chemical Communications* **28**, 2959-2958.
- Bauer, M. and Smith, G. P.** (1988). Filamentous phage morphogenetic signal sequence and orientation of DNA in the virion and gene-V protein complex. *Virology* **167**, 166-175.
- Beck, E., Sommer, R., Auerswald, E. A., Kurz, C., Zink, B., Osterburg, G., Schaller, H., Sugimoto, H., Sugisaki, H., Okamoto, T., and Takanami, M.** (1978). Nucleotide sequence of the bacteriophage fd DNA. *Nucleic Acids Research* **5**, 4495-4503.
- Benzer, S. and Champe, S. P.** (1962). A change from nonsense to sense in the genetic code. *PNAS* **48**, 1114-1121.
- Berkowitz, S. A., and Day, L. A.** (1980). Turbidity Measurements in an Analytical Ultracentrifuge. Determinations of Mass per Length for Filamentous Viruses fd, Xf, and Pf3. *Biochemistry* **19**, 2696-2702.

## References

---

**Berkowski, K. L., Plunkett, K. N., Yu, Q. and Moore, J. S.** (2005). Introduction to Photolithography: Preparation of Microscale Polymer Silhouettes. *Journal of Chemical Education* **82**, 1365-1369.

**Biacore AB** (1997). *BIAevaluation Software Handbook version 3.0*.

**Bock, A., Forchhammer, K., Heider, J. and Baron, C.** (1991). Selenoprotein synthesis: an expansion of the genetic code. *Trends in Biochemical Sciences* **16**, 463-467.

**Bradley, D. E.** (1964). The structure of some bacteriophages associated with the male strains of *Escherichia coli*. *Journal of General Microbiology* **35**, 471-482.

**Brissette, R., Prendergast, J. K. A. and Goldstein, N. I.** (2006). Identification of cancer targets and therapeutics using phage display. *Current Opinion in Drug Discovery and Development* **9**, 363-369.

**Brunner, T. A.** (2003). Why optical lithography will live forever. *Journal Vacuum Science and Technology B* **21**, 2632-2637.

**Brust, M., Walker, M., Bethell, D., Schiffrin, D. J. and Whyman, R.** (1994). Synthesis of Thiol-derivatised Gold Nanoparticles in a Two-phase Liquid-Liquid System. *Journal of the Chemical Society - Chemical Communications*, 801-802.

## References

---

**Burkhard, P., Stetefeld, J. and Strelkov, S. V.** (2001). Coiledcoils: a highly versatile protein folding motif. *Trends in Cell Biology* **11**, 82-88.

**Cahoon, L.** (2009). Bugs Build Batteries. *ScienceNOW* **403**, 1.

**Caro, L. G., and Schnoss, M.** (1966). The attachment of the male-specific bacteriophage f1 to sensitive strains of *Escherichia coli*. *PNAS* **56**, 126-132.

**Carrera, M. R. A., Kaufmann, G. F., Mee, J. M., Meijler, M. M., Koob, G. F. and Janda, K. D.** (2004). Treating cocaine addiction with viruses. *PNAS* **101**, 10416-10421.

**Chambers, I., Frampton, J., Goldfarb, P., Affara, N., McBain, W. and Harrison, P. R.** (1986). The structure of the mouse glutathione peroxidase gene: the selenocysteine in the active site is encoded by the 'termination' codon, TGA. . *The EMBO Journal* **5**, 1221-1227.

**Chasteen, L., Ayriss, J., Pavlik, P., and Bradbury, A. R. M.** (2006). Eliminating helper phage from phage display. *Nucleic Acids Research* **34**, 1-11.

**Chatellier, J., Hartley, O., Griffiths, A. D., Fersht, A. R., Winter, G. and Riechmann, L.** (1999). Interdomain interactions within the gene 3 protein of filamentous phage. *FEBS letters* **463**, 371-374.

**Clackson, T. and Lowman, H. B.** (2004). Phage Display: A Practical Approach: Oxford University Press.

## References

---

**Colace, L., Masini, G., Assanto, G., Luan, H-C., Wada, K. and Kimerling, L. C.** (2000). Efficient high-speed near-infrared Ge photodetectors integrated on Si substrate. *Applied Physics Letters* **76**, 1231-1233.

**Cookes-Goodson, W. J., Slocik, J. M., and Naik, R. R.** (2008). Bio-directed synthesis and assembly of nanomaterials. *Chemical Society Reviews* **37**, 2403-2412.

**Cross, G. H., Reeves, A. A., Brand, S., Popplewell, J. F., Peel, L. L., Swann, M. J. and Freeman, N. J.** (2003). A new quantitative optical biosensor for protein characterisation. *Biosensors and Bioelectronics* **19**, 383-390.

**Cseh, L. and Mehl, G. H.** (2007). Structure-property relationships in nematic gold nanoparticles. *Journal of Materials Chemistry* **17**, 311-315.

**Daniel, M.-C. and Astruc, D.** (2004). Gold Nanoparticles: Assembly, Supramolecular Chemistry, Quantum-Size-Related Properties, and Applications toward Biology, Catalysis, and Nanotechnology. *Chemical Reviews* **104**, 293-346.

**Day, L. A. and Wiseman, R. L.** (1978). A comparison of DNA packaging in the virions of fd, Xf, and Pf1. In *The Single-Stranded DNA Phages*, (ed. D. T. Denhardt, Dressler, D., and Ray, D.S.), pp. 605-625. Cold Spring Harbor, N.Y.: Cold Spring Harbor Laboratory.

## References

---

**Deng, L.-W., Malik, P., and Perham, R. N.** (1999). Interaction of the Globular Domains of pIII Protein of Filamentous Bacteriophage fd with the F-Pilus of *Escherichia coli*. *Virology* **253**, 271-277.

**Dietz, H., Douglas, S. M. and Shih, W. H.** (2009). Folding DNA into twisted and curved nanoscale shapes. *Science* **325**, 725-730.

**Dogic, Z. and Fraden, S.** (2006). Ordered phages of filamentous viruses. *Current Opinion in Colloid and Interface Science* **11**, 47-55.

**Donatan, S., Yazici, H., Bermek, H., Sarikaya, M., Tamerler, C. and Urgan, M.** (2009). Physical elution in phage display selection of inorganic-binding peptides. *Materials Science and Engineering C* **29**, 14-19.

**Donzeau, M., Bauersachs, S., Blum, H., Reichelt, P., Rochnisch, T. and Nagel, W.** (2006). Purification of His-tagged hybrid phage antibody. *Analytical Biochemistry* **352**, 154-156.

**Dotto, G. P., Enea, V., and Zinder, N. D.** (1981). Functional Analysis of Bacteriophage f1 Intergenic Region. *Virology* **114**, 463-473.

**Dujardin, E., Peet, C., Stubbs, G., Culver, J. N. and Mann, S.** (2003). Organization of Metallic Nanoparticles Using Tobacco Mosaic Virus Templates. *Nano Letters* **3**, 413-417.

## References

---

- Dulkeith, E., Morteani, A. C., Niedereichholz, T., Klar, T. A., Feldman, J., Levi, S., van Veggel, F. C. J. M., Reinhoudt, D. N., Moller, M. and Gittins, D. I.** (2002). Fluorescence quenching of dye molecules near gold nanoparticles: radiative and nonradiative effects. *Physical Review Letters* **89**, 2030021 - 2030024.
- Editorial, N. M.** (2009). Anniversary of a myth. *Nature Materials* **8**, 771.
- Enea, V. and Zinder, D.** (1982). Interference resistant mutants of phage f1. *Virology* **122**, 222-226.
- Eteshola, E., Brillson, L. J. and Lee, S. C.** (2005). Selection and characteristics of peptides that bind thermally grown silicon dioxide films. *Biomolecular Engineering* **22**, 201-204.
- Fang, Y., Poulsen, N., Dickerson, M. B., Cai, Y., Jones, S. E., Naik, R. R., Kroger, N. and Sandhage, K. H.** (2008). Identification of peptides capable of inducing the formation of titania but not silica via a subtractive bacteriophage display approach. *Journal of Materials Chemistry* **18**, 3871-3875.
- Feng, J.-N., Russel, M. and Model, P.** (1997). A permeabilized cell system that assembles filamentous bacteriophage. *PNAS* **94**, 4068-4073.
- Feng, J.-N., Model, P. and Russel, M.** (1999). A trans-envelope protein complex needed for filamentous phage assembly and export. *Molecular Microbiology* **34**, 745-755.

## References

---

**Feynman, R. P.** (1960). Plenty of Room at the Bottom. *Engineering and Science* **23**, 22-36.

**Firbank, S. J., Rogers, M., Hurtado-Guerrero, R., Dooley, D. M., Halcrow, M. A., Phillips, S. E. V., Knowles, P. F. and McPherson, M. J.** (2003). Cofactor processing in galactose oxidase. *Biochemical Society Transactions* **31**, 506-509.

**Fischer, N., Paleskava, A., Gromadski, K. B., Konevega, A. L., Wahl, M. C., Stark, H. and Rodnina, M. V.** (2007). Towards understanding selenocystine incorporation into bacterial proteins. *Biological Chemistry* **388**, 1061-1067.

**Flohe, L., Gunzler, W. A. and Schock, H. H.** (1973). Glutathione peroxidase: a selenoenzyme. *FEBS letters* **32**, 132-134.

**Flynn, C. E., Mao, C., Hayhurst, A., Williams, J. L., Georgiou, G., Iverson, B. and Belcher, A. M.** (2003). Synthesis and organization of nanoscale II-VI semiconductor materials using evolved peptide specificity and viral capsid assembly. *Journal of Materials Chemistry* **13**, 2414-2421.

**Fuh, G., Sidhu, S. S.** (2000). Efficient phage display of polypeptides fused to the carboxy-terminus of the M13 gene-3 minor coat protein. *FEBS letters* **480**, 231-234.

**Gao, C., Lin, C-H., Lo, C-H. L., Mao, S., Wirsching, P., Lerner, R. A. and Janda, K. D.** (1997). Making chemistry selectable by linking it to infectivity. *PNAS* **94**, 11777-11782.

---

## References

---

**Gao, C., Mao, S., Lo, C-H., L., Wirsching, P., Lerner, R. A. and Janda, K. D.** (1999). Making artificial antibodies: A format for phage display of combinatorial heterodimeric arrays. *PNAS* **96**, 6025-6030.

**Gao, C., Mao, S., Ditzel, H. J., Farnaes, L., Wirsching, P., Lerner, R. A. and Janda, K. D.** (2002). A Cell-Penetrating Peptide from a Novel pVII-pIX Phage-Displayed Random Peptide Library. *Bioorganic and Medicinal Chemistry* **10**, 4057-4065.

**Gaskin, D. J. H., Starck, K. and Vulfson, E. N.** (2000). Identification of inorganic crystal-specific sequences using phage display combinatorial library of short peptides: A feasibility study. *Biotechnology Letters* **22**, 1211-1216.

**Geider, K. and Kornberg, A.** (1974). Conversion of the M13 viral single-strand to the double-stranded replicative form by purified proteins. *Journal of Biological Chemistry* **249**, 3999-4005.

**Gerasopoulos, K., McCarthy, M., Royston, E., Culver, J. N. and Ghodssi, R.** (2008). Nanostructured nickel electrodes using the Tobacco mosaic virus for microbattery applications. *Journal of Micromechanics and Microengineering* **18**, 1-8.

**Gerasopoulos, K., McCarthy, M., Banerjee, P., Fan, X. Culver, J. N. and Ghodssi, R.** (2010). Biofabrication methods for the patterned assembly and synthesis of viral nanotemplates. *Nanotechnology* **21**, 1-11.

## References

---

- Goldman, E. R., Pazirandeh, M. P., Charles, P. T., Balighian, E. D. and Anderson, G. P.** (2002). Selection of phage displayed peptides for the detection of 2,4,6-trinitrotoluene in seawater. *Analytica Chimica Acta* **457**, 13-19.
- Graddis, T. J., Myszka, D. G. and Chaiken, I. M.** (1993). Controlled formation of model homo- and heterodimer coiled coil polypeptides. *Biochemistry* **32**.
- Grandbois, M., Beyer, M., Rief, M., Clausen-Schaumann, H. and Gaub, H. E.** (1999). How Strong Is a Covalent Bond. *Science* **283**, 1727-1730.
- Gray, C. W.** (1989). Three-dimensional structure of complexes of single-stranded DNA-binding proteins with DNA. I. *Ike* and *fd* gene 5 proteins form left-handed helices with single-stranded DNA. *Journal of Molecular Biology* **208**, 57-64.
- Greenwood, J., Willis, A. E. and Perham, R. N.** (1991). Multiple Display of Foreign Peptides on a Filamentous Bacteriophage. *Journal of Molecular Biology* **220**, 821-827.
- Grieco, S.-H., H., Lee, S., Dunbar, W. S, MacGillivray, R. T. A. and Curtis, S. B.** (2009). Maximizing filamentous phage yield during computer-controlled fermentation. *Bioprocess and Biosystems Engineering* **32**, 773-779.
- Griffith, J. and Kornberg, A.** (1974). Mini M13 bacteriophage: Circular Fragments of M13 DNA are replicated and packaged during Normal Infections. *Virology* **59**, 139-152.

## References

---

**Gungormus, M., Fong, H., Kim, I. W., Evans, J. S., Tamerler, C. and Sarikaya, M.** (2008). Regulation of in vitro Calcium Phosphate Mineralization by Combinatorially Selected Hydroxyapatite-Binding Peptides. *Biomacromolecules* **9**, 966-973.

**Herrmann, H., Haner, M., Brettel, M., Ku, N. O., Aebi, U.** (1999). Characterization of distinct early assembly units of different intermediate filament proteins. *Journal of Molecular Biology* **286**, 1403-1420.

**Herrmann, R., Neugebauer, K., Prikl, E., Zentgraf, H., and Schaller, H.** (1980). Conversion of Bacteriophage fd into an Efficient Single-Stranded DNA Vector System. *Molecular and General Genetics* **177**, 231-242.

**Hewitt, J. A.** (1975). Miniphage- a Class of Satellite Phage to M13. *Journal of General Virology* **26**, 87-94.

**Hill, D. F. and Petersen, G. B.** (1982). Nucleotide sequence of bacteriophage f1 DNA. *Journal of Virology* **44**, 32-46.

**Hofschneider, P. H.** (1963). Untersuchungen uber 'kleine' *E.coli* K-12 Bacteriophagen M12, M13, und M20. *Zeitschrift für Naturforschung C* **18**, 203-205.

**Homola, J., Yee, S. S. and Gauglitz, G.** (1999). Surface Plasmon Resonance Sensors: Review. *Sensors and Actuators B: Chemical* **54**, 3-15.

## References

---

**Horiuchi, K.** (1983). Co-evolution of a Filamentous Bacteriophage and its Defective Interfering Particles. *Journal of Molecular Biology* **169**, 389-407.

**Hu, N., and Zhao, B.** (2007). Key genes involved in heavy-metal resistance in *Pseudomonas putida* CD2. *FEMS Microbiology letters* **267**, 17-22.

**Huang, Y., Chiang, C. Y., Lee, S. W., Gao, Y., Hu, E. L. Yoreo, J. D., and Belcher, A. M.** (2005). Programmable Assembly of Nanoarchitectures Using Genetically Engineered Viruses. *Nano Letters* **5**, 1429-1434.

**Huber, R. E. and Criddle, R.S.** (1967). Comparison of the chemical properties of selenocysteine and selenocystine with their sulfur analogs. *Archives of Biochemistry and Biophysics* **122**, 164-173.

**Hunter, G. J., Rowitch, D. H. and Perham, R. N.** (1987). Interactions between DNA and coat protein in the structure and assembly of filamentous bacteriophage fd. *Nature* **327**, 252-254.

**Ilyichev, A. A., Minenkova, O.O., Tatkov, S.I., Karpyshev, N.N., Eroshkin, A.M., Petrenko, V.A. and Sandakhchiev, L.S.** (1989). Construction of M13 viable bacteriophage with the insert of foreign peptides into the major coat protein. *Doklady Biochemistry (Proceedings of the Academy of Sciences of the USSR)-English Translation* **307**.

## References

---

- Iori, F., Corni, S. and Felice, R. D.** (2008). Unravelling the Interaction between Histidine Side Chain and the Au(111) Surface: A DFT Study. *Journal of Physical Chemistry C* **112**, 13540-13545.
- Jadzinsky, P. D., Calero, G., Ackerson, C. J., Bushnell, D. A. and Kornberg, R. D.** (2007). Monolayer-Protected Gold Nanoparticle at 1.1 Å Resolution. *Science* **318**, 430-433.
- Jespers, L. S., Messens, J. H., De Keyser, A., Eeckhout, D., Van den Brande, I., Gansemans, Y. G., Lauwereys, M. J., Vlasuk, G. P. and Stanssens, P. E.** (1995). Surface expression and ligand-based selection of cDNAs fused to filamentous phage gene VI. *Biotechnology* **13**, 378-82.
- Johansson, L., Gafvelin, G. and Arner, E. S. J.** (2005). Selenocysteine in proteins-properties and biotechnological uses. *Biochimica et Biophysica Acta* **1726**, 1-13.
- Johnson, D.** (2005). Molecular Level Investigations of Coiled-Coil Proteins, vol. PhD (ed., pp. 205. Nottingham: University of Nottingham.
- Johnson, S., Evans, D., Laurenson, S., Paul, D., Davies, G., Ferrigno, P. K. and Walti, C.** (2008). Surface-Immobilized Peptide Aptamers as Probe Molecules for Protein Detection. *Analytical Chemistry* **80**, 978-983.
- Kastner, M. A.** (2000). The single electron transistor and artificial atoms. *Annals of Physics* **9**, 885-894.

## References

---

**Khalil, A. S., Ferrer, J. M., Brau, R. R., Kottmann, S. T., Noren, C. J., Lang, M. J., and Belcher, A. M.** (2007). Single M13 bacteriophage tethering and stretching. *PNAS* **104**, 4892-4897.

**Kohn, W. D., Mant, C. T. and Hodges, R. S.** (1997). Alpha-Helical Protein Assembly Motifs. *Journal of Biological Chemistry* **272**, 2583-2586.

**Kohn, W. D. and Hodges, R. S.** (1998). De novo design of alpha-helical coiled coils and bundles: models for the development of protein-design principles. *Trends in Biotechnology* **16**, 379-389.

**Komelli, A.** (2007). Molecular Mechanisms of Magnetosome Formation. *Annual Review of Biochemistry* **76**, 351-366.

**Krebber, A., Bornhauser, S., Burmester, J., Honegger, A., Willuda, J., Bosshard, H. R. and Pluckthun, A.** (1997). Reliable cloning of functional antibody variable domains from hybridomas and spleen cell repertoires employing a reengineered phage display system. *Journal of Immunological Methods* **201**, 35-55.

**Kremser, A., and Rasched, I.** (1994). The adsorption protein of filamentous phage fd: Assignment of its disulfide bridges and identification of the domain incorporated in the coat. *Biochemistry* **33**, 13954-13958.

**Kumar, S.** (2001). *Liquid Crystals*. Cambridge: Cambridge University Press.

---

## References

---

**Kwasnikowski, P., Kristensen, P. and Markiewicz.** (2005). Multivalent display system on filamentous bacteriophage pVII minor coat protein. *Journal of Immunological Methods* **307**, 135-143.

**Laemmli, U. K.** (1970). Cleavage of Structural Proteins during the Assembly of the Head of Bacteriophage T4. *Nature* **227**, 680-685.

**Landschulz, W. H., Johnson, P. F. and McKnight, S. L.** (1988). The leucine zipper: a hypothetical structure common to a new class of DNA binding proteins. *Science* **240**, 1759-1764.

**Lee, J. W., Sim, S. J., Cho, S. M. and Lee, J.** (2005). Characterization of a self-assembled monolayer of thiol on a gold surface and the fabrication of a biosensor chip based on surface plasmon resonance for detecting anti-GAD antibody. *Biosensors and Bioelectronics* **20**, 1422-1427.

**Lee, S.-K., Yun, D. S. and Belcher, A. M.** (2006). Cobalt Ion Mediated Self-Assembly of Genetically Engineered Bacteriophage for Biomimetic Co-Pt Hybrid Material. *Biomacromolecules* **7**, 14-17.

**Lee, S.-W., Mao, C., Flynn, C. E. and Belcher, A. M.** (2002). Ordering of Quantum Dots Using Genetically Engineered Viruses. *Science* **296**, 892-895.

## References

---

- Lee, S. Y., Royston, E., Culver, J. N. and Harris, M. T.** (2005). Improved metal cluster deposition on a genetically engineered tobacco mosaic virus template. *Nanotechnology* **16**, S435-S441.
- Lee, S. Y., Culver, J. N. and Harris, M. T.** (2006). Effect of  $\text{CuCl}_2$  concentration on the aggregation and mineralization of Tobacco mosaic virus biotemplate. *Journal of Colloid and Interface Science* **297**, 554-560.
- Lee, Y. J., Yi, H., Kim, W. J., Kang, K., Yun, D. S., Strano, M. S., Ceder, G., and Belcher, A. M.** (2009). Fabricating Genetically Engineered High-Power Lithium-Ion Batteries Using Multiple Virus Genes. *Science* **324**, 1051-1055.
- Levinson, A., Silver, D., and Seed, B.** (1984). Minimal size plasmids containing an M13 origin for production of single-strand transducing particles. *Journal of Molecular and Applied Genetics* **2**, 507-517.
- Liepold, L. O., Revis, J., Allen, M., Oltrogge, L., Young, M. and Douglas, T.** (2005). Structural transitions in Cowpea chlorotic mottle virus (CCMV). *Physical Biology* **2**, S166-S172.
- Lin, B. J.** (1986). Where is the lost resolution? *Proceedings of SPIE* **633**, 44-50.
- Lin, B. J.** (2006). Optical lithography - present and future challenges. *Comptes Rendus Physique* **7**, 858-874.

## References

---

- Linderoth, N. A., Simon, M. N., Russel, M.** (1997). The filamentous phage pIV multimer visualized by scanning transmission electron microscopy. *Science* **278**, 1635-1638.
- Ling, T. C., Loong, C. K., Tan, W. S., Tey, B. T., Abdullah, W. M. W., and Ariff, A.** (2004). Purification of Filamentous Bacteriophage M13 by Expanded Bed Anion Exchange Chromatography. *The Journal of Microbiology* **42**, 228-232.
- Liu, Y., Mao, J., Zhou, B. Wei, W. and Gong, S.** (2009). Peptide aptamers against titanium-based implants identified through phage display. *Journal of Materials Science: Materials in Medicine* **21**, 1103-1107.
- Lopez, J., and Webster, R. E.** (1983). Morphogenesis of filamentous bacteriophage f1: Orientation of extrusion and production of polyphage. *Virology* **127**, 177-193.
- Loiset, G. A., Kristinsson, S. G. and Sandlie, I.** (2008). Reliable titration of filamentous bacteriophages independent of pIII fusion moiety and genome size by using trypsin to restore wild-type pIII phenotype. *Biotechniques* **44**, 551-554.
- Lubkowski, J., Hennecke, F., Pluckthun, A. and Wlodawer, A.** (1998). The structural basis of phage display elucidated by the crystal structure of the N-terminal domains of g3p. *Nature Structural Biology* **5**, 140-147.

## References

---

- Makowski, L.** (1984). Structural diversity in filamentous bacteriophages. In *Biological macromolecules and assemblies. I. Virus structures*, (ed. F. A. a. M. Journak, A.), pp. 203-253. New York: Wiley.
- Malik, P. and Perham, R. N.** (1996). New vectors for peptide display on the surface of filamentous bacteriophage. *Gene* **171**, 49-51.
- Mandal, D., Bolander, M. E., Mukhopadhyay, D., Sarkar, G., and Mukherjee, P.** (2006). The use of microorganisms for the formation of metal nanoparticles and their application. *Applied Microbiology and Biotechnology* **69**, 485-492.
- Mandal, S., Selvakannan, P. R., Phadtare, S., Pasricha, R., and Sastry, M.** (2002). Synthesis of a stable gold hydrosol by the reduction of chloroaurate ions by the amino acid, aspartic acid *Journal of Chemical Sciences* **114**, 513-520.
- Mao, C., Flynn, C. E., Hayhurst, A., Sweeney, R., Qi, J., Georgiou, G., Iverson, B. and Belcher, A. M.** (2003). Viral assembly of orientated quantum dot nanowires. *PNAS* **100**, 6946-6951.
- Mao, C., Solis, D. J., Reiss, B. D., Kottman, S. T., Sweeney, R. Y., Hayhurst, A., Georgiou, G., Iverson, B. and Belcher, A. M.** (2004). Virus-Based Toolkit for the Directed Synthesis of Magnetic and Semiconducting Nanowires. *Science* **303**, 213-217.

## References

---

- Marciano, D. K., Russel, M. and Simon, S. M.** (2001). Assembling filamentous phage occlude pIV channels. *PNAS* **98**, 9359-9364.
- Marvin, D. A., and Hoffmann-Berling, H.** (1963). Physical and chemical properties of two new small bacteriophage. *Nature* **197**, 517-518.
- Marvin, D. A.** (1998). Filamentous phage structure, infection and assembly. *Current Opinion in Structural Biology* **8**, 150-158.
- Marvin, D. A. and Hoffman-Berling, H.** (1963). Physical and chemical properties of two new small bacteriophages. *Nature* **197**, 517-518.
- Marvin, D. A. and Hohn, B.** (1969). Filamentous bacterial viruses. *Bacteriological Reviews* **33**, 172-209.
- Marvin, D. A. and Wachtel, E. J.** (1966). The topology of DNA from the small filamentous bacteriophage fd. *Journal of Molecular Biology* **15**, 1-7.
- Matsuno, M. T., H., Overman, S. A. and Thomas, Jr., G. J.** (1998). Orientations of Tyrosines 21 and 24 in Coat Subunits of Ff Filamentous Virus: Determination by Raman Linear Intensity Difference Spectroscopy and Implications for Subunit Packing. *Biophysical Journal* **74**, 3217-3225.
- Mead, D., and Kemper, B.** (1986). Vectors: A survey of Molecular Cloning Vectors and Their Uses. Woburn, Massachusetts: Butterworth Publishers.

## References

---

- Mirkin, C. A., Letsinger, R. L., Mucic, R. C., and Storhoff, J. J.** (1996). A DNA-based method for rationally assembling nanoparticles into macroscopic materials. *Nature* **382**, 607-609.
- Moore, G. E.** (1965). Cramming more components onto integrated circuits. *Electronics* **38**, 1-4.
- Mou, T.-C., Gray, C. W. and Gray, D. M.** (1999). The Binding Affinity of Ff Gene 5 Protein Depends on the Nearest-Neighbor Composition of the ssDNA substrate. *Biophysical Journal* **76**, 1537-1551.
- Naik, R. R., Stringer, S. J., Agarwal, G., Jones, S. E., and Stone, M. O.** (2002). Biomimetic synthesis and patterning of silver nanoparticles. *Nature Materials* **1**, 169-172.
- Naik, R. R., Jones, S. E., Murray, C. J., McAuliffe, J. C., Vaia, R. A. and Stone, M. O.** (2004). Peptide Templates for Nanoparticle Synthesis Derived from Polymerase Chain Reaction-Driven Phage Display. *Advanced Functional Materials* **14**, 25-30.
- Nam, K. T., Pelle, B. R., Lee, S. W., and Belcher, A. M.** (2004). Genetically Driven Assembly of Nanorings Based on the M13 Virus. *Nano Letters* **4**, 23-27.
- Nam, K. T., Kim, D-W., Yoo, P. J., Chiang, C-Y., Meethong, N., Hammond, P. T., Chiang, Y-M. and Belcher, A. M.** (2006). Virus-Enabled Synthesis and Assembly of Nanowires for Lithium Ion Battery Electrodes. *Science* **312**, 885-888.

## References

---

- Nam, Y. S., Magyar, A. P., Lee, D., Kim, J. W., Yun, D. S., Park, H., Pollom Jr, T. S., Weitz, D. A., and Belcher, A. M.** (2010). Biologically templated photocatalytic nanostructures for sustained light-driven water oxidation. *Nature Nanotechnology* **5**, 340-344.
- Neumann, H., Wang, K., Davis, L., Garcai-Alai, M. and Chin, J. W.** (2010). Encoding multiple unnatural amino acids via evolution of a quadruplet-decoding ribosome. *Nature* **464**, 441-444.
- Newman, J. R. S. and Keating, A. E.** (2003). Comprehensive Identification of Human bZIP Interactions with Coiled-Coil Arrays. *Science* **300**, 2097-2101.
- Noren, K. A. and Noren, C. J.** (2001). Construction of High-Complexity Combinatorial Phage Display Peptide Libraries. *Methods* **23**, 169-178.
- Oakley, M. G. and Kim, P. S.** (1998). A Buried Polar Interaction Can Direct the Relative Orientation of Helices in a Coiled Coil. *Biochemistry* **37**, 12603-12610.
- O'Shea, E., K., Rutkowski, R. and Kim, P. S.** (1992). Mechanism of Specificity in the Fos-Jun oncoprotein Heterodimer. *Cell* **68**, 699-708.
- O'Shea, E. K., Klemm, J. D., Kim, P. S. and Alber, T.** (1991). X-ray structure of the GCN4 leucine zipper, a two stranded, parallel coiled coil. *Science* **254**, 539-544.

## References

---

- O'Shea, E. K., Lumb, K. J. and Kim, P. S.** (1993). Peptide 'Velcro': design of a heterodimeric coiled coil. *Current Biology* **3**, 658-667.
- Overman, S. A., Tsuboi, M., and Thomas Jr., G. J.** (1996). Subunit Orientation in the Filamentous Virus Ff(fd, f1, M13). *Journal of Molecular Biology* **259**, 331-336.
- Overman, S. A. and Thomas, Jr., G. J.** (1995). Raman Spectroscopy of the Filamentous Virus Ff (fd, f1, M13): Structural Interpretation for Coat Protein Aromatics. *Biochemistry* **34**, 5540-5451.
- Papavoine, C. H. M., Christiaans, B. E. C., Folmer, R. H. A., Konins, R. N. H., and Hilbers, C. W.** (1998). Solution Structure of the M13 Major Coat Protein in Detergent Micelles: A Basis for a Model of Phage Assembly Involving Specific Residues. *Journal of Molecular Biology* **282**, 401-419.
- Parmley, S. F. and Smith, G. P.** (1988). Antibody-selectable filamentous fd phage vectors: affinity purification of target genes. *Gene* **73**, 305-318.
- Peele, B. R., Krauland, E. M., Wittrup, K. D. and Belcher, A. M.** (2005). Design Criteria for Engineering Inorganic Material-Specific Peptides. *Langmuir* **21**, 6929-6933.
- Petrenko, V. A., Smith, G. P., Gong, X. and Quinn, T.** (1996). A library of organic landscapes on filamentous phage. *Protein Engineering* **9**, 797-801.

## References

---

- Petrenko, V. A. and Smith, G. P.** (2000). Phages from landscape libraries as substitute antibodies. *Protein Engineering* **13**, 589-592.
- Ponomarenko, L. A., Schedin, F., Katsnelson, M. I., Yang, R., Hill, E. W., Novoselov, K. S. and Geim, A. K.** (2008). Chaotic Dirac Billiard in Graphene Quantum Dots. *Science* **320**, 356-358.
- Rackham, O. and Chin, J. W.** (2005). A network of orthogonal ribosome mRNA pairs. *Nature Chemical Biology* **1**, 159-166.
- Rakonjac, J., Feng, J-N., and Model, P.** (1999). Filamentous Phage are Released from the Bacterial Membrane by a Two-step Mechanism Involving a Short C-terminal Fragment of pIII. *Journal of Molecular Biology* **289**, 1253-1265.
- Rakonjac, J. and Model, P.** (1998). Roles of pIII in filamentous phage assembly. *Journal of Molecular Biology* **282**, 25-41.
- Ramakrishnan, V.** (2002). Ribosome structure and the mechanism of translation. *Cell* **108**, 557-572.
- Rapoza, M. P. and Webster, R. E.** (1995). The products of gene I and the overlapping in-frame gene XI are required for filamentous phage assembly. *Journal of Molecular Biology* **248**, 627-638.

## References

---

- Reiss, B. D., Mao, C., Solis, D. J., Ryan, K. S., Thomson, T. and Belcher, A. M.** (2004). Biological Routes to Metal Alloy Ferromagnetic Nanostructures. *Nano Letters* **4**, 1127-1132.
- Ro, H.-S., Jung, S. O., Kho, B. H., Hong, H. P., Lee, J. S., Shin, Y-B., Kim, M. G. and Chung, B. H.** (2005). Surface Plasmon Resonance Imaging-Based Protein Array Chip System for Monitoring a Hexahistidine-Tagged Protein during Expression and Purification. *Applied and Environmental Microbiology* **71**, 1089-1092.
- Rowitch, D. H., Hunter, G. J., Perham, R. N.** (1988). Variable Electrostatic Interaction Between DNA and Coat Protein in Filamentous Bacteriophage Assembly. *Journal of Molecular Biology* **204**, 663-674.
- Russel, M.** (1991). Filamentous phage assembly. *Molecular Microbiology* **5**, 1607-1613.
- Salivar, W. O., Henry, T. J. and Pratt, D.** (1967). Purification and properties of diploid particles of coliphage M13. *Virology* **32**, 41-51.
- Salstrom, J. D. and Pratt, D.** (1971). Role of coliphage M13 gene 5 in single-stranded DNA production. *Journal of Molecular Biology* **61**, 489-501.
- Sandman, K. E., Benner, J. S. and Noren, C. J.** (2000). Phage Display of Selenopeptides. *Journal of American Chemical Society* **122**, 960-961.

## References

---

- Sandman, K. E., Tardiff, D. F., Neely, L. A. and Noren, C. J.** (2003). Revised *Escherichia coli* selenocysteine insertion requirements determined by in vivo screening of combinatorial libraries of SECIS variants. *Nucleic Acids Research* **31**, 2234-2241.
- Sanghvi, A. B., Miller, K. P.-H., Belcher, A. M. and Schmidt, C. E.** (2005). Biomaterials functionalisation using a novel peptide that selectively binds to a conducting polymer. *Nature Materials* **4**, 496-502.
- Sarikaya, M., Tamerler, C., Jen, A. K.-Y., Schulten, K. and Baneyx, F.** (2003). Molecular biomimetics: nanotechnology through biology. *Nature Materials* **2**, 577-585.
- Schlizerman, C., Atanassov, A., Berkovich, I., Ashkenasy, G. and Ashkenasy, N.** (2010). De Novo Designed Coiled-Coil Proteins with Variable Conformations as Components of Molecular Electronic Devices. *Journal of American Chemical Society* **132**, 5070-5076.
- Schneider, G. and Decher, G.** (2006). Distance-Dependent Fluorescence Quenching on Gold Nanoparticles Ensheathed with Layer-by-Layer assembled Polyelectrolytes. *Nano Letters* **6**, 530-536.
- Schon, A., Bock, A., Ott, G., Sprinzl, M., and Soll, D.** (1989). The selenocysteine-inserting opal suppressor serine tRNA from *E. coli* is highly unusual in structure and modification. *Nucleic Acids Research* **17**, 7159-7165.

## References

---

**Schuermann, M., Hunter, J. B., Henrig, G. and Muller R.** (1991). Non-leucine residues in the leucine repeats of Fos and Jun contribute to the stability and determine the specificity of dimerization. *Nucleic Acids Research* **19**, 739-746.

**Schüler, D., and Frankel, R. B.** (1999). Bacterial magnetosomes: microbiology, biomineralization and biotechnological applications. *Applied Microbiology and Biotechnology* **52**, 464-473.

**Selvakannan, P. R., Swami, A., Srisathiyannarayanan, D., Shirude, P. S., Paricha, R., Mandale, A. B., and Sastry, M.** (2004). Synthesis of aqueous Au core-Ag shell nanoparticles using tyrosine as a pH-dependent reducing agent and assembling phase-transferred silver nanoparticles at the air-water interface. *Langmuir* **20**, 7825-7836.

**Shen, C. K. J., Ikoku, A., and Heart, J. E.** (1979). Specific DNA orientation in the filamentous bacteriophage fd as probed by psoralen crosslinking and electron microscopy. *Journal of Molecular Biology* **127**, 163-175.

**Shenton, W., Douglas, T., Young, M., Stubbs, G. and Mann, S.** (1999). Inorganic-organic nanotube composites from template mineralization of tobacco mosaic virus. *Advanced Materials* **11**, 253-256.

**Short, J. M., Fernandez, J. M., Sorge, J. A. and Huse, W. D.** (1988).  $\lambda$  ZAP: a bacteriophage  $\lambda$  expression vector with in vivo excision properties. *Nucleic Acids Research* **16**, 7583- 7600.

## References

---

- Si, S., Bhattacharjee, R. R., Banerjee, A., and Mandal, T. K.** (2006). A Mechanistic and Kinetic Study of the Formation of Metal Nanoparticles by Using Synthetic Tyrosine-Based Oligopeptides. *Chemistry: A European Journal* **12**, 1256-1265.
- Silver, S.** (1996). Bacterial resistance to toxic metal ions - a review. *Gene* **179**, 9-19.
- Sinensky, A. K. and Belcher, A. M.** (2006). Biomolecular Recognition of Crystal Defects: A Diffuse-Selection Approach. *Advanced Materials* **18**, 991-996.
- Slawson, R. M., Van Dyke, M. I., Lee, H., and Trevor, J. T.** (1992). Germanium and silver resistance, accumulation and toxicity in microorganisms. *Plasmids* **27**, 73-79.
- Slocik, J. M., Naik, R. R., Stone, M. O., and Wright, D. W.** (2005). Viral templates for gold nanoparticle synthesis. *Journal of Materials Chemistry* **15**, 749-753.
- Slocik, J. M., Govorov, A. O. and Naik, R. R.** (2006). Optical Characterization of Bio-assembled Hybrid Nanostructures. *Supramolecular Chemistry* **18**, 415-421.
- Smith, G. P.** (1985). Filamentous fusion phage: novel expression vectors that display cloned antigens on the virion surface. *Science* **228**, 1315-1317.
- Smith, G. P.** (1988). Filamentous phage assembly: morphogenetically defective mutants that do not kill the host. *Virology* **167**, 156-165.

## References

---

- Smith, G. P. and Gingrich, T. R.** (2005). Hydroxyapatite chromatography of phage-display virions. *Biotechniques* **39**, 879-884.
- Specthrie, L., Bullitt, E., Horiuchi, K., Model, P., Russel, M., and Makowski, L.** (1992). Construction of a Microphage Variant of Filamentous Bacteriophage. *Journal of Molecular Biology* **228**, 720-724.
- Speir, J. A., Munshi, S., Wang, G., Baker, T. S. and Johnson, J. E.** (1995). Structures of the native and swollen forms of cowpea chlorotic mottle virus determined by X-ray crystallography and cryo-electron microscopy. *Structure* **3**, 63-78.
- Srinivasan, G., James, C. M. and Krzycki, J. A.** (2002). Pyrrolysine encoded by UAG in archaea: charging of a UAG-decoding specialized tRNA. *Science* **296**, 1459-1462.
- Stadtman, T. C.** (1996). Selenocysteine. *Annual Review of Biochemistry* **65**, 83-100.
- Stenberg, E., Persson, B., Roos, H. and Urbaniczky, C.** (1991). Quantitative Determination of Surface Concentration of Protein with Surface Plasmon Resonance using Radiolabeled Proteins. *Journal of Colloid and Interface Science* **143**, 513-526.
- Stengele, I., Bross, P., Garces, X., Giray, J., and Rasched, I.** (1990). Dissection of functional domains in phage fd adsorption protein: Discrimination between attachment and penetration sites. *Journal of Molecular Biology* **212**, 143-149.

## References

---

**Stevens, M. M., Allen, S., Sakata, J. K., Davies, M. C., Roberts, C. J., Tendler, S. J. B., Tirrell, D. A. and Williams, P. M.** (2004). pH-Dependent Behavior of Surface-immobilized Artificial Leucine Zipper Proteins. *Langmuir* **20**, 7747-7752.

**Stolz, J. F.** (1993). Magnetosomes. *Journal of General Microbiology* **139**, 1663-1670.

**Sweeney, R. Y., Park, E. Y., Iverson, B. L. and Georgiou, G.** (2006). Assembly of Multimeric Phage Nanostructures Through Leucine Zipper Interactions. *Biotechnology and Bioengineering* **95**, 539-545.

**Tamerler, C. and Sarikaya, M.** (2009). Molecular biomimetics: nanotechnology and bionanotechnology using genetically engineered peptides. *Philosophical Transactions of the Royal Society* **367**, 1705-1726.

**Toumey, C.** (2009). Plenty of room, plenty of history. *Nature Nanotechnology* **4**, 783-784.

**Turkevich, J., Stevenson, P. C., and Hiller, J.** (1951). A study of the nucleation and growth processes in the synthesis of colloidal gold. *Discussions of the Faraday Society* **11**, 55-75.

**Umetsu, M., Mizuta, M., Tsumoto, K., Ohara, S., Takami, S., Watanabe, H., Kumagai, I. and Adschiri, T.** (2005). Bioassisted Room-Temperature Immobilization and Mineralization of Zinc Oxide- The Structure Ordering of ZnO Nanoparticles into a Flower-Type Morphology. *Advanced Materials* **17**, 2571-2575.

## References

---

- Vieira, J., and Messing, J.** (1987). Production of Single-Stranded Plasmid DNA. *Methods in Enzymology* **153**, 3-11.
- Vos, W. L., Nazarov, P. V., Koehorst, R. B. M., Spruijt, R. B., and Hemminga, M. A.** (2009). From 'I' to 'L' and back again: the odyssey of membrane-bound M13 protein. *Trends in Biochemical Sciences* **34**, 249-255.
- Wang, L., Magliery, T. J., Liu, D. R. and Schultz, P. G.** (2000). A new functional suppressor tRNA/aminoacyl-tRNA synthetase pair for the in vivo incorporation of unnatural amino acids in proteins. *Journal of the American Chemical Society* **122**, 5010-5011.
- Wang, W., and Malcolm, B. A.** (1999). Two-Stage PCR Protocol Allowing Introduction of Multiple Mutations, Deletions and Insertions Using QuikChange Site-Directed Mutagenesis. *Biotechniques* **26**, 680-682.
- Wang, Y. A., Yu, X., Overman, S., Tsuboi, M., Thomas Jr., G. J., and Egelman, E. H.** (2006). The Structure of a Filamentous Bacteriophage. *Journal of Molecular Biology* **361**, 209-215.
- Wegner, G. J., Lee, H. J., Marriott, G. and Corn, R. M.** (2003). Fabrication of Histidine-Tagged Fusion Protein Arrays for Surface Plasmon Resonance Imaging Studies of Protein-Protein and Protein-DNA Interactions. *Analytical Chemistry* **75**, 4740-4746.

## References

---

Welsh, L. C., Symmons, M. F., Nave, C., Perham, R. N., Marseglia, E. A. and Marvin, D. A. (1996). Evidence for Tilted Smectic Liquid Crystalline Packing of fd Inovirus from X-ray Fiber Diffraction. *Macromolecules* **29**, 7075-7083.

Wen, Z., Q., Overman, S. A. and Thomas, G. J. (1997). Structure and interactions of the single-stranded DNA genome of filamentous virus fd: investigation by ultraviolet resonance Raman spectroscopy. *Biochemistry* **36**, 7810-7820.

Whaley, S. R., English, D. S., Hu, E. L., Barbara, P. F. and Belcher, A. M. (2000). Selection of peptides with semiconductor binding specificity for directed nanocrystal assembly. *Nature* **405**, 665-668.

Whittaker, M. M., and Whittaker, J. W. (1990). A tyrosine-derived free radical in apogalactose oxidase. *Journal of Biological Chemistry* **265**, 9610-9613.

Willats, W. G. T. (2002). Phage display: practicalities and prospects. *Plant Molecular Biology* **50**, 837-854.

Wolf, E., Kim, P. S. and Berger, B. (1997). MultiCoil: A program for predicting two- and three-stranded coiled coils. *Protein Science* **6**, 1179-1189.

Xie, J., Lee., J. Y., Wang, D. I. C., and Ting, Y. P. (2007). Identification of Active Biomolecules in the High-Yield Synthesis of Single-Crystalline Gold Nanoplates in Algal Solutions. *Small* **3**, 672-682.

## References

---

- Xie, J. and Shultz, P. G.** (2006). A chemical toolkit for proteins - an expanded genetic code. *Nature Reviews Molecular Cell Biology* **7**, 775-782.
- Yamaguchi, H., Terui, T., Noguchi, Y., Ueda, R., Nasu, K., Otomo, A. and Matsuda, K.** (2010). A photoresponsive single electron transistor prepared from oligothiophene molecules and gold nanoparticles in a nanogap electrode. *Applied Physics Letters* **96**, -.
- Yamamoto, K. R., and Alberts, B. M.** (1970). Rapid Bacteriophage Sedimentation in the Presence of Polyethylene Glycol and Its Application to large-Scale Virus Purification. *Virology* **40**, 734-744.
- Yi, H., Nisar, S., Lee, S-Y., Powers, M. A., Bentley, W. E., Payne, G. F., Ghodssi, R., Rubloff, G. W., Harris, M. T., and Culver, J. N.** (2005). Patterned Assembly of Genetically Modified Viral Nanotemplates via Nucleic Acid Hybridization. *Nano Letters* **5**, 1931-1936.
- Yoo, P. J., Nam, K. T., Qi, J., Lee, S. K., Park, J., Belcher, A. M. and Hammond, P. T.** (2006). Spontaneous assembly of viruses on multilayered polymer surfaces. *Nature Materials* **5**, 234-240.
- Zaharova, M. Y., Kozyr, A. V., Ignatova, A. N., Vinnikov, I. A., Shemyakin, I. G. and Kolesnikov, A. V.** (2005). Purification of filamentous bacteriophage for phage display using size-exclusion chromatography. *Biotechniques* **38**, 194-198.

## References

---

**Zeilstra-Ryalls, J., Fayet, O., and Georgopoulos, C.** (1991). The universally conserved GroE (Hsp60) chaperonins. *Annual Review of Microbiology* **45**, 301-25.

**Zeri, A. C., Mesleh, M. F., Nevzorov, A. A., and Opella, S. J.** (2003). Structure of the coat protein in fd filamentous bacteriophage particles determined by solid-state NMR spectroscopy. *PNAS* **100**, 6458-6463.

**Zhou, Y., Chen, W., Itoh, H., Naka, K., Ni, Q., Yamane, H., and Chujo, Y.** (2001). Preparation of a novel core-shell nanostructured gold colloid-silk fibroin bioconjugate by the protein *in situ* redox technique at room temperature. *Chemical communications* **23**, 2518-2519.

**Zhu, J. G., Zheng, Y., and Prinz, G. A.** (2000). Ultrahigh density vertical magnetoresistive random access memory. *Journal of Applied Physics* **87**, 6668-6673.

**Zinder, N. D. and Boeke, J. D.** (1982). The filamentous phage (Ff) as vectors for recombinant DNA - a review. *Gene* **19**, 1-10.

**Zinoni, F., Birkmann, A., Stadtman, T. C. and Bock, A.** (1986). Nucleotide sequence and expression of the selenocysteine-containing polypeptide of formate dehydrogenase (formate-hydrogen-lyase-linked) from *Escherichia coli*. *PNAS* **83**, 4650-4654.

# Appendix A

---

## Appendix A

### 1.0 DNA sequence of pM1

ACCGTCTATCAGGGCGATGGTCTAGAGCATATCTTTCTAGAAGATCTCCTAC  
AATATTCTCAGCTGCCATCGCCCTGATAGACGGTTTTTCGCCCTTTGACGTT  
GGAGTCCACGTTCTTTAATAGTGGACTCTTGTTCCAAACTGGAACAACACTC  
AACCCCTATCTCGGGCAAGCTTGGAACCGCCCTGTAGCGGCGCATTAAAGCGC  
GCGGGGTGTGGTGGTTACGGCGCAGCGTGACCGCTACACTTGCCAGCGCCCT  
AGCGCCCGCTCCCGGGATCGGAATTCCGGGCCATCGCCCTGATAGACGGTTTT  
TCGCCCTTTGACGTTGGAGTCCACGTTCTTTAATAGTGGACTCTTGTTCCAA  
ACTGGAAAACGTCTATCCACAGAATCAGGGATAACGCAGAAAGAAACATGT  
GGAGCCAAGCAGCAAGCCAGAACCGTAAAGGCGCGTTGTTGGCGTTTCCTA  
GGTCGCCCCCTGGCGAGATTCAAATTCACGCTCAGTCAAAGTGCAACGCACG  
GCTAAGATACACGTCCATGGAGATACTCTGGGGT

### 2.0 DNA sequence of pMicro plasmid

GGGGGTGTGGAGATGCGCAGATTGCTCTAGAGCCATCGCCCTGATAGACGGT  
TTTTCGCCCTTTGACGTTGGAGTCCACGTTCTTTAATAGTGGACTCTTGTTCC  
AAACTGGAACAACACTCAACCCTATCTCGGGCAAGCTTGGAACCGCCCTGT  
AGCGGCGCATTAAAGCGCGGGGGGTGTGGTGGTTACGGCGCAGCGTGACCGCT  
TCACTTGCCAGCCCCCTAGCGCCCGCTCCCGGGATCGGAATTCCGGGCCATC  
GCCCTGATAGACGGTTTTTCGCCCTTTGACGTTGGAGTCCACGTTCTTTAAT  
AGTGGACTCTTGTTCCAAACTGGAAAACGTCTGGATCCGCAATCTTTCTAGA  
AGATCTCCTACAATATTCTCAGCTGCCATGGAAAATCGATGTTCTTCTTTTAT

3.0 DNA sequence of pMicrokan

TTGGAGATGCGCAGATTGCTCTAGA **CCATCGCCCTGATAGACGGTTTTTCGC**  
**CCTTTGACGTTGGAGTCCACGTTCTTTAATAGTGGACTCTTGTTCCAAACTG**  
**GAACAACACTCAACCCTATCTCGGGCAAGCTTGGAGCGCCCTGTAGCGGG**  
**GCATTAAGCGCGGGCGGGTGTGGTGGTACCGCGACCGTGACCGCTACACTT**  
**CCGAGCGCCCTAGCGCCCGCTCC**CGGGATCGGAATTCAGGCGGTGCTACAG  
AGTTCTTGAAGTGGTGGCCTAACTACGGCTACACTAGAAGGACAGTATTTG  
GTATCTGCGCTCTGCTGAAGCCAGTTACCTTCGGAAAAAGAGTTGGTAGCTC  
TTGATCCGGCAAACAAACCACCGCTGGTAGCGGTGGTTTTTTTTGTTTGCAAG  
CAGCAGATTACGCGCAGAAAAAAGGATCTCAAGAAGATCCTTTGATCTTT  
TCTACGGGGTCTGACGCTCAGTGGAACGAAAACACTCACGTTAAGGGATTTTG  
GTCATGAACAATAAACTGTCTGCTTACATAAACAGTAATACAAGGGGTGT  
TATGAGCCATATTCAACGGGAAACGTCTTGCTCTAGGCCGCGATTAAATTCC  
AACATGGATGCTGATTTATATGGGTATAAATGGGCTCGCGATAATGTCGGG  
CAATCAGGTGCGACAATCTATCGATTGTATGGGAAGCCCGATGCGCCAGAG  
TTGTTTCTGAAACATGGCAAAGGTAGCGTTGCCAATGATGTTACAGATGAG  
ATGGTCAGACTAACTGGCTGACGGAATTTATGCCTCTTCCGACCATCAAGC  
ATTTTATCCGTACTCCTGATGATGCATGGTTACTCACCCTGCGATCCCCGG  
GAAAACAGCATTCCAGGTATTAGAAGAATATCCTGATTCAGGTGAAAATAT  
TGTTGATGCGCTGGCAGTGTTCTGCGCCGGTTGCATTTCGATTCCTGTTTGTA  
ATTGTCCTTTTAAACAGCGATCGCGTATTTTCGTCTCGCTCAGGCGCAATCACG  
AATGAATAACGGTTTGGTTGATGCGAGTGATTTTGATGACGAGCGTAATGG  
CTGGCCTGTTGAACAAGTCTGGAAAGAAATGCATAAACTTTTGCCATTCTCA  
CCGGATTCAGTCGTCACTCATGGTGATTTCTCACTTGATAACCTTATTTTTGA

## Appendix A

CGAGGGGAAATTAATAGGTTGTATTGATGTTGGACGAGTCGGAATCGCAGA  
CCGATACCAGGATCTTGCCATCCTATGGAAGTGCCTCGGTGAGTTTTCTCCT  
TCATTACAGAAACGGCTTTTTCAAAAATATGGTATTGATAATCCTGATATGA  
ATAAATTGCAGTTTCATTTGATGCTCGATGAGTTTTTCTAAGAATTAATTCAT  
GAGCGGATACATATGAATTCCGGCCATCGCCCTGATAGACGGTTTTTTCGCC  
TTTGACGTTGGAGTCCACGTTCTTTAATAGTGGACTCTTGTTCCAAACTGGA  
AAACGTCTGGATCCGCAATCTTTCTAGAAGATCTCCTACAATATTCTCAGCT  
GCCATGGA

### 4.0 DNA sequence of pM13CP

Highlighted bases, e.g. A, C, T, G, show the 5 silent mutations.

Position 1:

TAATGCTACTACTATTAGTAGAATTGATGCCACCTTTTCAGCTCGCGCCCCA  
AATGAAAATATAGCTAAACAGGTTATTGACCATTTGCGAAATGTATCTAAT  
GGTCAAACCTAAATCTACTCGTTCGCAGAATTGGGAATCAACTGTTATATGGA  
ATGAAACTTCCAGACACCGTACTTTAGTTGCATATTTAAAACATGTTGAGCT  
ACAGCATTATATTCAGCAATTAAGCTCTAAGCCATCCGCAAAAATGACCTCT  
TATCAAAGGAGCAATTAAGGTAAGTCTCTAATCCTGACCTGTTGGAGTTTG  
CTTCCGGTCTGGTTCGCTTTGAAGCTCGAATTAACGCGATATTTGAAGTC  
TTTCGGGCTTCCTCTTAATCTTTTTGATGCAATCCGCTTTGCTTCTGACTATA  
ATAGTCAGGGTAAAGACCTGATTTTTGATTTATGGTCATTCTCGTTTTCTGA  
ACTGTTTAAAGCATTGAGGGGGATTCA

Gene X:

ATGAATATTTATGACGATTCCGCAGTATTGGACGCTATCCAGTCTAAACATT  
TACTATTACCCCTCTGGCAAACTTCTTTTGCAAAAGCCTCTCGCTATTTT  
GGTTTTTATCGTCGTCTGGTAAACGAGGGTTATGATAGTGTGCTCTTACTA  
TGCTCGTAATTCCTTTTGGCGTTATGTATCTGCATTAGTTGAATGTGGTATT  
CCTAAATCTCAACTGATGAATCTTTCTACCTGTAATAATGTTGTTCCGTTAGT

## Appendix A

---

TCGTTTTATTAACGTAGATTTTTCTTCCCAACGTCCTGACTGGTATAATGAGC  
CAGTTCTTAAAATCGCATAAGGTAATTCACA

### Gene V:

ATGATTAAAGTTGAAATTAACCATCTCAAGCCCAATTTACTACTCGTTCTG  
GTGTTTCTCGTCAGGGCAAGCCTTATTCACTGAATGAGCAGCTTTGTTACGT  
TGATTTGGGTAATGAATATCCGGTTCTTGTCAAGATTACTCTTGATGAAGGT  
CAGCCAGCCTATGCGCCTGGTCTGTACACCGTTCATCTGTCCTCTTTCAAAG  
TTGGTCAGTTCGGTTCCTTATGATTGACCGTCTGCGCCTCGTTCGGGCTAA  
GTAAC

### Gene VII:

ATGGAGCAGGTCGCGGATTTTCGACACAATTTATCAGGCGATGATACAAATC  
TCCGTTGTACTTTGTTTCGCGCTTGGTATAATCGCTGGGGGTCAAAG

### Gene IX:

ATGAGTGTTTTAGTGTATTCTTTGCCTCTTTCGTTTTAGGTTGGTGCCTTCG  
TAGTGGCATTACGTATTTTACCCGTTTAATGGAAACTTCCTC

### Gene VIII:

ATGAAAAAGTCTTTAGTCCTCAAAGCCTCTGTAGCCGTTGCTACCCTCGTTC  
CGATGCTGTCTTTCGCTGCAGTATCTGGTTCTTCTCCGGACTCGGATCCCGC  
AAAAGCGGCCTTTAACTCCCTGCAAGCCTCAGCGACCGAATATATCGGTTAT  
GCGTGGGCGATGGTTGTTGTCATTGTGCGGCGCAACTATCGGTATCAAGCTGT  
TTAAGAAATTCACCTCGAAAGCAAGCTGATAAACCGATAACAATTAAGGCT  
CCTTTTGGAGCCTTTTTTTTGGAGATTTTCAAC

### Gene III:

GTGAAAAAATTATTATTCGCAATTCCTTTAGTGGTACCTTTCTATTCTCACTC  
GGCCGAAACTGTTGAAAGTTGTTTAGCAAAATCCCATACAGAAAATTCATTT  
ACTAACGTCTGGAAAGACGACAAAACCTTTAGATCGTTACGCTAACTATGAG  
GGCTGTCTGTGGAATGCTACAGGCGTTGTAGTTTGTACTGGTGACGAAACTC  
AGTGTTACGGTACATGGGTTCCATTGGGCTTGCTATCCCTGAAAATGAGGG  
TGGTGGCTCTGAGGGTGGCGGTTCTGAGGGTGGCGGTTCTGAGGGTGGCGG

## Appendix A

TACTAAACCTCCTGAGTACGGTGATACACCTATTCCGGGCTATACTTATATC  
AACCTCTCGACGGCACTTATCCGCCTGGTACTGAGCAAACCCCGCTAATC  
CTAATCCTTCTCTTGAGGAGTCTCAGCCTCTTAATACTTTTCATGTTTCAA<sup>1</sup>AA  
TAATAGGTTCCGAAATAGGCAGGGGGCATTAACTGTTTATACGGGCACTGT  
TACTCAAGGCACTGACCCCGTTAAACTTATTACCAGTACACTCCTGTATCA  
TCAAAGCCATGTATGACGCTTACTGGAACGGTAAATTCAGAGACTGCGCT  
TTCCATTCTGGCTTTAATGAGGATTTATTTGTTTGTGAATATCAAGGCCAATC  
GTCTGACCTGCCTCAACCTCCTGTCAATGCTGGCGGCGGCTCTGGTGGTGGT  
TCTGGTGGCGGT<sup>2</sup>CCTGAGGGTGGTGGCTCTGAGGGTGGCGGTTCTGAGGGT  
GGCGGCTCTGAGGGAGGCGGTTCCGGTGGTGGCTCTGGTTCGGTGATTTTG  
ATTATGAAAAGATGGCAAACGCTAATAAGGGGGCTATGACCGAAAATGCCG  
ATGAAAACGCGCTACAGTCTGACGCTAAAGGCAAACCTTGATTCTGTCGCTA  
CTGATTACGGTGCTGCTATCGATGGTTTCATTGGTGACGTTCCGGCCTTGCT  
AATGGTAATGGTGCTACTGGTGATTTTGCTGGCTCTAATCCCAAATGGCTC  
AAGTCGGTGACGGTGATAATCACCTTTAATGAATAATTTCCGTCAATATTT  
ACCTTCCCTCCCTCAATCGGTTGAATGTCGCCCTTTTGTCTTTGGCGCTGGTA  
AACCATATGAATTTTCTATTGATTGTGACAAAATAAACTTATCCGTGGTGT  
CTTTGCGTTTCTTTTATATGTTGCCACCTTTATGTATGTATTTTCTACGTTTG  
TAACATACTGCGTAATAAGGAGTCTTAATC

### Gene VI:

ATGCCAGTTCTTTTGGGTATTCCGTTATTATTGCGTTTCCTCGGTTTCCTTCT  
GGTAACTTTGTTCCGGCTATCTGCTTACTTTTCTTAAAAGGGCTTCGGTAAG  
ATAGCTATTGCTATTTTCATTGTTTCTTGCTCTTATTATTGGGCTTAACTCAAT  
TCTTGTGGGTTATCTCTCTGATAATTAGCGCTCAATTACCCTCTGACTTTGTTT  
AGGGTGTTCAGTTAATTCTCCCGTCTAATGCGCTTCCCTGTTTTTATGTTATT  
CTCTCTGTAAAGGCTGCTATTTTT<sup>3</sup>ATTTTTGACGTTAAACAAAAAATCGTTT  
CTTATTTGGATTGGGATAAATAAT

### Gene I:

ATGGCTGTTTATTTTGTAACCTGGCAAATTAGGCTCTGGAAAGACGCTCGTTA  
GCGTTGGTAAGATTCAGGATAAAATTGTAGCTGGGTGCAAATAGCAACTA  
ATCTTGATTTAAGGCTTCAAACCTCCCGCAAGTCGGGAGGTTTCGCTAAAAC  
GCCTCGCGTTCTTAGAATACCGGATAAGCCTTCTATATCTGATTTGCTTGCT  
ATTGGGCGCGGTAATGATTCCCTACGATGAAAATAAAAACGGCTTGCTTGTTT  
TCGATGAGTGCGGTAATTGGTTTAAATACCCGTTCTTGGAAATGATAAGGAAAG  
ACAGCCGATTATTGATTGGTTTCTACATGCTCGTAAATTAGGATGGGATATT  
ATTTTCTTGTTTCAGGACTTATCTATTGTTGATAAACAGGCGCGTTCTGCATT  
AGCTGAACATGTTGTTTATTGTCGTCGCTGGACAGAATACTTTACCTTTTG  
TCGGTACTTTATATTCTTATTACTGGCTCGAAAATGCCTCTGCCTAAATTA

CATGTTGGCGTTGTTAAATATGGCGATTCTCAATTAAGCCCTACTGTTGAGC  
GTTGGCTTTATACTGGTAAGAATTTGTATAACGCATATGATCTAAACAGGCT  
TTTTCTAGTAATTATGATTCCGGTGTATTCTTATTTAACGCCTTATTTATC  
ACACGGTCGGTATTTCAAACCATTAAATTTAGGTCAGAAGATGAAATTAAC  
TAAAATATATTTGAAAAAGTTTTCTCGCGTTCTTTGTCTTGCGATTGGATTG  
CATCAGCATTACATATAGTTATATAACCCAACCTAAGCCGGAGGTTAAAA  
AGGTAGTCTCTCAGACCTATGATTTTGATAAATTCACTATTGACTCTTCTCA  
GCGTCTTAATCTAAGCTATCGCTATGTTTTCAAGGATTCTAAGGGAAAATTA  
ATTAATAGCGACGATTTACAGAAGCAAGGTTATTCACTCACATATATTGATT  
TATGTACTGTTTCCATTAAAAAAGG TAAT

Gene XI

ATGAAATTAACATAAAATATATTTGAAAAAGTTTTCTCGCGTTCTTTGTCTTG  
CGATTGGATTTGCATCAGCATTACATATAGTTATATAACCCAACCTAAGCC  
GGAGGTTAAAAAGGTAGTCTCTCAGACCTATGATTTTGATAAATTCACTATT  
GACTCTTCTCAGCGTCTTAATCTAAGCTATCGCTATGTTTTCAAGGATTCTAA  
GGGAAAATTAATTAATAGCGACGATTTACAGAAGCAAGGTTATTCACTCAC  
ATATATTGATTTATGTACTGTTTCCATTAAAAAAGGTAATTCAA

Gene IV:

ATGAAG<sup>4</sup>TTGTTAAATGTAATTAATTTTGTCTTCTTGATGTTTGTTTCATCATC  
TTCTTTTGCTCAGGTAATTGAAATGAATAATTCGCCTCTGCGCGATTTTGTA  
ACTTGGTATTCAAAGCAATCAGGCGAATCCGTTATTGTTTCTCCCGATGTAA  
AAGGTACTGTTACTGTATATTCATCTGACGTTAAACCTGAAAATCTACGCAA  
TTTCTTTATTTCTGTTTTACGTGCAAATAATTTTGATATGGTAGGTTCTAACC  
CTCCATTATTCAGAAGTATAATCCAAACAATCAGGATTATATTGATGAATT  
GCCATCATCTGATAATCAGGAATATGATGATAATTCGCTCCTTCTGGTGGT  
TTCTTTGTTCCGCAAATGATAATGTTACTCAAACCTTTTAAAATTAATAACG  
TTCGGGCAAAGGATTTAATACGAGTTGTCGAATTGTTTGTAAGTCTAATAC  
TTCTAAATCCTCAAATGTATTATCTATTGACGGCTCTAATCTATTAGTTGTTA  
GTGCTCCTAAAGATATTTTAGATAACCTTCCTCAATTCCTTTCAACTGTTGAT  
TTGCCAACTGACCAGATATTGATTGAGGGTTTGATATTTGAGGTTTCAGCAAG  
GTGATGCTTTAGATTTTTCAATTTGCTGCTGGCTCTCAGCGTGGCACTGTTGCA  
GGCGGTGTTAATACTGACCGCCTCACCTCTGTTTTATCTTCTGCTGGTGGTTC  
GTTCCGGTATTTTAAATGGCGATGTTTTAGGGCTATCAGTTCGCGCATTAAG  
ACTAATAGCCATTCAAAAATATTGTCTGTGCCACGATTCTTACGCTTTTCAG  
GTCAGAAGGGTTCTATCTCTGTTGGCCAGAATGTTCCTTTTATTACTGGTCGT  
GTGACTGGTGAATCTGCCAATGTAAATAATCCATTTTCAGACGATTGAGCGTC  
AAAATGTAGGTATTTCCATGAGCGTTTTTTCCTGTTGCAATGGCTGGCGGTAA  
TATTGTTCTGGATATTACCAGCAAGGCCGATAGTTTGAGTTCTTCTACTCAG

## Appendix A

---

GCAAGTGATGTTACTACTAATCAAAGAAGTATTGCTACAACGGTAAATTTGC  
GTGATGGACAGACTCTTTTACTCGGTGGCCTCACTGATTATAAAAACACTTC  
TCAGGATTCTGGCGTACCGTTCCTGTCTAAAATCCCTTTAATCGGCCTCCTGT  
TTAGCTCCCGCTCTGATTCTAACGAGGAAAGCACGTTATACGTGCTCGTCAA  
AGCAACCATAGTACGCGCCCTGTAGCGGCGCATTAAAGCGCTGCAGAGAACA  
TGGCTTCATGTAGCAGGAGAAAAAAGGCTGCACCGGTGCGTCAGCAGAATA  
TGTGATACAGGATATATTCCGCTTCCTCGCTCACTGACTCGCTACGCTCGGT  
CGTTCGACTGCGGCGAGCGGAAACGGCTTACGAACGGGGCGGAGATTTCT  
GGAAGATGCCAGGAAGATACTTAACAGGGAAAGTGAGAGGGCCGCGGCAA  
GCCGTTTTTCCATAGGCTCCGCCCCCTGACAAGCATCACGAAATCTGACGC  
TCGAATCAGTGGTGGCGAAACCCGACAGGACTATAAAGATACCAGGCGTTT  
CCCCCTGGCGGCTCCCTCGTGCGCTCTCCTGTTCTCCTGCCTTTCCGTTTACCGG  
TGTCATTCCGCTGTTATGGCCGCGTTTGTCTCATTCCACGCCTGACACTCAGT  
TCCGGGTAGGCAGTTCGCTCCAAGCTGGACTGTATGCACGAACCCCCCGTTC  
AGTCCGACCGCTGCGCCTTATCCGGTAACTATCGTCTTGAGTCCAACCCGGA  
AAGACATGCAAAGCACCACTGGCAGCAGCCACTGGTAATTGATTTAGAGG  
AGTTAGTCTTGAAGTCATGCGCCGGTTAAGGCTAAACTGAAAGGACAAGTT  
TTGGTACTGCGCTCCTCCAAGCCAGTTACCTCGGTTCAAAGAGTTGGTAGC  
TCAGAGAACCTTCGAAAAACCGCCCTGCAAGGCGGTTTTTTTCGTTTTTCAGAG  
CAAGAGATTACGCGCAGACCAAACGATCTCAAGAAGATCATCTTATTAAG  
GGGTCTGACGCTCAGTGGAACGAAAACCTCACGTTAAGGGATTTTGGTCATG  
ACAATAAAACTGTCTGCTCTGCAG

Chloramphenicol resistance gene:

ACGCGTGTCCGAATTTCTGCATTCATCCGCTTATTATCACTTATTCAGGCGTA  
GCAACCAGGCGTTTAAGGGCACCAATAACTGCCTTAAAAAAATTACGCCCC  
GCCCTGCCACTCATCGCAGTACTGTTGTAATTCATTAAGCATTCTGCCGACA  
TGGAAGCCATCACAAACGGCATGATGAACCTGAATCGCCAGCGGCATCAGC  
ACCTTGTCGCCTTGCGTATAATATTTGCCCATGGTGAAAACGGGGGCGAAG  
AAGTTGTCCATATTGGCCACGTTTAAATCAAACTGGTGAAACTCACCCAG  
GGATTGGCTGAGACGAAAAACATATTCTCAATAAACCTTTAGGGAAATAG  
GCCAGGTTTTTACCGTAACACGCCACATCTTGCGAATATATGTGTAGAACT  
GCCGGAAATCGTCGTGGTATTCACTCCAGAGCGATGAAAACGTTTCAGTTTG  
CTCATGGAAAACGGTGTAACAAGGGTGAACACTATCCCATATCACCAGCTC  
ACCGTCTTTCATTGCCATACGGAATTCGGGATGAGCATTATCAGGCGGGCA  
AGAATGTGAATAAAGGCCGGATAAACTTGTGCTTATTTTTCTTTACGGTCT  
TTAAAAGGCCGTAATATCCAGCTGAACGGTCTGGTTATAGGTACATTGAG  
CAACTGACTGAAATGCCTCAAATGTTCTTTACGATGCCATTGGGATATATC  
AACGGTGGTATATCCAGTGATTTTTTTCTCATTTTAGCTTCCTTAGCTCCTG  
AAAATCTCGATAACTCAAAAAATACGCCCCGGTAGTGATCTTATTTTCATTATG  
GTGAAAGTTGGAACCTCTTACGTGCCGATCAACGTCTCATTTTCGCCAAAAG  
TTGGCCAGGGCTTCCCGGTATCAACAGGGACACCAGGATTTATTTATTCTG





# Appendix A

5491 TCC ATG AGC GTT TTT CCT GTT GCA ATG GCT GGC GGT AAT ATT GTT CTG GAT ATT ACC AGC AAG GCC GAT AGT TTG AGT TCT TCT ACT CAG  
1831 S M S V F P V A M A G G N I V L D I T S K A D S L S S S T Q

5581 GCA AGT GAT GTT ATT ACT AAT CAA AGA AGT ATT GCT ACA ACG GTT AAT TTG CGT GAT GGA CAG ACT CTT TTA CTC GGT GGC CTC ACT GAT  
1861 A S D V I T N Q R S I A T T V N L R D G Q T L L L G L L F S S R S D S N

5671 TAT AAA AAC ACT TCT CAG GAT TCT GGC GTA CCG TTC CTG TCT AAA ATC CCT TTA ATC GGC CTC CTG TTT AGC TCC CGC TCT GAT TCT AAC  
1891 Y K N T S Q D S G V F F L E K I P L I G L L F S S R S D S N

5761 GAG GAA AGC ACG TTA TAC GTG CTC GTC AAA GCA ACC ATA GTA CGC GCC CTG TAG CGG CGC ATT AAG CGC TGC AGA GAA CAT GGC TTC ATG  
1921 E E S T L Y V L V K A T I V R A L - R B I K R C R E H G F M

5851 TAG CAG GAG AAA AAA GGC TGC ACC GGT GGC TCA GCA GAA TAT GTG ATA CAG GAT ATA TTC CGC TTC CTC GCT CAG TGA CTT GCT ACG CTC  
1951 - O E K K G C T G A S A E Y V I Q D I F R F L A H - L A T L

5941 GGT CGT TCG ACT GCG GCG AGC GGA AAC GGC TTA CGA ACG GGG CGG AGA TTT CCT GGA AGA TGC CAG GAA GAT ACT TAA CAG GGA AGT GAG  
1981 G R S T A A S G N G L R T G R R P P G R C Q E D T - Q G S E

6031 AGG GCC GCG GCA AAG CCG TTT TTC CAT AGG CTC CGC CCC CCT GAC AAG CAT CAC GAA ATC TGA CGC TCG AAT CAG TGG TGG GAA AAC CCG  
2011 R A A A K P P F H R P P V D K H H E I -

6121 ACA GGA CTA TAA AGA TAC CAG GCG TTT CCC CTT GGC GGC TCC CTC GTG CGC TCT CCT GTC CCT GCC TTT CGS TTT ACC GGT GTC ATT CCG  
2041 T G L - R Y Q A F P P G G S L V R S P V P A F R F T G V I P

6211 CTG TTA TGG CCG GTT TCT CAT TCC ACG CCT GAC ACT CAG TTC CGG GTA GGC AGT TCG CTC CAA GCT GGA CTG TAT GCA CGA ACC CCG  
2071 L U W P R L S H S T F D T Q F R V G S S L Q A G L Y A R T P

6301 CGT TCA GTC CGA CCG CTG CCG CTT ATC CGG TAA CTA TCG TCT TGA GTC CAA CCC GGA AAG ACA TGC AAA AGC ACC ACT GCG AGC AGC CAC  
2101 R S V R P L S I R L S - V Q P G K T C K S T T T G S S H

6391 TGG TAA TTG ATT TAG AGG AGT TAG TCT TGA AGT CAT GCG CCG GTT AAG GCT AAA CTG AAA GGA CAA GTT TTG TGT ACT GCG CTC CTC CAA  
2131 W - L I - R S - S - S H A P V K A K L K G Q V L V T A L L Q

6481 GCC AGT TAC CTC GGT TCA AAG AGT TGG TAG CTC AGA GAA CCT TCG AAA AAC CGC CCT GCA AGG CGG TTT TTT CGT TTT CAG AGC AAG AGA  
2161 A S Y L G S K S W - L R E P S K N R P A R R F -

6571 TTA CGC GCA GAC CAA AAC GAT CTC AAG AAG ATC ATC TTA TTA AGG GGT CTG ACG CTC AGT GGA ACG AAA ACT CAC GTT AAG GGA TTT TGG  
2191 L R A D Q N D L K K I I L L R G L T L S G T K T H V K G F W

6661 TCA TGA ACA ATA AAA CTG TCT GCT CTG CAG ACG CGT GTC CGA ATT TCT GCA TTC ATC CGC TTA TTA TCA CTT ATT CAG GCG TAG CAA CCA  
2221 S - T I K L S A L I S A F I R L L S L I Q A R T Q P

6751 GGC GTT TAA GGG CAC CAA TAA CTG CCT TAA AAA AAT TAC CGC CCG CCC TGC CAC TCA TCG CAG TAC TGT TGT AAT TCA TTA AGC ATT CTG  
2251 G V - G H C - L F - K N Y A P P C H S S Q Y C C N S L S I L

6841 CCG ACA TGG AAG CCA TCA CAA ACG GCA TGA TGA ACC TGA ATC GCC AGC GGC ATC AGC ACC TTG TCG CTT GCA TAA TAT TTG CCC ATG  
2281 P T W K P S O T A T T I A S G T S T L S P C V - Y L P M

6931 GTG AAA ACG GGG GCG AAG AAG TTG TCC ATA TTG GCC ACG TTT AAA TCA AAA CTG GTG AAA CTC ACC CAG GGA TTG GCT GCG AAG AAA AAT  
2311 Y K T R L S I L S I L A T F S - V K L V K J T C Q G L A E T K N

7021 ATA TTC TCA ATA AAC CCT TTA GGG AAA TAG GCC AGG TTT TCA CCG TAA CAC GCC ACA TCT TGC GAA TAT ATG TGT AAG AAC TGC CGS AAA  
2343 I F S I N P L G K - A R F S P - H A T S C E Y M C R N C R K

7111 TCG TCG TGG TAT TCA CTC CAG AGC GAT GAA AAC GIT TCA GIT TGC TCA TGG AAA ACG GTG TAA CAA GGG TGA ACA CTA TCC CAT ATT ACC  
2371 S S W Y S F I A T E R N S G - A F J F R A R M - I K A G - N L C

7201 AGC TCA CCG TCT TTC ATT GCC ATA CCG AAT TCC GGA TGA GCA TTC ATC AGG CGG GCA AGA ATG TGA ATA AAG GCC GGA TAA AAC TTG TGC  
2401 S S P S F I A T E R N S G - A F J F R A R M - I K A G - N L C

7291 TTA TTT TTC TTT ACG GTC TTT AAA AAG GCC GTA ATA TCC AGC TGA ACG GTC TGG TTA TAG GTA CAT GCA ACT GCA TGA AAT GCC TCA  
2431 L F P P F T V P K K A V I S S T V W L - V H - A T D - N A S

7381 AAA TGT TCT TTA CGA TGC CAT TGG GAT ATA TCA ACG GTG GTA TAT CCA GTG ATT TTT TTC TCC ATT TTA GCT TCC TTA GCT CCT GAA AAT  
2461 K C S L R C H W D I S T V V Y P V I P F S I L A S L A P E N

7471 CTC GAT AAC TCA AAA AAT ACG CCC GGT AGT GAT CTT ATT TCA TTA TGG TGA AAG TTG GAA CCT CTT ACG TGC CGA TCA ACG TCT CAT TTT  
2491 L D N S K N T P G S D L I S L W - K L E P L T C R S T S R F

7561 CGC CAA AAG TTG GCC CAG GGC TTC CCG GTA TCA ACA GGG ACA CCA GGA TTT ATT TAT TCT GCG AAG TGA TCT TCC GTC ACA GGT ATT TAT  
2521 R Q K L A K R G F P V S T G T P G T P G F I Y S A K -

7651 TCG ACG CGT CCT ATT GGT TAA AAA ATG AGC TGA TTT AAC AAA AAT TTA ATG CGA ATT TTA ACA AAA TAT TAA CGT TTA CAA TTT AAA TAT  
2551 S T R P I G - K M S - F N K N L M R I L T K Y - R L Q P K Y

7741 TTG CTT ATA CAA TCT TCC TGT TTT TGG GGC TTT TCT GAT TAT CAA CCG GGC TAC ATA TGA TTG ACA TGC TAG TTT TAC GAT TAC CGT TCA  
2581 L L I Q S S C F W G F S D Y O P G Y I - L T C - F Y D I R S

7831 TCG ATT CTC TTG TGT GCT CCA GAC TCT CAG GCA ATG ACC TGA TAG CCT TTG TAG ATC TCT CAA AAA TAG CTA CCC TCT CCG GCA TTA ATT  
2611 S I L L S A P D S Q A M T - P L - I S Q K - L P S P A L I

7921 TAT CAG CTA GAA CCG TTG AAT ATC ATA TTG ATG GTG ATT TGA CTG TCT CCG GCC TTT CTC ACC CTT TTG AAT CTT TAC CTA CAC ATT ACT  
2641 Y O L E R L N I I L M V I - L S P A F L T L L N L Y L H I T

8011 CAG GCA TTG CAT TTA AAA TAT ATG AGG GTT CTA AAA ATT TTT ATC CTT CCG TTG AAA TAA AGG CTT CTC CCG CAA AAG TAT TAC AGG GTC  
2671 Q A L H L K Y M R V L K I F I L A L K - R L L P Q K Y Y R V

8101 ATA ATG TTT TTG GTA CAA CCG ATT TAG CTT TAT GCT CTG AGG CTT TAT TGC TTA ATT TTG CTA ATT CTT TGC CTT GCC TGT ATG ATT TAT  
2701 I M F L V C P I - L Y A L R L Y C L I L L I L C L A C M I Y

8191 TGG ATG T  
2731 W M

**This page is intentionally blank**

# Appendix B

---

## Appendix B

### 1.0 DNA sequence of M13pIIISel phage

pIII start codon

CTTTTTTTTGGAGATTTTCAACGTGAAAAATTATTATTCGCAATTCCTTTAG  
TGGTACCTTTCTATTCTCACTCTAGCGCTCGTGTCTGACACGGCCCATCGGTT  
GCAGGTCTGCACCAATCGGCCGAAACTGTTGAAAGTTGTTTAGCAAATCC  
CATACAGAAAATTCATTTACTAACGTCTGGAAAGACGACAAAACCTTTAGAT  
CGTTACGCTAACTATGAGGGCTGTCTGTGGAATGCTACAGGCGTTGTAGTTT  
GTACTGGTGACGAAACTCAGTGTTACGGTACATGGGTTCTATTGGGCTTGC  
TATCCCTGAAAATGAGGGTGGTGGCTCTGAGGGTGGCTGTTCTGAGGGTGG  
CGGTTCTGAGGGTGGCGGTAATAACCTCCTGAGTACGGTGATACACCTATT  
CCGGGCTATACTTATATCAACCCTCTCGACGGCACTTATCCGCCTGGTACTG  
AGCAAACCCCGCTAATCCTAATCCTTCTCTTGAGGAGTCTCATCCCTCTTA  
TACTTTCATGTTTCCAAAAAATAAGTTCTCAAAAAAGGACAGGAGAAC

Yellow = Selenocysteine peptide DNA sequence

### 1.1 DNA and protein sequence of M13pIIISel phage

1 CTT TTT TTG GAG ATT TTC AAC GTG AAA AAA TTA TTA TTC GCA ATT CCT TTA GTG GTA CCT TTC TAT TCT CAC TCT AGC GCT CGT GTC TGA CAC  
1 L F L E I F N V K K L L F A I P L V V P F Y S H S S E A R V U R  
94 GGC CCA TCG GTT GCA GGT CTG CAC CAA TCG GCC GAA ACT GTT GAA AGT TGT TTA GCA AAA TCC CAT ACA GAA AAT TCA TTT ACT AAC GTC TGG  
32 G P S V A G L H Q S A E T V E S C L A K S H T E N S F T N V W  
187 AAA GAC GAC AAA ACT TTA GAT CGT TAC GCT AAC TAT GAG GGC TGT CTG TGG AAT GCT ACA GGC GTT GTA GTT TGT ACT GGT GAC GAA ACT CAG  
63 K D D K T L D R Y A N Y E G C L W N A T G V V V C T G D E T Q  
280 TGT TAC GGT ACA TGG GTT CCT ATT GGG CTT GCT ATC CCT GAA AAT GAG GGT GGT GGC TCT GAG GGT GGC TGT TCT GGT GGC GGT TCT GAG  
94 C Y G T W V P I G L A I P E N E G G G S E G G C S E G G S E  
373 GGT GGC GGT ACT AAA CCT CCT GAG TAC GGT GAT ACA CCT ATT CCG GGC TAT ACT TAT ATC AAC CCT CTC GAC GGC ACT TAT CCG CCT GGT ACT  
125 G G S T K P P E Y G D T P I P G Y T Y I N P L D G T Y P P G T  
466 GAG CAA AAC CCC GCT AAT CCT AAT CCT TCT CTT GAG GAG TCT CAT CCC TCT TAT ACT TTC ATG TTT CCA AAA AAT AAG TTC TCA AAA AAG GAC  
156 E Q N P A N P N P S L E E S H P S Y T F M P P K N K P S K R D  
559 AGG AGA AC  
187 K P

**2.0 DNA sequence of M13pIII C phage**

pIII start codon

TTTTTTTTGGAGATTTTCAACGTGAAAAAATTATTATTCGCAATTCCTTTAGT  
 GGTACCTTTCTATTCTCACTCTAGCGCTCGTGTCTGCCACGGCCCATCGGTTG  
 CAGGTCTGCACCAATCGGCCGAAACTGTTGAAAGTTGTTTAGCAAAATCCC  
 ATACAGAAAATTCATTACTAACGTCTGAAAAGGACCGGACC

Yellow = Cysteine peptide DNA sequence

**2.1 DNA and protein sequence of M13pIII C phage**

```

1 TTT TTT TTG GAG ATT TTC AAC GTG AAA AAA TTA TTA TTC GCA ATT CCT TTA GTG GTA CCT TTC TAT TCT CAC TCT AGC GCT CGT GTC TGC CAC
1 F F L L E I F N V K K L L F A I P L V V F F Y S H S S A R V C H
94 GGC CCA TCG GTT GCA GGT CTG CAC CAA TCG GCC GAA ACT GTT GAA AGT TGT TTA GCA AAA TCC CAT ACA GAA AAT TCA TTA CTA ACG TCT GAA
32 G P S V A S L H Q S A E T V E S C L A K S H T E N S L L T S E
187 AAG GAC CGG ACC
63 K D R T
  
```

**3.0 DNA and protein sequence of wild-type pIII**

```

1 GTG AAA AAA TTA TTA TTC GCA ATT CCT TTA GTG GTA CCT TTC TAT TCT CAC TCG GCC GAA ACT GIT GAA AGT TGT TTA GCA AAA TCC CAT
1 V K K L L L F A I F L V V F F Y S H S S A E T V E S C L A K S H
91 ACA GAA AAT TCA TTT ACT AAC GTC TGG AAA GAC GAC AAA ACT TTA GAT CGT TAC GCT AAC TAT GAG GGC TGT CTG TGG AAT GCT ACA GGC
31 T E N S F T N V W K D D K T L D R Y A N Y E G E G L W N A T G
181 GTT GTA GTT TGT ACT GGT GAC GAA ACT CAG TGT TAC GGT ACA TGG GTT CCT ATT GGG CTT GCT ATC CCT GAA AAT GAG GGT GGT GGC TCT
61 V V V C T G D E T Q C Y G T W V F I G L A I F E N E G G G S
271 GAG GGT GGC GGT TCT GAG GGT GGC GGT TCT GAG GGT GGC GGT ACT AAA CCT CCT GAG TAC GGT GAT ACA CCT ATT CCG GGC TAT ACT TAT
91 E G G G S E G G G S E G G G T K P F E Y G D T F I F G Y T Y
361 ATC AAC CCT CTC GAC GGC ACT TAT CCG CCT GGT ACT GAG CAA AAC CCC GCT AAT CCT AAT CCT TCT CTT GAG GAG TCT CAG CCT CTT AAT
121 I N F L D G T Y P P G T E Q N F A N P N P S L E E S O F L N
451 ACT TTC ATG TTT CAG AAT AAT AGG TTC CGA AAT AGG CAG GGG GCA TTA ACT GIT TAT ACG GGC ACT GIT ACT CAA GGC ACT GAC CCC GIT
151 T F M F Q N N R F R N R Q S A L T V Y T G T V T Q G T D P V
541 AAA ACT TAT TAC CAG TAC ACT CCT GTA TCA TCA AAA GCC ATG TAT GAC GCT TAC TGG AAC GGT AAA TTC AGA GAC TGC GCT TTC CAT TCT
181 K A T Y Y Q Y T P V S S K A M Y D A Y W N G K F R D C A P H S
631 GGC TTT AAT GAG GAT TTA TTT GTT TGT GAA TAT CAA GGC CAA TCG TCT GAC CTG CCT CAA CCT CCT GTC AAT GCT GGC GGC GGC TCT GGT
211 G F N E D L F V C E Y Q G G S S D L F Q P P V N A G G G S G
721 GGT GGT TCT GGT GGC GGC TCT GAG GGT GGT GGC TCT GAG GGT GGC GGC TCT GAG GGA GGC GGT TCC GGT GGT GGC
241 G G S G G S E G G G S E G G G S E G G G S E G G G S E G G G
811 TCT GGT TCC GGT GAT TTT GAT TAT GAA AAG ATG GCA AAC GCT AAT AAG GGG GCT ATG ACC GAA AAT GCC GAT GAA AAC GCG CTA CAG TCT
271 S G S G D F D Y E K M A N A N K G A M T E N A D E N A L Q S
901 GAC GCT AAA GGC AAA CTT GAT TCT GTC GCT ACT GAT TAC GGT GCT GCT ATC GAT GGT TTC ATT GGT GAC GTT TCC GGC CTT GCT AAT GGT
301 D A K S K L D S V A T D Y G A A I D G F I G D V S G L A N G
991 AAT GGT GCT ACT GGT GAT TTT GCT GGC TCT AAT TCC CAA ATG GCT CAA GTC GGT GAC GGT GAT AAT TCA CCT TTA ATG AAT AAT TTC CGT
331 N G A T G D F A G S N S Q M A Q V G D G D N S P L M N N F R
1081 CAA TAT TTA CCT TCC CTC CCT CAA TCG GTT GAA TGT CGC CCT TTT GTC TTT GGC GCT GGT AAA CCA TAT GAA TTT TCT ATT GAT TGT GAC
361 Q Y L P S L P Q S V E C R P F V F G A G K P Y E F S I D C D
1171 AAA ATA AAC TTA TTC CGT GGT GTC TTT GCG TTT CTT TTA TAT GIT GCC ACC TTT ATG TAT GTA TTT TCT ACG TTT GCT AAC ATA CTG CGT
391 K I N L F R G V F A F L L Y V A T P M Y V P S T F A N I L R
1261 AAT AAG GAG TCT TAA
421 N K E S
  
```

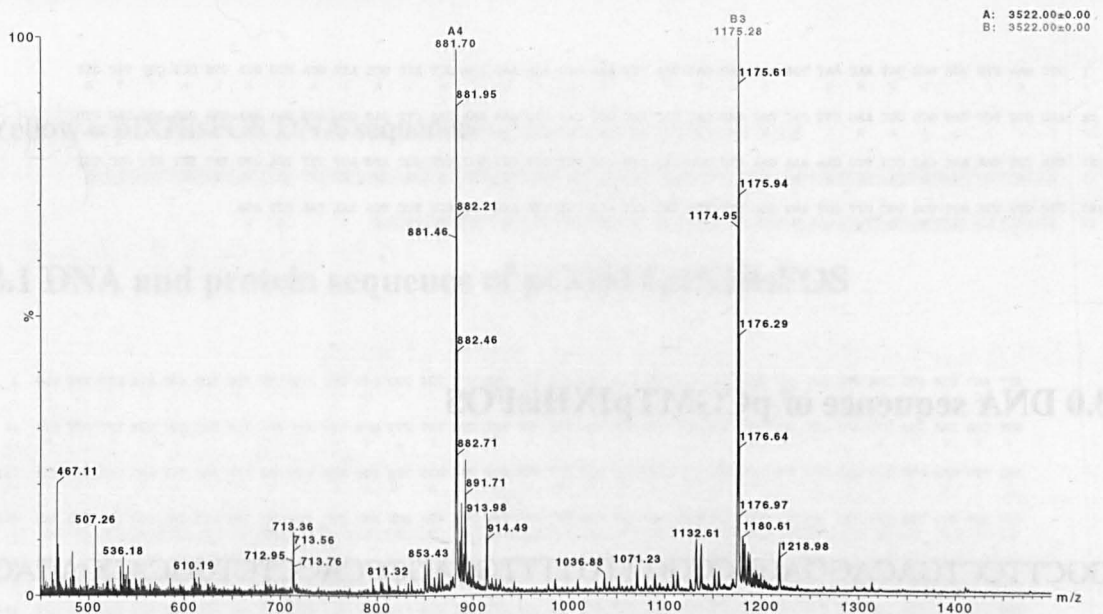
**This page is intentionally blank**

# Appendix C

---



1.3 HPLC purified ACIDap peptide



2.0 DNA sequence of pCGMTpIXHisACIDap

GTGGAATTGTGAGCGGATAACAATTGAATTCAGGAGGAATTTAAAATGAAA  
AAGACAGCTATCGCGATTGCAGTGGCACTGGCTGGTTTCGCTACCGTGGCCC  
AGGCGGCCAAGCTTCACCACCACCACCACGCGCAGCTGGAAAAAGAAC  
TTCAGGCGCTGGAAAAAGAACTGGCGCAGCTGGAATGGGAAAACCAGGCG  
CTGGAAAAAGAACTGGCGCAGCTGCAGTCTGGTGGTGGTTCTGGCATGAGT  
GTTTTAGTGTATTCTTTCGCCTCTTTCGTTTTAGGTTGGTGCCTTCGTAGTGG  
CATTACGTATTTACCCGTTTAATGGAACTTCCTCATAATAAGCTAGAT

Yellow = pIXHisACID DNA sequence

## Appendix C

### 2.1 DNA and protein sequence of pCGMTpIXHisACIDap

```
1 GTG GAA TTG TGA GCG GAT AAC AAT TGA ATT CAG GAG GAA TTT AAA ATG AAA AAG ACA GCT ATC GCG ATT GCA GTG GCA CTG GCT GGT TTC GCT
1 V E L A D N N I Q E E F K M K K T A I A I A V A L A G F A
94 ACC GTG GCC CAG GCG GCC AAG CTT CAC CAC CAC CAC CAC CAC GCG CAG CTG GAA AAA GAA CTT CAG GCG CTG GAA AAA GAA CTG GCG CAG CTG
32 T V A Q A A K L R H R H R H A Q L E K E L Q A L E K E L A Q L
187 GAA TGG GAA AAC CAG GCG CTG GAA AAA GAA CTG GCG CAG CTG CAG TCT GGT GGT TCT GGC ATG AGT GTT TTA GTG TAT TCT TTC GCC TCT
63 E W E N Q A L E K E L A Q L Q S G G G S G M S V L V Y S F A S
280 TTC GTT TTA GGT TGG TGC CTT CGT AGT GGC ATT ACG TAT TTT ACC CGT TTA ATG GAA ACT TCC TCA TAA TAA GCT AGA
94 F V L G W C L R S G I T Y F T R L M E T S S A R
```

### 3.0 DNA sequence of pCGMTpIXHisFOS

```
GGCTTCCTGACAGGAGGCCGtTTTGT TTTGCAGCCACCTCTGGCAGACAG
GTTTCCCGACTGGAAAGCGGGCAGTGAGCGCAACGCAATTAATGTGAGTTA
GCTCACTCATTAGGCACCCAGGCTTTACACTTTATGCTTCCGGCTCGTATG
TTGTGTGGAATTGTGAGCGGATAACAATTGAATTCAGGAGGAATTTAAAAT
GAAAAAGACAGCTATCGCGATTGCAGTGGCACTGGCTGGTTTCGCTACCGT
GGCCCAGGCGGCCAAGCTTCACCACCACCACCACCACCTGAACGATACCTT
GCAAGCGGAAACCGATCAGCTGGAAGATGAAAAAAGCGCGCTGCAAACCG
AAATTGCGAACCTGCTGAACGAAAAAGAAAACTGGAATTTATTCTGGCGG
CGCATCTGCAGTCTGGTGGTGGTTCTGGCATGAGTGTTTTAGTGTATTCTTTC
GCCTCTTTCGTTTTAGGTTGGTGCCTTCGTAGTGGCATTACGTATTTACCCG
TTTAATGGAACTTCCTCATAATAAGCTAGATAATTAATTAGGAGGAATTTA
AAATGAAATACCTATTGCCTACGGCAGCCGCTGGATTGTTATTACTCGCTGC
CCAACCAGCCATGGCCAGGATTCCGGGTGTTGCGGGCGGGGGATCATTGGGC
GCGGGGGGTGTGTTCTGGCGGGCTCCATGGAGCAGGTCGCGGATTTCGA
CACAATTTATCAGGCGATGATACAAATCTCCGTTGTACTTTGTTTCGCGCTT
GGTGTAATCGCTGGGGGTCAAAGATAATAAGGCCTCGCGGGCCAGATCTGC
```

## Appendix C

TCTCTGAGGAGGATCTGGGAAATTGTAAGCGTTAATATTTTGTAAAATTTCG  
CGTAAATTTTGTAAATCAGCTCATTTTTAAACCAATAGGCCG

Yellow = pIXHisFOS DNA sequence

### 3.1 DNA and protein sequence of pCGMTpIXHisFOS

```
1 GGC TTC CTG ACA GGA GGC CGT TTT GTT TTG CAG CCC ACC TCT GGC ACG ACA GGT TTC CCG ACT GGA AAG CGG GCA GTG AGC GCA ACG CAA TTA
1 G F L T G G R F V L Q P T S G T T G F P T G K R A V S A T Q L
94 ATG TGA GTT AGC TCA CTC ATT AGG CAC CCC AGG CTT TAC ACT TTA TGC TTC CGS CTC GTA TGT TGT GTG GAA TTG TGA GCG GAT AAC AAT TGA
32 M V S S L I R H P R L Y T L C F R L V C C V E L A D N N -
187 ATT CAG GAG GAA TTT AAA ATG AAA AAG ACA GCT ATC GCG ATT GCA GTG GCA CTG GCT GGT TTC GCT ACC GTG GCC CAG GCG GCC AAG CTT CAC
63 I Q E E F K M K K T A I A I A V A L A G F A T V A Q A A K L H
280 CAC CAC CAC CAC CTG AAC GAT ACC CTG CAA GCG GAA ACC GAT CAG CTG GAA GAT GAA AAA AGC GCG CTG CAA ACC GAA ATT GCG AAC CTG
94 H H H H H L N D T L Q A E T D Q L E D E K S A L Q T E I A N L
373 CTG AAC GAA AAA GAA AAA CTG GAA TTT ATT CTG GCG GCG CAT CTG CAG TCT GGT GGT GGT TCT GGC ATG AGT GTT TTA GTG TAT TCT TTC GCC
125 L N E K E K L E F I L A A H L Q S G G G S G M E V L V Y S F A
466 TCT TTC GTT TTA GGT TGG TGC CTT CGT AGT GGC ATT ACG TAT TTT ACC CGT TTA ATG GAA ACT TCC TCA TAA TAA GCT AGA TAA TTA ATT AGG
156 S F V L G W C L R S G I T Y F T R L M E T S S - - A R - L I R
559 AGG AAT TTA AAA TGA AAT ACC TAT TGC CTA CCG CAG CCG CTG GAT TGT TAT TAC TCG CTG CCC AAC CAG CCA TGG CCA GGA TTC CGG GTG TTG
187 R N L K - N T Y C L R Q P L D C Y Y S L P N Q P W P G F R V L
652 CGG CGG GGG ATC ATT GGG CGC GGG GGG TGT GTT CTG GCG GCG GCT CCA TGG AGC AGG TCG CGG ATT TCG ACA CAA TTT ATC AGG CGA TGA TAC
218 R R G I I G R G G C V L A A A P W S R S R I S T Q F I R R - Y
745 AAA TCT CCG TTG TAC TTT GTT TCG CGC TTG GTG TAA TCG CTG GGG GTC AAA GAT AAT AAG GCC TCG CGG GCC AGA TCT GCT CTC TGA GGA GGA
243 K S P L Y F V S R L V - E L G V K D N K A S R A R S A L - S G
838 TCT GGG AAA TTG TAA GCG TTA ATA TTT TGT TAA AAT TCG CST TAA ATT TTT GTT AAA TCA GCT CAT TTT TTA ACC AAT AGS CCG
280 S G K L A L I F C - N S R - I F V K S A H F L T N R P
```

### 4.0 DNA sequence of M13pIIIACIDap

pIII start codon

TTTTTTTTGGAGATTTTCAACGTGAAAAAATTATTATTCGCAATTCCTTTAGT  
GGTACCTTTCTATTCTCACTCTGCGCAGCTGGAAAAAGAACTTCAGGGCGCTG  
GAAAAAGAACTGGCGCAGCTGGAATGGGAAAACCAGGGCGCTGGAAAAAGA  
ACTGGCGCAGCTGCAGTCTGGTGGTGGTTCTGCCGAAACTGTTGAAAGTTGT  
TTAGCAAAATCCCATACAGAAAATTCATTTACTAACGTCTGGAAAGACGAC  
AAAACCTTTAGATCGTTACGCTAACTATGAGGGCTGTCTGTGGAATGCTACAG  
GCGTTGTAGTTTGTACTGGTGACGAACTCAGTGTTACGGTACATGGGTTC  
TATTGGGCTTGCTATCCCTGAAAATGAGGGTGGTGGCTCTGAGGGTGGCTGT  
TCTGAGGGTGGCGGTTCTGAGGGTGGCGGTAATAACCTCCTGAGTACGGT  
GATACACCTATCCGGGCTATACTTATATCAACCCTCTCGACGGCACTTATC

# Appendix C

CGCCTGGTACTGAGCAAACCCCGCTAATCCTAATCCTTCTCTTGAGGAGTC  
TCATCCCTCTTATACTTTTCATGTTTCCAAAAAATAAGTTCTCAAAAAAGGAC  
AGGAGA

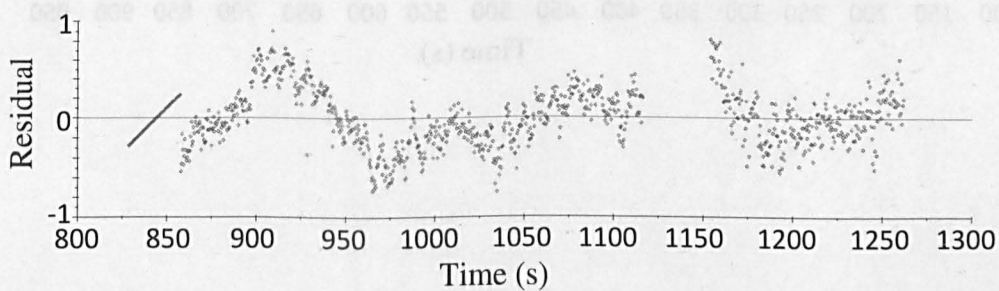
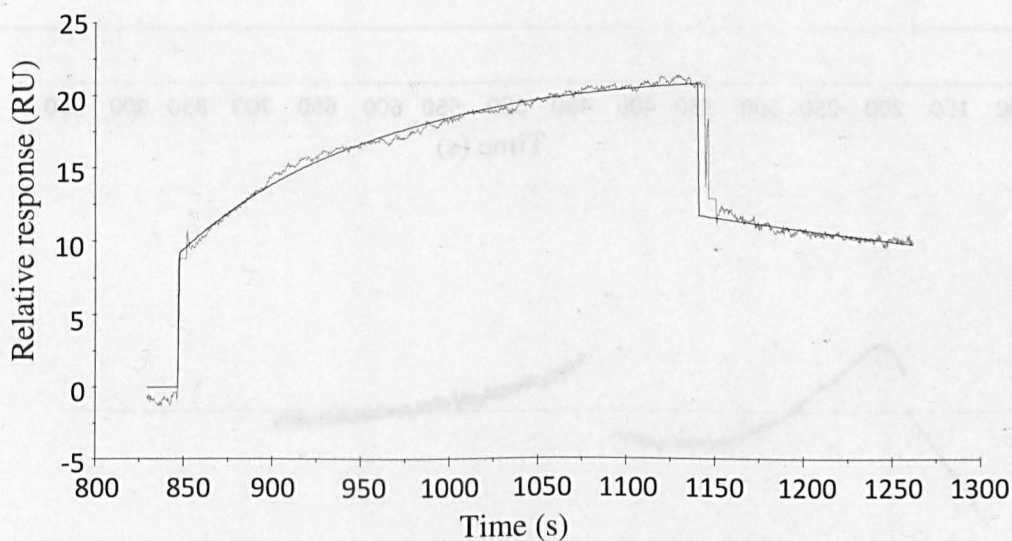
Yellow = ACID peptide DNA sequence

## 4.1 DNA and protein sequence of M13pIIIACIDap

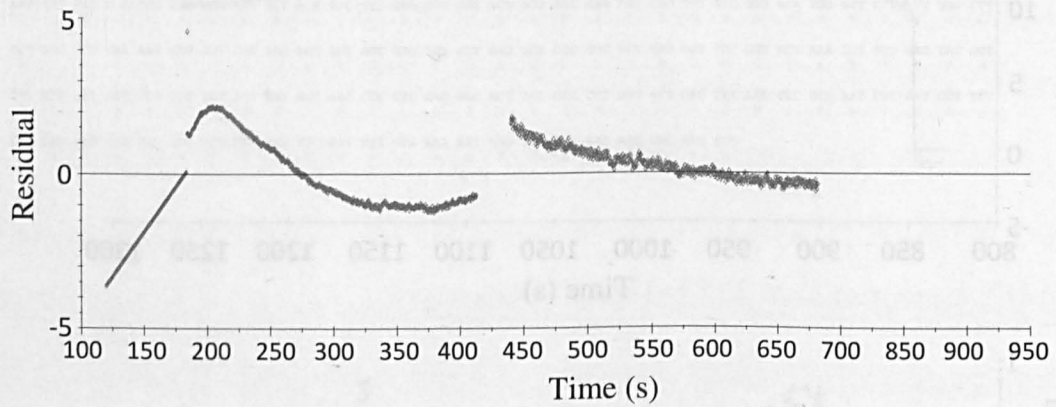
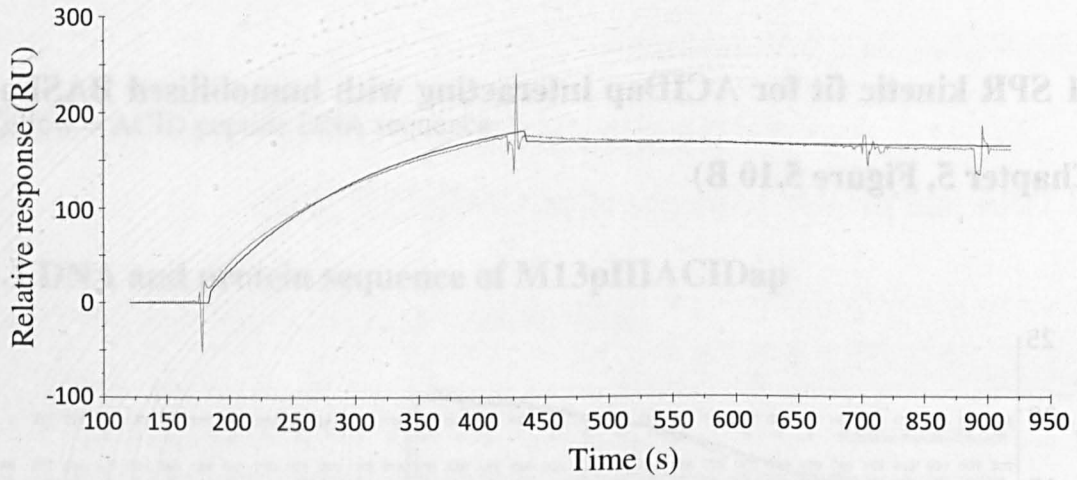
```
1 TTT TTT TTG GAG ATT TTC AAC GTG AAA AAA TTA TTA TTC GCA ATT CCT TTA GTG GTA CCT TTC TAT TCT CAC TCT GCG CAG CTG GAA AAA GAA
1 F F F L E I F N V K K L L F A I P L V V P F Y S H S A Q L E K K E
94 CTT CAG GCG CTG GAA AAA GAA CTG GCG CAG CTG GAA TGG GAA AAC CAG GCG CTG GAA AAA GAA CTG GCG CAG CTG CAG TCT GGT GGT GGT TCT
32 H Q A L E K E L A Q L E W E N Q A L E K E L A Q L Q S G G G S
187 GCC GAA ACT GTT GAA AGT TGT TTA GCA AAA TCC CAT ACA GAA AAT TCA TTT ACT AAC GTC TGG AAA GAC GAC AAA ACT TTA GAT CGT TAC GCT
63 A E T V E S C L A K S H T E N S F T N V W K D D K T L D R Y A
280 AAC TAT GAG GGC TGT CTG TGG AAT GCT ACA GGC GTT GTA GTT TGT ACT GGT GAC GAA ACT CAG TGT TAC GGT ACA TGG GTT CCT ATT GGG CTT
94 N Y E G C L W N A T G V V V C T G D E T D C Y G T W V P I G L
373 GCT ATC CCT GAA AAT GAG GGT GGT GGC TCT GAG GGT GGC TGT TCT GAG GGT GGC GGT TCT GAG GGT GGC GGT ACT AAA CCT CCT GAG TAC GGT
125 A I P E N E G G G S E G G C S E G G G S E G G G T K P P E Y G
466 GAT ACA CCT ATT CCG GGC TAT ACT TAT ATC AAC CCT CTC GAC GGC ACT TAT CCG CCT GGT ACT GAG CAA AAC CCC GCT AAT CCT AAT CCT TCT
156 D T P I P G Y T Y I N F L D S T Y K P G T E Q N P A N F N P S
559 CTT GAG GAG TCT CAT CCC TCT TAT ACT TTC ATG TTT CCA AAA AAT AAG TTC TCA AAA AAG GAC AGG AGA
187 L E E S H P S Y T F M F P K N K P E K K D P R
```

**5.0 SPR kinetic fits for ACIDap and M13pIXHisACID interacting with immobilised BASEap peptide**

**5.1 SPR kinetic fit for ACIDap interacting with immobilised BASEap (Chapter 5, Figure 5.10 B)**



5.2 SPR kinetic fit for M13pIXHisACIDap interacting with immobilised BASEap (Chapter 5, Figure 5.13 B)



1.0 DNA sequence of M13Y

AATTCGGTAAAGAAATTCCTATGAAAGTCTATGCTCCAAAGGC  
TGTAGCCGTTCTAGCTGTTTCTGATGCTGCTTGTCTGATGCTG  
GATCCGCAATAGCCGCTTAACTCTGCAATCTGATGCTGATG  
TTGGTTATGCTGCTGCTGCTGCTGCTGCTGCTGCTGCTGCTG  
ATCAAGCTTTAAGAAATTCCTATGAAAGTCTATGCTCCAAAGGC  
ATTAAGGCTCTTGGAGCTTTTCTGATGCTGCTTCTCAACGTA  
TTAATTCGCAATTCCTGATGCTGCTTCTATGCTGCTGCTGCTG  
TCTGCAAGCCATCGTTGAGGCTGCAACAAATGGTGGAACTGTT

# Appendix D

Yellow = pVII and protein DNA sequence

Green = G to T substitution for D to Y replacement

1.1 DNA and protein sequence of M13Y

1.2 DNA and protein sequence of wild-type M13 pVII

## Appendix D

### 1.0 DNA sequence of M13Y

AATTCCGGTTAATGGA<sup>ACTTCCCTCATGAAAAAGTCTTTAGTCCTCAAAGCC</sup>  
TCTGTAGCCGTTGCTAC<sup>CTCGTTCCGATGCTGTCTTTCGCTGCTGAGGGTTA</sup>  
CGATCCCGCAA<sup>AGCGGCCTTTAACTCCCTGCAAGCCTCAGCGACCGAATA</sup>  
TATCGGTTATGCGTGGGCGATGGTTGTTGTCATTGTCGGCGCAACTATCGGT  
ATCAAGCTGTTTAA<sup>GAAATTCACCTCGAAAGCAAGCTGATAAACCGATACA</sup>  
ATTAAAGGCTCCTTTTGGAGCCTTTTTTTTGGAGATTTTCAACGTGAAAAA  
TTATTATTCGCAATTCCTTTAGTGGTACCTTTCTATTCTCACTCTAGCGCTCG  
TGTCTGACACGGCCCATCGGTTGCAGGTCTGCACCAATCGGCCGAAACTGTT

Yellow = pVIII coat protein DNA sequence

Underline = G to T substitution for D to Y replacement

### 1.1 DNA and protein sequence of M13Y

```
1  AIT CCG GTT AAT GGA ACT TCC CTC ATG AAA AAG TCT TTA GTC CTC AAA GCC TCT GTA GCC GTT GCT ACC CTC GTT CCG ATG CTG TCT TTC GCT
1  I P V N G T S L M K K S L V L K A S V A V A T L V P M L S P A
94  GCT GAG GGT TAC GAT CCC GCA AAA GCG GCC TTT AAC TCC CTG CAA GCC TCA GCG ACC GAA TAT ATC GGT TAT GCG TGG GCG ATG GTT GTT GTC
32  A E G Y D P A K A A F N S L Q A S A T E Y I G Y A W A M V V V
187 AIT GTC GGC GCA ACT ATC GGT ATC AAG CTG TTT AAG AAA TTC ACC TCG AAA GCA AGC TGA TAA ACC GAT ACA ATT AAA GGC TCC TTT TGG AGC
63  I V G A T I G I K L F K K F T S K A S - - T D T I K G S P W S
280 CTT TTT TTT GGA GAT TTT CAA CGT GAA AAA ATT ATT ATT CGC AAT TCC TTT AGT GGT ACC TTT CTA TTC TCA CTC TAG CGC TCG TGT CTG ACA
94  L F F G D P Q R E K I I I R N S F S G T F L F S L - P S C L T
373 CGG CCC ATC GGT TGC AGG TCT GCA CCA ATC GGC CGA AAC TGT T
129 R P I G C R S A P I G R N C
```

### 2.0 DNA and protein sequence of wild-type M13 pVIII

```
1  AIT AAA AAG TCT TTA GTC CTC AAA GCC TCT GTA GCC GTT GCT ACC CTC GTT CCG ATG CTG TCT TTC GCT GCT GAG GGT GAC GAT CCC GCA AAA
1  M K K S L V L K A S V A V A T L V P M L S F A A E G D D P A K
94  GCG GCC TTT AAC TCC CTG CAA GCC TCA GCG ACC GAA TAT ATC GGT TAT GCG TGG GCG ATG GTT GTT GTC ATT GTC GGC GCA ACT ATC GGT ATC
32  A A F N S L Q A S A T E Y I G Y A W A M V V V I V G A T I G I
187 AAG CTG TTT AAG AAA TTC ACC TCG AAA GCA AGC TGA
63  K L F K K F T S K A S -
```